Project No. 13-5144

A Pebble-Bed Breed and Burn Reactor

Reactor Concepts Research Development and Demonstration

Ehud Greenspan
University of California, Berkeley

Thomas Sowinski, Federal POC
Jess Gehin, Technical POC

NEUP Nuclear Energy University Programs
U.S. Department of Energy

A Pebble-Bed Breed and Burn Reactor

Summary Report for Project

NEUP Project 13-5144

University of California, Berkeley

March 31, 2016

A Pebble-Bed Breed and Burn Reactor

NEUP PROJECT 13-5144 SUMMARY REPORT

Covering Period:	January 02, 2014 through January 01, 2016
Date of Report:	March 15, 2016
Recipient:	University of California, Berkeley
Award Number:	DOE-Battelle project award number DE-NE70000701
Project Number:	13-5144
Principal Investigator:	Ehud Greenspan, 510-6439983, gehud@nuc.berkeley.edu
Collaborating PI:	Taek K. Kim, tkkim@anl.gov

Contributing students and researchers

UCB

- PI: Ehud Greenspan – University of California, Berkeley
- CO-PI: Per Peterson – University of California, Berkeley
- Students and post-docs
    - David Frazer, Phil Gorman, Kelly Rowland, Daniel Wooten, PhD students
    - Jason Hou, Post Doc
    - Staffan Qvist, Post Doc

ANL collaborators

- ANL PI: Taek Kyum Kim – Argonne National Laboratory
- Florent Heidet
- Roger Kellogg
- Kun Mo, Walid Mohamed and Abdellatif Yacout

Table of Contents

Table of Contents.....i

Project Abstract..... 1

Project Summary 3

1. Background and Introduction..... 3

2. List of Issues Addressed 7

3. Summary of Work Done and Findings..... 8

3.1 Pebble-bed core concepts and findings 8

3.2 Alternative pin-type segmented core design capable for 3-D fuel shuffling.....10

3.2.1 Developing a robust segmented assembly design for enabling the 3-D fuel shuffling 10

3.2.2 Developing vented fuel rod design for segmented fuel assemblies. 13

3.2.3 Developing generic design of 2-D and 3-D shuffling B&B cores. 14

3.3 Establish deterministic 3-D fuel shuffling capability. 16

3.4 Develop the computational capability for an automatic search of the optimal 2-D and 3-D shuffling pattern. 19

3.5 Compare the optimal 3-D shuffled core characteristics against those of an optimal conventional B&B core design that features 2-D fuel shuffling. 24

3.6 Comparing the neutron balance in 3-D versus 2-D shuffled cores.....29

3.7 The effect of 3-D fuel shuffling patterns of different complexities on the optimal core performance. 34

3.8 The effect of core power density on the core performance. 37

3.9 Effect of 3-D fuel shuffling on safety-related parameters of optimized 3-D shuffled B&B cores versus the 2-D shuffled core. 39

3.10 Develop B&B core models in Hexagonal-Z geometry and investigate the difference between the R-Z and Hexagonal-Z models. 45

3.11 3-D fuel management in modular sodium-cooled B&B fast reactors.....48

3.12 3-D fuel shuffling concept viability assessment and technology roadmap. 51

3.12.1 Fuel rod design 52

3.12.2 Venting mechanism 54

3.12.3 Technology roadmap of 3-D fuel shuffling in B&B reactors 58

4. Conclusions and Recommendations 59

5. Acknowledgements 63

6. Project Publications.....64

References 66

Appendices 72

Project Abstract

The overall objective of this project was to investigate the feasibility of designing a sodium-cooled fast reactor that will be able to establish and maintain a breed-and-burn (B&B) mode of operation when fueled with depleted uranium while discharging the fuel at a peak radiation damage that is significantly closer to 200 dpa than to ~550 dpa present designs call for. The proposed approach was to design the core to enable an effective three-dimensional (3-D) fuel shuffling to reduce the axial variation of the discharge burnup and, thereby, reduce the peak burnup and corresponding minimum required peak radiation damage. Only 2-D shuffling can be realized when using conventional fuel assemblies made of fuel rods and these fuel rods peak-to-average (axially) discharge burnup is in the vicinity of 1.7. [1] [2]

The first part of the project was devoted to study the feasibility of a breed-and-burn (B&B) core made of a bed of metallic fuel pebbles that are clad with HT-9 and are continuously recirculating. Pebble fuel performance analysis concluded that the large stress that would be produced in the pebble cladding from the containment of the fission gases greatly reduces the smear density of the fuel in the pebble. To load enough heavy metal into the core that will enable to reach sustainable B&B mode of operation at acceptable burnup would require such a high smear density that will cause large stress in the cladding and, most likely cladding failure. The phenomenon most limiting the smear density of the fuel is the thermal creep strain of the cladding. Venting of the pebbles will allow high smear density of the pebble fuel but a reliable mechanism needs to be developed to allow venting of the gaseous fission products without significantly reducing the fraction of pebble volume available for the fuel while preventing ingress of the Na coolant and preserving the spherical shape of the outer pebble surface.

Moreover, the thermal-hydraulic analysis concluded that the coolant pressure drop across the pebble bed greatly limits the attainable core power for a neutronically acceptable core height making the pebble-based designs much less economical than an analogous pin-based design. Furthermore, the maximum fuel volume fraction possible to achieve in the pebble-bed core is significantly smaller than of a pin-type core and this significantly impairs the neutronics performance.

As a result, the project focused on assessing the feasibility of performing 3-D fuel shuffling in a core made by segmented fuel assemblies consisting of axially stacked sub-assemblies (also called fuel segments). Each segment is constituted of short vented fuel rods. During fuel shuffling each shuffled fuel assembly is generally made of a different combination of

subassemblies that are axially stacked in different order before the reconstituted assembly is shuffled to another radial location in the core. A combinatorial optimization search methodology of the optimal 3-D shuffling pattern based on the Simulated Annealing (SA) algorithm was developed and implemented; it aims to identify that 3-D Shuffling Pattern (SP) that will minimize the peak radiation damage while, to the extent possible, reducing the burnup reactivity swing, radial power peaking factor and maximum change of assembly power over a cycle. A number of alternative 3-D shuffling scheme variants were also investigated in an attempt to minimize the complexity of the 3-D shuffling strategy and the associated refueling time without significantly penalizing the improvements in the B&B core performance.

It was found that compared with the optimal conventional 2-D fuel shuffling, the optimal 3-D shuffling pattern offers a 1/3 reduction of the minimum peak radiation damage level required for establishing a B&B mode of operation – down to ~350 dpa; a 45% increase in the average fuel discharge burnup – up to ~15% FIMA, and hence the uranium utilization, without violating all major neutronics and thermal-hydraulics constraints. The depleted uranium utilization of this B&B reactor is ~30 times the natural uranium utilization of contemporary LWR when measured per unit of generated electricity. For the same peak dpa level, the average discharge burnup of the optimal 3-D shuffled core is 2.23 times that of the 2-D shuffled core. These significant improvements may enable an earlier commercialization of B&B reactors than otherwise. A successful deployment of the B&B core along with optimal 3-D fuel shuffling could provide at least 30-fold increase in uranium utilization over current once-through Light Water Reactors (LWRs), and hence significantly improve the sustainability of the once-through nuclear fuel cycle. In fact, large 3-D shuffled B&B reactors could supply the total current US electricity needs for hundreds of years in a once-through cycle (no reprocessing) using only the depleted uranium stockpiles accumulated for fuelling the light water reactor fleet and for the start-up loading (first generation) of new B&B reactors. The 30-fold increase in uranium utilization over current LWRs effectively expands the potential for nuclear energy without reprocessing to a technology that is able to supply all of the world's electricity needs for centuries to come, and thus warrants detailed and intense further study.

Project Summary

1. Background and Introduction

Present day commercial Light Water Reactors (LWRs) can extract only ~0.6% of the potential energy that is available in the natural uranium mined for making LWR fuel. Approximately 90% of the unused uranium goes to the depleted uranium (DU) stream of the enrichment process and ~95% of the enriched uranium is left in the used nuclear fuel (UNF). Fast Breeder Reactors (FBRs) can, in principle, fission almost all the DU "waste", although high uranium utilization cannot be achieved in a single irradiation campaign because the radiation damage accumulated by the fuel and cladding challenges the mechanical integrity of the fuel rod. Consequently, the approach that enables attaining high uranium utilization involves multiple fuel recycling. Fuel recycling includes removal of the fuel cladding, removal of the fission products, addition of some DU make up fuel, fabrication of new fuel assemblies and reloading them into the reactor core for another irradiation cycle. Such recycling is commonly required every 10% to 15% fissions per initial heavy metal atom (FIMA), depending on the core neutron spectrum and fuel type. Although technically feasible, the fuel recycling was not acceptable to many U.S. administrations and by other countries due to economic viability and proliferation concerns.

FBRs could, in principle, also operate without fuel recycling. That is, using a once-through fuel cycle as do the majority of LWRs. Although the standard FBR discharge burnup of 10% to 15% FIMA is two to three times higher than that of LWRs, the uranium utilization of a once-through FBR is not significantly different from that of a once-through LWR because the level of uranium enrichment required to achieve criticality in the FBR is often three times that required to fuel the LWR.

To achieve significant uranium utilization without resorting to fuel recycling, special class of fast reactors known as Breed-and-Burn (B&B) reactors has been proposed and studied since the 1950s. The unique feature of a B&B reactor is that it can breed plutonium in depleted or natural uranium feed fuel and then fission a significant fraction of the bred plutonium without having to reprocess the fuel. Once the initial criticality is established with the assistant of either enriched uranium (EU) or plutonium with or without minor actinides, the B&B reactor is capable of continuing its operation fed only with fertile fuel such as DU or natural uranium.

There are two basic types of B&B reactors: Travelling Wave Reactors (TWRs) and Stationary (or Standing) Wave Reactors (SWRs). In TWRs, like the CANDLE reactor concept [3] and the one proposed by Teller et al. [4], the breeding and burning wave travels axially through

the long core from one end to the other. In SWRs, like the one presently being pursued by TerraPower [5] [6], the location of the fission reaction in the core is maintained nearly stationary by adequate radial, i.e., 2-dimensional (2-D) shuffling of fuel assemblies. The TWR concept is considered difficult to implement due to its poor neutron economy and excessive level of radiation damage the fuel has to accumulate [7]. Therefore, this study focuses on the SWR type of B&B reactor and its fuel shuffling strategy.

In order to sustain the B&B mode of operation by feeding the core with fertile fuel such as DU, the burnup the fuel needs to accumulate has to exceed a certain threshold, which strongly depends on the core neutron balance. In a sodium-cooled metallic-fueled B&B core featuring high fuel volume fraction and low-leakage, the minimum required peak burnup is above 20% FIMA and the corresponding peak radiation damage of the fuel cladding is in the vicinity of 500 displacements per atom (dpa). [8] The maximum radiation damage cladding materials were exposed to so far in fast reactors is 200 dpa, experienced by the ferritic-martensitic steel HT-9 in the Fast Flux Test Facility (FFTF) [9]. This means that the SWRs cladding material must withstand a radiation damage more than double the level that has been proven feasible. A combination of development of advanced structural and fuel materials and irradiation experiments are likely to increase the permissible clad radiation damage beyond 200 dpa but proving the practicality and licence-ability of cladding material up to ~500 dpa may take significant time and resources.

Three approaches for operation in the B&B mode without exceeding the 200 dpa constraint had recently been investigated: (1) reconditioning the fuel whenever the cladding reaches 200 dpa. The function of the reconditioning is to remove the cladding, remove the gaseous and some volatile fission products, and load the fuel into a new cladding [10]. (2) Double-clad the fuel [11] after removal of the gaseous fission products. (3) Using excess neutrons from transmutation of trans-uranium elements from LWR UNF to drive a subcritical B&B blanket up to 200 dpa [12].

The overall objective of this project is to investigate a different approach for reducing the minimum required peak radiation damage level – use of 3-dimensional (3-D) in-core fuel management strategy to reduce the axial variation of the discharge burnup and, thereby, reduce the peak burnup and corresponding peak radiation damage. In the 2-D shuffled system, as the plutonium builds up near the axial center faster than at the bottom and top of the fuel assembly, the axial power and burnup distribution in B&B cores is significantly more centrally peaked than in conventional (uniform axial composition) sodium-cooled fast reactor (SFR) cores. In a typical

low-leakage B&B core the peak-to-axially average discharge burnup can far exceed 1.7. If the axial profile of burnup or fast fluence can be flattened down to close to 1.0, the peak dpa level may be reduced significantly.

The NEUP project initially proposed to explore the feasibility of designing a breed-and-burn (B&B) core made of a bed of metallic fuel pebbles that are clad with HT-9 and are continuously circulating. Pebble fuel performance analysis concluded that the stress that would build-up in the pebble cladding from the containment of the fission gases could only be accommodated by greatly reducing the smear density of the fuel in the pebble. To load enough heavy metal into the core that will enable to reach sustainable B&B mode of operation at acceptable burnup would require such a high smear density that will cause large stress in the cladding and, most likely cladding failure. The phenomenon most limiting the smear density of the fuel is the thermal creep strain of the cladding. Venting of the pebbles will allow high smear density of fuel in the pebbles but a design needs to be developed to allow venting of gaseous fission products but prevent ingress of Na coolant. It is not certain that such a design could be developed and be licensable. Moreover, thermal-hydraulic analysis concluded that the coolant pressure drop greatly limits the attainable core power for a neutronically acceptable core height making the pebble-based designs much less economical than an analogous pin-based design. Furthermore, the maximum fuel volume fraction possible to achieve in the pebble-bed core is significantly smaller than of a pin-type core and this significantly impairs the neutronics performance.

As a result, the project focused on assessing the feasibility of performing three-dimensional fuel shuffling in a core made by segmented fuel assemblies made of axially stacked sub-assemblies. Each subassembly is made of short vented fuel pins. In the current design, each full-length assembly is constituted of 2 to 4 assembly segments and during the refueling stage, the fuel assembly is disconnected to allow shuffling of the segments in both radial and axial location. The mechanical design of the segmented fuel assemblies was later improved to be more robust and have enhanced stability of the assembly segments during reactor operation and improved mobility during refueling.

The search for the optimal 3-D Shuffling Pattern (SP) was initially based on a user specified trial-and-error approach and was limited to few trials applied to a single core. The 3-D SP optimization presents a large decision space – for the reference core given in Ref. [8] that features 12-batches and 4 axially stacked subassemblies there are on the order of 10^{61} SP combinations. Hence, an exhaustive search is not feasible using the trial-and-error approach

since using it is extremely computationally expensive. Moreover, the optimal core design should meet several constraints including the burnup reactivity swing, radial power peaking factor and relative assembly power change over the cycle. This makes a manual selection of SP impractical. In addition, the optimal SP is highly sensitive to the core dimensions and number of radial and axial shuffling zones. An automated optimization capability that is able to account for all the constraints was developed in this study based on a stochastic Simulated Annealing (SA) algorithm and applied to the search for the optimum SP in both 2-D and 3-D shuffled systems.

The next major question addressed in this project was the dependence of the improvements in the B&B core performance made possible by 3-D fuel shuffling on the core design complexity, such as number of axially stacked sub-assemblies and constraining the subassemblies to a given assembly. A number of core design simplification approaches have been proposed and evaluated to maximize the improvements of B&B core performance while minimizing the penalties on the refueling effort imposed by 3-D fuel shuffling. The project also quantified the dependence of 3-D shuffled core performance on the core power level and core dimensions.

The list of issues addressed during the two years of the project is given in Section 2 while our findings pertaining to each of these issues are briefly summarized in Section 3. Detailed description of the studies performed in order to reach these findings can be found in the referenced publications a subset of which is included to this report as Appendices. Section 4 summarizes the more important conclusions derived from this project and gives recommendations for future work.

2. List of Issues Addressed

Following is a list of the issues addressed in this project:

1. Pebble-bed core concepts and findings
2. Alternative pin-type segmented core design capable for 3-D fuel shuffling; including:

   2.1 Developing a robust segmented assembly design for enabling the 3-D fuel shuffling

   2.2 Developing vented fuel rod design for segmented fuel assemblies.

   2.3 Developing generic design of 2-D and 3-D shuffling B&B cores.
3. Establish deterministic 3-D shuffling capacity and verify it against a Monte Carlo method.
4. Develop a computational capability for an automatic search of the optimal 2-D and 3-D shuffling pattern (SP). The search for the optimal fuel management is based on a Simulated Annealing (SA) algorithm.
5. Compare the optimal 3-D shuffled core characteristics against those of a conventional B&B core design that features 2-D fuel shuffling.
6. Extend the neutron balance analysis of 0-D unit cell model to actual 3-D core model. Apply this analysis to optimized 2-D and 3-D shuffled core to understand the improvement offered by the 3-D shuffling.
7. Investigate the effect of different simplifications of 3-D fuel shuffling strategies on the optimal core performance.
8. Determine the effect of core power density on 3-D shuffled core performance.
9. Compare the effects of 3-D fuel shuffling on safety related parameters of optimized 3-D shuffled B&B core relative to 2-D shuffled core.
10. Develop Hexagonal-Z models for B&B cores and quantify the difference between the predictions of the Hexagonal-Z and the previously used R-Z core models.
11. Apply 3-D fuel management to relatively small modular sodium-cooled B&B fast reactors and quantify the improvement of core performance made possible by 3-D shuffling. The reactor core chosen for this study is a small B&B core with thermal power of 1000 MW having a diameter comparable to the diameter of the Super-PRISM (S-PRISM) core.
12. 3-D fuel shuffling concept viability assessment and technology roadmap.

3. Summary of Work Done and Findings

3.1 Pebble-bed core concepts and findings

The first design approach was to use a bed of spherical pebbles with continuous feeding and pebble circulation [13]. A pebble bed approach was chosen because pebbles can be well-shuffled in, essentially, three dimensions, without need for complicated shuffling mechanisms. In addition, the cladding in spherical pebbles would withstand the pressure from the fission gases better than a rod would.

The specific approach first tried is to use the pebble-bed B&B core schematically illustrated in Figure 1 [13]. The colored zones are loaded with fuel pebbles of different burnup levels while the white zone that radially surrounds the fuel pebble zones contain steel pebbles that function as a reflector and also protect the reactor vessel from radiation damage. If needed, absorber pebbles could be added at the outer side of the reflector to better shield the reactor vessel. There are no structural partitions in the pebble-bed; the radial and axial grid shown in the figure denotes different depletion zone used for preliminary simulation of this B&B core neutronics performance. Experimental studies performed with graphite pebbles at UCB found that it is feasible to radially segregate the pebbles in the core without any structural partition.

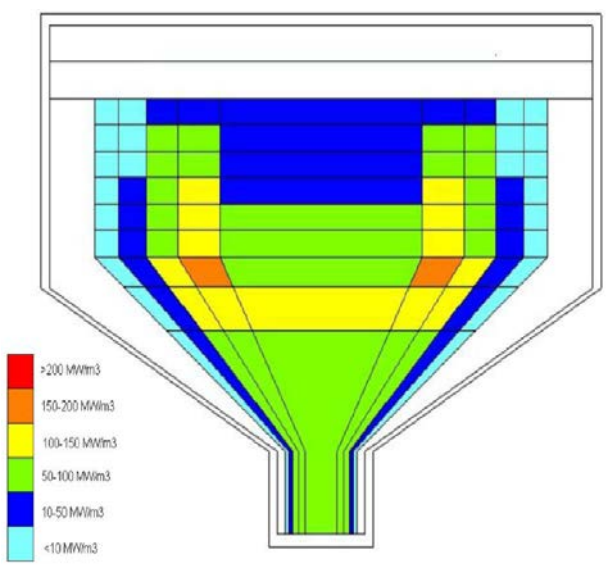

Figure 1 Schematic vertical cut through a very preliminary PB-B&B core design arrived at prior to the initiation of this NEUP project

The pebble-bed examined is divided into 5 radial zones (with no partition) to be numbered sequentially from 1 for the outermost to 5 the innermost. The new depleted U containing pebbles are loaded, from the top, into the outermost radial zone 1 and are slowly circulated

downwards. Pebbles discharged from the outermost radial zone are inserted at the top of zone 2. When the pebbles come out from the bottom of zone 2, they are circulated to the top of zone 5 (radial core center), then to zone 4 and finally to zone 3. This particular shuffling scheme was found to provide a desirable peak-to-average power density. The circulation of the pebbles through the core is envisioned continuous; the pebbles residence time is the time it takes to reach the minimum discharge burnup level that is required for sustaining a B&B mode of operation at a full power k_{eff} value of 1.0.

This design approach resulted in reducing the average discharge radiation damage required for sustaining the B&B mode of operation to a remarkable low value of about 310 dpa; the peak radiation damage was not calculated, but due to the multi-circulation of the fuel pebbles, it is expected to be almost the same as the average. However, there were a number of practical issues with this design; most significantly, it was difficult to introduce control elements to the pebble core without introducing control rod guide tubes that present a mechanical challenge; radiation damage life limit and impaired neutronics performance. Additionally, the coolant pressure drop required for achieving economically acceptable power density was exceptionally large and, due to lack of engineered channels, it was difficult to predict or control the coolant flow pattern throughout the core. This could result in a low average-to-peak coolant temperature rise across the core along with a penalty on the attainable thermodynamic efficiency and hot-spot safety concern.

In order to alleviate the feasibility issues identified for this design concept, another design approach involving pebble fuel was attempted [14]. The pebbles were placed in an ordered lattice within stacked segmented fuel assemblies. This design enabled control blade placement between fuel assemblies, as well as coolant flow orificing for each assembly. The ordered lattice provided a significant reduction of the pressure drop compared to a randomly packed bed of pebbles but at the cost of requiring a complicated shuffling scheme in order to move the pebbles in a 3-D pattern across the core. In this design approach, although the pebble packing fraction was close to that of the random bed, the volume fraction of pebbles in the core was significantly lower due to the volume consumed by the assembly walls and inter-assembly gaps.

It was found that although the 3-D shuffling might have significantly reduced the peak-to-average discharge burnup and peak radiation damage, the lack of a fission gas plenum led to enormous strain on the pebble cladding due to thermal creep. This could be accommodated by reducing the fuel smear density but the reduced fuel loading would make the breed-and-burn mode of operation impractical. The strain would also be made acceptable if the pebbles were

vented; however, no practical solution for venting pebbles without allowing sodium ingress into the pebble could be identified. Additionally, although the pressure drop was lower than in the pebble bed core arrangement, it was still significantly higher than in a rod-type core, which led to comparatively lower power densities. More technical details are provided in Appendix H. These findings led to a change in the fuel concept from pebbles to short cylindrical rods.

3.2 Alternative pin-type segmented core design capable for 3-D fuel shuffling

3.2.1 Developing a robust segmented assembly design for enabling the 3-D fuel shuffling

This section describes a newly perceived design of the segmented fuel assembly to facilitate the 3-D shuffling. In the original design concept [15], assembly segments were axially connected with upper and lower connecting grapplers to form a full-length assembly, while the segment at the bottom of the core is connected to a shielding and flow orificing block that is designed to remain in a fixed location in the reactor for the lifetime of the core.

A recent mechanical concept review performed by ANL mechanical design experts identified a number of mechanical engineering challenges associated with the original design, including difficulties to provide core stability under all operating conditions and to move fuel segments reliably in the sodium coolant. [16] Both of these challenges must be met in a manner that introduces as little as possible fuel-free volume in the core. Therefore, the original design has been modified and the upgraded solution arrived at is described below.

An important guiding principle is that fuel segments should be free stacking without axial joining connections to avoid penalties on fuel-free volume and the introduction of a reliability weakness. As a result, a nesting tapered conic interface is proposed for the segment-segment interface, as illustrated in Figure 2. The top cap (blue) has a protruding hexagonal cone, and the bottom cap (green) has a re-entrant hexagonal cone. The generous tapered hexagonal cone provides a self-centering zone that is larger than the resolution limits of the refueling machine; it also provides robustness against axial fuel segment movements. Adequate passages are also provided on the conic surface for coolant flow.

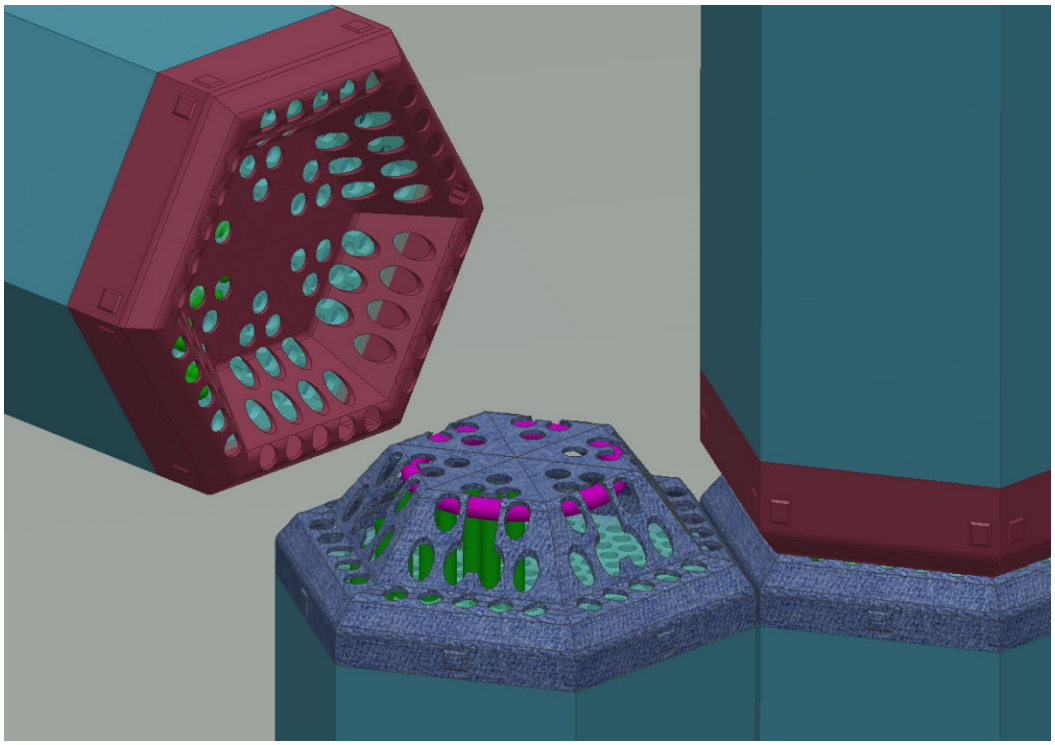

Figure 2 Top and bottom cap of the newly proposed fuel segment design for 3-D fuel shuffling.

Upper and lower external edges of the fuel segments have bevels to provide additional self-centering and resistance to snagging on adjacent fuel assemblies. This contributes significantly to eliminating difficulties with placing segments in the core, especially the last few segments placed in the array, as neighbouring ones that tend to lean toward the open space can be pushed back into proper position as the new fuel segment is inserted.

Centering buttons on the side of the top and bottom cap provide a consistent lateral positioning of the assembly segment in the core and maintain consistent gaps between segments, as shown in Figure 3. Two buttons are designed at the bottom of the segment in order to maintain rotational registry with the core grid, while a single button at the top is adequate to maintain the position of the top of the segment. This arrangement minimizes the dragging of one segment against its neighbours when being inserted or removed. These centering buttons can also provide a measure of tolerance for bowing or twisting of fuel assemblies over their service life.

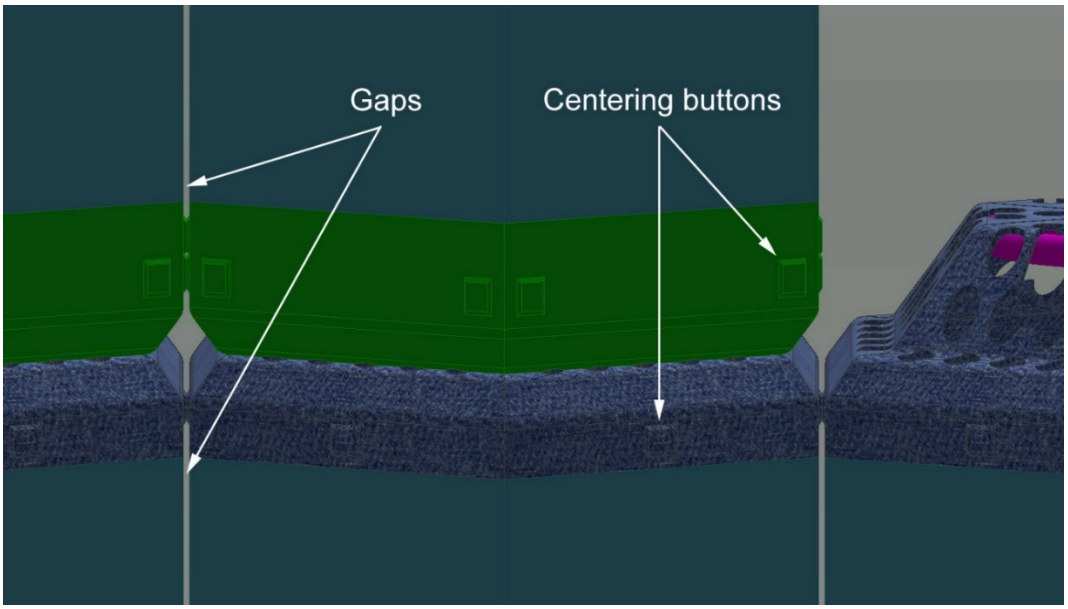

Figure 3 Stacked fuel assembly segments with a demonstration of centering buttons at the top and bottom of the segment and the gaps between segments.

Figure 4 (left) depicts the design of the fuel handling gripper with 3 jaws, which is positioned at the end of the refueling mast. A robust reinforcing ring (also shown in Figure 2) is placed in the top of the fuel segment to distribute gripper forces and provide adequate wear surfaces for the life of the segment. A central rod actuator can actuate 3 jaws equally. During the refueling process, the refueling mast is positioned over the assembly segment and extended downwards to reach the segment. The segment is then attached with the handling gripper and lifted up. The gripper is smaller than the footprint of a segment, thus allowing it to reach a fuel segment on the lowest course without removing neighboring segments. Figure 4 (right) shows the attachment of the gripper to one of the sub-assemblies sitting on top of the stacked segments during the refueling process.

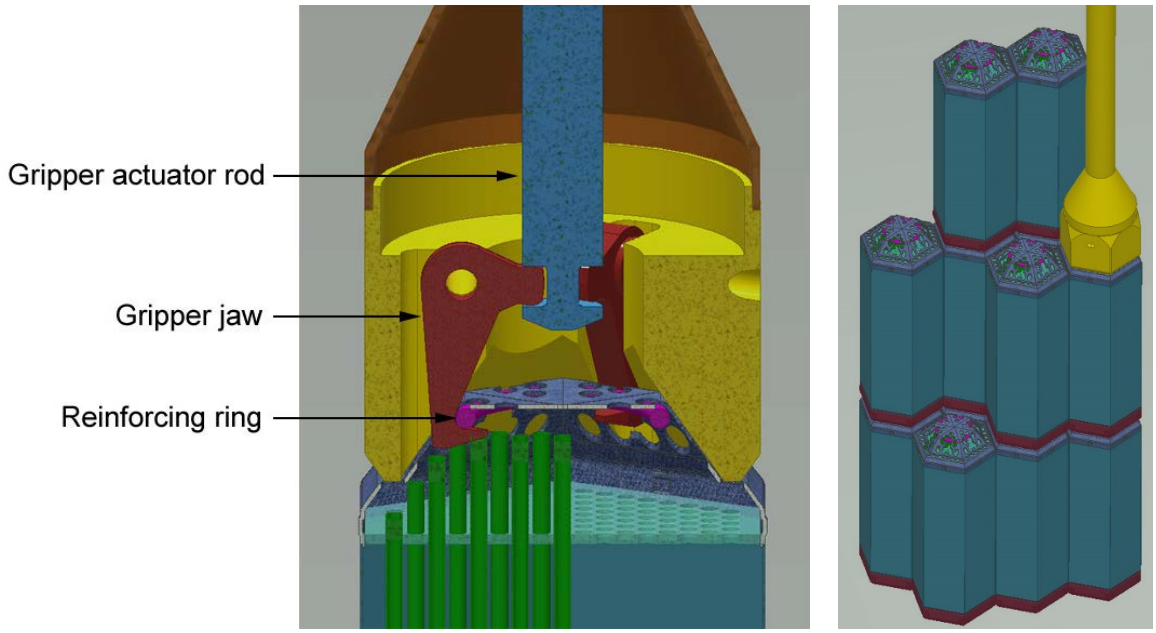

Figure 4 Section view of the fuel gripper mechanism (left); and stacked fuel segments, representing a portion of a core (right).

3.2.2 Developing vented fuel rod design for segmented fuel assemblies.

The assembly segments are constituted of conventional rod-type fuel, which are designed to allow for continuous release of gaseous fission products through a thin porous filter followed by small openings in the upper end cap, as illustrated in Figure 4. This is because the use of any type of un-vented fuel would make the segmentation of the fuel assemblies impractical as the gas plenum at the top of the fuel sub-assembly will take a large fraction of the core volume and will therefore have a significant negative impact on the neutron economy. The only identified option to design high actinide-density axially segmented solid fuel rods is to vent the gaseous fission products directly to the coolant. Because of the relatively large space required for accommodating any type of hydrostatic venting devices, continuous release of fission gas through small openings in the upper end cap is assumed in this study.

The depleted uranium metal fuel, which was selected as the feed fuel for the purpose of maximizing the actinide density, is known to swell axially in the range of 8-10% at burnup of ~20% FIMA caused by the internal pressure of fission gas bubbles, and requires a liquid bond due to low melting temperature. [17] In a segmented fuel rod design, the free volume reserved for fuel swelling and the displacement of the bonding liquid will also have detrimental effects on the neutron economy. As a result, an annular fuel rod design was adopted to avoid both of these issues. The annular fuel is mechanically bonded to a 30-μm vanadium liner [18], which acts as a

diffusion barrier to avoid fuel/cladding chemical interaction (FCCI). When the fuel swells inwards with burnup, the bonding restrains the fuel from swelling axially. These features are described in details in Appendix A.

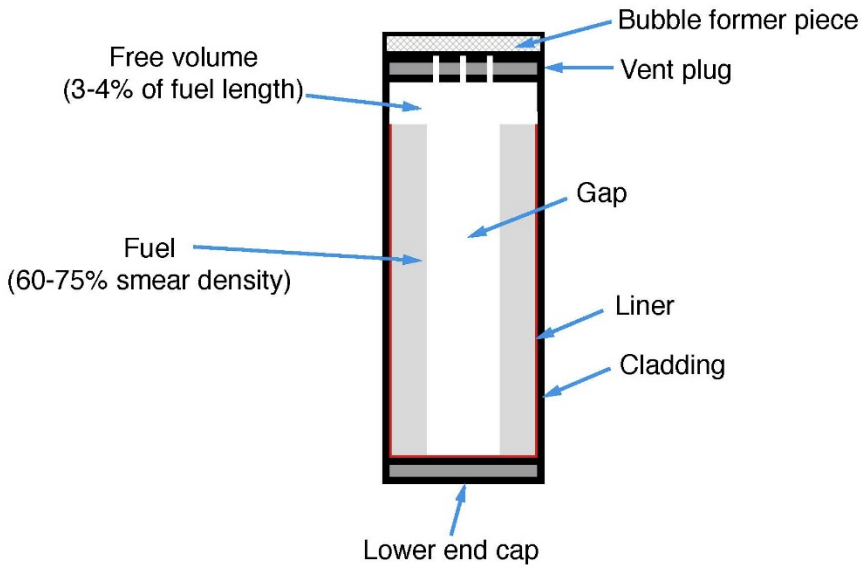

Figure 5 Axially segmented initially annular fuel rod design for 3-D fuel shuffling.

The upgraded design is adequate to maintain the core stability under various operating conditions and the reliability of 3-D fuel shuffling in the sodium coolant, without significant enlargement of the non-fuel volume in the assembly or significant harming of the neutron economy.

3.2.3 Developing generic design of 2-D and 3-D shuffling B&B cores.

A generic 2-D shuffled optimal B&B core concept OBB-I (Optimized B&B, type I) upon which the 3-D shuffled cores were developed in this study is a large SFR fed with DU with 0.25% ^{235}U. The unirradiated nominal fuel density is 18.66 g/cm^3 at 800 K, and a smear density of 75% is assumed to accommodate the fuel swelling with burnup. The cladding material, which is the ferritic-martensitic alloy HT-9, and the coolant have densities of 7.87 and 0.830 g/cm^3, respectively, both at 800 K. The effective core height is 300 cm and equivalent diameter of the simulated core is ~493 cm, giving a total active core volume of 57.19 m^3, and a volumetric power density of 52.45 MW/m^3 for a total core thermal power of 3000 MW. This reference design adopts the vented fuel rod concept [19]. The diving bell type ventilating device allows the release of the fission gas, but prevents the reverse-flow of the coolant into the fuel pin. [19]

Venting the released fission gases from the fuel pin into the primary reactor coolant will maintain cladding stresses at low levels to high burnup. The fraction of core volume that is required for the control system was not accounted for in the preliminary core design because the required number of control assemblies cannot be estimated before detailed calculation for safety parameters is performed. The general characteristics and assumed volume fraction of the active core ingredients are presented in Table 1.

Table 1 Main parameters of reference B&B core

Thermal power (MW)		3000
Core equivalent radius (cm)		246.34
Active fuel length (cm)		300
Gas plenum height (cm)		100
Feed fuel		DU (0.25% ^{235}U) with 75% smear density
Coolant		Sodium
Inlet/outlet coolant temperature (ºC)		355.0/506.8
Structural material (cladding, duct, wire-wrap, reflector pin)		HT-9
Fuel assembly volume fraction (%)	Fuel	40.70
	Gap	13.57
	Cladding+Wire	13.04
	Duct	6.28
	Coolant	26.41
Density (g/cc)	Fuel (theoretical)	18.99
	Cladding	7.87
	Coolant	0.83

In the 3-D shuffled version of OBB-I, the full-length fuel assembly is made of four 77 cm long sub-assemblies (an alternative term for assembly segment) making a 301 cm active core height. This core has three 7 cm thick fuel-free layers at the top of each of the three lower sub-assemblies due to the design of the sub-assembly fuel rods illustrated in Figure 5. The effective

fuel volume fraction of the resulting core is lower than of the 2-D shuffled core. The total power of the 3-D shuffled core with segmented fuel assemblies is the same as of the 2-D reference core.

3.3 Establish deterministic 3-D fuel shuffling capability.

The core characteristics compared in this study pertain to the critical equilibrium cycle. The search for the equilibrium cycle was performed using the DIF3D/REBUS-3 codes [20] [21] which are part of the Argonne Reactor Computation (ARC) system obtained from the Argonne National Laboratory (ANL) collaborator. The finite difference diffusion method was employed in the flux and eigenvalue solver DIF3D as it is the only available option for R-Z geometry. A variable mesh structure that can be defined in both radial and axial directions provide a higher resolution of the results, including flux and power etc. The fuel shuffling was modelled explicitly on a fuel batch basis in REBUS-3 calculations. For a given core geometry and constituents volume fraction, the design variables are the shuffling pattern and cycle length.

Burnup region-dependent 33-group cross section sets were generated from the ENDF/B-VII.0 data library using the ETOE-2/MC2-3/TWODANT sequence of codes of the ARC package. [22] [23] Specifically, the MC2-3 code first calculates 0-dimensional (0-D) neutron spectra and condenses point-wise cross sections prepared by ETOE-2 into an ultrafine group structure (~2000 groups). For non-multiplying regions such as reflectors and shield, leaking spectra from the fueled region is used for the condensation. Then, a 2-D ultrafine group transport calculation is conducted by TWODANT to take into account realistic leakage and the calculated spectra are fed back to MC2-3 for the final cross section condensation. As shown in Appendix C, it was found in previous studies that in order to accurately account for spectral variation in the B&B core, the best approach is to use burnup and location dependent group constants for the core simulation. However, it is impossible to generate cross sections without knowing the zone-wise equilibrium composition beforehand. It is also difficult to assign cross sections to burnup zones while performing fuel shuffling in REBUS-3. Therefore, the preliminary core calculation was carried out using a cross section set generated for the fuel composition pertaining to intermediate burnup (~10% FIMA). This approximation is acceptable for the initial exploration of the effects to be expected from the newly proposed B&B core design and fuel management.

An external module has been developed to post-process REBUS-3 simulation results and produce key performance characteristics for the equilibrium core such as the zone-wise fuel burnup, infinite multiplication factor, power, and leakage. In particular, the radiation damage accumulated by HT-9 cladding is evaluated by folding cell averaged multi-group flux from REBUS-3 results with the isotopic neutron dpa cross sections. (see Appendix B)

The capability of the simplified DIF3D/REBUS-3 model for determining equilibrium composition of B&B cores has been verified [8] by comparing against a continuous energy Monte Carlo (MC) code Serpent. [24] Both deterministic and MC calculations used the ENDF/B-VII.0 cross section library and assumed uniformity of temperature distribution for fuel/clad (800 K) and coolant (600 K) in the active core to have consistency between the two models. They differ, however, in the depletion calculations – whereas Serpent uses a detailed burnup chain, the REBUS-3 calculations use a pre-stored plutonium-uranium burnup chain to simplify the input preparation in two ways. First, it does not include all the heavy metal nuclides prepared in the cross section library. Second, the effect of fission products is accounted for using lumped fission product (LFP) cross sections for 4 different fissionable isotopes that were created from cross sections of 137 individual fission products using fission yields for ^{235}U, ^{238}U, ^{239}Pu, and ^{241}Pu. It was found in Appendix E that the relative difference of the core characteristics such as cycle length, discharge burnup, reactivity swing, and power peaking factor, is within 4%, indicating that the deterministic approach is adequate for quantifying the relative difference in the performance of B&B cores designed using 3-D versus 2-D fuel shuffling. The computational time for an equilibrium cycle search using REBUS-3 is ~12 min on the UNIX cluster at UCB, which is a significant reduction when compared with ~23 h required for Serpent.

REBUS-3 has the capability of modeling the core in R-Z and Hexagonal-Z geometry. It is desirable to further reduce the code modeling effort even using deterministic codes, especially when performing shuffling pattern optimization as will be discussed in later sections. Therefore, the assembly-based hexagonal B&B core is represented in R-Z geometry, which consists of a number of equal-volume concentric fuel batches. The discrepancy of using the simplified R-Z model, which primarily stems from depleting all the assemblies of a given batch with the same power level, is considered acceptable for a preliminary feasibility study aimed at estimating the relative difference on the B&B core characteristics resulting from 3-D versus 2-D fuel shuffling; these differences will be illustrated in later sections. The R-Z model enables a 70-80% reduction in the neutronics computational time and thus expedites the optimization process.

The above mentioned standalone neutronics study of the equilibrium performance of the B&B core assumes that the core can operate at the designed power level without violating any thermal-hydraulics constraints. However, the peak assembly power depends on the radial power distribution which depends on the fuel shuffling scheme. Therefore, thermal-hydraulics calculations are incorporated into the core optimization process through coupling with neutronics calculations using the ADOPT code [25]. ADOPT aims to automatically search for the optimal fuel assembly design that maximizes the fuel volume fraction while adhering to set constraints for all component temperatures, pressure drop, coolant velocity and structural integrity limits, subjected to a specified peak assembly power level. The coupling scheme used to converge on thermal-hydraulic and neutronics solutions for the critical equilibrium cycle of B&B cores is given in Figure 6. A separate module – PyRebus, was developed to prepare the input files, control data exchange, and check the convergence of the iterative process. For a given core specification (defined by geometry, material, SP, etc.), the process starts with REBUS by searching for the equilibrium critical cycle and calculating its performance parameters. Then, the power distribution is sent to the ADOPT model, which has the identical core specification as in REBUS, to generate the volume fraction of all constituents that will enable the peak power assembly to meet all the design constraints. If different from the previous iteration, this information is fed back to REBUS to repeat the search for equilibrium core using the revised assembly design until a converged critical core design has been found. The fuel volume fraction and the maximum cycle radial power peaking factor require 4-5 iterations to converge to an error less than 2%.

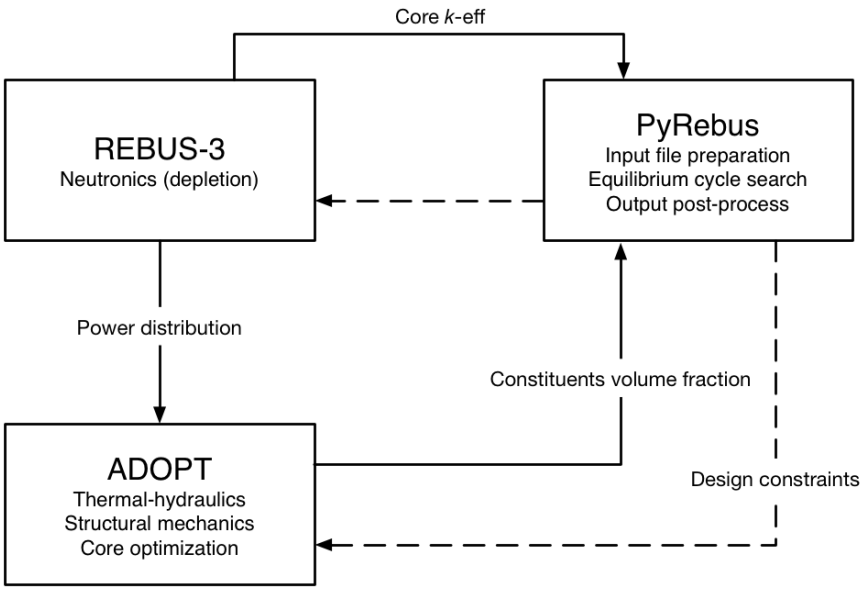

Figure 6 Coupled neutronics-TH calculation scheme for equilibrium B&B core search.

The thermal-hydraulics constraints accounted for in this study are:

(1) maximum core pressure drop: 0.9 MPa, [15]
(2) maximum sodium velocity across the core: 12 m/s, [26]
(3) maximum fuel-cladding interface temperature: 650 °C, [27] and
(4) maximum peak fuel temperature: 1000 °C. [28]

3.4 Develop the computational capability for an automatic search of the optimal 2-D and 3-D shuffling pattern.

The search for optimum 3-D shuffling pattern in the early stage of the project was based on a user specified trial-and-error approach and was limited to few trials applied to a single core. The 3-D SP optimization presents a large decision space – for the reference core given in Appendix E that features 12-batches and 4 axially stacked subassemblies per assembly there are on the order of 10^{61} SP combinations. Hence, an exhaustive trial-and-error search is not feasible since it is extremely computationally expensive. Moreover, the optimal core design should meet several constraints in addition to criticality including the burnup reactivity swing, radial power peaking factor and relative assembly power change over the cycle. This makes a manual search for the optimal SP impractical. In addition, the optimal SP is highly sensitive to the core dimensions and number of radial and axial shuffling zones. Thus, an automated optimization

capability that is able to account for all the constraints is desirable. The Simulated Annealing (SA) algorithm was adopted as the optimization method for this study.

SA is a stochastic optimization technique motivated by an analogy to annealing in metallurgy, which involves repeatedly heating and cooling of a material to increase the crystal size and remove defects so as to alter its physical properties. It was first introduced as a tool of finding equilibrium configuration of a system of particles at a given temperature, and then applied it to combinatorial optimization problems, in which a family of candidate solutions to minimize the objective function is generated following a Markov chain sampling. [29] [30] Its major advantage over other methods is an ability to avoid being trapped at local minima, because the random search not only accepts changes that improve the solution performance but also some changes that worsen it.

In the general implementation of the SA method, a control parameter *T* is introduced for system (metal) temperature, and the energy difference between the two states of the material is replaced by the difference between the value of the current objective function and the proposed objective function. The variable of the optimization problems considered in this work is the SP; and the objective function is used to guide the search for the SP. The algorithm begins with an initial guess at the optimal solution and then seeks successively improved solutions through a continuing examination of randomly generated solutions in the neighborhood of the ever-changing optimum. Candidates that decrease the objective function are, of course, accepted, while candidates that increase the objective function are accepted as new solutions with a probability. The more the solution (SP) degrades the objective function, the less likely it will be chosen as the optimum solution for the next iteration. A strategy flowchart of the optimization process is displayed in Figure 7, in which the term “evaluate SP” refers to the estimation of the augmented objective function outcome for a specific SP using REBUS.

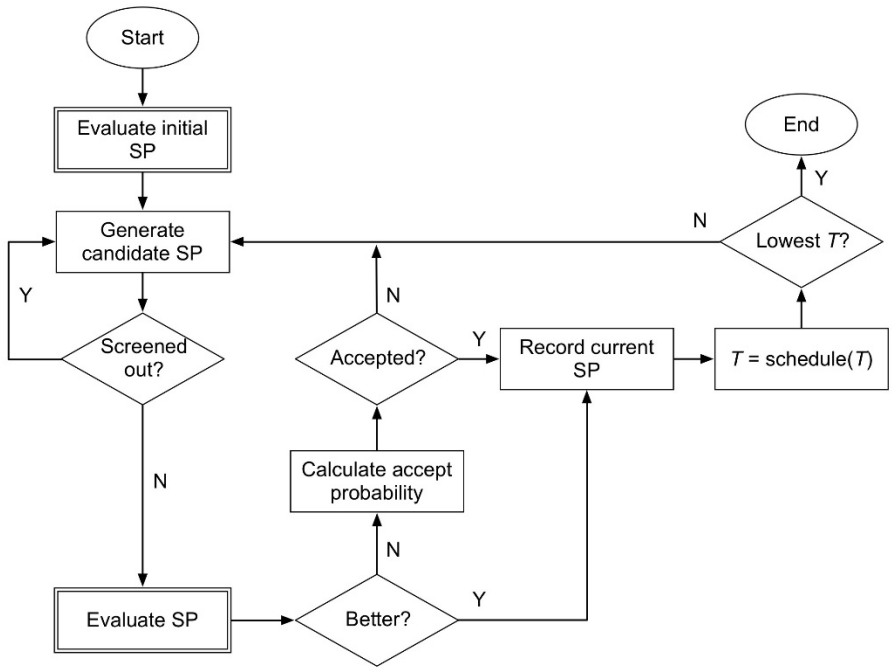

Figure 7 Flow diagram of shuffling pattern optimization process using simulated annealing.

The primary objective of the SP optimization is to reduce the peak minimum required radiation damage as much as possible. However, it is desirable to account for other design constraints including:

(1) Reactivity swing during the cycle: $\Delta\rho \leq \Delta\rho^{\mathrm{lim}}$

(2) Change of batch power over the cycle: $\Delta \mathrm{P_B} \leq \Delta \mathrm{P_B^{lim}}$

(3) Radial power peaking factor: $\mathrm{F_R} \leq \mathrm{F_B^{lim}}$

The burnup reactivity swing FBRs are usually designed not exceed 3.5%. A smaller reactivity swing implies a smaller number of required control assemblies or smaller worth of each control assembly. The former leads to a higher core average fuel volume fraction and therefore a better neutron economy, while the latter can reduce consequences of a transient overpower accident (UTOP). The minimization of the maximum relative change in the batch power will result in maximum core average coolant exit temperature and, hence, highest possible energy conversion efficiency. This is because the radial coolant flow distribution must be designed, via orificing, for the peak-power conditions and cannot be adjusted over the cycle. Minimization of the radial peaking factor results in minimization of the peak assembly power and maximization of the fuel volume fraction and, hence, of the neutron economy.

In the current study, these additional design constraints are handled in the optimization by augmenting the main objective function (peak dpa) with penalties terms, which reflect the extent of violation of the constraints. For each constraint related objectives other than the peak radiation damage, its contribution to the augmented objective function is measured by the relative differences of current value of the parameter from the pre-defined design constraints. As a result, the current problem is considered as the multi-objective optimization problem aiming at finding the best SP to have the lowest possible peak radiation damage (R*), the smallest burnup reactivity swing (Δρ), the least relative change of batch power (ΔP_B) and the smallest radial power peaking factor (F_R). The augmented objective function is of the following form:

$$\bar{F} = \gamma R^* + \sum_{i=1}^{I} \lambda_i \Omega_i \tag{1}$$

where the first term on the right side of Eq. (1) is the main objective function corresponding to the evaluation of peak radiation damage, and each penalty term in the summation represents the contribution of one of the constraint related objectives to the augmented objective function. The violation functions Ω, taking the forms given in Table 2, are the relative differences of current value of the parameter from the pre-defined design constraints, of which the values in the 3rd column of the same table were adopted in this study. The impact factor λ are introduced to adjust the importance of each objective; for example, in the case where reactivity swing minimization takes the priority in SP optimization, all that must be done for the objective function transition is to increase the impact factor associated to Ω_1. γ is a multiplication constant used to adjust *R** to the order of magnitude of the penalty terms in Eq. (1); a value of 0.01 is used in this study.

Table 2 Elements and constraints of augmented objective function

Description	Violation function	Constraint
Reactivity swing during burnup cycle	$\Omega_1(\Delta\rho) = \frac{\Delta\rho}{\rho^{lim}} - 1$	$\Delta\rho^{lim} = 7.0$
Max change of batch power	$\Omega_2(\Delta P_b) = \frac{\Delta P_b}{\Delta P_b{}^{lim}} - 1$	$\Delta P_B^{lim} = \frac{P_{th}}{N_b}$ ǂ
Radial power peaking factor	$\Omega_3(F_R) = \frac{F_R}{F_R{}^{lim}} - 1$	$F_R^{lim} = 2.5$

‡ P_{th} refers to the core thermal power; N_b denotes the number of radial fuel batches in the core.

The performance of the SA algorithm has been extensively examined by optimizing the SP for both the 2-D and 3-D shuffled B&B cores. An example of the optimization performance is given here for the 3-D shuffled OBB-I core, which is defined in previous sections. The behavior of the augmented objective function, as well as of its components is displayed in Figure 8 as a function of cooling stage. In the first 500 cooling stages in the optimization history, all components of the augmented objective function clearly exhibit a decreasing trend, with larger oscillations at the early stage and smaller towards the end. It implies that the SA algorithm allows a wide exploration of the design space by accepting solutions degrading the core performance, and tightens the acceptance criterion as the simulation proceeds. It could also be seen that penalty terms reached their minima at different rates, and the minimum value of the augmented objective function is found at cooling stage 464. In this case, most of the SPs generated after the 400 simulation cycle are preferred from the neutronics point of view, among which four SPs with low radial power peaking factor were selected for thermal-hydraulics evaluation. For each of the SPs, it took no more than five iterations for the REBUS-ADOPT approach to arrive at converged volume fractions and radial power peaking factor, and generate the best 3-D SP that can meet all thermal-hydraulics constraints.

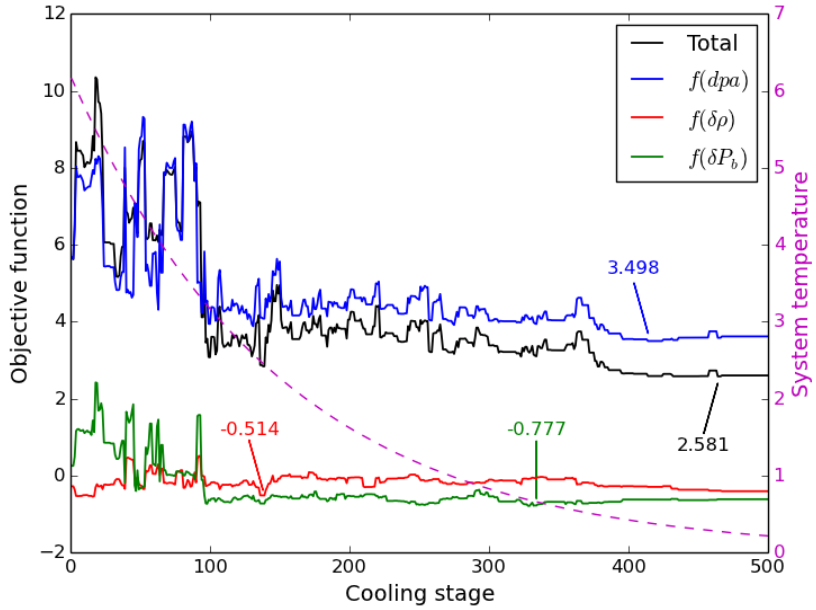

Figure 8 Convergence history of SP optimization with SA algorithm.

Detailed development of the SA algorithm for the current problem can be found in Appendix B, including the formation of the augmented objective, the selection of system temperature and the random generation of the updated (perturbed) SP in both 2-D and 3-D shuffled systems.

3.5 Compare the optimal 3-D shuffled core characteristics against those of an optimal conventional B&B core design that features 2-D fuel shuffling.

The optimum SP obtained by the SA automated search is depicted in Figure 9 and Figure 10 for, respectively, the 2-D and 3-D shuffled OBB-I core.

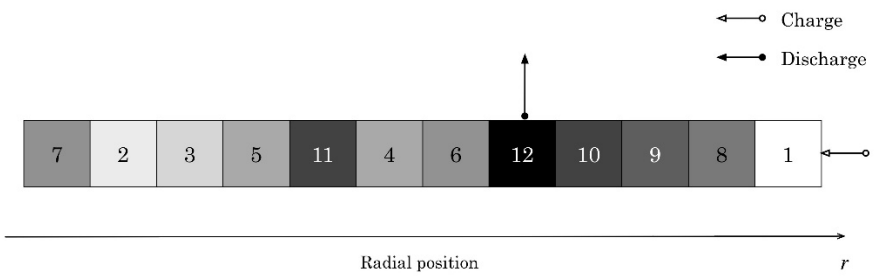

Figure 9 Optimum 2-D shuffling pattern for OBB-I core.

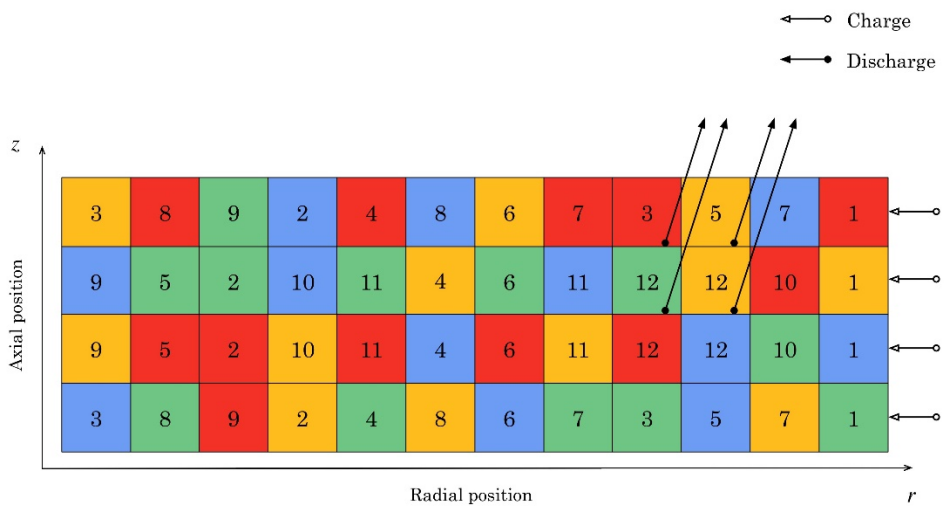

Figure 10 Optimum 3-D shuffling pattern for OBB-I core.

Table 3 compares the equilibrium core performance of the optimal 2-D and 3-D SP described above. The 3-D shuffling enables a 34% reduction of the peak radiation damage – from 534.2 dpa for the 2-D shuffling case to 351.0 dpa for the 3-D case. Even though the peak burnup was reduced proportionally, the corresponding average discharge burnup increased from 9.91% to 14.49% FIMA, which implies an approximately 45% increase in the depleted uranium fuel utilization. This is despite of the higher neutron leakage probability from the 3-D shuffled core. If normalized to the same dpa level, the average discharge burnup of the 3-D shuffled core is 2.23 times that of the 2-D shuffled core! The 14.49% FIMA corresponds to approximately (14.49/0.6=) ~25 times higher natural uranium utilization of LWRs per unit of fission energy generated or nearly (25*0.4/0.33=) 30 times higher per unit of generated electricity . As a result of the higher average burnup, the equilibrium cycle length was increased from 1083 for 2-D to 1566 effective full power days (EFPD) for 3-D shuffled systems.

Correspondingly, the burnup reactivity swing increases from 2.81% of the 2-D to 4.66% of the 3-D shuffled system implying an increase of the fraction of neutrons that are absorbed in the reactivity control system. However, per unit time or given amount of energy generated, the burnup reactivity swing is comparable: 1.09% versus 0.95% Δk/k per effective full power year (EFPY).

Table 3 Comparison of performance characteristics of the optimal 2-D and 3-D shuffled OBB-I core.

Equilibrium parameter		2-D shuffled	3-D shuffled
Burn cycle time (EFPD)		1083	1566
Burnup reactivity swing (% Δk/k)		2.81	4.66
Average discharge BU (% FIMA)		9.91	14.49
Peak discharge BU (% FIMA)		23.62	15.69
Peak radiation damage (dpa)		534.2	351.0
Peak fast fluence (n/cm^2)		1.28E+24	9.88E+23
Axial/radial leakage probability (%)		1.00/2.67	1.56/2.75
Axial/radial power peaking factor		2.35/1.64	2.00/1.70
Peak batch power change (%)		17.07	22.14
Pitch-to-diameter ratio		1.065	1.070
Core volume fractions (%)	Fuel	40.16	39.77
	Gap	13.39	13.26
	Cladding+Wire	12.85	12.77
	Duct	6.59	6.57
	Coolant	27.03	27.63

Although 351 dpa is still beyond the proven radiation damage limit for HT-9 cladding, it is expected that ongoing and future irradiation experiments and new material development will enable to reach this dpa value much sooner and with higher certainty than the >500 dpa required for 2-D shuffling cores. The thermal-hydraulics corrected fuel volume fraction was 40.16% and 39.77%, corresponding to the fuel pin pitch-to-diameter (P/D) ratio of 1.065 and

1.070, for 2-D and 3-D shuffled system, respectively, due to the somewhat higher radial power peaking factor of the 3-D shuffled core.

The radial and axial power distributions of the 2-D and 3-D shuffled cores, shown in Figure 11 and Figure 12, are quite similar. The radial power distribution peaks at the 8th radial batch since a large portion of the high burnup and, therefore, high k_∞ fuel is located in radial batches 8 through 10. Over the cycle the radial power distribution tends to shift towards the core center as the fissile contents builds up steeply with burnup at the low burnup fuel that is loaded at the inner region of the core. Due to the axial shuffling of the segmented assemblies, the axial peaking factor was brought down from 2.35 in 2-D to 2.00 in 3-D shuffled core. As a result, the leakage probability from the 3-D shuffled core is 17% higher.

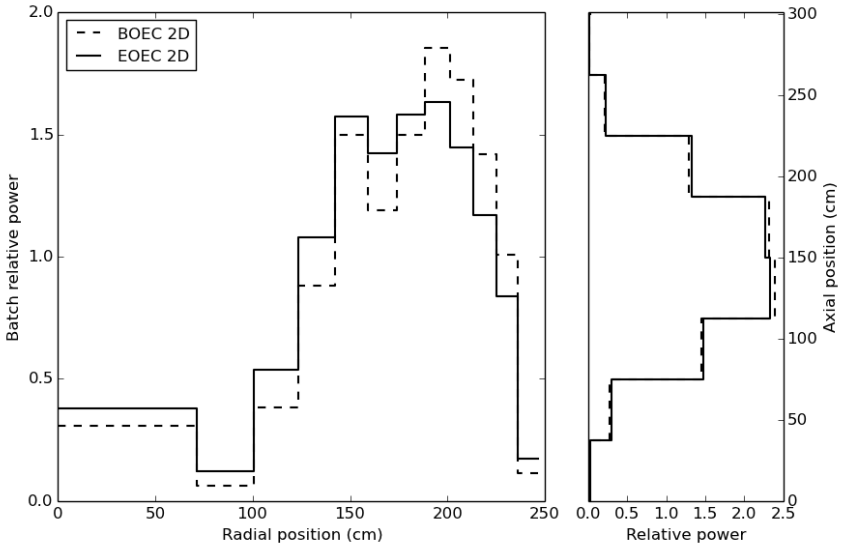

Figure 11 Radial and axial power distribution for 2-D shuffled OBB-I core.

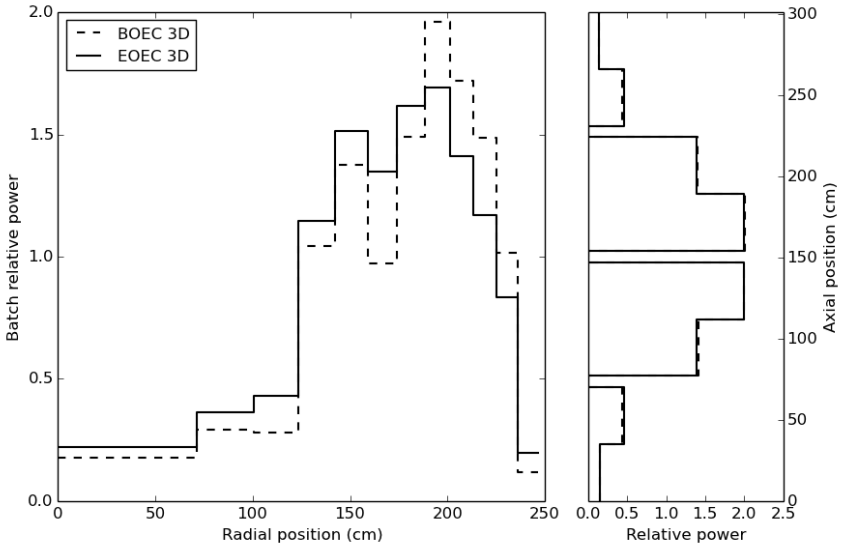

Figure 12 Radial and axial power distribution for 3-D shuffled OBB-I core.

In summary, 3-D shuffling offers an increase of 45% in the average discharge burnup, and hence the fuel utilization, along with a 34% reduction in the minimum required peak HT-9 dpa – from 534.2 to 351.0 dpa. The 3-D shuffled OBB-I core therefore far outperforms the 2-D shuffled reference core on both economics (average burnup and cycle time) and radiation damage.

3.6 Comparing the neutron balance in 3-D versus 2-D shuffled cores

The 0-D neutron balance analysis developed in previous studies [2] [31] can be used to estimate the net number of excess neutrons generated by a unit volume of fuel, N_{ex}, as a function of burnup as follows:

$$\mathrm{N_{ex}} = \mathrm{N_{HM}} \int_0^{\mathrm{BU}} \left[1 - \frac{1}{\mathrm{k(BU)} \times \mathrm{P_{NL}} \times \mathrm{P_{NRC}}}\right] \bar{\nu}(\mathrm{BU})\mathrm{dBU} \tag{2}$$

In the above, $k(BU)$ refers to the k_∞ evolution with burnup in the control volume. Although in practice fuel is shuffled in the reactor core and is thus depleted with variable power density during its lifetime, the k_∞ evolution curve in the infinite medium with fixed power density can be used to understand its behavior as a function of burnup, as illustrated as the black curve in Figure 13. It can be seen that for the metallic DU fuel as used in the reference B&B core, k_∞ increases rapidly with burnup before it reaches 1.0 and the change slows down in the vicinity of its maximum value.

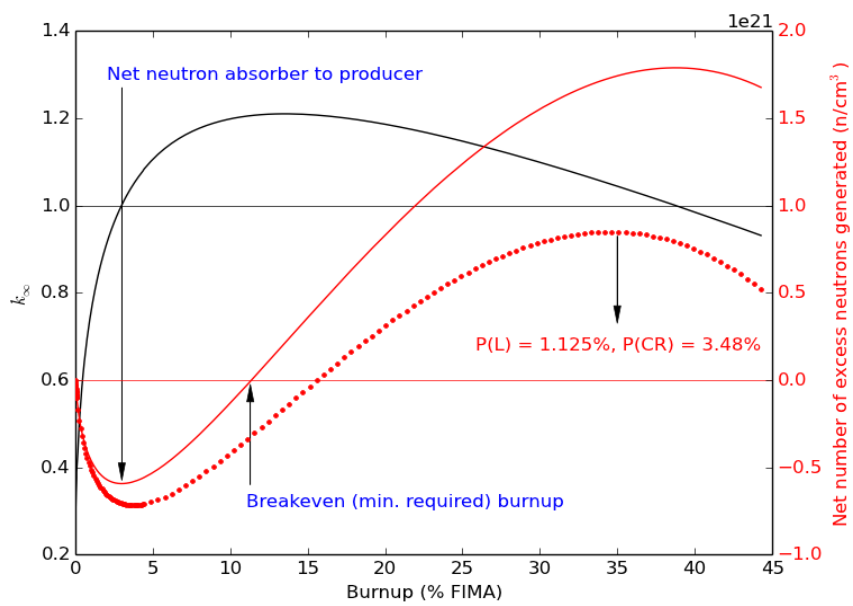

Figure 13 k_∞ evolution and neutron balance with burnup of metallic DU fuel in a typical B&B core.

In Eq. (2), N_{HM} is the Heavy Metal (HM) atom density, BU is the burnup expressed in FIMA, $\bar{\nu}$(BU) is the average number of neutrons released per fission, P_{NL} (= 1 − P_L) is the non-leakage probability and P_{NRC} (= 1 − P_{RC}) is the probability that a fission-born neutron will escape capture in the control elements used to compensate for the burnup reactivity swing over the

equilibrium cycle. The minimum burnup required for sustaining a B&B operation is that burnup for which N_{ex} = 0. In the case where neutron loss is neglected (P_L = 0 and P_{RC} = 0), shown as the red curve in Figure 13, the minimum required burnup is smaller than that where neutron loss is included in the analysis (red dotted curve). The lowest point of the neutron balance curve is the point that features equal neutron loss rate and generation rate, and pertains to the burnup at which the fuel turns from anet neutron absorber to a net neutron producer.

This simple neutron balance analysis, although developed based on the 0-D reactor model, was found useful to determine the minimum required and maximum attainable (not shown in the figure) burnup for sustaining a B&B mode of operation. However, the fuel is depleted with different power almost everywhere in the real core and the rate of depletion is highly sensitive to the neutron spectrum imposed by the neighboring fuel assemblies, especially for the low burnup fuel. In addition, the strong axial variation of burnup that exists in the fuel assembly in the 2-D shuffled core complicates the problem thus makes it difficult to understand the difference between 2-D and 3-D shuffling from the neutronics point of view relying only on the average burnup of the assembly. Therefore, the neutron balance analysis has been extended from the 0-D to 3-D core model by tracking the burnup accumulation of each of the burnup zones throughout its residency in the reactor core.

Each fuel assembly is subdivided into 8 axial burnup fuel zones to account for the burnup variation, with zone A corresponding to the lowest 1/8, while zone H corresponds to the highest 1/8 of the fuel assembly. In the 3-D shuffled case, this means the discretization of each sub-assembly into 2 equal-volume axial zones, as shown in Figure 14. The tracking of the fuel content creates a fuel management path, which represents a unique shuffling sequence of this burnup zone. A neutron balance analysis is carried out for each of the 8 axial equal burnup fuel batches as they traverse the core from loading to discharge. The burnup dependent infinite multiplication factor of each of these fuel batches is calculated as the ratio of neutron production rate to neutron absorption rate. The neutron production from (n, 2n) and (n, 3n) reactions is assumed negligible. It is assumed that the neutron loss is constant throughout the cycle and equals to the average of its BOEC and EOEC values.

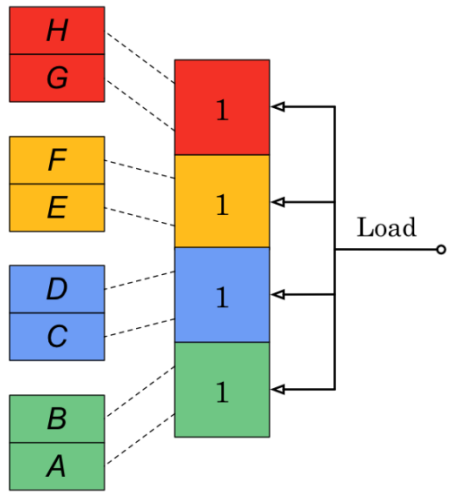

Figure 14 Axial discretization of fuel zones.

Figure 15 and Figure 16 plot the neutron balance curves of 4 out of the 8 axial fuel burnup batches for the optimal 2-D and 3-D shuffled cores following each batch shuffling path as defined in Figures 8 and 9. Because of near axial symmetry, the neutron balance of the other four axial fuel burnup paths is very similar. The turning point of the neutron balance plots from a negative to a positive slope corresponds to k_∞ of 1.0; at smaller burnups the fuel is a net neutron consumer – i.e., it absorbs more neutrons than it generates, while at higher burnups the rate of fission neutrons the fuel generates exceeds the rate of neutrons it absorbs. A negative sign at the end of the neutron balance plot implies that there is a net cumulative neutron loss, whereas a positive sign implies that a net excess of neutrons has been generated by a unit fuel volume.

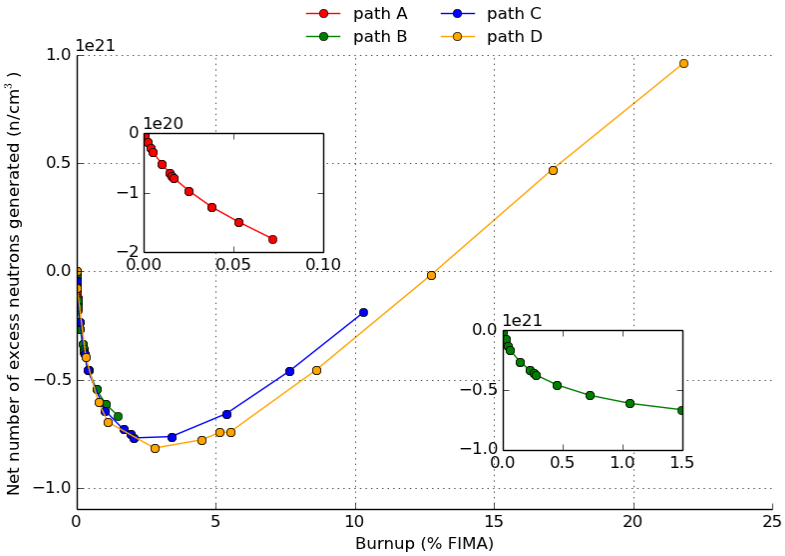

Figure 15 Fuel path dependent neutron balance of 2-D shuffling for OBB-I core.

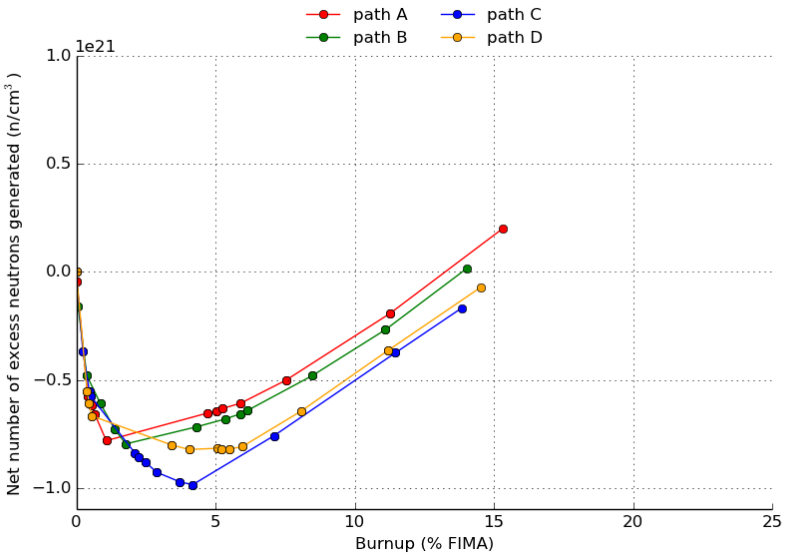

Figure 16 Fuel path dependent neutron balance of 3-D shuffling for OBB-I core.

In the 2-D shuffled reference core, The fuel of path A and B remained a net neutron absorber throughout its residence in the core; the neutron balance of these burnup batches did not even reach the turning point implying that their discharge $k_\infty < 1.0$. The fuel of path C, although becoming a net neutron producer, did not manage to pay back the number of neutrons it absorbed. Only the axially central fuel path D (and its counterpart E) exceeded the zero

balance line and by a large extent as it has to make up for the neutron deficiency of the other three fuel paths.

In the 3-D shuffled OBB-I core on the other hand, the fuel of each of the paths has paid back all or most of the neutrons it absorbed; it's neutron balance at discharge is in the vicinity of zero, as can be seen in Figure 16. This is because the 3-D fuel shuffling significantly flattens the burnup distribution of the discharged fuel as can be deduced from the burnup corresponding to the end point of the neutron balance curve of each of the fuel paths shown in Figure 16. The 3-D fuel shuffling also significantly increases the average discharge burnup and therefore also the cycle length. The longer cycle increases the positive burnup reactivity swing from 2.81% of the 2-D to 4.66% of the 3-D shuffled and therefore also of the fraction of neutrons that are absorbed in the reactivity control system. However, per unit time or given amount of energy generated, the burnup reactivity swing is comparable: 1.09% versus 0.95% $\Delta k/k$ per effective full power year (EFPY).

The peak dpa of the fuel discharged from each of the 8 fuel management paths of the 2-D and 3-D shuffled cores is displayed in Figure 17. In the 2-D shuffled core the dpa strongly peaks at the core axial center (Paths D and E) while with 3-D fuel shuffling the peak discharge dpa is within ±3% of the average.

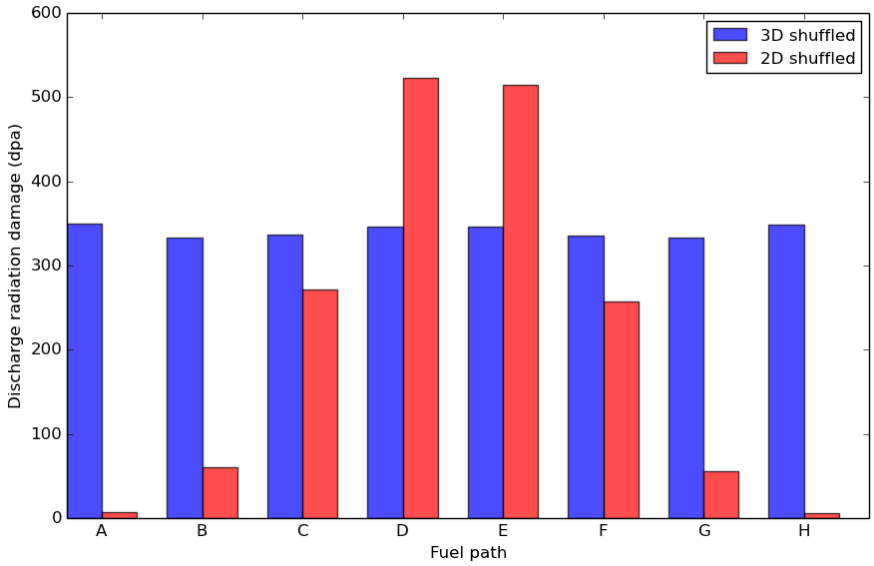

Figure 17 HT-9 discharge dpa for OBB-I core.

3.7 The effect of 3-D fuel shuffling patterns of different complexities on the optimal core performance.

The implementation of the 3-D fuel shuffling strategy considered in the previous section will require significantly longer refueling time, more complicated refueling machine and, possibly, two separate refueling machines to cut down the total refueling time, [15] and larger workspace above the core to disassemble and reassemble the fuel assemblies relative to 2-D fuel shuffling. Therefore, a number of design approaches for 3-D shuffling simplifications were examined and their effect on the core performance improvements relative to 2-D fuel shuffling was quantified.

The first approach was to restrict the shuffling of sub-assemblies to axial shuffling within the same fuel assembly in OBB-I without changing the design parameters of the core, so that radial shuffling will be performed for entire fuel assemblies as in a 2-D shuffling strategy. More specifically, at the refueling outage, a fuel assembly is lifted from the core segment by segment, then the fuel assembly is reassembled from the same segments but in a different axial order. This shuffling strategy will greatly reduce the workspace and time required for refueling, because the relocation of one fuel assembly does not affect the rest of the assemblies in the core except for the assembly at the targeting location - as is the case in 2-D shuffling.

The second approach was to reduce the number of segmented assemblies used to constitute one fuel assembly. This design, called OBB-II core, is loaded with fuel assemblies made of 3 axially stacked segments, each having identical dimensions as of OBB-I. The active core height is 228 cm (consisting of 3 segmented rods and 2 volumes of fuel-free space in the axial direction), giving a core volume of 42.70 m^3. The core thermal power of OBB-II is adjusted to achieve the same fuel specific power as of OBB-I, which is 7.22 kW/kg, and the resulting core power is 2340 MW.

The third approach (named OBB-III) reduces the number of fuel batches from 12 to 8 and uses 3 sub-assemblies to constitute one fuel assembly. As a result, the number of assembly segments contained in OBB-III core is only half of that in OBB-I core. Based on the OBB-II core, the assembly pitch in this OBB-III core is increased to 18.78 cm while maintaining the number of full-length assemblies within each batch and total core cross-sectional area, as shown in Figure 18. By matching the fuel specific power of OBB-I, the core power of OBB-III is 2335 MW with volumetric power of 54.68 MW/m^3. The design parameters and the resulting performance characteristics of the alternative cores are presented in, respectively Table 4 and Table 5.

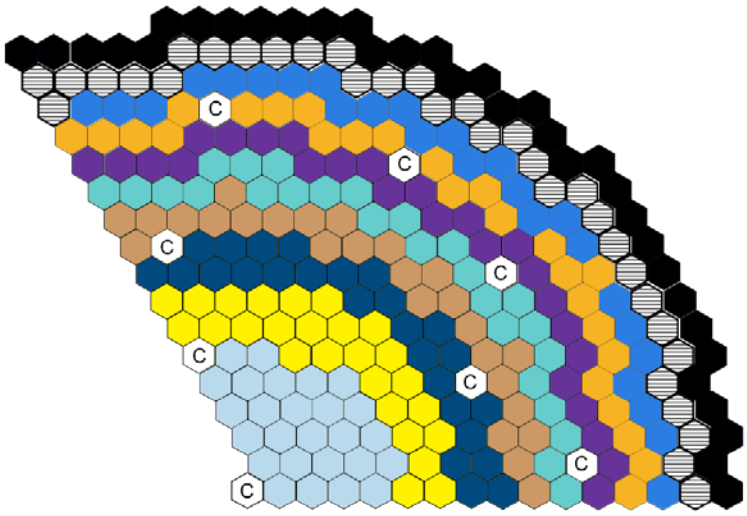

Figure 18 Schematic view of the 8-batch OBB-III B&B core. The outer two layers are reflector (dashed) and shield (black).

Table 4 Design parameters of alternative B&B core designs with 3-D fuel shuffling

Design Parameter	OBB-I	OBB-II	OBB-III
No. of sub-assemblies per assembly	4	3	2
Total fuel length in assembly (cm)	280	210	280
Core thermal power (MW)	3000	2340	2935
Active core height (cm)	301	224	287
Equivalent core radius (cm)	246.34	246.34	246.34
Active core volume (m^3)	57.38	42.70	54.71
Power density (MW/m^3)	56.20	54.80	53.64

As shown in Table 5, the equilibrium cycle length and discharge burnup of the OBB-I core with axially-constrained shuffling (3rd column) are 1728 EFPD and 16.02% FIMA, respectively-both slightly larger than those of the unconstrained case (2nd column). By placing segments with high burnup fuel at the axial periphery of the core before the discharge, this shuffling strategy is able to flatten the axial power peaking factor to 1.37, but inevitably causes a higher axial leakage probability of 3.84%. The radial power peaking factor of 1.78 is slightly higher than the 1.70 of the unrestricted 3-D shuffled core; it is necessary to reduce the fuel

volume fraction from 39.77% to 39.27% in order to meet the thermal-hydraulic constraints. The increase of core leakage and the reduction of fuel volume fraction are the major contributors to the 25 dpa increase in the minimum required peak radiation damage to the HT-9 cladding, when compared with the unconstrained core design.

The OBB-II core performance is summarized in the 4th column of Table 5. The reduction of the number of axially stacked sub-assemblies from 4 to 3 along with a 25% reduction in the total active fuel length does not significantly penalize the core performance. The minimum required peak radiation damage is 359.8 dpa – only 2.5% higher than of the optimal 3-D shuffled OBB-I core. Due to the reduced core height and therefore reduced pressure drop, the fuel volume fraction could be increased to 41.45%.

The peak radiation damage of the OBB-III core, shown in the rightmost column of Table 5, is 376.3 dpa – only about 4.6% higher than of the optimal 3-D shuffled OBB-II core while the average discharge burnup and, hence, fuel utilization, is even slightly higher. When compared with OBB-I core with 2-D shuffling (Table 3), the OBB-III core enables a ~30% reduction in peak radiation damage, from 534.2 to 376.3 dpa, while providing a ~131% increase in cycle length, primarily due to the increased DU loading per batch. The number of shuffling operations this core requires is only approximately doubled, assuming this number is directly proportional to the number of assembly segments in the core. With the significantly extended cycle length, the number of shuffling operations required per year in OBB-III core is even ~14% less than that in the 2-D shuffled OBB-I core. However, the burnup reactivity swing of this core is significantly higher and this may force an increase in the number of batches that will enable to shorten the cycle. A search for alternative SP that features a smaller burnup reactivity swing is worth trying as well.

Table 5 Performance characteristics of optimal 3-D shuffled B&B core of various designs.

Shuffling type	OBB-I unconstrained	OBB-I axially-constrained	OBB-II	OBB-III
Core thermal power (MW)	3000	3000	2340	2335
Burn cycle time (EFPD)	1566	1728	1598	2506
Burnup reactivity swing (% $\Delta k/k$)	4.66	3.26	4.85	5.52
Peak/ave. discharge BU (% FIMA)	15.69/14.49	17.16/16.02	14.95/14.64	15.78/15.36

Peak radiation damage (dpa)	351.0	375.8	359.8	376.3
Axial/radial leakage probability (%)	1.56/2.75	3.84/3.05	1.72/0.89	1.83/1.31
Axial/radial power peaking factor	2.00/1.70	1.37/1.78	2.18/1.85	2.02/1.89
Peak batch power change (%)	22.14	16.28	12.19	14.00
Pitch-to-diameter ratio	1.070	1.076	1.055	1.052
Fuel volume fraction (%)	39.77	39.27	41.45	41.27

3.8 The effect of core power density on the core performance.

The core designs shown above are characterized by low power density, which is typical to B&B cores. The sensitivity of the core performance, especially the peak radiation damage, to the core power density was investigated for OBB-II core. The results are presented in Table 6 for 2500 MW, 3000 MW and 3500 MW OBB-II-like cores as compared to the original 2340 MW core. All three cores adopt the same core geometric configuration and optimal SP as used in previous calculations and meet the thermal-hydraulic and structural constraints.

As the core power increases from 2340 MW to 3500 MW, a larger coolant flow area is required to meet the thermal hydraulic constraints – in particular the pressure drop, leading to an increase of P/D ratio and decrease of fuel inventory, which harms the neutron economy. As a result of the impaired neutron economy higher fuel burnup is required to sustain the B&B mode of operation, and consequently, the minimum required peak radiation damage increases with an increase in the core power level. Since in the vicinity of the discharge burnup the reactivity increase with burnup is much smaller than in the low burnup range, the increase of overall fuel burnup when going to a higher power level results in a decrease in the burnup reactivity swing. The impact of core power level on some of the design parameters is illustrated in Figure 19. It can be seen that except for the peak dpa level, all other parameters are slightly improved with power upgrade. Overall it appears desirable to increase the core power level – a ~50% increase in the power level will result in an additional 10% increase in fuel utilization and incur a penalty of only a ~6% increase in the dpa the cladding will have to accommodate.

Table 6 Sensitivity of OBB-II core performance to power density

Core design	2500 MW	3000 MW	3500 MW

Burn cycle time (EFPD)		1488	1236	1062
Burnup reactivity swing (% Δk/k)		4.66	4.30	3.97
Average discharge BU (% FIMA)		14.87	15.41	16.02
Peak discharge BU (% FIMA)		15.23	15.87	16.57
Peak radiation damage (dpa)		362.84	370.93	381.35
Peak fast fluence (n/cm^2)		1.18E+24	1.19E+24	1.20E+24
Axial/radial leakage probability (%)		1.84/0.96	2.07/1.09	2.30/1.21
Axial/radial power peaking factor		2.15/1.81	2.10/1.75	2.04/1.69
Peak batch power change (%)		12.08	11.92	11.37
Pitch-to-diameter ratio		1.055	1.074	1.093
Core volume fractions (%)	Fuel	40.99	39.44	37.99
	Gap	13.66	13.15	12.66
	Cladding+Wire	13.03	12.69	12.42
	Duct	6.61	6.56	6.52
	Coolant	25.71	28.16	30.41

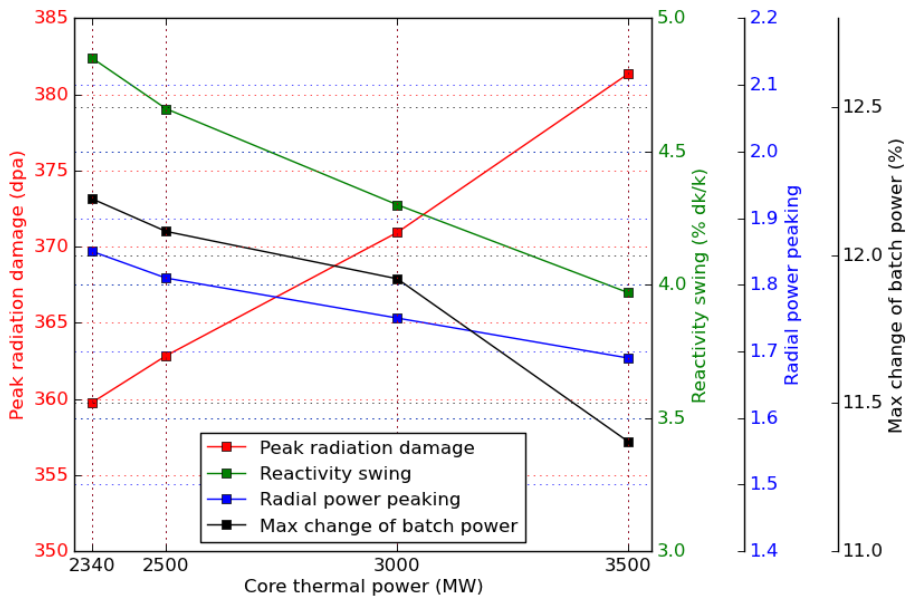

Figure 19 Optimal core performance of OBB-II as a function of core power.

3.9 Effect of 3-D fuel shuffling on safety-related parameters of optimized 3-D shuffled B&B cores versus the 2-D shuffled core.

An important challenge is to design the large low-leakage B&B cores to be passively safe; these cores tend to feature a larger positive coolant temperature reactivity coefficient and coolant voiding reactivity feedback than conventional fast reactor cores. In order to understand the effect of 3-D fuel shuffling on the reactivity feedback in B&B cores, a preliminary study was performed to calculate the space-dependence of important reactivity coefficients, including the fuel Doppler coefficient, coolant density coefficient and void worth, in addition to a set of kinetics parameters such as the delayed neutron fraction and prompt neutron lifetime.

The perturbation and sensitivity analysis code VARI3D included in the ARC code system was used to perform these calculations; it utilizes DIF3D as the flux solver. The calculations were performed for the B&B core model in R-Z geometry due to the limitation of the VARI3D code. The burnup zone dependent core composition at both Beginning of Equilibrium Cycle (BOEC) and End of Equilibrium Cycle (EOEC) were obtained in the equilibrium cycle calculations for the OBB-I cores.

Kinetics parameters

Table 7 and Table 8 present the delayed neutron fraction and prompt neutron lifetime values for the 2-D and 3-D shuffled OBB-I cores, respectively. The average delayed neutron fraction β_{eff} in both cases is ~0.38%, which is slightly larger than of typical SFRs (0.33-0.35%). This may be because β_{eff} decreases with increasing atomic number of the fissioning isotopes and the B&B cores under study have considerable fast fission probability of ^{238}U.

Table 7 Kinetic parameters of the B&B OBB-I core with 2-D shuffling.

	BOEC		EOEC	
Delayed neutron group	Fractional yield β	Decay constant λ (s^{-1})	Fractional yield β	Decay constant λ (s^{-1})
1	8.06E-05	0.0134	8.02E-05	0.0134
2	6.08E-04	0.0311	6.04E-04	0.0311
3	5.41E-04	0.119	5.35E-04	0.119
4	1.37E-03	0.312	1.34E-03	0.312
5	8.21E-04	0.89	8.05E-04	0.89

6	3.10E-04	2.97	3.03E-04	2.97
Effective delayed neutron fraction β_{eff}	0.0037		0.0037	
Effective delayed neutron lifetime (s)	9.54		9.61	
Prompt neutron lifetime (s)	1.88E-07		1.89E-07	
Neutron generation time (s)	1.88E-07		1.83E-07	

Table 8 Kinetic parameters of the OBB-I B&B core with 3-D shuffling.

	BOEC		EOEC	
Delayed neutron group	Fractional yield β	Decay constant λ (s^{-1})	Fractional yield β	Decay constant λ (s^{-1})
1	8.13E-05	0.0134	8.05E-05	0.0134
2	6.11E-04	0.0311	6.05E-04	0.0311
3	5.49E-04	0.119	5.37E-04	0.119
4	1.39E-03	0.313	1.35E-03	0.312
5	8.38E-04	0.89	8.09E-04	0.89
6	3.18E-04	2.97	3.05E-04	2.97
Effective delayed neutron fraction β_{eff}	0.0038		0.0037	
Effective delayed neutron lifetime (s)	9.46		9.59	
Prompt neutron lifetime (s)	1.93E-07		1.93E-07	
Neutron generation time (s)	1.92E-07		1.84E-07	

Doppler coefficient

The Doppler broadening of resonance cross sections reduces the resonance self-shielding with increasing temperature, yielding an increase in effective cross sections. In order to calculate the Doppler coefficient, a perturbed cross section library has been generated at a higher fuel temperature (1300 K) than its nominal value of 900 K. The VARI3D calculation was

then performed assuming a uniform change in fuel temperature across the core. The code is capable of calculating the reactivity worth for each individual burnup zone in the expression of multi-group perturbation based on the first-order perturbation theory. Specifically, the reactivity worth due to fuel temperature increase in each burnup zone is obtained from

$$\rho = \frac{-\int \sum_g \phi_g^* \delta\Sigma_{ag} \phi_g dV + \int \sum_g \phi_g^* \chi_g \left[\sum_{g'} \delta\left(\nu\Sigma_f\right)_{g'} \phi_{g'}\right] dV}{\int \sum_g \phi_g^* \chi_g \left[\sum_{g'} \delta\left(\nu\Sigma_f\right)_{g'} \phi_{g'}\right] dV} \quad (3)$$

where ϕ and ϕ^* represent the forward and adjoint flux, $\delta\Sigma_a$ and $\delta(\nu\Sigma_f)$ terms reflect changes in the absorption and fission neutrons birth probability due to fuel heating. The integrals are over the burnup zone and the summations are over all energy groups. The variation of reaction rates are being weighted with adjoint fluxes to determine the effect on reactivity. The first integral in the numerator accounts for the increase in the effective absorption cross sections of the fertile and fissile isotopes; this is a negative reactivity effect for an increase in fuel temperature. The second term accounts for the positive contribution of the increase in the effective number of fission neutrons birth rate with an increase in fuel temperature.

The burnup zone dependent reactivity worth introduced by the fuel temperature increase is depicted in Figure 20 for the OBB-I core with 2-D and 3-D fuel shuffling, both at EOEC. It can be seen that the distribution of the reactivity worth in the two cases is similar, and it indicates that the effectiveness of Doppler feedback due to heating of the fuel is significantly higher at the center of the 6th and 7th batches than at the rest of the core; it follows a similar trend as does the power distribution, shown in Figure 11 and Figure 12.

The core Doppler coefficient was then obtained by summing the burnup zone reactivity worth over the core ($\rho_T = \sum\rho$) and dividing it by the temperature variation (400 K). It can be seen in Table 9 that the negative Doppler coefficient (given in ₵/K) is slightly larger in the 3-D shuffled core than that of the 2-D core, although the difference is small. The magnitude of the B&B core Doppler coefficient is smaller than that of the 1000 MW Advanced Burner Reactor (ABR), which is -0.13 ₵/K. [32]

Table 9 Core average Doppler coefficient for 2-D and 3-D shuffled OBB-I core (unit: ₵/K).

	BOEC	EOEC
2-D shuffled core	-0.086	-0.082
3-D shuffled core	-0.094	-0.085

The approach used in this preliminary study is an approximation because it does not account for the fuel temperature distribution in the actual core. The spatial change in fuel temperature will be taken into account in a future study.

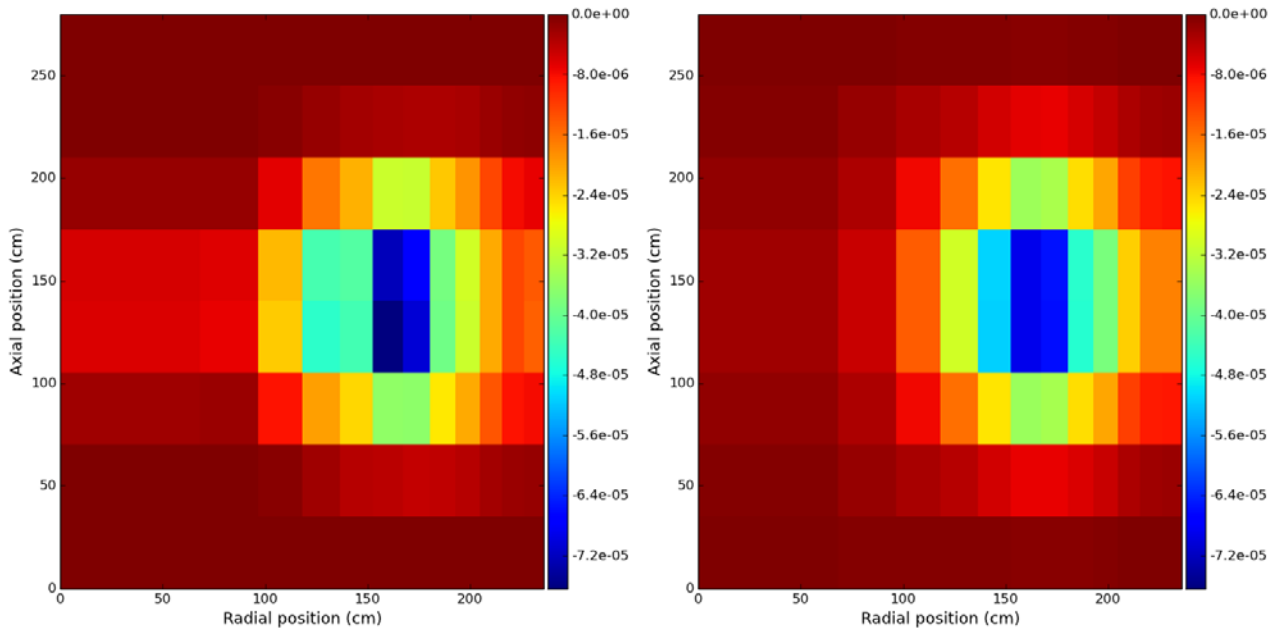

Figure 20 Doppler reactivity worth for 2-D (left) and 3-D (right) OBB-I B&B core.

Sodium void worth

The reactivity change that occurs when sodium density is reduced or voided from a reactor can be separated into spectral, leakage, and capture components. The spectral effect results from the reduced moderation with decreasing sodium density; it is a positive reactivity effect in fast reactors because of increasing fissile η and increasing fertile fission probability with increasing in fissioning neutrons energy. Reduction in sodium density results in increased neutron leakage probability and this introduces a negative reactivity effect. A reduced sodium density also decreases the parasitic neutron capture in sodium and this results in a positive reactivity effect, but this is of a relatively minor contribution.

Since the peak minimum required radiation damage, which is directly related to the average discharge burnup, is to be the lowest possible, the B&B reactors studied in this project are large cores featuring low leakage. This is reflected in the comparison results of the sodium void worth between OBB-I B&B core and the 1000 MW ABR [32] presented in Table 10. These values were obtained by voiding the sodium in the active core and above core regions.

Table 10 Sodium void worth by component for OBB-I B&B and for ABR cores (unit: $).

Core type		Capture	Spectral	Leakage	Total
2-D shuffled B&B core	BOEC	0.48	13.25	-2.75	10.98
	EOEC	0.47	13.08	-2.50	11.05
3-D shuffled B&B core	BOEC	0.50	13.13	-2.67	10.97
	EOEC	0.48	12.85	-2.31	11.02
1000 MW ABR	BOEC	0.5	9.9	-5.2	4.4
	EOEC	0.5	9.1	-5.5	4.9

It was found that the difference between the sodium void worth for 2-D and 3-D shuffled B&B cores is almost negligible. The average sodium void worth over the equilibrium cycle for both cases is ~$11.0, which is significantly larger than that of the ABR. This is primarily due to large positive spectral effect and small negative leakage effect in the large B&B cores. A novel engineered negative reactivity insertion system passively actuated by coolant temperature increase has been recently invented to compensate for the low-leakage and large spectral reactivity effects. [33]

The distribution of sodium void worth based on radial locations of the fuel batch is given in Figure 21 and Figure 22 for 2-D and 3-D shuffled cores, respectively. They were obtained following the same approach used in the zone-dependent Doppler coefficient calculation except for the perturbed condition being complete voiding of sodium in the active core. A similar trend is found in the comparison of the two distributions although the peaking is slightly higher in 3-D shuffled core. It can be seen that the positive effect increases from core center (low power) gradually with radius until it reaches a maximum in Batch 8. The only negative value, although of a small magnitude, occurs at the outermost batch due to its higher leakage probability. This distribution can be used in future studies as a useful guidance for determination of the control assembly locations.

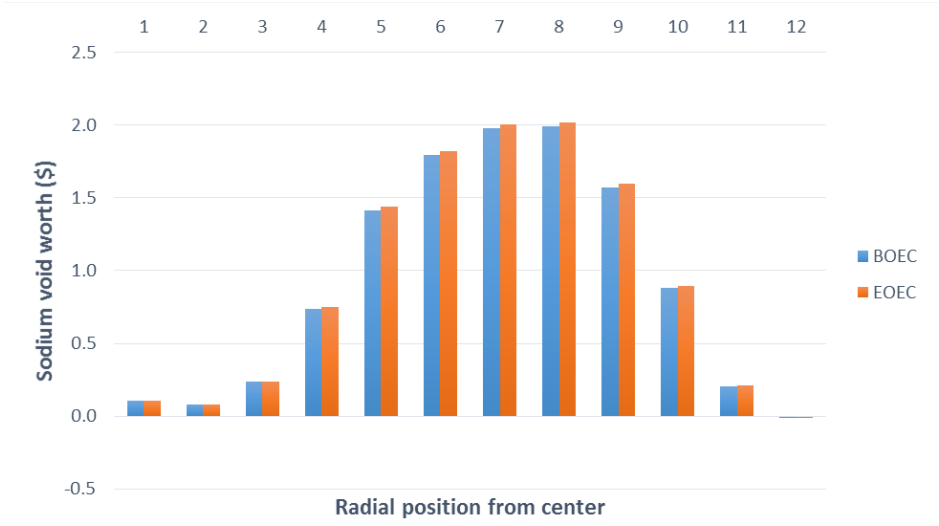

Figure 21 Batch dependent sodium void worth for the OBB-I B&B core with 2-D shuffling.

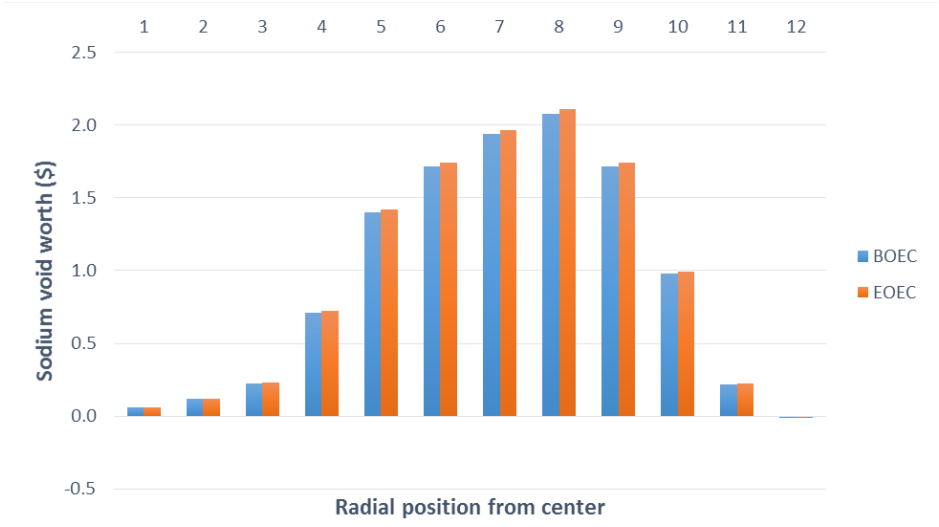

Figure 22 Batch dependent sodium void worth for OBB-I B&B core with 3-D shuffling.

Sodium density worth

The sodium density worth has also been evaluated for small coolant density changes such as due to sodium temperature increase or to partial sodium voiding. The sodium density worth curve, shown in Figure 23, was determined by direct eigenvalue difference of the base and a series of voided coolant conditions. It can be seen that the inserted percent reactivity increases with the void fraction in a linear manner over the range of 0-20% void, and a change in sodium density of 10% would cause approximately 0.4% increase in reactivity, which corresponds to ~$1.0 of reactivity insertion.

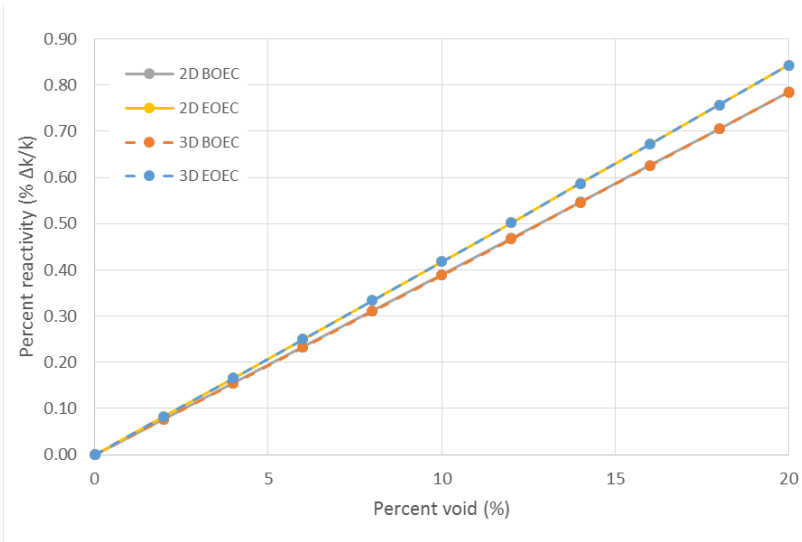

Figure 23 Sodium density worth curve for 0-20% void fraction.

No significant differences were found in the value of the kinetic parameters and reactivity coefficients when using 3-D versus 2-D fuel shuffling. An autonomous reactivity control system that is passively actuated by coolant temperature increase may be required to compensate for the large positive coolant voiding reactivity worth and ensure that large B&B cores can be designed to be inherently safe.

3.10 Develop B&B core models in Hexagonal-Z geometry and investigate the difference between the R-Z and Hexagonal-Z models.

The preliminary study that aims to understand trends in core performance improvement introduced by the 3-D fuel shuffling, used a simplified R-Z geometry (left of Figure 24) for the core simulation. This model greatly simplifies the optimal SP search. However, a more realistic core representation should use an assembly-by-assembly hexagonal geometry. The right of Figure 24 is the assembly-by-assembly configuration of the OBB-I 3-D shuffled core constructed to match the optimal core identified using the R-Z geometry.

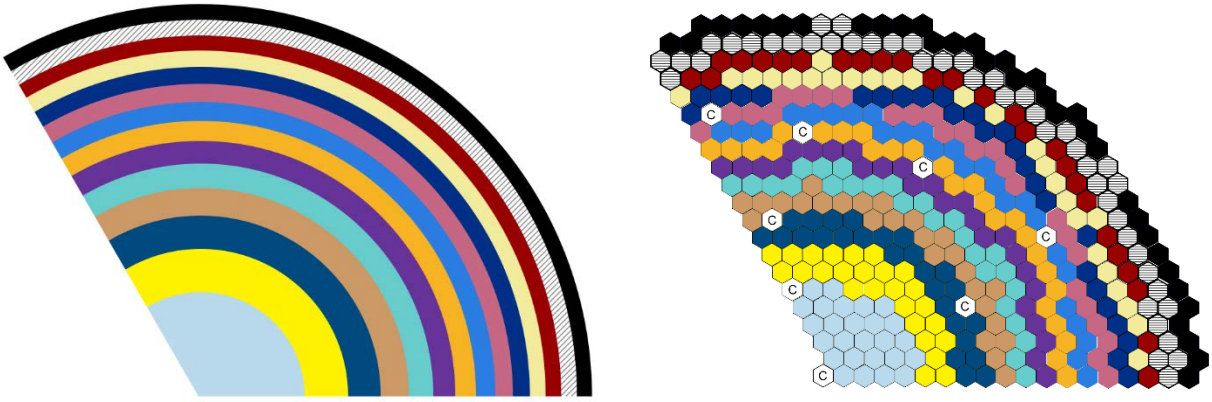

Figure 24 Schematic view of B&B core in R-Z (left) and Hex-Z (right) geometry.

For the neutronics calculations using REBUS the core model has been discretized in the axial direction using the identical mesh size as of the R-Z geometry, and in the radial direction based on the one- mesh-per-assembly configuration. The core flux, power and fuel composition were therefore calculated for each assembly segment instead of the whole fuel batch. As a result, the corresponding computational time was approximately 6-7 times longer in Hex-Z geometry than that of the R-Z geometry. The equilibrium core performance of the 3-D shuffled OBB-I core in R-Z and Hex-Z geometry is presented in Table 11.

Very good agreement can be found in the comparison with Hex-Z model having a slightly longer equilibrium cycle length and corresponding average discharge fuel burnup, primarily due to larger core leakage in both radial and axial direction. This is because in the hexagonal model the outmost batch filled with the fresh fuel does not have enough assemblies to completely surround the inner batches. However, the corresponding increase in the peak discharge burnup and the peak radiation damage is only 1.6% and 1.9%, respectively, and the peak radiation damage of the discharge fuel is 357.7 dpa. The thermal-hydraulics corrected fuel volume fraction was 39.77% and 40.31%, corresponding to the fuel pin pitch-to-diameter (P/D) ratio of 1.070 and 1.068, for R-Z and Hex-Z core, respectively, due to the somewhat lower radial power peaking factor of the Hex-Z core.

Table 11 3-D shuffled OBB-I B&B core characteristics in R-Z and Hex-Z geometry.

	R-Z geometry	Hex-Z geometry
Burn cycle time (days)	1566	1647
Reactivity swing (% dk/k)	4.66	4.41
Ave discharge BU (% FIMA)	14.49	14.88

Peak discharge BU (% FIMA)		15.69	15.94
Peak radiation damage (dpa)		351.0	357.7
Axial/radial leakage probability (%)		1.56/2.75	1.72/3.15
Axial/radial power peaking factor		2.00/1.70	1.93/1.67
Max change of batch power (%)		22.14	20.73
Core volume fractions (%)	Fuel	39.77	40.31
	Gap	13.26	13.44
	Cladding + Wire	12.77	12.92
	Duct	6.57	6.46
	Coolant	27.63	26.88

It is concluded that the difference between core performance predicted using Hex-Z and R-Z geometry is small enough, so that it is adequate to search for the optimal shuffling pattern using the R-Z model and then convert it to an Hex-Z model to obtain higher-resolution results.

A MATLAB visualization tool has been developed to gather and plot REBUS output such as the flux and power associated with either the computational mesh or the whole assembly. In this study each assembly is discretized into 64 axial meshes. A 2-D view of the 1/3 core power distribution calculated using the Hex-Z geometry was obtained by integrating the node power over the entire assembly and displayed in Figure 25 and Figure 26. Each hexagon represents a fuel assembly and the scale of the color bar represents the range of power of all assemblies. The lower left corner is the core center.

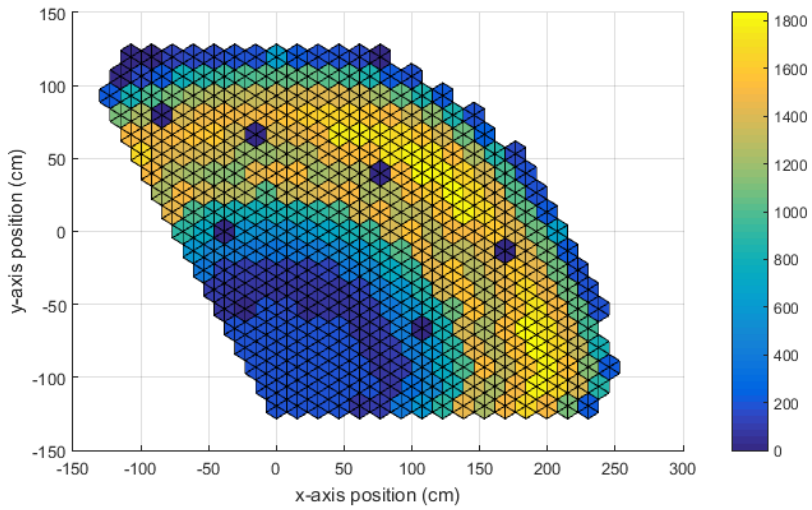

Figure 25 2-D view of assembly power (in KW) distribution of 3-D shuffled OBB-I core.

A 3-D histogram image can also be generated using the same information with assembly power be distinguished by both color and height of the hexagonal prism, as shown in Figure 26. This type of visulization can help identify the peak location of assembly power.

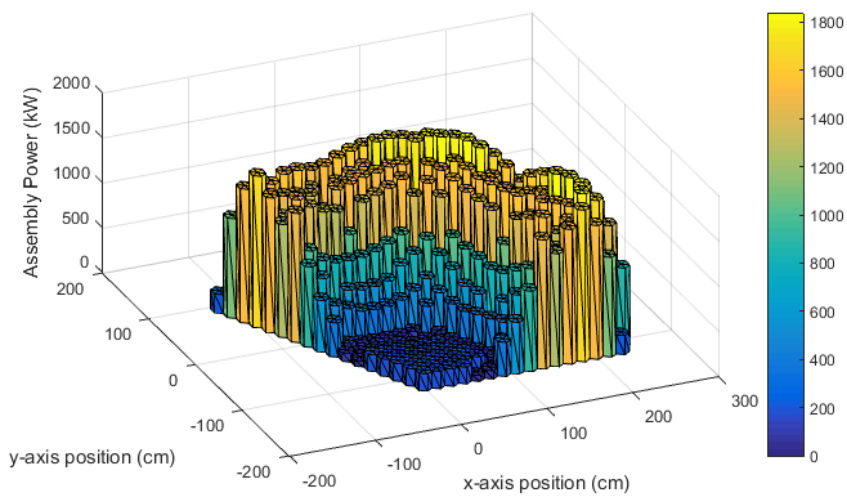

Figure 26 3-D view of assembly power distribution of 3-D shuffled OBB-I core.

3.11 3-D fuel management in modular sodium-cooled B&B fast reactors

Although the current design effort of the B&B core focuses on large size sodium-cooled fast reactor cores that feature low neutron leakage for the purpose of improving the neutron economy, a preliminary study was undertaken to quantify the extent to which 3-D fuel shuffling can improve the performance of modular sodium-cooled B&B reactors. The reactor core chosen

for this study is a small B&B core with thermal power of 1000 MW that could fit within a reactor vessel of the dimensions of Super-PRISM (S-PRISM). [34] The S-PRISM reactor was considered the most advanced and most promising U.S. fast reactor design. It was designed by General Electric (GE) to be the largest modular sodium-cooled fast reactor that could be passively safe using a reactor vessel air cooling system for passive decay heat removal by ambient air natural circulation. It was also considered to be licensable.

The S-PRISM-sized B&B core studied is conceptually similar to the large B&B cores shown in previous sections; it is sodium cooled and uses metallic DU fuel. The active core height is 1.42 m, and the active core, including radial blanket diameter, is 3.65 m; these dimensions are the same as of the oxide fueled reference S-PRISM design. The reactor has 450 full-length fuel assemblies with assembly pitch of 16.142 cm, 78 shield assemblies and 13 reactivity control assemblies. In the 3-D shuffled version, the core consists of fuel assemblies that are made of 4 axial segments, each 73.2 cm long. The non-fuel region in the fuel segment takes 7.0 cm on top of the annular fuel region as used for the large B&B cores examined in the previous sections. In the 2-D shuffled core, the large gas plenum in the original design is replaced by the hydrostatic venting device (diving bell or DISCA type) to ensure the core can achieve the B&B mode of operation. The active fuel length is identical in 2-D and 3-D cores. The main design parameters of this core can be found in Table 12.

Table 12 Main characteristics of 1000 MW SPRISM-sized B&B core.

Core configuration	2-D shuffled	3-D shuffled
Core equivalent radius (cm)	182.50	
No. of fuel batches	12	
Active fuel length (cm)	264.74	
No. of fuel segments	--	4
Total length of non-fuel region (cm)	28.0	
Core power density (MW/m^3)	36.10	
Number of fuel assemblies (Driver + Internal Blanket + Radial Blanket + Gas Expansion Module + Reflector in original design)	450	
Number of control assemblies (Primary + Secondary in original design)	13	

The same method has been applied for core modeling and shuffling pattern optimization to this core as used in Section 3.3 and 3.4, respectively. The thermal-hydraulics constraints applied to the coupled core calculation are identical to those described before except for the pressure drop -- 0.48 MPa is used as in the original S-PRISM core design. The resulting performance of the ptimal 2-D and 3-D cores arrived at are compared in Table 13.

Table 13 Performance characteristics of the optimal S-PRISM-size B&B core.

		2-D shuffled	3-D shuffled
Burn cycle time (days)		1684	2800
Burnup reactivity swing (% dk/k)		3.14	5.08
Peak/average discharge BU (% FIMA)		24.49/10.14	16.75/16.37
Max discharge BU (% FIMA)		24.49	16.75
Peak radiation damage (dpa)		571.1	396.3
Axial/radial leakage probability (%)		0.38/1.32	1.46/2.38
Radial power peaking factor		2.22	1.91
Peak batch power change (%)		18.16	16.65
Core volume fraction (%)	Fuel	38.81	39.91
	Gap	12.94	13.30
	Cladding + Wire	12.35	12.61
	Duct	6.02	6.05
	Coolant	29.88	28.12

It is found that changing from 2-D to 3-D shuffling enables a reduction of the minimum required peak radiation damage from 571.1 down to 396.3 dpa. Although the radiation damage level is higher than in any of the previously investigated large core designs, the 3-D shuffling still offers a 26% reduction from the optimal 2-D shuffling. The fuel path dependent distribution of peak discharge dpa for 2-D and 3-D shuffled cases is plotted in Figure 27. It can be seen that the 3-D shuffling can effectively minimize the peaking factor and the peak radiation damage is within only ±2.3% of the average, whereas the distribution is strongly peaked at the core axial

center in the 2-D shuffled core. The 2-D shuffled core features higher radial power peaking factor and correspondingly a lower fuel volume fraction caused by the need for a higher P/D ratio that is imposed by thermal-hydraulics analysis.

Since the 3-D shuffled S-PRISM core and the simplified large core OBB-III (discussed in Section 3.7) have the same number of assembly segments in the core, the refueling time required in these two cores is expected to be comparable. But with a relatively longer fuel cycle – 2800 EFPD (or 7.67 EFPY) primarily due to the low core power determined by the original S-PRISM design, the 3-D shuffled S-PRISM core can further increase the availability factor and minimize the relative shuffling effort. However, it is also worth mentioning that the burnup reactivity swing of this design is larger than 5% Δk/k, which increases the requirement on the control system and a quantitative study of the control assembly reactivity worth is suggested for future study.

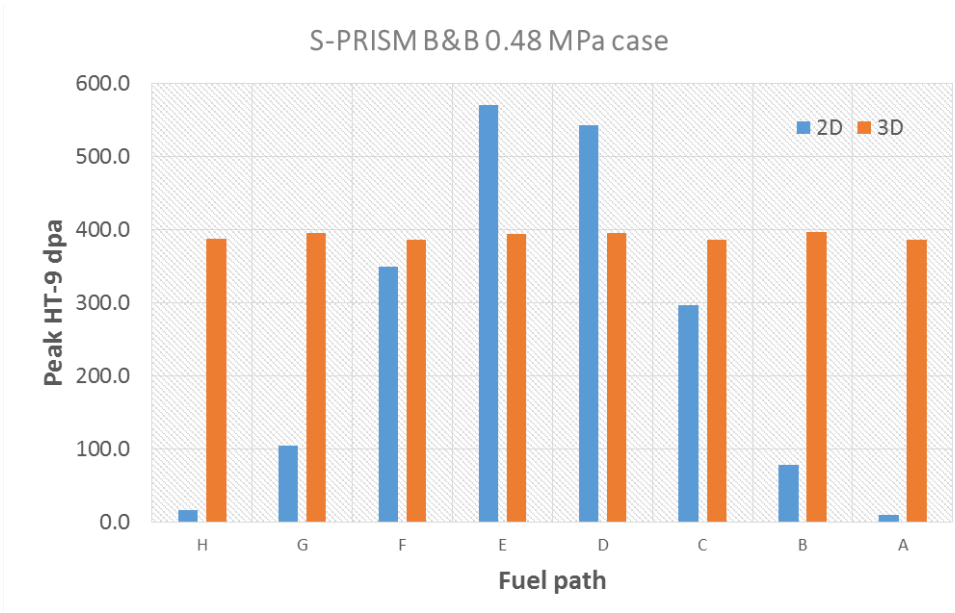

Figure 27 HT-9 discharge dpa for SPRISM-sized B&B core.

3.12 3-D fuel shuffling concept viability assessment and technology roadmap.

Although the optimal 3-D shuffled B&B core designs arrived at in this project offer significant improvements over 2-D shuffled cores – especially reduced peak radiation damage and increased fuel discharge burnup, and thus fuel utilization, concerns exist about the design viability, primarily with regard to the use of short vented fuel rods and segmented assembly

design. Concept viability issues related to the current design include the following: the feasibility of using an alloy-less depleted uranium (DU) metallic fuel; the fabrication of annular fuel; the mechanical bonding of the fuel to the cladding via a diffusion barrier; the feasibility of designing a short venting device on top of each fuel pin; and the impact of the direct release of fission gas into the sodium coolant on the core reactivity and reactor maintenance and safety.

3.12.1 Fuel rod design

Use of practically alloy-less metal fuel

Conventional uranium dioxide fuel cannot sustain the B&B mode of operation in any configuration when fed by fertile fuel due to the poor neutron economy [31]. A critical equilibrium cycle could theoretically be reached using either nitride or carbide fuel, but such designs would suffer excessively high levels of radiation damage and require a very low neutron leakage probability [35]. The only realistic fuel option for at least the first generation of B&B systems is metallic fuel. In order to minimize the minimum required burnup it is desirable to maximize the actinide density and minimize the fraction of alloying components. In conventional metallic fueled fast breeder reactor (FBR) the actinides are typically alloyed with 10 w% Zr [17]. Due to the low power density of B&B cores, it may be possible to use a lower fraction of alloying material and even use nearly pure metallic uranium. A reduction of the Zr-component from 10% down to pure metallic uranium enables an 18% increase in the fuel density, from 15.8 to 18.8 g/cm^3 at 500°C, while reducing the solidus temperature from ~1200 °C to ~1100 °C [36]. All the core calculations reported previously were performed based on this fuel temperature constraint, and it was shown that the low power density of B&B cores makes peak fuel temperatures sufficiently low that this reduction in solidus temperature is acceptable, while the neutron economy benefits from the increased fuel density is a major contributor to lowering the level of required average discharge burnup and peak radiation damage.

Fabricating annular fuel at nominal density while providing for fuel swelling with burnup into the central voided volume

The fuel annulus, cladding and liner could potentially be manufactured using a co-extrusion process. Alternatively, the cladding and liner could be manufactured separately from the fuel, with the fuel then manufactured with a slightly smaller outer diameter than the inner diameter of the cladding liner. When co-extruded, the fuel is bonded with the cladding steel from the very beginning. If separately manufactured, the fuel annulus would quickly fill the space between its

original outer diameter and the inner wall of the cladding liner, due to differential thermal expansion and fuel swelling.

A fabrication process based on the bottom pour casting has been recently proposed for metallic fuel [37] in which the range of metal (alloy) compositions are not as limited as in the case of injection cast fuel. The liquid alloy metal fuel may be bottom poured from the crucible into a graphite mold or block, which may include one or more cylindrical holes lined with cladding tubes. In an approximate center of each tube may be a steel rod or a threaded solid graphite rod, which is coated with a thin ceramic layer, such as titanium nitride. After the metal fuel is cast into the graphite mold, the annular fuel slug can be removed from the graphite with a central hole and the cladding tube surrounding it.

Annular metallic fuel was manufactured by Argonne National Laboratory (ANL) in the early 1960s and tested in the Experimental Breeder Reactor (EBR-1). Results from these campaigns show that the fuels swell inward to fill up the void annulus and exhibit practically no axial swelling, but fuels were only tested to a volume-averaged burnup of about 2.2% [38]. Annular helium-bonded metallic fuel using pure uranium metal (and an inner liner on the cladding acting as a diffusion barrier) will be tested in the Advanced Test Reactor (ATR) in the AFC-3 and ACF-4 campaigns [39]. Results from these experiments, should verify whether the fuel rod designs developed in this study could in fact be used in axially segmented fuel assembly designs utilizing fuel shuffling in three dimensions.

Mechanically bonding the annular fuel with the cladding using a thin vanadium buffer layer in between to provide diffusion barrier

It was proposed in the current design that instead of primarily relying on the fuel-alloy zirconium-content to avoid fuel/cladding chemical interaction (FCCI), annular fuel will be mechanically bonded to a 30 μm vanadium (or possible chromium) liner that acts as a diffusion barrier to avoid FCCI. In a recent investigation candidate diffusion barrier materials were tested by diffusion couple annealing tests with commercial metallic foils. [18]

Diffusion couples of U–Zr–X (X refers to the diffusion barrier candidate) vs. ferritic martensitic steels (FMS) incorporating metallic diffusion barrier foils showed that inter-diffusion was inhibited effectively by the presence of thin foils of about 20~30 μm even above the eutectic melting temperature of U–Zr alloys and FMS. Comparing the interactions between U–Zr–X and various diffusion barrier materials, it is concluded that an element with a limited

solubility of U and no intermediate phases with U should be used for the diffusion barrier material. V and Cr showed good diffusion barrier performance during the diffusion couple tests.

The upcoming irradiation campaigns of “mechanically bonded” metallic fuel in the Indian Fast Breeder Test Reactor (FBTR) will hopefully demonstrate the viability of this type of fuel [40].

3.12.2 Venting mechanism

Feasibility of designing the venting fixture within ~7 cm

The components of the assembly segment include: the assembly duct, the space reserved for the refueling mechanism and for attaching to the axially neighboring assembly duct and the fuel rods; in addition to the active fuel length the fuel rod includes a space for fuel expansion and the venting device. The duct thickness, calculated by the assembly design optimization code ADOPT, is 2.5 mm if using the HT-9 steel.

A space-efficient way, and probably the only acceptable way, of venting the fuel in B&B cores is through a simple porous plug. The fuel rod has at its upper end a metallic or ceramic plug with one side exposed to the coolant and the other side exposed to the fission gas in the space between the fuel and the plug. In the original designs of vent plugs, the vent would have to allow the fission gas to pass while keeping out the sodium coolant [41]. On top of the plug a bubble-former piece is implemented to vent the gases as large enough bubbles to maximize the probability of fission gas transport to the cover gas for coolant velocities up to 12 m/s.

An innovative gripper mechanism was designed for the assembly segment to actualize the fuel shuffling, as shown in Figure 4 (right). The fuel handling gripper has 3 jaws and is positioned at the end of the refueling mast. A robust reinforcing ring is placed at the top of the fuel segment to distribute gripper forces and provide adequate wear surfaces for the life of the segment. It is assumed in this study that the gripper jaw with its tip thickness of 15 mm and a reinforcing ring with diameter of 10 mm are enough to ensure adequate attachment of the segment during movement, since the assembly segment is considerably shorter and lighter than the conventional SFR fuel assembly.

The test of annular metallic fuel manufactured by ANL showed that the fuels swell inward to fill up the void annulus and exhibit no axial swelling at all, but the fuels were only tested to a volume-averaged burnup of about 2.2% [38]. Since the bulk of total swelling occurs within the first few percent of burnup, these results, while inconclusive for high-burnup systems, are highly encouraging. In order to remain conservative and make provision for the potential swelling by solid fission products, the assumption in this study (until newer experimental results

are available) is that the fuel may swell by up to 0.2% of its initial length per % of burnup at burnups higher than 3%. The target B&B range of average discharge burnup is 15-20%, which means that the B&B fuel rod is designed to accommodate an axial fuel swelling of 4%. In the first design of the 3-D shuffled B&B core the length of the fuel region in each of the assembly segments is 70 cm, and thus the fuel expansion space is 28 mm.

The non-fuel region in each assembly segment is made up of the following axial components (from bottom to top):

- Lower duct thickness: 2.5 mm
- Fuel expansion space: 28 mm (4% of fuel length)
- Porous vent-plug: 8 mm
- Bubble-former piece: 2 mm
- Reinforcing ring: 10 mm
- Thickness of the gripper jaw tip: 15 mm
- Upper duct thickness: 2.5 mm

The estimated length of the non-fuel region on top of the fuel is approximately 70 mm. More careful calculation and experiments must be performed to confirm the above estimations.

Feasibility of continuous venting

A number of fission gas vent-to-coolant devices have been developed for use in SFRs, but studies of fission gas venting systems have primarily been focused on use in gas-cooled reactors [42] [43] [44]. Peach Bottom Unit 1 in the US, a 40-MWe helium-cooled reactor, was an early US reactor to utilize fission gas venting [45]. The only liquid metal cooled reactor that has operated with a vent-to-coolant fuel rod design is the NaK-cooled Dounreay Fast Reactor (DFR) in the UK, in operation between 1959 and 1974. While it has been shown that venting could improve the performance of standard SFRs, venting is not strictly needed and complicates system operation and licensing, which is likely why it is rarely a design choice for SFRs. The primary focus of SFR venting system design studies have been on hydrostatic venting, particularly variants of the “diving bell” concept invented by General Electric in the early 1960s [19] [46].

A major safety concern in the vented fuel concept is the potential for gas entrainment in the primary coolant. Several potential problems can result from gas recirculation, such as cavitation of the pumps, formation of hot spots possibly near grid spacers (when used), and flow blockage. Fission gas recirculation has been shown to be highly probable, especially in loop-type reactors when venting directly out to the flowing coolant using the pinhole-type vents as in hydrostatic venting devices [47]. To avoid this issue for the porous-plug vent, the venting is

designed to be from the top rather than the side of the fuel pin. It may be possible to add a fixture on top of the porous plug carefully designed to vent the gases as large enough bubbles to maximize the probability of fission gas transport to the cover gas for coolant velocities up to 12 m/s.

Assuming that an average of about 0.27 gaseous fission products are produced in each fission reaction [48], a 3 GWt FBR produces about 4.2×10^{-5} moles/sec of the gaseous fission products Bromium, Iodine, Xenon and Krypton, 100% of which is assumed to be released from the metallic fuel. At 500°C and near-atmospheric pressure, this corresponds to a summed total of about 2.7 cm^3/s of gas release from all the pins of the core. For the 3-D shuffling design, most of this gas will be released inside the active core. An SFR of this size has a volumetric coolant flow on the order of 20 m^3/s, and the fission gas release inside the 3-D shuffled core could thus create an equivalent "void" of 1.35×10^{-5} %.

Assuming continuous removal, the concentration of the gaseous fission products in the cover gas is expected to be very small as the cover gas flow rate is expected to be much higher than the fission gas release rate; for example, the cleanup system flow rate In EBR-II was 25 cm^3/s.

In our recent study, the sodium density worth has been evaluated for small coolant density changes such as due to sodium temperature increase or to partial sodium voiding. [49] From the sodium density worth curve shown in Figure 23, it can be seen that the inserted percent reactivity increases with the void fraction in a linear manner over the range of 0-20% void.

The equivalent void created in the coolant, according to the relation shown in Figure 23, corresponds to a core reactivity insertion of 5.34E-7 (absolute value) or $1.44E-4, given the effective delayed neutron fraction being 0.0037 at EOEC of the 3D shuffled system. This calculation is done under the approximation that fission gas release rate and void worth are both uniformly distributed across the core, which may not be adequate to capture the local effects.

Two assumptions were made for calculating the peak local reactivity insertion due to fission gas release. First, the local fission gas release rate is proportional to the pin power, and the peak release rate in the core can be estimated by multiplying the average release rate by the overall peak-to-average power ratio. Based on the radial and axial power distribution for the 3-D shuffled core as presented in Figure 12, it can be calculated that the peak local void created

by the fission gas release is ~4.35E-5%, which would introduce a local reactivity insertion of $4.65E-4 if all burnup zones were to have equal contributions to the core total reactivity.

Second, the distribution of the sodium density worth across the core is identical to that of the sodium void worth, which can be obtained by performing first-order perturbation calculations using VARI3D and assuming a complete void of coolant across the core. The burnup zone dependent reactivity worth is depicted in Figure 28. It can be seen that the center-peaked positive effect increases from core center (low power) gradually with radius until it reaches a maximum in the outer regions. The only negative value occurs at the center of the outermost batch due to its higher leakage probability, although the magnitude is small. By multiplying the peaking factor of this distribution, the resulting upper-bound reactivity worth is found to be ~$2.71E-3, which still can be considered negligible.

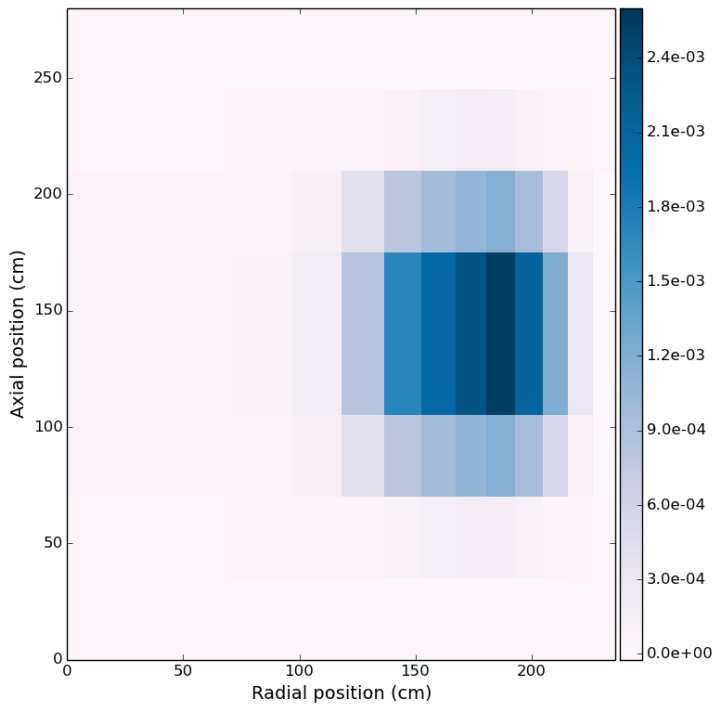

Figure 28. Void reactivity worth distribution for 3D shuffled core.

The above estimation is performed in a very conservative way; therefore, it is adequate to conclude that the vent-to-coolant is not expected to have significant effects on the B&B core reactivity and cooling.

3.12.3 Technology roadmap of 3-D fuel shuffling in B&B reactors

The general direction of future work for B&B technology is clear: structural materials such as the steels that make up the cladding, wire and ducts inside the core need to be qualified for significantly higher levels of neutron irradiation damage than has been proven experimentally in the past. For the 3-D shuffled designs introduced in this study, significant focus must be put on the feasibility of the proposed shuffling machine and mechanism. Dimensional changes to the connecting pieces must be small enough to ensure adequate attachment and detachment of assembly segments throughout the lifetime of the core, without exceeding withdrawal-force limits of the shuffling machine itself.

The 3-D shuffling involves many more operations and is significantly more complex, and will therefore need very comprehensive further study. Even using fuel assemblies made of only 2 segments each will cause a considerable increase in the time and workspace required for fuel handling. A refuelling machine with the capability of transferring more than one assembly segment at a time can be a potential solution to reduce the down time associated with fuel shuffling. [50] Industrial robots in the manufacturing industry routinely perform pre-programmed operations more advanced than what is envisioned of the shuffling device, but they are not exposed to the same extreme environment of being submerged in hot and opaque liquid sodium in a strong radiation field. Further studies that apply the advanced robotics to the fuel shuffling in nuclear reactor is highly recommended.

In addition, a safe core response to unprotected transients such as loss of flow, loss of heat sink and transient overpower scenarios (such as the rapid withdrawal of an inserted control assembly) is a difficult challenge. It appears likely that the introduction of Autonomous Reactivity Control (ARC) systems [51] will assure passive safety for both 2D and 3D-shuffling B&B systems, and this will be hopefully verified in detailed time-dependent studies to be undertaken in a new NEUP project (15-8251; started October 2015).

Additional recommended undertakings include the following: (1) How to effectively use the In-vessel storage space for storing and manipulating the subassemblies? The number of fuel segments in the 3-D shuffled core can be several times the number of assemblies in the 2-D shuffled core. (2) Could 3-D fuel shuffling reduce the time for commercialization of B&B reactors and if so, to what extent? (3) Could 3-D fuel shuffling improve the economic viability (reduce the cost of electricity) of B&B reactors, and to what extent? (4) Which of the 3-D shuffling strategies is the most economically promising? (5) What is the effect of 3-D fuel shuffling on the cost of waste disposal?

4. Conclusions and Recommendations

This project investigated the feasibility of three-dimensional (3-D) fuel shuffling in breed-and-burn (B&B) reactor cores for the purpose of reducing the peak minimum required radiation damage level while increasing the peak fuel discharge burnup.

As a by-product of this project, the following calculational schemes were developed to facilitate the design, analysis and optimization of self-sustaining B&B and other type of fast reactors:

- The Simulated Annealing (SA) algorithm for automated search for the optimum shuffling pattern (SP). This algorithm is based on the Markov chain incorporating large number of equilibrium core calculations, core performance evaluation, and probabilistic decision-making. It can be flawlessly applied to optimization problem for other types of fast reactors, and all types of reactors in general, by modifying the formulation of the objective function and optimizing the control parameter.
- Coupled scheme for fast reactor analysis simultaneously taking into account of neutronics, thermal-hydraulics and structural constraints. This method was developed based on the REBUS code available in the Argonne Reactor Computation (ARC) tool suite and the in-house developed Assembly Design OPTimization (ADOPT) code.
- A utility script for 3-D visualization of computational mode based core parameters in a realistic assembly-by-assembly core model. This capability is compatible with REBUS output format primarily for generating power or flux distribution images.

The use of 3-D in-core fuel management enables to reduce the axial variation of the discharge burnup and, thereby, reduce the peak burnup and corresponding peak radiation damage. In contrast, using 2-D shuffling in B&B cores the plutonium builds up near the axial center faster than at the top and bottom of the fuel assembly so that the axial power and burnup distribution in B&B cores is significantly more centrally peaked than in conventional (uniform axial composition) sodium cooled fast reactor (SFR) cores. This study confirmed that the peak dpa level can be significantly reduced if the burnup and dpa level of the fuel discharged from the B&B cores are flattened down to a peaking factor close to 1.0.

The initially proposed design approach, which was to design a B&B core made of a bed of metallic fuel pebbles that are clad with HT-9 and are continuously circulating, was found impractical. The pebble fuel performance analysis concluded that in order to load enough heavy metal into the core that will enable to reach sustainable B&B mode of operation at acceptable

burnup would require a high smear density that will cause large stress in the cladding and most likely cladding failure. Venting of the pebbles will allow high smear density of the pebble fuel but no mechanism that allows venting of gaseous fission products but prevents ingress of sodium coolant could be found. Moreover, the thermal-hydraulic analysis suggested that the coolant pressure drop greatly limits the attainable core power for a neutronically acceptable core height making the pebble-bed design approach much less economical than an analogous pin-based design. Furthermore, the maximum fuel volume fraction possible to achieve in the pebble-bed core was found significantly smaller than in a pin-type core and this significantly impairs the neutronics performance.

As a result of the preliminary evaluation, an alternative approach was adopted to enable three-dimensional (3-D) fuel shuffling; in this design approach the B&B core is made of axially segmented fuel assemblies. The 3-D shuffling is achieved by axially reconstituting, after each cycle, a fuel assembly by different segments or the same segments but in different order and radially shuffling the reconstituted assemblies as in conventional Sodium Fast Reactor (SFR) cores. Each of the assembly segments is composed of relatively short fuel pins that are vented to enable continuous release of gaseous fission products into the coolant flow and thus eliminate the need for long fission gas plena between the fuel segments. The project worked out a mechanical design of the fuel pins and their venting mechanism as well as their integration into a fuel subassembly and integration of the fuel subassemblies into a fuel assembly. In the course of the project this design has been carefully evaluated and modified -- especially the connecting mechanism of the subassemblies, to ensure the core stability under all operating conditions and fuel assembles integrity when moved in the sodium coolant. At the refueling stage, the assembly segments are disconnected, then connected to make new assemblies and these new assemblies are shuffled to new radial locations as guided by the SP optimization.

Compared with the optimal conventional 2-D fuel shuffling, the optimal 3-D SP was found to offer a 34% reduction of the peak radiation damage level – down to ~350 dpa; a 45% increase in the average fuel discharge burnup and, hence, the depleted uranium utilization, without violating all major neutronics and thermal-hydraulics design constraints. For the same peak dpa level, the average discharge burnup – depleted uranium utilization, of the optimal 3-D shuffled core is 2.23 times that of the optimal 2-D shuffled core These significant improvements may enable an earlier commercialization of B&B reactors than possible otherwise. A successful deployment of B&B reactors that use optimal 3-D fuel shuffling could provide at least 30-fold increase in the depleted uranium utilization than natural uranium utilization in current once-

through LWRs that generate the same amount of electricity and, hence, a significantly improvement in the once-through nuclear fuel cycle.

In fact, a 3-D fuel shuffling could also increase the average burnup between recycling of conventional fast reactors by flattening the axial burnup distribution and thereby reduce the recycling capacity required per unit of electricity generated and thus reduce the fuel cycle cost and increase the reactor capacity factor. The improvement potential is a factor close to 1.45 -- the typical peak-to-average discharge burnup in conventional 2-D shuffled SFR cores such as S-PRISM.

The introduction of the axially segmented fuel assembly design will inevitably increase the complexity of the refuelling strategy and will increase the refueling time. A number of variations of the standard 3-D shuffled design approach to alleviate these drawbacks were investigated. It was found possible to reduce by 50% the number of refueling operations in 3-D shuffling while extending the cycle length and thereby reducing the number of shuffling operations required per unit of reactor operation time when compared with 2-D shuffling. There results a nearly 40 dpa penalty on the minimum burnup required for establishing the B&B mode of operation. A similar penalty results from another promising simplification of the 3-D shuffling – restricting the shuffling of sub-assemblies to axial shuffling within the same fuel assembly so that radial shuffling will be performed for entire fuel assemblies as in a 2-D shuffling strategy.

The impact of power level increase on the minimum required peak dpa level was investigated for one of the B&B cores. It was found that a ~50% increase in the power level (or power density) will require only a ~6% increase in the peak dpa the cladding will have to accommodate without violating the thermal-hydraulic and structural constraints.

Safety related parameters were calculated for the 3-D and 2-D optimized B&B cores. No significant differences were found in the value of the kinetic parameters and reactivity coefficients. An autonomous reactivity control system that is passively actuated by coolant temperature increase invented at UC Berkeley in a companion NEUP project will most likely have to be used to compensate for the relatively large positive coolant voiding reactivity worth and ensure that large B&B cores can be designed to be inherently safe.

While offering significant improvements of the B&B core performance as discussed above, the 3-D fuel shuffling also gives rise to a number of mechanical feasibility issues. First, the segmented fuel assembly design requires further evaluation and optimization. The venting fixtures on top of the fuel rods in the sub-assemblies have to be carefully designed and tested

and the gaseous fission products vented into the reactor primary loop have to be properly handled. Dimensional changes in the sub-assembly connecting pieces must be small enough to ensure adequate attachment and detachment throughout the lifetime of the fuel assemblies without exceeding withdrawal-force limits of the shuffling machine.

A refuelling machine and refuelling strategies have to be designed for disconnecting sub-assemblies and reconnecting them to make new assemblies. Even using only 2 segments per fuel assembly will cause a considerable increase in the time and workspace above the core required for fuel handling. Thus, a cost/benefit analysis must be performed in order to assess the tradeoff between the improved core performance offered by 3-D fuel shuffling versus the complexity in the fuel handling devices and increased reactor down time and a corresponding decrease in the nuclear plant capacity factor. A refueling machine with the capability of transferring more than one assembly segment at a time can be a potential solution to reduce the down time associated with 3-D fuel shuffling.

It is also recommended to extend the study of the simulated-annealing algorithm for shuffling-pattern optimization, especially for the simplified B&B core designs featuring 3-D fuel shuffling aiming to minimize the refuelling effort and time. For example, some of the cores feature relatively large burnup reactivity swing which may force an increase in the number of batches that will enable to shorten the cycle, although the rest of the design constraints have been satisfied. A search for alternative SP that features a smaller burnup reactivity swing is worth trying.

B&B reactors are the most resource-efficient once-through reactors ever proposed, potentially being able to extract at least ~15% of the available fission energy out of depleted uranium that is readily available in large quantities as waste material from uranium enrichment facilities. 3-D shuffled 3000 MW B&B cores like those conceptually designed in this study could, if expected performance extensions to advanced fast reactor steels are realized, may become commercial sooner than 2-D shuffled B&B cores. They could supply the total current US electricity needs for hundreds of years in a once-through cycle (no reprocessing) using only the depleted uranium stockpiles accumulated for fueling the light water reactor fleet and the start-up loading (first generation) of B&B cores. The 30-fold increase in uranium utilization over current LWRs and once-through fast reactors effectively expands the potential for nuclear energy without reprocessing to a technology that is able to supply all of the world's electricity needs for centuries to come, and thus warrants detailed and intense further study.`

5. Acknowledgements

This research was performed using funding received from the DOE Office of Nuclear Energy's Nuclear Energy University Programs (NEUP 13-5144). The technical assistance and feedback of experts at the Argonne National Laboratory (ANL) is highly appreciated. In particular, the authors would like to thank Dr. T.K. Kim and Dr. Florent Heidet for their assistance.

6. Project Publications

The following publications summarize most of the work performed in the framework of this project. They are included in the Appendices and should be considered as part of this projects' summary.

Journal papers:

1. S. Qvist, J. Hou and E. Greenspan, "Design and performance of breed-and-burn reactors," *Annals of Nuclear Energy*, 85, 93-114 (2015) {Appendix A}
2. J. Hou, S. Qvist, R. Kellogg and E. Greenspan, "3D in-core fuel management optimization for breed-and-burn reactors," *Progress in Nuclear Energy*, XX, pp. xxx-xxx (2016) {Appendix B}

Conference papers:

3. J. Hou, F. Heidet, P. Gorman and E. Greenspan, "On multi-group cross sections for breed-and-burn reactors," in Transaction of the American Nuclear Society, Anaheim, CA, 2014. {Appendix C}
4. S. Qvist and E. Greenspan, "3D shuffling in Breed and Burn reactors," in American Nuclear Society Winter Meeting, Anaheim, CA, USA, 2014. {Appendix D}
5. J. Hou, S. Qvist and E. Greenspan, "3-D fuel shuffling for reduced peak burnup and increased uranium utilization of breed-and-burn reactors," in Proceedings of ICAPP 2015, Nice, France, 2015. {Appendix E}
6. J. Hou, S. Qvist and E. Greenspan, "In-fuel management optimization for breed-and-burn reactors with 3D fuel shuffling," in Proceedings of PHSOR 2016, Sun Valley, ID, 2016. {Appendix F}

Technical reports:

7. R. Kelloge, "Mechanical Concept Review of 3D Fuel Shuffling in Breed-and-Burn Reactors," Nuclear Engineering Division, Argonne National Laboratory Technical Memo, 2015. {Appendix G}

Presentations:

8. J. Hou, "3-D fuel shuffling in breed-and-burn reactors," Presentation given at Meeting of Fast Reactor Technologies and Reactor Methods, Argonne National Laboratory, Nov 20, 2015.

9. J. Hou, “Design and Performance of Breed-and-Burn Reactors with 3D Fuel Shuffling,” Seminar, Center for Advanced Energy Studies, Idaho Falls, ID, July 2015.

References

[1] L. L. C. TerraPower, "Traveling-wave reactors: a truly sustainable and full-scale resource for global energy needs," in *Proc. Int. Cong. Advances in Nuclear Power Plants (ICAPP)*, San Diego, CA, 2010.

[2] F. Heidet, R. Petroski and E. Greenspan, "Minimum burnup required for sustainable operation of fast reactors without recycling," in *Proceedings International Conference on Fast Reactors and Related Fuel Cycles: Challenges and Opportunities-FR09*, Kyoto, Japan, 2009.

[3] H. Sekimoto and K. Ryu, "A New Reactor Burnup Concept “CANDLE”," in *Proc. of PHYSOR 2000*, Pittsburgh, PA, USA, 2000.

[4] E. Teller, M. Ishikawa and L. Wood, "Completely automated nuclear reactors for long-term operation II," in *In Proceeding of ICENES’96, International Conference on Emerging Nuclear Energy Systems*, Obninsk, Russia, 1996.

[5] C. Ahlfeld, T. Burke, T. Ellis, P. Hejzlar, K. Weaver, C. Whitmer and J. Gilleland, "Conceptual design of a 500 MWe traveling wave demonstrator reactor plant," in *Proc. ICAPP 2011*, Nice, France, 2011.

[6] P. Hejzlar, R. Petroski, J. Cheatham, N. Touran, M. Cohen, B. Truong, R. Latta, M. Werner, T. Burke, J. Tandy, M. Garrett, B. Johnson, T. Ellis, J. McWhirter, A. Odedra, P. Schweiger, D. Adkisson and J. Gilleland, "TerraPower, LLC Traveling Wave Reactor Development Program Overview," in *Proceedings of ICAPP 2013*, Jeju Island, Korea, 2013.

[7] E. Greenspan, "A phased development of breed-and-burn reactors for enhanced nuclear energy sustainability," *Sustainability,* vol. 4, no. 10, pp. 2745-2764, 2012.

[8] J. Hou, S. Qvist and E. Greenspan, "3-D fuel shuffling for reduced peak burnup and increased uranium utilization of breed-and-burn reactors," in *Proceedings of ICAPP 2015*, Nice, France, 2015.

[9] M. B. Toloczko, F. A. Garner and C. R. Eiholzer, "Irradiation creep and swelling of the US fusion heats of HT9 and 9Cr-1Mo to 208 dpa at ~400°C," *Journal of Nuclear Materials,*

Vols. 212-215, pp. 604-607, 1994.

[10] E. Greenspan and F. Heidet, "Energy Sustainability and Economic Stability with Breed and Burn Reactors," *Progress in Nuclear Energy,* vol. 53, pp. 794-799, 2011.

[11] C. Di Sanzo, J. Cohen, T. Cisneros, B. Ludewight and E. Greenspan, "An Accelerator Driven Energy Multiplier for Doubling Uranium Ore Utilization," in *Proc. of Accelerator Application Topical Meeting*, Knoxville, TN, US, 2011.

[12] G. Zhang, E. Greenspan, A. Jolodosky and J. Vujic, "SFR with Once-through Depleted Uranium Breed & Burn Blanket," *Progress in Nuclear Energy,* 2014.

[13] X. L. G. Soto, "Study of the Feasibility of a Pebble Bed Breed & Burn Reactor," University of California, Berkeley, 2012.

[14] P. G. P. G. K. R. D. W. D. Frazer, "A Pebble Based Breed & Burn Reactor Capable of 3-D Shuffling," University of California, Berkeley, 2013.

[15] S. Qvist, J. Hou and E. Greenspan, "Design and performance of breed-and-burn reactors," *Annal of Nuclear Energy,* vol. 85, pp. 93-114, 2015.

[16] R. Kelloge, "Mechanical Concept Review of 3D Fuel Shuffling in Breed-and-Burn Reactors," Nuclear Engineering Division, Argonne National Laboratory Technical Memo, 2015.

[17] Y. I. Chang, "Technical rationale for metal fuel in fast reactors," *Nuclear Engineering and Technology,* vol. 39, no. 3, pp. 161-170, 2007.

[18] H. Ryu, B. O. Lee, S. J. Oh, J. H. Kim and C. B. Lee, "Performance of FCCI barrier foils for U-Zr-Z metallic fuel," *Journal of Nuclear Materials,* vol. 392, no. 2, pp. 206-212, 2009.

[19] G. L. O'Neill, "Safety and Economic Aspects of Vented Fuel in Sodium-Cooled Reactors,," in *Proceedings of the Conference on Safety, Fuels, and Core Design in Large Fast Power Reactors,*, 1965.

[20] K. L. Derstine, "DIF3D: A Code to Solve One-, Two-, and Three-Dimensional Finite Difference Diffusion Theory Problems," 1984.

[21] B. L. Toppel, "A User’s Guide to the REBUS-3 Fuel Cycle Analysis Capability," 1983.

[22] C. H. Lee and W. S. Yang, "MC2-3: Multigroup Cross Section Generation Code for Fast

Reactor Analysis," 2013.

[23] R. E. Alcouffe, F. W. Brinkley, D. R. Marr and R. D. O'Dell, "User's Guide for TWODANT: A Code Package for Two-Dimensional, Diffusion-Accelerated, Neutral Particle Transport," 1990.

[24] J. Leppänen, "Serpent Monte Carlo Physics Code," in *AER Symposium on VVER Reactor Physics and Reactor Safety*, Espoo, Finland, 2010.

[25] S. Qvist and E. Greenspan, "The ADOPT code for automated fast reactor design," *Annals of Nuclear Energy,* vol. 71, pp. 23-36, 2014.

[26] "Fast Reactor Database 2006 Update," 2006.

[27] A. Suspluagas and E. Greenspan, "Implementation of the ENHS Thermal Hydraulic Optimization Code for Recent ENHS Design Improvement," University of California, Berkeley, 2005.

[28] A. Bleise, P. Danesi and W. Burkart, "Properties, use and health effects of depleted uranium (DU): a general overview," *Journal of Environmental Radioactivity,* vol. 64, no. 2-3, pp. 93-112, 2003.

[29] N. Metropolis, A. Rosenbluth, M. Rosenbluth, A. Teller and E. Teller, "Equation of State Calculations by Fast Computing Machines," *J. Chem. Phys.,* vol. 21, p. 1087, 1953.

[30] S. Kirkpatrick and M. P. Vecchi, "Optimization by simmulated annealing," *Science,* vol. 220, no. 4598, pp. 671-680, 1983.

[31] F. Heidet and E. Greenspan, "Neutron Balance Analysis for Sustainability of Breed-and-Burn Reactors," *Nuclear Science and Engineering,* vol. 171, no. 1, pp. 13-31, 2012.

[32] W. Yang, T. Kim and R. Hill, "Performance characteristics of metal and oxide fuel cores for a 1000 MWt advanced burner reactor," in *ARWIF2008*, Fukui, Japan, 2008.

[33] S. Qvist and E. Greenspan, "Inherent safety of minimum-burnup breed & burn reactors," in *Proc. of ICAPP 2012*, Chicago, IL, US, 2012.

[34] A. E. Dubberley, K. Yoshida, C. E. Boarman and T. Wu, "SuperPRISM oxide and metal fuel core designs," in *Proceedings of ICONE 8*, 2000.

[35] S. Qvist and E. Greenspan, "Design space analysis for breed-and-burn reactor cores," *Submitted to Nuclear Science and Engineering [in review],* 2015.

[36] F. A. Rough, "An Evalutation of Data on Zirconium-Uranium Alloys," 1955.

[37] L. C. Walters, "Sheathed, annular metal nuclear fuel". US Patent 9008259, 12 Jan 2011.

[38] J. A. Horak, J. H. Kittel and F. L. Yaggee, "Irradiation behavior of restrained and vented uranium-2 w/o zirconium alloy," Argonne, IL, US, 1962.

[39] Idaho National Laboratory, "Advanced Fuels Campaign 2013 Accomplishments," Idaho Falls, Idaho, US, 2013.

[40] S. Kaity, J. Banerjee, K. Ravi, R. Keswani, T. R. Kutty, Kumar A and G. J. Prasad, "Characterization and property evaluation of U-15wt%Pu alloy for fast reactor," *Journal of Nuclear Materials,* vol. 433, no. 1-3, pp. 206-214, 2012.

[41] S. Dorner and W. Sommer, "Investigation into a Fuel Element Sealing of Sinter Metal in Liquid Sodium".

[42] General Atomics, "Gas-Cooled Fast Breeder Reactor Preliminary Environmental Report on 300-MW(e) Demonstration Plant," 1974.

[43] R. W. Schleicher, H. Choi and J. Rawls, "The Energy Multiplier Module: Advancing the Nuclear Fuel Cycle Through Technology Innovations," *Nuclear Technology,* vol. 184, pp. 169-180, 2013.

[44] M. T. Farmer, E. A. Hoffman and P. F. Pfeiffer, "Generation IV Nuclear Energy System Initiative Pin Core Subassembly Design," 2006.

[45] K. P. Steward, "Final Summary Report on the Peach Bottom End-of-Life Program," 1978.

[46] M. J. McNelley, "Liquid Metal Fast Breeder Reactor Design Study [1000 Mw(electrical)] UO2-PuO2 Fueled Plant," 1964.

[47] A. J. Lipps, "Evaluation of Vented-to-Coolant Designs for Sodium-Bonded Carbide Fuel Rods: Task I Report, Follow-on Study for a 1000 MWe LMFBR," Madison, Pennsylvania, 1968.

[48] A. E. Waltar, D. R. Todd and P. V. Tsvetkov, Fast Spectrum Reactors, New York: Springer,

2012.

[49] J. Hou and E. Greenspan, "Quarterly report for Project 13-5144: period August 1, 2015 - October 31, 2015," Nuclear Engineering University Program (NEUP), 2015.

[50] R. Meuschke and L. Malandra, "Refueling machine". US Patent 5,687,207, 11 1997.

[51] S. Qvist and E. Greenspan, "An Autonomous Reactivity Control System for Improved Fast Reactor Safety," *Progress in Nuclear Energy,* vol. 77, pp. 32-47, 2014.

[52] J. Hou, F. Heidet, P. Gorman and E. Greenspan, "On Multi-Group Cross Sections for Breed-and-Burn Reactors," in *Transaction of the American Nuclear Society*, Anaheim, CA, 2014.

[53] M. R. I. T. M.J. Norgett, "A Proposed Method of Calculating Displacement Dos Rates," *Nucl. Eng. and Design,* vol. 33, pp. 50-54, 1975.

[54] L. Greenwood, "SPECOMP calculations of radiation damage in compounds," in *Sixth ASTM-EURATOM Symposium on Reactor Dosimetry*, Jackson Hole, WY, 1987.

[55] K. A. Dowsland and C. R. Reeves, Morden Heuristic Techniques for Combinatorial Problems, McGraw-Hill, 1995.

[56] A. Dubberley, *Private communication.*

[57] J. Hou, S. Qvist, R. Kelloge and E. Greenspan, "3D In-core Fuel Management Optimization for Breed-and-Burn Reactors," *Progress in Nuclear Energy,* Revised.

[58] S. Qvist and E. Greenspan, "3D shuffling in Breed and Burn reactors," in *American Nuclear Society Winter Meeting*, Anaheim, CA, USA, 2014.

[59] P. Poon and G. Parks, "Application of genetic algorithms to in-core nuclear management optimization," in *Proc. Joint Int. Conf. Mathematical Methods Supercomputing Nuclear Applications*, Karlsruhe, Germany, 1993.

[60] M. DeChaine and M. Feltus, "Nuclear fuel management optimization using genetic algorithms," *Nucl. Tech.,* vol. 111, pp. 109-114, 1995.

[61] G. Parks, "Multiobjective pressurized water reactor reload core design by nondominated genetic algorithm search," *Nucl. Sci. Eng.,* vol. 124, pp. 178-187, 1996.

[62] V. G. Toshinsky, H. Sekimoto and G. I. Toshinsky, "Multiobjective fuel management optimization for Self-Fuel-Providing LMFBR using genetic algorithms," *Annals of Nuclear Energy,* vol. 26, no. 9, pp. 783-802, 1999.

[63] V. Toshinsky, H. Sekimoto and G. Toshinsky, "A method to improve multiobjective genetic algorithm optimization of a self-fuel-providing LMFBR by niche induction among nondominated solutions," *Annals of Nuclear Energy,* vol. 27, pp. 397-410, 2000.

[64] P. J. Turinsky and G. T. Parks, "Advances in nuclear fuel management for light water reactors," *Advances in Nuclear Science and Technology,* pp. 137-165, 1999.

[65] J. G. Stevens, K. S. Smith, K. R. Rempe and T. J. Downar, "Optimization of pressurized water reactor shuffling by simulated annealing with heuristics," *Nuclear science and engineering,* vol. 121, no. 1, pp. 67-88, 1995.

[66] T. K. Park, H. G. Joo, C. H. Kim and H. C. Lee, "Multiobjective loading pattern optimization by simulated annealing employing discontinuous penalty function and screening technique," *Nuclear Science and Engineering,* vol. 162, no. 2, pp. 134-147, 2009.

Appendices

All appendices are attached below in the order:

APPENDIX	Publication Title	Pages
A	S. Qvist, J. Hou and E. Greenspan, "Design and performance of breed-and-burn reactors," *Annals of Nuclear Energy*, **85**, 93-114 (2015)	22
B	J. Hou, S. Qvist, R. Kellogg and E. Greenspan, "3D in-core fuel management optimization for breed-and-burn reactors," *Progress in Nuclear Energy*, **88**, 58-74 (2016)	17
C	J. Hou, F. Heidet, P. Gorman and E. Greenspan, "On multi-group cross sections for breed-and-burn reactors," in Transaction of the American Nuclear Society, Anaheim, CA, 2014.	4
D	S. Qvist and E. Greenspan, "3D shuffling in Breed and Burn reactors," in American Nuclear Society Winter Meeting, Anaheim, CA, USA, 2014	4
E	J. Hou, S. Qvist and E. Greenspan, "3-D fuel shuffling for reduced peak burnup and increased uranium utilization of breed-and-burn reactors," in Proceedings of ICAPP 2015, Nice, France, 2015 (paper 15144)	9
F	J. Hou, S. Qvist and E. Greenspan, "In-fuel management optimization for breed-and-burn reactors with 3D fuel shuffling," to be published in Proceedings of PHSOR 2016, Sun Valley, ID, 2016	16
G	R. Kelloge, "Mechanical Concept Review of 3D Fuel Shuffling in Breed-and-Burn Reactors," Nuclear Engineering Division, Argonne National Laboratory Technical Memo, 2 Sept. 2015.	12
H	David Frazer, Priyanka Gaurav, Phil Gorman, Kelly Rowland, Daniel Wooten, "A Pebble Based Breed & Burn Reactor Capable of 3-D Shuffling" NE-265 Project Report (Partial), December 2013	40

APPENDIX A

APPENDIX B

APPENDIX C

APPENDIX D

APPENDIX E

APPENDIX F

APPENDIX G

APPENDIX H

Appendix A

S. Qvist, J. Hou and E. Greenspan, “Design and performance of breed-and-burn reactors,” *Annals of Nuclear Energy*, 85, 93-114 (2015)

Annals of Nuclear Energy 85 (2015) 93–114

Contents lists available at ScienceDirect

Annals of Nuclear Energy

journal homepage: www.elsevier.com/locate/anucene

Design and performance of 2D and 3D-shuffled breed-and-burn cores

Staffan Qvist [a,b,*], Jason Hou [b], Ehud Greenspan [b]

[a] Department of Physics and Astronomy, Uppsala University, Sweden
[b] Department of Nuclear Engineering, University of California Berkeley, United States

ARTICLE INFO

Article history:
Received 13 January 2015
Received in revised form 6 April 2015
Accepted 8 April 2015

Keywords:
Breed and burn
Traveling Wave
Core design
Fast reactor
Shuffling
LMFBR

ABSTRACT

The primary objective of this work is to find design approaches that will enable 3D fuel shuffling in stationary breed-and-burn (B&B) cores and to quantify the attainable reduction in peak DPA and change in additional performance characteristics going from conventional 2D to 3D fuel shuffling strategies. An additional objective is to establish the tradeoff between the minimum required DPA (displacements per atom) and average required burnup (fuel utilization) for B&B cores spanning a core power range from 1250 to 3500 MWth. It is found possible to design a B&B core fuelled with depleted uranium to have a peak radiation damage at or below 350 DPA when using 3D-shuffling. Relative to conventional 2D-shuffling, 3D-shuffling offers between 30% and 40% reduction in the peak DPA along with up to 30% increase in the average discharge burnup and, hence, in the depleted uranium utilization as well as significant increase in the core average and specific power density. Per DPA, the 3D shuffling option offers up to 60% higher uranium utilization. Even though 350 DPA is above the 200 DPA peak radiation damage HT9 steels were exposed to so far, it is below the 400 DPA advanced structural materials are expected to tolerate.

© 2015 Elsevier Ltd. All rights reserved.

1. Introduction

Present-day light water reactors (LWR) extract only ~0.6% of the potential fission energy of the natural uranium mined to make their fuel. About 90% of the unused uranium is depleted uranium (DU) and the remaining >9% is left over as used nuclear fuel (UNF). Based on the information from the 2006 US Department of Energy (DOE) UF_6 cylinder information database, there is approximately 479,000 tons of depleted uranium stored in the form of UF_6 in the US alone (Schneider et al., 2007). This material is currently located outside three large enrichment facilities (in Kentucky, Tennessee and Ohio) in metallic canisters. About 1330 tons of this material is ^{235}U, with a concentration in the range of 0.2–0.3% ^{235}U. The volume-averaged ^{235}U-concentration of the US DU stockpile is 0.279%.

This material can, in principle, be utilized for energy production in fast reactors via, primarily, conversion of ^{238}U by neutron capture to ^{239}Pu. Direct fission of the ^{238}U can contribute between 10% and 20% of the total fissions in a hard spectrum core. The conventional approach for attaining high uranium utilization is to use it to fuel fast breeder reactors (FBR) coupled with periodic fuel re-cycling. When the radiation damage accumulated by the fuel and its cladding threatens the mechanical integrity of the fuel rods, the fuel assemblies are discharged and reprocessed and the heavy metal is recycled back to the reactor core with the addition of depleted uranium makeup. Fuel reprocessing involves removal of the fuel cladding, removal of the fission products, addition of some DU to make up for the uranium that has been fissioned, fabrication of new fuel assemblies and reloading the fuel assemblies into the reactor core for another irradiation cycle. This process enables utilization (fission) of all the mined uranium minus inevitable losses in, primarily, the reprocessing operations.

Reprocessing of LWR fuel currently in use in both Europe and Japan uses the PUREX (Plutonium Uranium Redox EXtraction (Anderson and Asprey, 1947) process to create mixed oxide (MOX) fuel for use in thermal reactors. Recycling in any thermal spectrum reactor, however, cannot be done indefinitely since maintaining criticality requires increasing the Pu loading and this tends to make the coolant density reactivity coefficient positive. Moreover, as the conversion ratio of thermal reactors is smaller than 1, they need continuous feed of enriched uranium. Thus, France and Japan are contemplating a single recycle of plutonium through their thermal spectrum reactors. This will raise the level of uranium utilization up to only ~1%.

Although reprocessing is currently in use in several countries for LWRs, there is significant objection in the United States and elsewhere to fuel reprocessing due to uncertainties regarding costs, and more importantly proliferation concerns. The proliferation concern is that the chemical or electrochemical processes that

* Corresponding author at: Ångström Lab, Lägerhyddsvägen 1, 752 37 Uppsala, Sweden. Tel.: +46 765624043.
E-mail address: staffan.qvist@physics.uu.se (S. Qvist).

http://dx.doi.org/10.1016/j.anucene.2015.04.007
0306-4549/© 2015 Elsevier Ltd. All rights reserved.

have been developed for fuel reprocessing could be used for the extraction and diversion of fissile materials for the clandestine production of nuclear weapons. Scientific arguments have been put forth that the reprocessing technology most suited for FBR applications (electrochemical) is non-proliferating by design (Hannum et al., 1997), meaning that the recycled materials could not be used to make a nuclear weapon without significant further processing (DeVolpi, 1986). These facts have so far had little effect on the positions of political opponents of fuel reprocessing.

Fast breeder reactors could, in principle, also operate without fuel recycling. That is, using a once-through fuel cycle as do the overwhelming majority of LWRs. Although the standard FBR discharge burnup of 10–15% FIMA (Fission of Initial Metal Atom) is two to three times higher than that of LWRs, the uranium utilization of a once-through FBR is not significantly different from that of a once-through LWR because the level of uranium enrichment required to achieve criticality in the FBR is often three times that required to fuel the LWR. A conventional FBR operating without reprocessing is thus not able to use fuel resources more efficiently or make any use of the untapped energy potential of the available DU stockpiles.

To enable a significantly higher utilization of uranium while using a once-through fuel cycle, a special class of fast nuclear reactors, collectively known as "breed-and-burn" (B&B) reactors, has been under consideration since the late 1950s. Theoretical studies have proven the principle of a traveling B&B deflagration wave through fertile material (so called "Traveling Wave Reactors"), but realistic designs utilizing this principle for power-producing cores have been difficult to achieve. The unique feature of a B&B reactor is that it can breed plutonium in low ^{235}U containing uranium feed fuel and then fission a significant fraction of the bred plutonium without having to reprocess the fuel. In order to initiate the chain reaction, the initial fuel loading of the B&B core has to have an adequate amount of fissile material – either enriched uranium (EU) or plutonium with or without minor actinides. Thereafter, the B&B core is capable to continue its operation while only being fed with fertile fuel such as natural or depleted uranium. Eventually, the uranium utilization will approach the fraction of the loaded uranium that has been fissioned.

An extensive though most definitely not complete chronologic history of B&B research and development up until the start of the Terrapower efforts in 2006 is shown in Fig. 1. The first or most important publication from each identified B&B research group in Fig. 1 is given in references: (Feinberg and Kunegin, 1958; Fuchs and Hessel, 1961; Kouts et al., 1979; Atefi, 1980; Slesarev et al., 1983; Feoktistov, 1988; Goldin and Anistratov, 1992; Seifritz, 1995; Teller et al., 1996; Toshinsky, 1997; Akhiezer et al., 1999; Sekimoto and Ryu, 2000; Van Dam, 1998, 2000; Khizhnyak, 2001; Pilipenko et al., 2003; Fomin et al., 2005; Chen et al., 2005; Yarsky, 2005; Heidet and Greenspan, 2010; Gaveau et al., 2005; Gilleland, 2008). Since 2006, when Bill Gates announced support and funding for the idea (TerraPower, 2015), a large number of groups have started research on the topic. Some of the more recently published researched is presented in references (Pavlovich et al., 2007; Rusov, 2011; Hartanto and Kim, 2012; Osbourne et al., 2012; Choi et al., 2013; Si, 2013; Heidet and Greenspan, 2013a,b).

B&B reactors come in two basic flavors: Traveling Wave Reactors (TWR) and Standing (or Stationary) Wave Reactors (SWR) (Greenspan, 2012). TWRs are long cores of static fuel with a small, enriched, "starter" region typically on one axial end. The starter region initiates a breeding and burning wave that travels axially through the fertile fuel material toward the other end. To propagate the burning wave through low-enriched material such as DU, a very high level of fast neutron fluence is needed, which exposes core structures (like fuel rod cladding and fuel assembly duct wall steel) to excessive levels of radiation damage.

Current fast reactor structural steels – specifically the ferritic–martensitic HT9 steel, were exposed, so far, to a peak fast neutron fluence of 3.9×10^{23} n/cm^2 ($E > 0.1$ MeV), corresponding to a radiation damage of ~200 DPA (displacements per atom) (Toloczko et al., 1994). Realistic TWR designs using DU as fertile fuel require a minimum peak fast neutron fluence of at least 2.5×10^{24} n/cm^2 ($E > 0.1$ MeV) (Tak et al., 2012), which corresponds to around ~1200 DPA – six times above the currently accepted limit. In other estimates, the peak TWR discharge fluence is as high as 4.2×10^{24} n/cm^2 ($E > 0.1$ MeV) (Kim and Taiwo, 2010). This situation makes TWRs impractical to implement until new materials or new design solutions for accommodating the excessive radiation damage can be found. One design solution investigated by *Sekimoto* and colleagues is to reclad the fuel rods with new steel every ~10 years of operation (Nagata and Sekimoto, 2007; Nagata et al., 2009).

In SWRs, while burned fuel assemblies are discharged, remaining fuel assemblies are shuffled radially in the core and new fertile (DU) fuel assemblies are loaded. In this way, the breed-and-burn wave can stay stationary while the fuel "travels" through the wave. SWRs are more neutron-efficient than TWRs, because they lose a smaller fraction of neutrons to leakage or non-fuel absorption. Correspondingly, the minimum peak fast fluence required to sustain SWR B&B-type operation in an optimized core with DU feed fuel is $\sim 1 \times 10^{24}$ n/cm^2 ($E > 0.1$ MeV), corresponding to about 500 DPA (Heidet, 2010; Qvist, 2013). While this is significantly more likely realizable than the values for TWRs, it still requires the cladding steel to survive radiation damage level more than double the current experimental limit. Two approaches to tackle this problem have been pursued in previous work. Recently, the TerraPower design was adjusted to use natural rather than depleted uranium as feed fuel to lower the peak radiation damage down to 480 DPA (Gilleland, 2014). At UC Berkeley, researchers have looked into the possibility of B&B operation with periodic and limited fuel reconditioning (Greenspan and Heidet, 2011), as well the option to double-clad the fuel (Di Sanzo et al., 2011). With limited fuel reconditioning, fuel rods are taken out of the core once the cladding reaches 200 DPA, part of the fission products (primarily the gaseous ones) are removed and the cladding is replaced prior to fuel reuse in the reactor.

A different option, recently introduced and studied in detail in this paper, is to introduce three-dimensional fuel shuffling in B&B cores in order to minimize the peak DPA (Qvist and Greenspan, 2014). The axial peaking-factor (maximum value divided by the average value) for fluence, burnup and DPA in a typical SWR B&B is on the order of 1.7–2.7. If the axial DPA-profile could be flattened down to a peaking-factor close to 1.0, peak DPA levels could be brought down significantly.

The primary objective of this work is to find design approaches that will enable 3D shuffling in SWR cores and to quantify the attainable reduction in peak DPA and change in additional performance characteristics going from conventional two-dimensional to three-dimensional fuel shuffling strategies. An additional objective is to establish the tradeoff between the minimum required DPA and average required burnup (fuel utilization) for varying core sizes and power outputs.

Section 2 briefly reviews fundamentals of B&B reactor physics that will help understanding the special requirements and challenges faced in B&B core design. Sections 3 and 4 covers the fuel rod and assembly design considerations of 2D and 3D-shuffled B&B cores respectively. Section 5 defines the fuel rod design that is used for all B&B cores in this study. Section 6 covers the design of the core and its structural components, particularly with regards to the 3D-shuffling options. Section 7 presents the approach of incorporating autonomous reactivity control (ARC) systems to tackle the challenges of inherent safety performance of large B&B

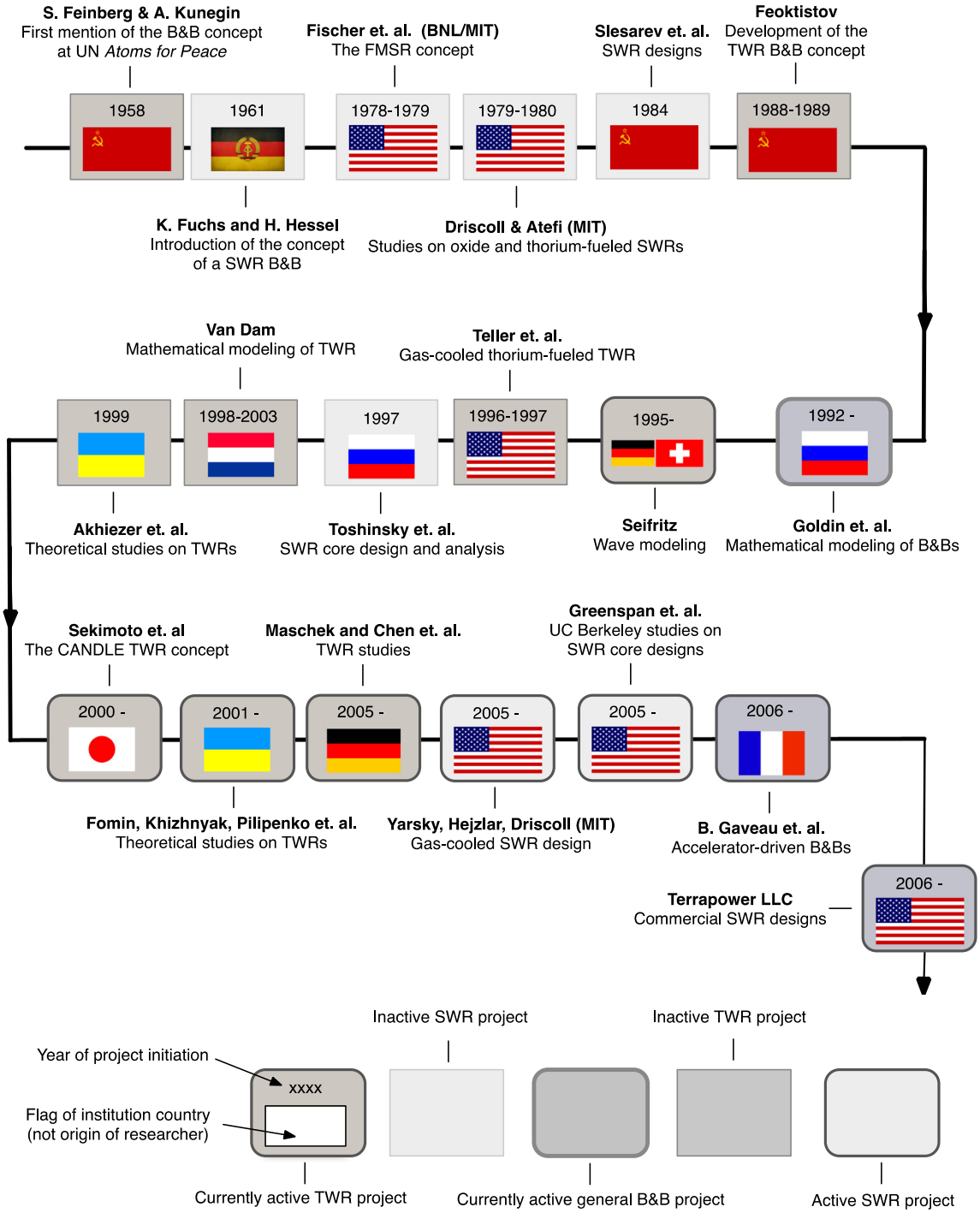

Fig. 1. The history of breed-and-burn reactor R&D until 2006.

cores. Sections 8 and 9 summarize the core design and shuffling scheme methodologies respectively. The results are summarized in Section 10, and Section 11 defines conclusions and the direction of future research.

2. Fundamentals of breed-and-burn reactor physics

2.1. The neutron balance concept and minimum required burnup

To estimate between what levels of average discharge burnup an SWR B&B core can operate at when at equilibrium, one can follow a batch of fertile material (metallic depleted uranium) from its introduction into the core until its discharge. When loaded, the fertile batch is a neutron sink, absorbing far more neutrons than it generates (k_∞ of a typical liquid–metal cooled core composition loaded with metallic DU fuel is ~0.25). As neutrons are absorbed, the ^{239}Pu concentration quickly builds up and the fuel eventually becomes a net neutron producer (k_∞ goes above unity at 3.5–4% FIMA). Until reaching this break-even burnup level, the batch accumulates a neutron deficit. If the batch is discharged before it has paid back this deficit by net neutron production, it will not be possible to sustain a critical B&B equilibrium cycle. Because of this,

uniquely for B&B systems, there is a strict minimum level of burnup required for equilibrium cycle operation where the total batch neutron production and absorption equals.

Following the derivation used by Heidet and Greenspan (Heidet, 2010; Heidet and Greenspan, 2012) (in principle similar to the method used by Yu et al. (2002)), the range of average discharge burnup accessible for B&B mode of operation can be estimated by solving the *neutron balance equation*:

$$\int_0^{Bu} \bar{\upsilon}(Bu) \times \left[1 - \frac{1}{k_\infty(Bu) \times (1-L)}\right] dBu = 0 \quad (1)$$

In which Bu is the fuel burnup measured in FIMA (Fission of Initial Metal Atom), $\bar{\upsilon}$ is the average number of neutrons released per fission and L is the fraction of neutrons lost to leakage and absorption in control elements.

For realistic nuclear reactor core designs, Eq. (1) can have either zero (B&B operation not possible) or two non-trivial solutions. The first non-trivial solution to Eq. (1) for any given system determines the minimum required average discharge burnup of a B&B core at equilibrium. Contrary to all other types of reactors, designers of B&B cores are attempting to bring the level of the minimum required burnup down rather than up. This is because in any FBR, the maximum discharge burnup is usually limited by the radiation damage to the structural materials rather than by the neutron economy. The minimum required burnup is the primary design requirement that challenges the viability of B&B reactors.

It can be inferred from Eq. (1) that the minimum required average burnup will be reduced by reducing the neutron leakage probability from the core and by increasing k_∞. The leakage probability can be reduced by increasing the core volume and optimizing the core height-to-diameter ratio. The infinite neutron multiplication can be increased by hardening the neutron spectrum. This can be achieved by increasing the loading of actinides per unit of core volume while avoiding low atomic number fuel constituents such as oxygen.

2.2. Power and fluence peaking factors

The radial power peaking factor – maximum axially averaged power in an assembly divided by the average assembly power level, depends primarily on the strategy chosen for fuel shuffling and will be discussed in more detail in Section 8, covering the principles of determining the fuel shuffling path. The axial peaking factor of burnup, fluence and DPA of an SWR B&B core at equilibrium with conventional 2D-shuffled fuel assemblies is essentially not strongly affected by either the shuffling scheme or the specifics of the core design excluding the core height. In a fresh fuel batch, ^{239}Pu will preferentially start building up near the axial center of the fuel, since this is where the axial flux distribution peaks. The production of fissile material near the center will further increase the flux in this region relative to the top and bottom of the fuel, which maintains a high axial peaking factor even as burnup progresses.

Only the length and the average discharge burnup of the fuel affect the equilibrium axial peaking factor. Using a very short fuel column (<100 cm) evens out the axial power and burnup distribution, but use of such a short fuel results in unacceptably high axial neutron leakage probability. As the average discharge burnup increases, breeding closer to the axial ends of the fuel causes a reduction in the peaking factor. SWR B&B cores feature axial burnup and DPA peaking factors of 1.7–2.7 rather than 1.2–1.35 in conventional fast reactor cores. There are no design fixes that can significantly reduce axial peaking and thus the peak radiation damage of an SWR B&B core at equilibrium using standard fuel assemblies and 2D shuffling. To achieve the reduction desired, 3D shuffling (radial and axial) options are being examined to flatten the axial burnup, fluence and DPA profile.

3. Fuel rod and assembly design for B&B cores

3.1. Fuel rod design

The design of the fuel rod has a significant effect on the minimum required burnup and peak radiation damage via the following design variables – fuel material and density, fission gas plenum length and lattice pitch.

Conventional uranium dioxide fuel cannot sustain the B&B mode of operation in any configuration when fed by fertile fuel due to the poor neutron economy (Heidet and Greenspan, 2012; Qvist and Greenspan, 2015). A critical equilibrium cycle could theoretically be reached using either nitride or carbide fuel, but such designs would suffer excessively high levels of radiation damage and require a very low neutron leakage probability (Qvist and Greenspan, 2015). The only realistic fuel option for at least the first generation of B&B systems is metallic fuel. In order to minimize the minimum required burnup it is desirable to maximize the actinide density and minimize the fraction of alloying components. In conventional metallic fuelled FBR the actinides are alloyed with 10 wt.% Zr (Chang, 2007). Due to the low power density of B&B systems, it is possible to use a lower fraction of alloying material and even use pure metallic uranium. A reduction of the Zr-component from 10% down to pure metallic uranium enables an 18% increase in the fuel density, from 15.8 to 18.8 g/cm^3 at 500 °C, while reducing the solidus temperature from ~1200 °C to ~1100 °C (Rough, 1955). The low power density of B&B systems makes peak fuel temperatures sufficiently low that this reduction in solidus temperature is acceptable, while the neutron economy benefit of the increased fuel density is a major contributor to lowering the level of required average discharge burnup. Instead of primarily relying on the fuel-alloy zirconium-content as a diffusion barrier to avoid fuel/cladding chemical interaction (FCCI), the inner surface of the cladding steel is coated with a diffusion-barrier liner, described in more detail in Section 5.

Ten different metallic fuel rod design options were examined and evaluated in this work. They are shown in Fig. 2, ranked from left-to-right in order of increasing attractiveness for B&B applications. Definition and description of the different options are given in Table 1. The high level of burnup causes the release of a large volume of gaseous fission products from the fuel. To deal with this issue, the standard metallic fast reactor fuel rod design (option C in Fig. 2) features a large above-core fission gas plenum volume. The large gas plenum volume is meant to keep the pressure in the pin low and enable a thin cladding wall. This reduces the amount of steel inside of the active core, which maximizes the neutron economy. In theory, one could also use a significantly smaller plenum by increasing the thickness of the cladding steel (design options A and B of Fig. 2), but the resulting negative neutronic impact of the increased mass of steel in the active core is typically so large that such designs have never been seriously considered (see Table 2).

The location of the plenum depends on whether one is using a liquid bonded fuel – as required for conventional cylindrical metallic fuel rods, or if it is possible to use a gaseous bond. Using an annular or "mechanically bonded" fuel design without a liquid bond between the fuel and the inner cladding wall enables the designer to put the bulk of the plenum volume below the active core where temperatures and thus gas pressures are lower, as is often done in ceramic-fuelled fast reactors. Annular metallic fuel is manufactured with an internal circular void, and the fuel swells inward to fill up this void rather than outward toward the cladding as a conventional fuel rod.

The fuel annulus, cladding and liner could potentially be manufactured using a co-extrusion process. Alternatively, the cladding

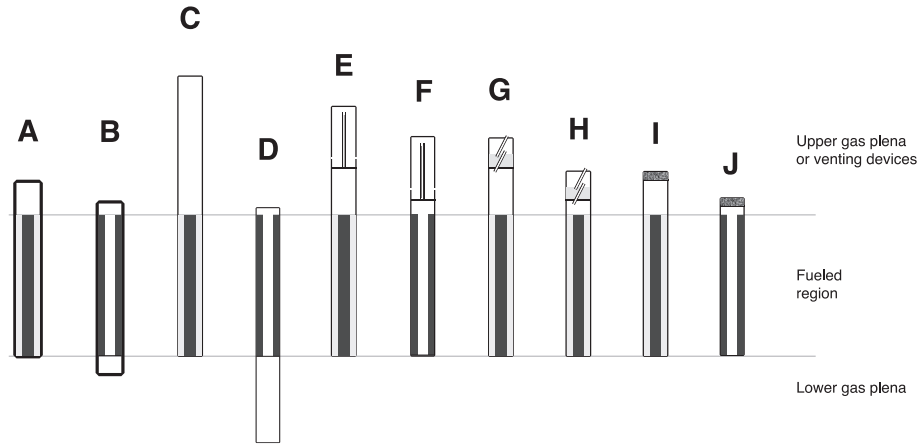

Fig. 2. Fuel rod design options using metallic fuel.

Table 1
Fuel rod design options and their neutronic impact.

Rod ID	Fuel type	Fission gas management principle	Neutronic impact
A B	Cylinder, sodium bond, thick clad Annular, no liquid bond, hick clad	Thick cladding wall maintains integrity at high pressure	Severe spectral softening and parasitic absorption due to the large volume fraction of cladding steel in the active core region
C D	Cylinder, sodium bond, thin clad Annular, no liquid bond, thin clad	Large fission gas plenum volume (either above or below the core depending on bond) maintains integrity by keeping pressures low	The very long overall fuel rods increases pressure drop and thus reduces the attainable fuel volume fraction in the active core
E F	Cylinder, sodium bond, thin clad Annular, no liquid bond, thin clad	Vent-to-coolant of fission gas through hydrostatic diving bell venting device at top of the rod	Marginal improvements over options C & D (for core designs with high coolant flow velocity) due to considerable length requirements of the venting device itself
G H	Cylinder, sodium bond, thin clad Annular, no liquid bond, thin clad	Vent-to-coolant of fission gas through hydrostatic DISCA-type venting device (Martini and Gerosa, 1973) at top of the rod	Significant further improvement over options E–F since the DISCA design requires far less axial space
I J	Cylinder, sodium bond, thin clad Annular, no liquid bond, thin clad	Vent-to-coolant of fission gas through porous plug at top of the rod	Enables a very short overall fuel rod length as well as a thin cladding, making it the best neutronic option for the B&B application

Table 2
Core design parameters assumed for this study.

Parameter		Value
Thermal power		1250, 2500 and 3500 MW
Fuel type (see Sections 3.2 and 3.3)		Annular pure metallic (no alloying materials) depleted uranium alloy (0.25% ^{235}U) with 75% smear density
Fuel batches	2D	12
	3D	12 radial batches with 4 independent axial fuel paths
Primary coolant		Sodium
Plant layout		Pool-type
Structure (cladding, wire, duct, reflector pin)		HT9 steel
Absorber material and layout (shield, control system)		All shield and absorber material is B_4C with natural composition boron. 19 independent control assemblies are used in each core design (regardless of core size). 25 cm of shielding material is placed at the bottom of each fuel rod, and one row of shielding assemblies is located at the radial periphery.
Coolant friction pressure loss in the primary cycle outside of the core		17% of total (assumed)
Coolant inlet and average outlet temperature		355–510 °C (ΔT_{co} = 155 °C)
Fuel rods per assembly		$\geqslant$169
Rod spacing		Wrapped wires with a pitch (pitch: the axial length of a 360° revolution around the pin) 25 times that of the outer diameter of the rod
Fission gas plenum		None (plug-venting of fission gas)
Cladding thickness ratio (CTR) The thickness of the cladding (T_c) is calculated as T_c = CTR * D, where D is the outer fuel rod diameter		0.05

and liner could be manufactured separately from the fuel, with the fuel then manufactured with a slightly smaller outer diameter than the inner diameter of the cladding liner. When co-extruded, the fuel is bonded with the cladding steel from the very beginning. If separately manufactured, the fuel annulus would quickly fill the space between its original outer diameter and the inner wall of the cladding liner, due to differential thermal expansion and fuel swelling. In both cases, the mechanical contact between fuel and

cladding results in very low thermal resistance, which enables such fuel to avoid the need for a liquid bond. This also reduces the required length of the rod, which in turns reduces the pressure drop through the system for a given flow velocity, fuel rod diameter and lattice pitch. Thus, for a given pressure drop constraint, the below-core plena design options allow for a slightly smaller fuel pin pitch and thereby higher fuel volume fraction in the core, which is part of why they are ranked as more attractive than their above-core plenum counterparts.[1]

In order to keep both a thin cladding wall thickness and a short overall fuel rod, various methods of venting the gaseous fission products directly to the flowing coolant have been developed; they are featured in options E–J in Fig. 2. The issues regarding fission gas venting are covered in detail in Section 3.3.

Out of all the design options studied, annular metallic fuel with venting of fission gases through a porous plug (option J) was identified as the neutronically most desirable. It offers the shortest overall fuel rod length while maintaining a thin-wall cladding, thus offering the best neutron economy of all options studied. The annular fuel (option J) outperforms the cylindrical fuel (option I) due to a lower resulting pressure drop as well as a smaller neutron moderation and parasitic absorption due to the absence of a sodium bond. Fortuitously, it is also the only fuel design option that can meet the design requirements of 3D-shuffling B&B cores, as is explained in more detail in Section 4.

3.2. Fission gas venting

A number of fission gas vent-to-coolant devices have been developed for use in sodium cooled fast reactors (SFR), but studies of fission gas venting systems have primarily been focused on use in gas-cooled reactors (General Atomics, 1974; Schleicher et al., 2013; Farmer et al., 2006). Peach Bottom Unit 1 in the US, a 40-MWe helium-cooled reactor, was an early US reactor to utilize fission gas venting (Steward, 1978). The only liquid metal cooled reactor that has operated with a vent-to-coolant fuel rod design is the NaK-cooled Dounreay Fast Reactor (DFR) in the UK, in operation between 1959 and 1974. While it has been shown that venting could improve the performance of standard SFRs, venting is not strictly needed and complicates system operation and licensing[2], which is likely why it is rarely a design choice for SFRs. The primary focus of SFR venting system design studies has been on hydrostatic venting, particularly variants of the "diving bell" concept invented by General Electric in the early 1960s (O'Neill, 1965; McNelley, 1964). The design and principle of the diving bell and further-developed "DISCA"-type hydrostatic venting device designs are shown in Fig. 3.

The hydrostatic venting devices are designed to allow gas to be released to the coolant without coolant intrusion into the pin. Gas is released from a capillary into a gas volume above the fueled region of the rod, which in turn has a pinhole through which gas can be released into the coolant flow. The pressure build-up of gas inside of this volume pushes the coolant level in the volume downward toward the pinhole and finally allows the release of fission gas bubbles. The gas pressure also keeps the coolant from entering the capillary and reaching the fueled part of the rod. The DISCA device relies on the same principle but instead of pinholes out the side of the rod has an outlet capillary at the top of the rod (Martini and Gerosa, 1973). Hydrostatic venting devices such as the diving bell or DISCA can significantly reduce the length and required cladding thickness of a fast reactor fuel rod compared to the standard fission gas plenum design, especially for designs reaching a high level of burnup. However, even the DISCA device, which takes up the least axial space of the hydrostatic systems, require more than 20 cm of axial space, which is far longer than could be accepted in an axially segmented 3D-shuffling system (Martini and Gerosa, 1973).

A much more space-efficient way of venting is through a simple porous plug mechanism. The fuel rod then has a metallic or ceramic plug in the end of the fuel rod with one side exposed to the coolant and the other side exposed to the fission gas. In the original designs of vent plugs, the vent would have to allow the fission gas to pass while keeping out the sodium coolant (Lipps, 1968). Some investigations into the wetting characteristics of metallic-plug vents made of iron, nickel and chromium-nickel with pore sizes between 1 and 5 μm were done at Karlsruhe in the 1960s and it was found that sodium leakage through the plug started at a pressure of 150 kPa with sodium at 500 °C (Smidt and Sommer, 1965a).

Venting systems that do not allow coolant penetration into the pin is mandatory for UO_2 fuel rods since UO_2 is incompatible with sodium. On the other hand, metallic fuel is chemically compatible with sodium (standard metallic fuel has a sodium bond). However, when communication of the coolant with the fueled region of the rod is allowed (regardless of fuel type), there is a risk for additional activity in the sodium. This additional activity will increase the shielding required for the primary loop and will complicate maintenance and detection of failed fuel. The fission products do not greatly increase the shielding requirements since their activity is masked by the intrinsic activity of the sodium, as confirmed by studies conducted by Westinghouse Electric for sodium-bonded carbide fuel rods which indicated there would be only a small effect on the system if the bond and coolant sodium are mixed (Lipps, 1968). There is also a possibility that fissionable material will enter the coolant stream and deposit somewhere in the loop. The loop must therefore be designed to minimize the locations where fissionable materials can collect. These problems appear much less severe for metallic fuel, since RCBC (run beyond cladding breach) tests have confirmed that fuel loss of metallic fuel at moderate temperature – which is expected in B&B cores due to their low-power density, even when directly exposed to sodium coolant flow during extended periods of time is practically zero. Fig. 4 shows the result of experiments exposing metallic and oxide fuel to sodium (Chang, 2007). The oxide suffers a significant loss of fuel to the sodium while the metallic fuel has shown no sign of interaction with the sodium after 169 days of continuous contact[3], including many start-up and shutdown transients.

A simpler, more efficient but less studied venting strategy is possible in principle: direct venting. Direct venting simply means that a number of small holes are drilled in the upper fuel rod end cap, which allows for free communication between the internals of the fuel rod and the primary coolant loop. While such a design would require the least axial space, a major disadvantage of direct venting is that the fission gas isotopes will have little time to decay within the fuel rod itself, which will result in a significantly higher activity of the fission gases reaching the cover gas (Keilholtz and Battle, 1969). Calculations indicate that the relative equilibrium activity of the cover gas is reduced by 80% with fission gas retained within the rod for 1 day on average, and by 90% with a 5-day retention period (O'Neill, 1965). The preferred option for the B&B cores

[1] While using a below-core gas plenum decreases the overall length of the fuel rod, there are potential safety implications. A failure of the rod that releases the trapped gas below the core would cause bubbles to axially traverse the active core, which is equivalent to a localized coolant voiding. In larger fast reactors and all B&B reactor designs this causes both a deterioration of the cooling efficiency as well as a positive reactivity insertion.

[2] Fission gas venting effectively removes one of the barriers between radioactive material and the environment, and is thus a step away from the well-known design philosophy of "defense-in-depth".

[3] Metallic fuel-sodium contact has been established in RBCB (run beyond cladding breach) tests for up to 223 days, but the specific metallic fuel rod shown in Fig. 4 was tested in the reactor in a breached state for 169 days.

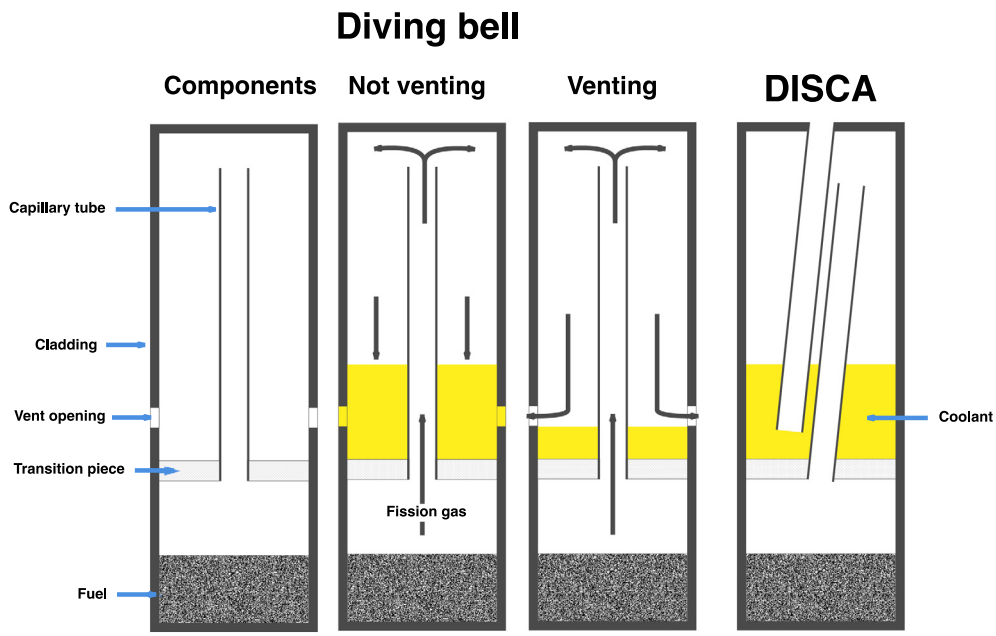

Fig. 3. Diving bell and DISCA hydrostatic venting device schematics.

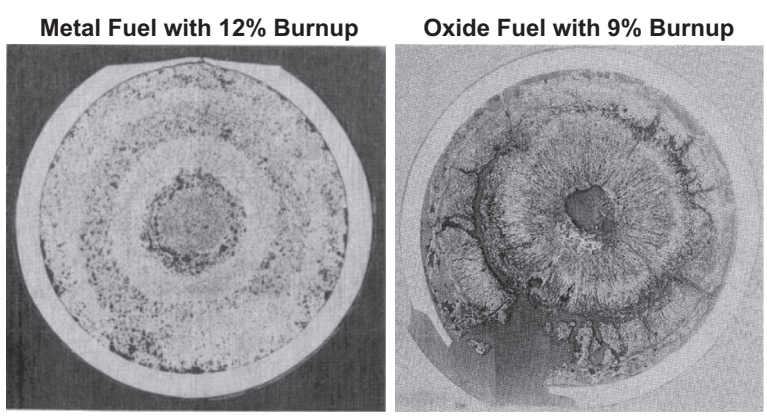

Fig. 4. Result of fuel/coolant contact for metallic and oxide fuel (Chang, 2007).

is therefore to vent through a short (~1 cm) porous filter-plug, which is designed to retain fission gases for an average of at least 5 days.

The major safety concern in the vented fuel concept is the potential for gas entrainment in the primary coolant. Several potential problems can result from gas recirculation, such as cavitation of the pumps, formation of hot spots possibly near grid spacers (when used), and flow blockage. Fission gas recirculation has been shown to be highly probable, especially in loop-type reactors when venting directly out to the flowing coolant using the pinhole-type vents as in hydrostatic venting devices (Lipps, 1968). To avoid this issue for the porous-plug vent, the venting is designed to be from the top rather than the side of the fuel pin. It may be possible to add a fixture on top of the porous plug carefully designed to vent the gases as large enough bubbles to maximize the probability of fission gas transport to the cover gas for coolant velocities up to 12 m/s.

Assuming that an average of about 0.27 gaseous fission products are produced in each fission reaction (Waltar et al., 2012), a 3 GWt FBR produces about 4.2×10^{-5} moles/s of the gaseous fission products, 100% of which is assumed to be released from the metallic fuel. At 500 °C and near-atmospheric pressure, this corresponds to a summed total of about 2.7 cm^3/s of gas release from all the pins of the core. For the 3D-shuffling design, most of this gas will be released inside the active core. An SFR of this size has a volumetric coolant flow on the order of 20 m^3/s, and the fission gas release inside the 3D-shuffling core could thus create an equivalent "void" of 1.35×10^{-5}%, too small to have any noticeable effect on core reactivity and cooling.

It has been shown that in extremely severe accident scenarios in sodium-cooled reactors with conventional metallic fuel rods (Type C of Fig. 2), the interplay between melting/molten fuel, liquid sodium bond and pressurized fission gas acts as a self-limiting accident mitigation feature (Cahalan et al., 1994). At present it is not at all clear to what extend the same features are present when using an annular plug-vented fuel (type J of Fig. 2).

3.3. Fuel assembly design

The fuel assembly design of the 2D-shuffled B&B core of this study follows the conventional ducted hexagonal assembly design that is used in most fast reactor designs. The major differences are a thicker-than-reference duct wall due to the long residence time;

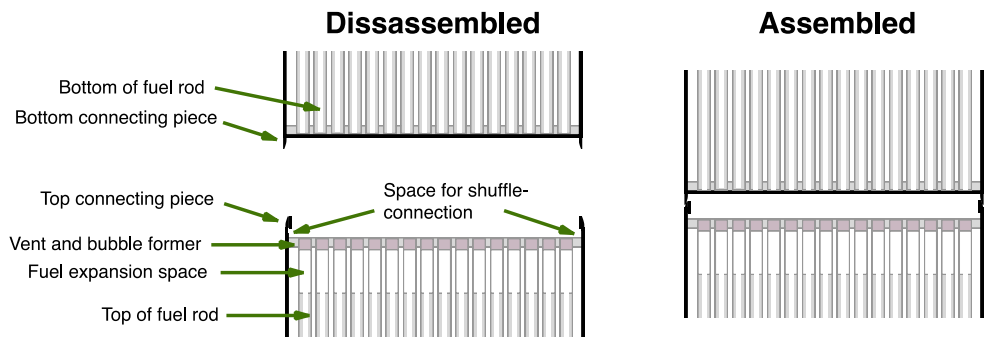

Fig. 5. Concept of connecting assembly segments (not to scale).

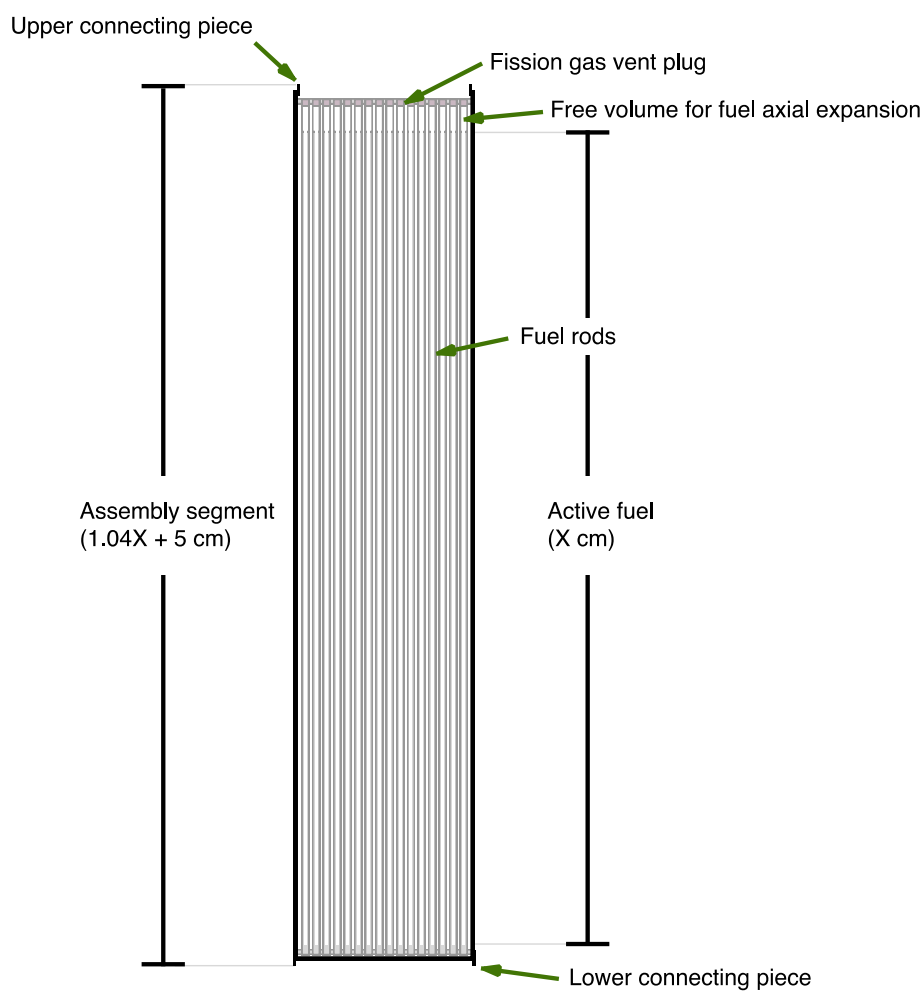

Fig. 6. Fuel sub-assembly schematic design for 3D B&B.

a longer assembly; a high pressure differential due to high coolant pressure drop; and high levels of fast neutron fluence (Qvist, 2015).

4. Design considerations for 3D-shuffling of B&B cores

One of the objectives of this study is to design a B&B core in which 3D fuel shuffling can be implemented. The fuel assembly design for the 3D-shuffled B&B core presents a number of new challenges. The general approach taken is to axially subdivide the fuel assembly into several segments or "sub-assemblies", which can be axially connected to form a fuel assembly equivalent to that used for the 2D-shuffled core design. When the reactor is shut down for shuffling, the sub-assemblies are disconnected from each other by the fueling machine and can be moved individually to new positions in the core both radially and axially.

The fuel sub-assemblies are connected with upper and lower connecting pieces by sliding on to one another as illustrated in Fig. 5. In the reference design, the top 15 mm of the duct, above the top end of the fuel rods, is chamfered inwards. In the bottom of the assembly segment, the duct wall is chamfered outward for an additional 15 mm below the fuel rods. In this way, the outward

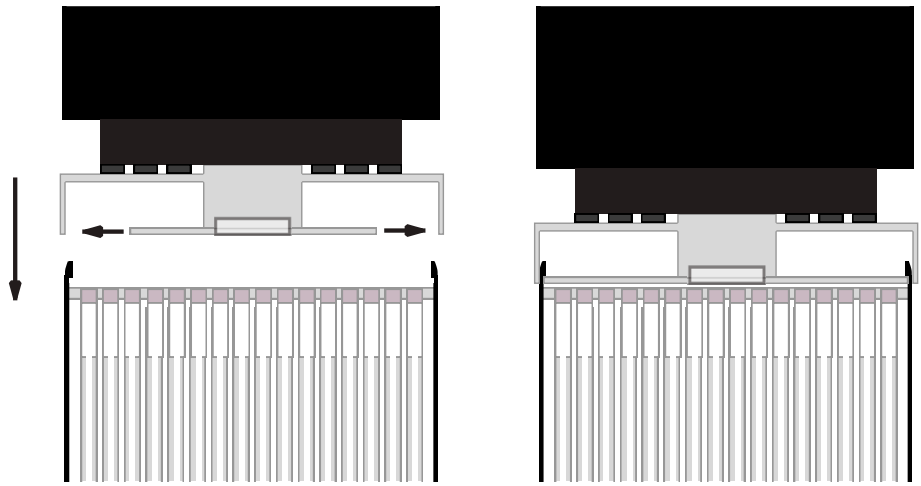

Fig. 7. Concept of shuffling machine connection to assembly segments.

bending of the bottom connecting piece slides on to the inward bending part of the connecting piece at the top, forming a continuous assembled unit of several segments. In addition, the duct wall is thickened at a section of the top to provide a ledge below which the shuffling machine may connect for lifting the assembly segment. Each individual sub-assembly rests on top of the sub-assembly below using the chamfered connectors design approach. They are not mechanically attached but pressed in place by an assembly hold-down mechanism attached to the upper internal structure (UIS) above the core. The sub-assemblies at the axial bottom rest on top of shielding and orificing pieces that are designed to remain in place throughout the life of the core. These components have chamfered upper connecting pieces that are identical to that of the fuel sub-assemblies.

The standard fast reactor fuel rod design approach (Type C of Fig. 2) is not practical for the fuel rods of the sub-assemblies since a relatively large volume fission gas plena will have to be incorporated within the active core volume which will have a detrimental impact on the neutron economy. Similarly, there is no possibility in the axially segmented 3D-shuffling design to provide accommodation within the pin for the expulsion of a liquid bond. Finally, conventional metallic fuel is known to swell axially by up to 10% (Chang, 2007), which will require an increase in the plenum length.

The 3D-shuffling core requires a fuel design of minimal axial length, no liquid bond and, if possible, minimized axial swelling of the fuel itself. The only identified option that could work is the annular plug-vented design that was already determined to be the neutronically optimal from the more general study of Section 3.1. Since the annular metallic fuel is in mechanical contact with the cladding steel at or near beginning of life, it is expected that it will be significantly inhibited in its axial swelling compared to that of a conventional rod (Walters, 2011). Fuel performance modeling for the Advanced Fuels Campaign (AFC) using the BISON code indicates that axial swelling is reduced at least by a factor of 5 going from solid cylinder to annular fuel (Medvedev, 2012).

Annular helium-bonded metallic fuel using pure uranium metal (and an inner liner on the cladding acting as a diffusion barrier) will be tested in the Advanced Test Reactor (ATR) in the AFC-3 and ACF-4 campaigns (Idaho National Laboratory, 2013). In addition, upcoming irradiation campaigns of "mechanically bonded" metallic fuel in the Indian Fast Breeder Test Reactor (FBTR) will make it possible to more clearly estimate the axial growth of this type of fuel (Kaity et al., 2012). Results from these experiments, the first of which will finish in early 2015 (Maloy, 2014), should verify whether the fuel rod designs developed in this study could in fact be used in axially segmented core designs utilizing fuel shuffling in three dimensions.

Annular metallic fuel was manufactured by Argonne National Laboratory in the early 1960s and tested in the Experimental Breeder Reactor (EBR-1). Results from these campaigns show that the fuels swell inward to fill up the void annulus and exhibit no axial swelling at all, but the fuels were only tested to a volume-averaged burnup of about 2.2% (Horak et al., 1962). Since the bulk of total swelling occurs within the first few percent of burnup, these results, while inconclusive for high-burnup systems, are highly encouraging. In order to remain conservative and make provision for the potential swelling by solid fission products, the assumption in this study (until newer experimental results are available) is that the fuel may swell by up to 0.2% of its initial length per % of burnup at burnups higher than 3%. The target B&B range of average discharge burnup is 15–20%, which means that the B&B fuel rod is designed to accommodate an axial swelling of 4%.

The general design concept for the assembly segments using annular plug-vented fuel (Type J of Fig. 2) of a 3D-shuffling B&B core is shown in Fig. 6.

Each sub-assembly is made up of the following axial components (from bottom to top):

- Lower connecting piece: 15 mm.
- Fuel: X cm (design variable).
- Fuel expansion space: 0.04*X cm (4% of fuel length).
- Porous vent-plug: 8 mm.
- Bubble-former piece: 2 mm.
- Free space for shuffling machine connector: 10 mm.
- Upper connecting piece: 15 mm.

An idea for the design of the lower connecting part of the pantograph shuffling machine is shown in Fig. 7. Fig. 7 is conceptual drawing and is not backed up by any engineering calculations or detailed study. The detailed design and analysis of a 3D shuffling machine suitable for this application will be the focus of future studies.

The total length of a fuel assembly segment (or sub-assembly) is given by:

$$L = 1.04X + 5[\text{cm}] \tag{2}$$

where X is the length of the fuel.

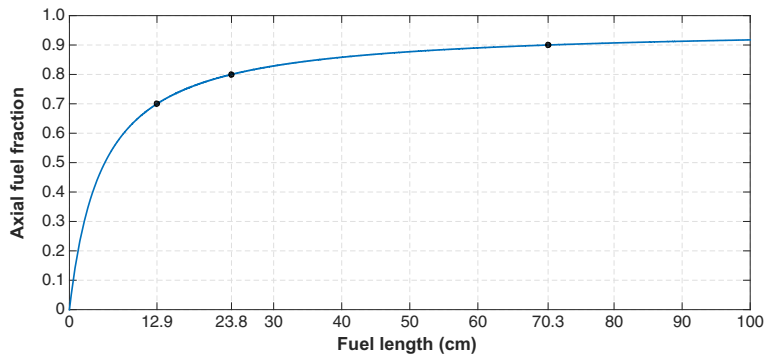

Fig. 8. Axial fraction of fuel vs. the fuel length in segmented assemblies.

The axial fraction of fuel is therefore:

$$F_x = \frac{X}{1.04X + 5} \tag{3}$$

Fig. 8 shows F_x dependence on L. With increasing fuel sub-assembly length, the importance of the 5 cm space for fuel axial expansion, venting, shuffling and connection pieces that are fuel-length-independent diminishes. There is a trade-off in the design of segmented fuel assemblies regarding the number of axial segments. A larger number of segments allows for a more even final burnup distribution and a more tailored shuffling path through the core. At the same time, the volume fraction of fuel in the core decreases with the number of segments, since the length of the unfueled segment of the sub-assembly (in this design, 5 cm) is independent of the sub-assembly length. This trend is shown in Fig. 8.

Due to these considerations and the fact that total fuelled lengths exceeding 300 cm is undesirable primarily due to pressure drop limitations, the 3D-shuffling B&B core designs of this study were confined to the following design space:

$$\begin{aligned} &3 \leqslant \#\text{ of axial segments} \leqslant 5 \\ &50\text{ cm} < \text{fuel length in segment} < 70\text{ cm} \\ &\text{Total fuelled length} \leqslant 300\text{ cm} \end{aligned} \tag{4}$$

There are numerous technical difficulties for implementation of the proposed 3D B&B core design, but the single most challenging part is the design and operation of the shuffling machine mechanism. Industrial robots in the manufacturing industry routinely perform pre-programmed operations more advanced than what is envisioned of the shuffling device, but they are not exposed to the same extreme environment of being submerged in hot and opaque liquid sodium in a strong radiation field. US fast reactor experts recently pointed out the difficulty of successful fuel shuffling from the experience in conventional 2D-shuffled cores such as EBR-II and JOYO in Japan (Sackett and Grandy, 2013).

3D-shuffling involves many more operations and is significantly more complex, and will therefore need very comprehensive further study. A large SWR B&B core may have as many as 400–600 fuel assemblies, meaning a total of 1200–3000 fuel assembly segments to be moved. In order to finish a complete fuel shuffling (every assembly segment relocated to a new position) within 1 month, the average time spent moving each assembly to its new location must be on the order of ~30 min. One advantage of the assembly segmentation is that the lifting force required for moving a single assembly segment piece is much smaller than for the full-length conventional fuel assemblies of corresponding size.

The present study focuses on quantifying the performance benefits that could be provided by 3D fuel shuffling assuming that such a shuffling could be technically realized. If the benefits turn out to be significant enough, it will be justified to embark upon the mechanical design as well as an extensive computational study to find the optimal set of operations to move each fuel assembly segment in a time-optimized practical manner.

5. Suggested B&B core fuel rod design

Figs. 9 and 10 show an axial and radial view respectively of the reference B&B fuel rod design using porous-plug fission gas venting and annular metallic fuel. The annular fuel is mechanically bonded to a 30 μm vanadium (or possible Zirconium) liner (Ryu et al., 2009), which acts as a diffusion barrier to avoid fuel/cladding chemical interaction (FCCI).

The ferritic/martensitic HT9 steel was chosen as the cladding material because it has the largest experimental database for high-dose neutron irradiation. As mentioned in Section 1, HT9 has been proven up to 200 DPA without excessive swelling or material property degradation. The incubation period before high-rate swelling sets in for optimized heats of HT9 is not yet determined, and could well exceed 300 DPA. HT9 steel irradiated in the Fast Flux Test Facility/Materials Open Test Assembly (FFTF/MOTA) campaigns and the FFTF ACO-3 duct has reached 160–200 DPA. Samples of these steels are currently under further irradiation in the BOR-60 reactor in Russia to extend the knowledge base for HT9 steel to at least 250–300 DPA (Maloy, 2014).

The DPA limit of the cladding steel is the principal technical issue holding back the performance of any fast reactor design, but the situation is critical for B&B cores due to the high neutron fluence required for sustained equilibrium cycle operation. While HT9 might be used for the structural components (cladding, wire and duct steel) of the first generation of B&B systems, advanced ferritic/martensitic steels such as NF616 or Oxide Dispersion Strengthened (ODS) alloys will likely replace HT9 as the reference material once sufficient irradiation data becomes available (Maloy, 2014). Ion irradiation results up to 500 DPA indicate that ODS steels such as MA957 and 14YWT will likely far outperform HT9. Void swelling at 500 DPA of ion irradiation was 9.9% for HT9, 4.6% for MA957 and a mere 1.6% for 14YWT (Maloy, 2014). These experiments need to be supplemented by neutron irradiation campaigns as well as a more complete understanding of the equivalence between the results from neutron and ion irradiations.

6. Core and core structure design considerations

The B&B reactors considered in this study are assumed to be of the conventional large pool-type sodium fast reactors design with pumps and intermediate heat exchangers (IHX) located inside the reactor vessel. Due to the axial segmentation of fuel assemblies in the 3D-shuffling system, a number of modifications to the reactor vessel and its components have been implemented. A preliminary conceptual design of a 3D-shuffling core with 4 axial fuel assembly

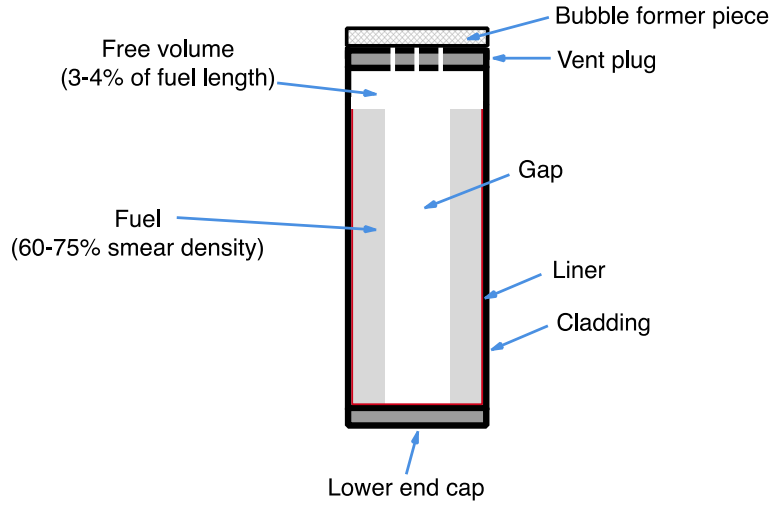

Fig. 9. Axial cut of vented B&B fuel rod design (not to scale).

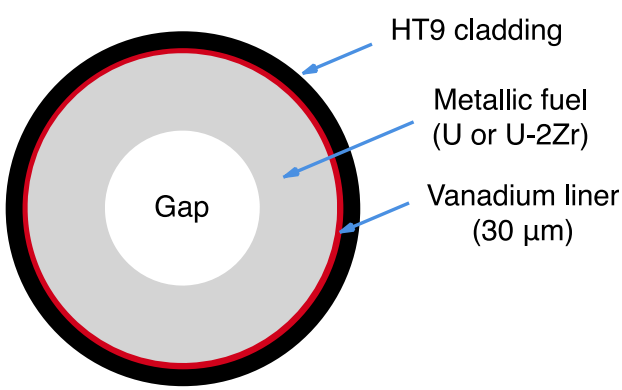

Fig. 10. Radial cut of a fuel rod for B&B core. Fuel smear density is 75%. To scale.

segments, not including components such as heat exchangers and pumps, is given in Fig. 11.

In the 3D-shuffling design, the assembly segment at the bottom of the core (Assembly segment 1/4 in Fig. 11) connects to a shielding and flow orificing block that is designed to remain in place in the reactor for the lifetime of the core. The shielding consists of vented enriched B_4C rods (90% ^{10}B) that protect the steel in the coolant inlet and orificing piece as well as the lower grid plate. In the 2D-shuffling design, axial shielding of the same type is installed at the bottom of the fuel assembly itself. At the radial periphery in both 2D and 3D shuffling core designs, one or more rows of static reflector & shield assemblies also remain in place for the entire core life and provide protection for the core barrel and vessel, as well as pumps and pump piping.

The 3D-shuffling design shown in Fig. 11 makes use of double rotating plugs with two separately off-center attached pantograph-type fuel shuffling devices. If proved feasible in more detailed analysis, the use of two semi-independent (the movements of one shuffling machine will restrict the movement options for the second) shuffling machines could significantly cut down the total time spent moving fuel assembly segments. In addition, a dedicated fuel loading and off-loading machine with full axial and limited radial movement is installed. Assembly segments to be discharged are placed on top of the radial shield assemblies in one of the 6 adjacent positions that can be reached by the fuel-loading machine. In principle, separate machines could be used for loading and discharge of spent segments, which could further speed up the process. A cost/benefit analysis will have to be performed in order to assess what complexity in fuel handling devices is beneficial as opposed to an increased time in fuel handling and a corresponding increase in reactor downtime.

Because of the relative frailty of the connecting pieces in the 3D-shuffling design, the radial bending of the stacked assembly segment need to be limited to avoid damage. It is therefore needed to use load pads on each assembly segment to ensure that the core is completely constrained radially and is not allowed to bow (or "flower") outward as temperatures rise. This design alteration effectively reduces the magnitude of the negative core radial expansion reactivity feedback that is of crucial importance for the safety of the standard SFR core design. This might be compensated by incorporating in the core autonomously operating reactivity feedback devices, as described in the following section. The continuous contact between assembly segments out to the core barrel can produce mechanical stresses if and when radial temperature and pressure gradients build up in the core, which will need to be accommodated by thicker duct walls as compared to the limited-free-bow design of the 2D-shuffling B&B core.

7. Safety systems and control

As mentioned in Section 2.1, the neutron economy required for B&B reactors operating with DU-feed fuel at equilibrium dictates the cores to be large with a low neutron leakage probability. This requirement presents a challenge to safety, since it is well known from previous studies that reactivity coefficients change for the worse with increasing core size and decreasing nominal neutron leakage probability (Wade and Fujita, 1987; Qvist and Greenspan, 2012) – the coolant temperature and void coefficients become more positive while fuel axial and core radial coefficients become less negative. In addition, the segmented fuel design of the 3D-shuffling B&B requires the core to be constrained radially, which reduces the magnitude of the negative radial expansion reactivity feedback coefficient because assemblies cannot bow outward. It is therefore not likely that these cores can be proven to be inherently safe in anticipated transient scenarios based on the feedback parameters of the core itself, implying the need for an additional engineered passive safety device.

The Autonomous Reactivity Control (ARC) system is a new safety device that can passively provide negative reactivity feedback in fast reactors that is sufficient to compensate for the positive coolant density reactivity feedback even in large low-leakage

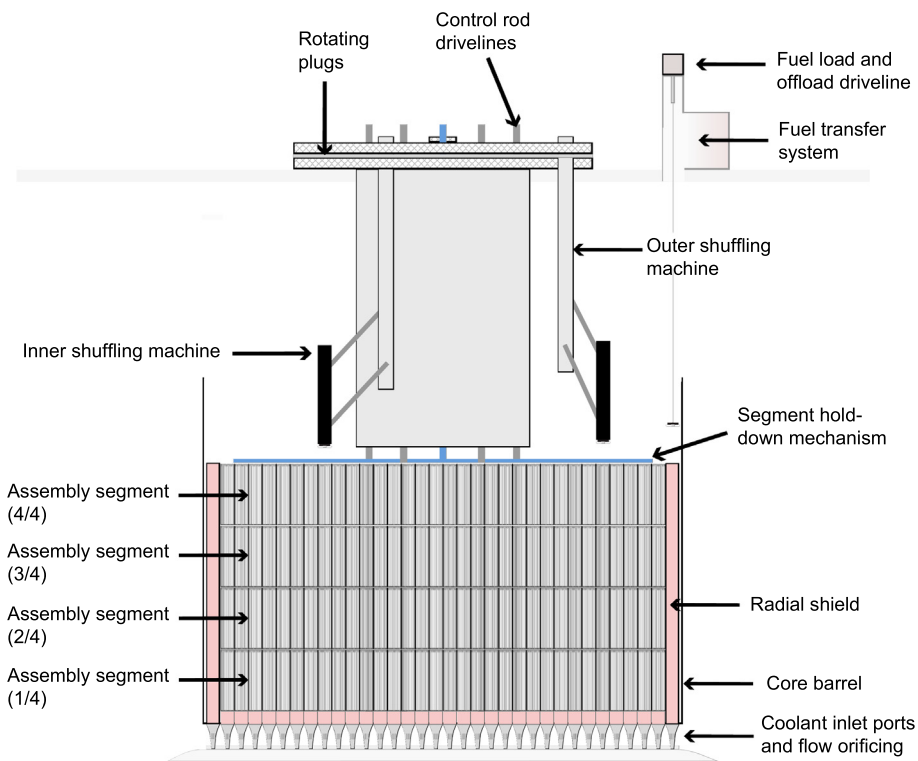

Fig. 11. A preliminary conceptual layout of a 3D-shufflinging B&B reactor.

cores (Qvist and Greenspan, 2014). The ARC system is actuated by the inherent physical property of thermal expansion, and has a very small effect on core neutronics at standard operating conditions. In its reference design, the ARC involves a replacement of a limited number of fuel rods in each assembly with pins that fill a specific safety role. Because the 3D SWR B&B requires axially segmented fuel assemblies, the standard ARC design cannot be implemented in such a core. Rather than replacing individual fuel rods within assemblies, some assembly locations within the core are reserved for dedicated control assemblies containing both active conventional solid-absorber control rods as well as passive ARC systems.

Fig. 12 illustrates ARC systems proposed for 2D shuffling core (left) and for 3D shuffling core (right). The ARC assemblies consist of an upper (located above the core) and lower (located below the core) reservoir of liquid, connected by tubes. The reservoirs are filled with two separate liquids that stay liquid and immiscible throughout the applicable temperature range of fast reactor operation. The lower reservoir contains a "neutron poison" liquid (^{6}Li) with a high neutron absorption cross-section. The upper reservoir is filled with a separate liquid with a small neutron absorption cross-section (Potassium). As the temperature of the coolant increases, the liquids in the reservoirs thermally expand, effectively pushing the absorbing liquid in the lower reservoir up toward the active core region while compressing the inert gas that fills the volume above the liquid between the inner and outer tubes of the ARC system.

Unfortunately, some of the unique advantages of the ARC system are lost when installed in a 3D-shuffling core. Since in 3D-cores the ARC-system cannot be installed within the fuel assemblies, the time-delay of actuation of the system will be increased and the redundancy will be lower (since a smaller number of systems will be present in the core). The ARC principle of actuation, shown in Fig. 13, is the same in both implementations. At state A (shutdown or refueling), the core is cold and the volume of the expansion liquid is small, leaving the liquid level of ^{6}Li far below the active core. At state B, the core is at nominal operating temperature and the liquids have expanded to bring the level of ^{6}Li up closer to the active core. Finally, in the transient event C, the temperatures have increased above those expected during standard operation and ^{6}Li is injected (contained within the ARC-tube) into the active core region and slows down the neutron chain reaction. Once the actuation of the system has brought temperatures back down, the liquids contract and re-equilibrate with the gas-pressure of the ARC-tube at the original state (B).

By installing a number of ARC-assemblies at fixed locations in the 3D SWR B&B core, it is hoped that acceptable core transient reactivity response can be achieved. Significant further R&D work is needed to assess the feasibility of the ARC-principle to assure passive safety of 3D SWR B&B cores and, if feasible, to optimize the ARC system design. Detailed safety analysis will be performed in future work to quantify these issues.

8. Core design of 2D and 3D-shuffling SWR B&Bs

8.1. General core design objectives and parameters

The primary objective of the B&B core design optimization enable equilibrium cycle operation on depleted uranium feed fuel while minimizing the peak DPA of the cladding steel, subjected to the design constraints as specified in Section 8.2. Optimal core design is searched for three power levels: 1250, 2500 and 3500 MWt (the core power levels considered covers the range of practical interest for B&B reactors); each for two fuel shuffling methods – 2D and 3D. The core volumetric power density for all systems was kept in the range of 70–90 MW/m^3, in between the typical values for Boiling Water Reactors (~50 MW/m^3) and Pressurized Water Reactors (~100 MW/m^3) Lewis, 2008. The design variables used for this study include the diameter and spacing of fuel rods, the thickness of the cladding and duct, the spacing between fuel assemblies and the irradiation cycle time.

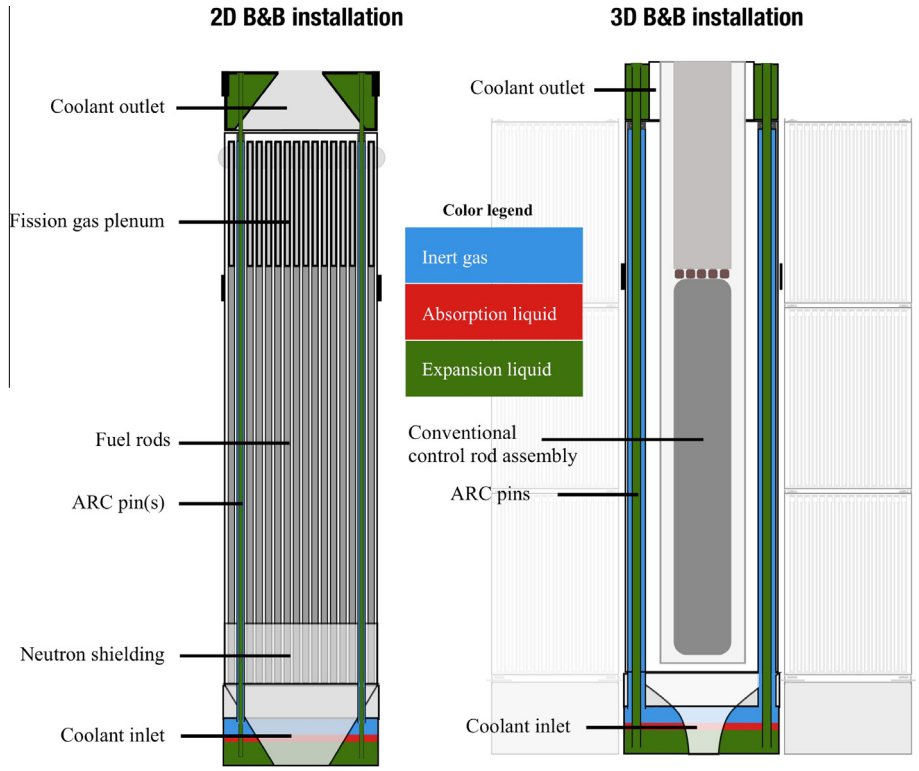

Fig. 12. ARC installation in conventional 2D (left) and 3D B&B cores (right).

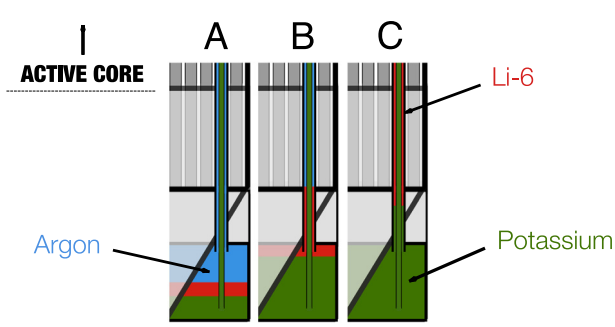

Fig. 13. States of actuation of an ARC installation: A = refueling/shutdown, B = standard operation, C = high temperature transient.

8.2. Design constraints

8.2.1. Thermal hydraulic constraints

Design constraints related to primary coolant flow often dictate the geometric parameters of the core. The most limiting constraint is coolant pressure drop, which is imposed by the mechanical limitations of the pump: the allowable nozzle-to-nozzle pressure difference and the volumetric flow rate. For a single-stage mechanical impeller sodium pump, the pressure limitation has been reported as ~1.38 MPa (200 psi) Barthold, 1974, so conservatively 1 MPa was adopted as a constraint for this study. In the US, the Clinch River Breeder Reactor Plant (CRBRP) design featured single-stage centrifugal primary pump with a pump head of 1.12 MPa (International Atomic Energy Agency, 1991), but the plant and pump were never built. The 20 MWe KNK-II reactor in Germany (operated between 1971 and 1991) had a reported primary cycle pressure drop of 1.5 MPa according to the IAEA "LMFBR Plant Parameters" report, which is the highest value of any fast reactor that has been in operation (International Atomic Energy Agency, 1991), but we have been unable to verify this number with additional sources.

The peak flow rate limitation of a single pump is not an issue since it can be avoided by simply adding more pumps. The coolant flow velocity is indirectly limited by the pressure drop constraint, but also by concerns for corrosion, cavitation and mechanical vibration of core components. This limit is not precisely defined and depends on parameters such as system temperatures and the coolant oxygen concentration. The Phenix 233 MWe SFR reactor (operated successfully between 1973 and 2009 at Marcoule in France), allowed a peak core coolant velocity of 12 m/s (International Atomic Energy Agency, 1991), which is now a generally applied limitation on the peak flow velocity of sodium.

Tighter limitations are imposed by inherent safety considerations. An inherently safe core must be able to terminate the fission chain reaction and remove the residual decay heat without the use of active systems. This implies that the decay heat from the core should be removed at acceptable system temperatures by natural circulation. The buoyancy pressure (P_{nc}) developed by a difference in coolant density is given by:

$$\Delta P_{nc} = gH_{xc}(\rho_{\text{heatsink}} - \rho_{\text{core}}) \text{ [Pa]} \tag{5}$$

where g is the gravitational constant (9.82 m/s^2), H_{xc} is the thermal center elevation between the core and the heat sink (m), and ρ is the density (kg/m^3) of the coolant at the thermal centers.

The pressure head for sodium as given by Eq. (5) for natural circulation flow at the nominal coolant temperature range (355–510 °C), becomes $P_{nc} = 358H_{xc}$. The friction pressure drop in the primary coolant loop is given by:

$$\Delta P_f = Xf_x m_x^2 \text{ [Pa]} \tag{6}$$

where X is a set of geometrical factors (of no importance for this discussion), f_x is the friction factor and m_x is the coolant mass flow rate.

One minute after the termination of the neutron chain reaction, around 3% of the nominal mass flow rate is required to remove decay heat while approximately maintaining the nominal core coolant temperature rise. Friction pressure drop scales by the square of the mass flow rate. The friction factor (f_x) increases as a function of Reynolds number – at 3% of nominal mass flow rate; the friction factor is about 3 times larger than at full-flow conditions (Qvist and Greenspan, 2014). This very crude analysis method can be used to estimate the required thermal center elevation between the core and primary coolant system heat sink to remove the heat by natural circulation as:

$$H_{xc} = \frac{\Delta P_{100\%} N_{\text{flow}}^2 N_{\text{friction}}}{g(\rho_{\text{heatsink}} - \rho_{\text{core}})} [m] \quad (7)$$

where $\Delta P_{100\%}$ is the full-flow pressure drop, N_{flow} is the normalized flow rate at the analysis conditions (3% = 0.03) and N_{friction} is the normalized friction factor of the fuel bundle

For the 3D SWR B&B the approximate values are $\Delta P_{100\%}$ = 1.0 MPa, N_{flow} = 0.03, N_{friction} = 3, which indicates a required thermal elevation distance of ~10 m for a temperature range of 355–510 °C. While this is a large value, several fast reactors have been constructed with internal vessel heights in excess of 17 m, which could accommodate such a heat transport loop (International Atomic Energy Agency, 1991).

8.2.2. Structural constraints

The solidus temperature of uranium metallic fuel is ~1100 °C (Rough, 1955). Applying a 30% margin-to-melt at standard operation gives a peak allowable fuel temperature of 770 °C. The cladding and duct steel are limited to a peak temperature of 560 °C to limit the drop in mechanical strength. The steel stress limits are taken from the American Society of Mechanical Engineers (ASME) code ASME, 2005. The duct thickness and inter-assembly gaps for all cores were calculated using the ADOPT methodology (Qvist, 2015), but will require more detailed future analysis of the special requirements of duct-connecting pieces in the 3D-shuffled design.

8.2.3. Summary of applied constraints

The constraints that were applied in this study to the core design are summarized in Table 3.

No direct constraints were imposed on parameters such as the reactivity swing over a cycle, the power peaking factors and the power change in a batch over a cycle. These shuffle-scheme-dependent factors are instead regarded as optimization parameters, based on which the relative merits of different shuffling schemes can be determined.

8.3. Core design methodology

The core design and optimization process has been automated to a large degree by coupling the ADOPT and Serpent code packages (Qvist and Greenspan, 2014; Leppänen, 2010). The EDIS code (Qvist, 2013) was added as a function in the ADOPT code to perform the fuel shuffling and enable automated search of the equilibrium core for the specified shuffling scheme. The ADOPT code takes the set of general input parameters and design constraints as defined in Sections 8.1 and 8.2 and optimizes the core geometry by performing thermal–hydraulic and structural-mechanic calculations. ADOPT produces a full-detail Serpent input file pertaining to the "optimized" core geometry and composition, and then iteratively runs Serpent to update initial guesses for most importantly the power peaking factors, and finally converge on the core power & flux distribution (which cannot be known a priori). Both the ADOPT and EDIS codes were re-written for this study to enable the simulation of the unconventional geometry of the 3D-shuffling B&B cores.

Table 3
Design constraints.

Parameter		Value
Thermal hydraulics	Primary loop pressure drop limit	1 MPa
	Sodium flow velocity	<12 m/s
Mechanical	Duct & cladding stress	$<2/3\sigma_y$, $1/3\sigma_{\text{uts}}$
Temperature	Fuel	770 °C
	Cladding	560 °C
	Duct	

The codes and structure employed in the B&B core design search is illustrated in Fig. 14. ADOPT/ADODPT-3D produces a core design using best-guess initial values, which are then sent to EDIS/EDIS-3D, which iteratively runs the Serpent code to find the critical cycle time of the given system. Once a critical system is found, the power and flux distributions of the core as calculated by Serpent are fed back into ADOPT/ADOPT-3D to restart the process. This scheme is repeated until a converged critical core design has been found. In general, the EDIS/EDIS-3D code can find the critical cycle time within 3 attempts. The power distribution and the maximum cycle radial power peaking factor (which determines the thermal–hydraulic solution and volume fraction of fuel) require 4–5 iterations to converge to an error less than 2%. This means that for each core design option, around 12–15 full equilibrium cycles need to be analyzed. Parallelization techniques for the computational analysis were extensively used on UC Berkeley and Uppsala University computational clusters in order to cut down the total simulation time.

The ADOPT code methodology is built on the principle of "Constrained Nuclear Design" (Barthold, 1974) to optimize the core design. Optimized here refers to a core design that pushes core performance to the limits of the thermal–hydraulic and structural-mechanical constraints that confine the design space. This means, for example, that the primary coolant velocity will be at precisely the value allowed by the velocity and pressure drop constraints, which will give the most efficient (optimized) heat removal capability, allowing the highest volumetric core power density. If a constraint is violated, for instance if the peak centerline temperature of the fuel is too high; the code adjusts one variable – in this case, the number of fuel rods in the assembly, and reruns all calculations until all constraints are met simultaneously. In this way, an optimized design can be arrived at quickly for a single defined set of operational parameters and constraints.

8.4. Neutronic analysis method

The neutron transport calculations were performed using the Serpent neutron transport code with the ENDF/B-VII.0 cross-section library (Leppänen, 2010; Chadwick, 2006). To speed up calculations, the active cores were modeled as 108 equi-volume burnup zones of homogenized composition in the 2D-shuffled cores (9 axial burnup zones) and 144 zones in the 3D-shuffling cores—3 burnup zones per fuel segment in the 3D-shuffling cores. This modeling approach has been shown to be accurate for modeling of fast spectrum B&B core equilibrium cycle analysis (Heidet, 2010).

9. B&B fuel shuffling paths

9.1. Principles of B&B shuffling

Three-dimensional shuffling of 48 fuel batches (12 radial, 4 axial) can be arranged in a near-infinite number of ways.

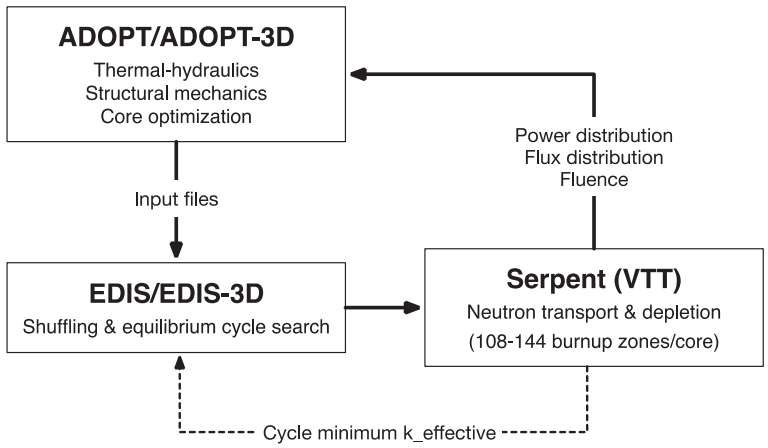

Fig. 14. Equilibrium B&B cores search methodology.

Complete optimization of the shuffling path is not amenable to brute-force numerical studies using the computationally intensive simulation tools presently in our use. Previous studies searched for optimal 2D SWR B&B shuffling using genetic algorithms that improve the shuffling path through thousands of iterations (Toshinsky et al., 1999, 2000). Such methods are not practical to apply when using a Monte Carlo transport code; they will be implemented in the future using deterministic diffusion theory based codes. In the present work the search for optimal shuffling path is guided by five considerations – simultaneously minimizing:

A. peak steel DPA.
B. neutron leakage probability.
C. reactivity swing during the cycle.
D. power change within a single batch during the cycle.
E. radial power peaking factor.

For any rational shuffling scheme that does not place high k_∞ fuel near the core periphery (resulting in a high neutron leakage probability), the minimum average discharge burnup is relatively insensitive to the shuffling path, assuming the same radial power peaking factor. A typical evolution of k_∞ with burnup of a metallic DU-fuel batch in a sodium-cooled reactor is shown in Fig. 15. The system reactivity swing and the power change within one batch during the cycle are both minimized by ensuring that the batches climb the steepest part of the "k_∞-ladder" (region 1 of Fig. 15) at a low flux low importance location – usually outside of the core central region.

When the batch is within region 1, and k_∞ increases from ~0.25 to above 1.0, the batch will experience a large change in relative power output, regardless of where it is placed in the core. If the batch is in or near the core periphery (in a low flux region), it may take a number of cycles to make this climb in k_∞ and the absolute change in the batch power will remain low, a situation which is easily managed. If the batch were to be placed near the core center while still in region 1, the high flux would cause it to rapidly climb in both k_∞ and power output, and its total impact on core reactivity and power would be far higher. A large change in batch power output during the cycle will penalize the energy conversion efficiency of the reactor. This is because the flow rate must be designed to handle the peak-power conditions so that the batch will be significantly over-cooled for the bulk of the cycle. Overcooling implies reduced coolant average outlet temperature and, hence, reduced thermodynamic efficiency. In principle, it may be possible to design the batch coolant flow rate to vary over the cycle, but such an approach will complicate the design and will introduce safety and reliability concerns. The larger positive reactivity swing over the cycle that results from placing region-1 fuel in the center of the core will have to be compensated by more extensive reactivity control system.

From the viewpoint of minimizing C (Reactivity swing) and D (Batch power-change), it appears clear that the batches should initially be kept near the core periphery, and once they have reached region 2 of Fig. 15, they may enter a higher-worth region of the core. This approach means that only batches with the highest value of k_∞ (producing the most excess neutrons) are placed near the core center, which also represents the most neutronically effective shuffling strategy since the neutron leakage probability is minimized. The resulting shuffling scheme considering factors A, C

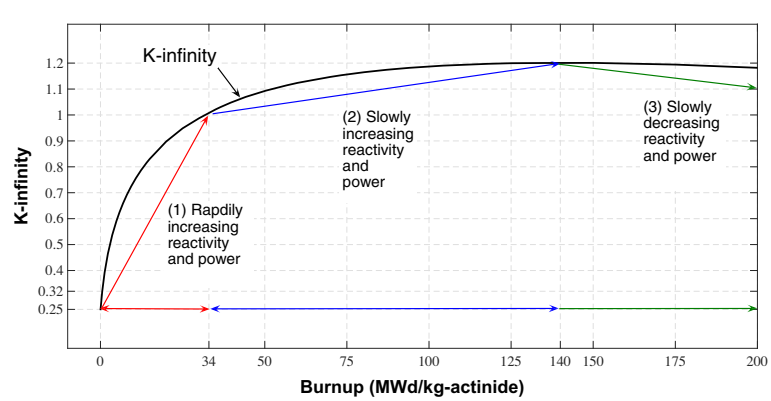

Fig. 15. Infinite multiplication factor change regimes with burnup.

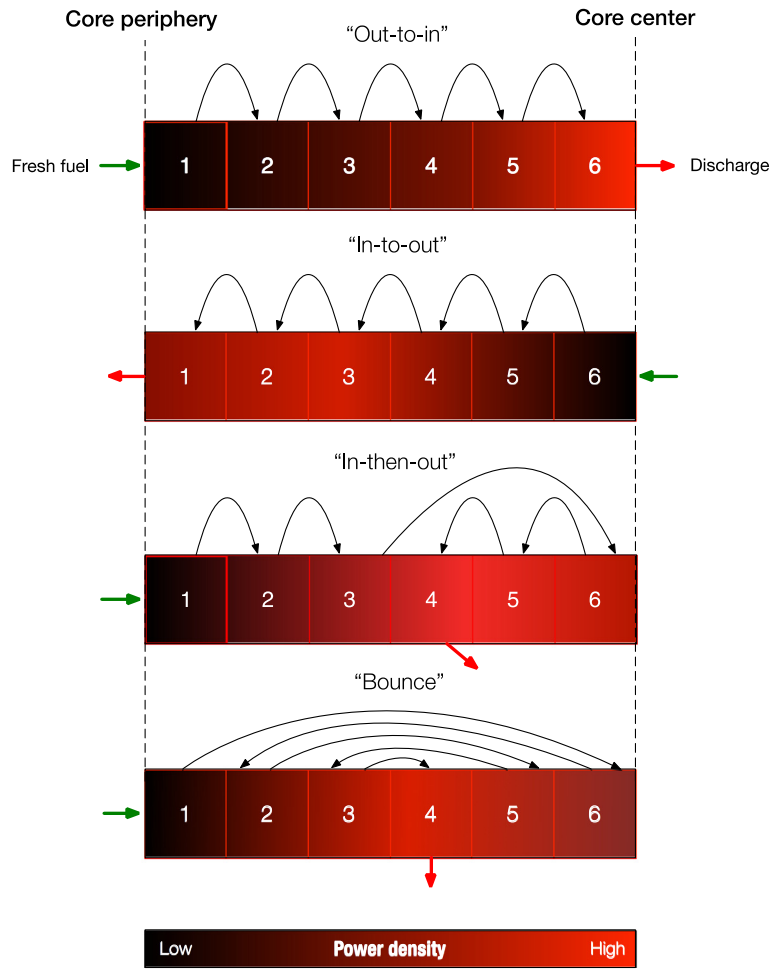

Fig. 16. Classification of strategies for radial B&B shuffling in a 6-batch system.

and D is thus simply an "out-to-in" strategy: load fuel at the core periphery and then sequentially move it inwards and finally discharge it from the center of the core. Unfortunately, the out-to-in shuffling strategy leads to an extreme radial power peaking, since fuel with high k_∞ is in the highest-worth spatial region and vice versa. The result is that the majority of power is produced near the radial center of the core, with the peripheral zones contributing next-to-nothing. For a given nominal core power a higher peak power density leads to a need for a larger coolant volume fraction and therefore lower effective actinide density and, thereby, increased peak DPA.

The opposite strategy ("in-to-out"), to load depleted uranium at the radial center of the core and then shuffle it outwards, leads to other but no less severe problems. In such a shuffling scheme, very low k_∞-fuel is placed in the inner radial regions, while higher k_∞-fuel is situated farther out toward the radial periphery. The radial power peaking factor is reduced significantly – from up to 7.0 in the case of out-to-in down to around 1.6 for in-to-out, but this comes at the cost of a very high neutron leakage probability, which requires prohibitively high levels of discharge fluence and DPA.

A compromise between the two extreme alternatives (out-to-in and in-to-out) is a shuffling scheme based on a "bounce" or "in-then-out" movement of assemblies. Fresh assemblies are loaded at the core periphery, but are then moved in and out of the more central regions of the core until they are finally discharged near the radial mid-point between the center and periphery. The shuffling path and power densities resulting from these four shuffling strategies are shown for a simplified 6-batch core in Fig. 16. Schemes such as the "bounce" and "in-then-out" maintain the good neutron economy of the out-to-in strategy while having a radial power peaking factor as low as ~1.8–2.0. Using a higher number of batches allows for more complex and potentially more optimal shuffling schemes, usually as a combination of the general "bounce" and "in-then-out" ideas.

9.2. Studied shuffling paths

The 12-batch shuffling scheme used for the 2D-shuffling cores in this study (shown at the top of Fig. 17) is based on the result of previous parametric studies by Heidet (2010). The 3D-shuffling scheme is illustrated in the bottom Fig. 17 for a core having 12 radial batch-zones using 4 independent axial fuel paths. The different colors of the 3D shuffling schemes as shown in the bottom of Fig. 17 indicate the four independent shuffling paths, while the numbers indicate the fuel location as a function of the step in the burnup cycle (1 where the fuel is loaded and 12 where the fuel is discharged).

This 3-D shuffling scheme was arrived at guided by the following considerations that aimed to maintain a low core leakage probability while minimizing the radial power peaking:

- Fresh depleted uranium fuel is loaded at the core outermost radial zone so as to minimize neutron loss via leakage in the radial direction. Considering the small thickness of the outer radial zones, once or twice burned fuel should also be loaded in the adjacent regions.

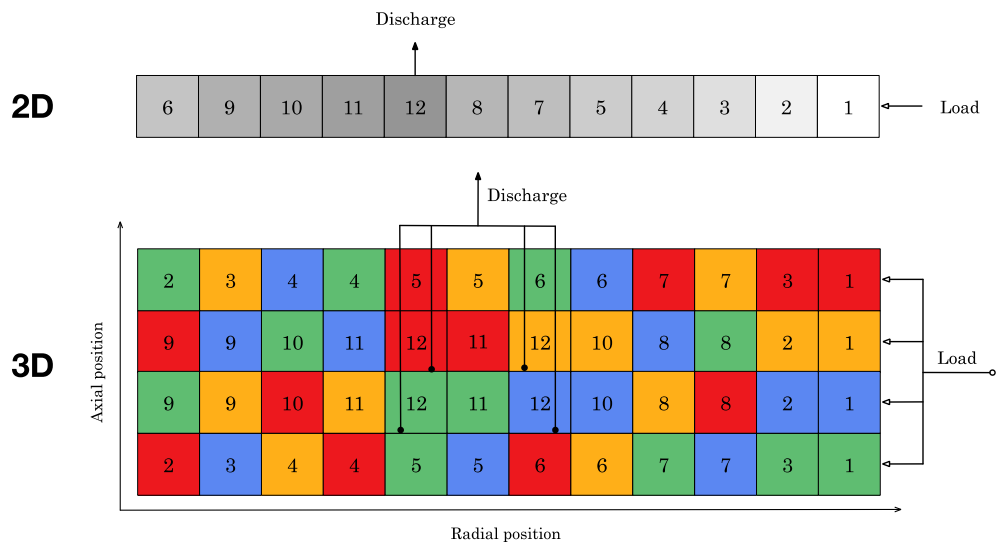

Fig. 17. Shuffling paths for the reference 2D (top) and 3D (bottom) cores.

Table 4
Design parameters of the 1250 MWt cores.

Core type		2D shuffling	3D shuffling
Active fuel height		200 cm	
Equivalent core diameter		300 cm	
Active core volume		14.1 m^3	
Volumetric power density		88.4 MW/m^3	
Fuel assemblies		204	
Total fuel rod(s) length		235 cm	256 cm
		1 cm lower end plug	1 cm lower end plug
		25 cm lower shield	25 cm lower shield
		200 cm fuel	200 cm total fuel
		8 cm expansion space	4 × 2.0 cm expansion space
		1 cm venting	4 × 5.5 cm venting and 3D-connections
Pitch-to-diameter ratio		1.100	1.069
Fuel actinide loading mass		92×10^3 kg	100×10^3 kg
Core volume fractions (%)	Fuel	36.00	38.30
	Gap	12.00	12.77
	Cladding + wire	11.86	12.29
	Duct	8.09	8.26
	Coolant	32.03	28.39

- A low burnup and, hence, a low fissile content fuel should be loaded at top and bottom zones to avoid strong axial leakage. Although the top and bottom locations are interchangeable because of the core near symmetry, it is desirable to keep axial burnup gradient outward (such that the more burned fuel is in the axial center) in order to reduce the leakage.
- A high burnup fuel batch with largest reactivity worth should be loaded at the axially middle zones, but not in radial innermost location to avoid large radial power peaking, or outer locations to prevent high neutron leakage.
- Intermediate burnup fuel is loaded in the rest of the locations in the axial core center. The burnup zones should be shuffled between the upper and lower halves of the core during their residence time to minimize the axial burnup gradient within subassemblies. This is particularly important for high fissile content fuel, since its reactivity worth is high and the burnup accumulates much faster within the burnup zone.

10. Results

The 1250 MWt cores were designed with 200 cm active fuel and an equivalent active core diameter of 300 cm, giving a core volume of 14.1 m^3 and a volumetric power density of 88.4 MW/m^3. The designs and calculation results for the 1250 MWt cores are given in Tables 4 and 5, respectively.

Table 5
Selected performance characteristics of the 1250 MWt cores.

Core type	2D shuffling	3D shuffling
Peak discharge HT9 DPA	529	400
Peak discharge fluence	20.5×10^{23} n/cm^2	15.5×10^{23} n/cm^2
Cycle time	1015 days	1250 days
Average discharge burnup	184 MWd/kg	219 MWd/kg
Peak discharge burnup	338 MWd/kg	227 MWd/kg
Axial burnup peaking factor	1.84	1.04
Reactivity swing	3.9%	4.8%
Neutron leakage probability	4.6%	5.8%
Peak absolute batch power change	9 MW	81 MW
Max/ave radial power peaking factor	2.36/2.31	1.82/1.72
Max/ave axial power peaking factor	2.07/1.84	2.23/2.03

Because of the significantly lower radial power peaking factor of the 3D-shuffling core, the volume fraction (and mass) of fuel in the core is higher and the pitch-to-diameter ratio is lower. This gives the 3D-shuffling core a neutronic advantage, which further enhances its performance with regards to the minimum required

Table 6
Design parameters 2500 MWt cores.

Core type		2D shuffling	3D shuffled
Active fuel height		250 cm	
Equivalent core diameter		384 cm	
Active core volume		29.0 m^3	
Volumetric power density		86.2 MW/m^3	
Fuel assemblies		348	
Total fuel rod(s) length		287 cm	308 cm
		1 cm lower end plug	1 cm lower end plug
		25 cm lower shield	25 cm lower shield
		250 cm fuel	250 cm total fuel
		10 cm expansion space	4×2.5 cm expansion space
		1 cm venting	4×5.5 cm venting and 3D-connections
Pitch-to-diameter ratio		1.159	1.094
Fuel actinide loading mass		179.0×10^3 kg	203.5×10^3 kg
Core volume fractions (%)	Fuel	33.27	37.67
	Gap	11.09	12.56
	Cladding + wire	11.81	12.33
	Duct	7.54	7.71
	Coolant	36.29	29.74

radiation damage. The average discharge burnup of the 3D-shuffling system is 19% higher, but the uniform axial burnup shape gives a 33% reduction in the peak burnup and a 25% reduction in the peak HT9 DPA. The 3D-shuffling core outperforms the 2D-shuffling core on both economics (average burnup and cycle time) as well as meeting the radiation damage constraint. However, the 2D-shuffled core suffers a less severe reactivity swing over the cycle and a smaller absolute power change within one batch (both of which are direct results of the difference in the shuffling schemes).

The designs and calculation results for the 2500 MWt cores are given in Tables 6 and 7 respectively.

The general trends found between the 1250 MWt 2D and 3D-shuffling cores apply to the 2500 MWt cores, but since the larger cores have a better neutron economy, radiation damage values are lower. Perhaps the most important difference is that axial burnup peaking of the 2D-shuffling core has increased from 1.84 up to 2.10, while the axial burnup peaking remains almost unchanged in the 3D-shuffling system. This fact gives a larger relative reduction in the peak radiation damage – 30% compared to 25%, when introducing 3D-shuffling. The peak radiation damage of the 2D-shuffling B&B core is 483 DPA, which is hoped to be attainable with optimized HT9 steel (Gilleland, 2014). The 3D-shuffling 2500 MWt core requires less than 350 DPA, which makes this design implementable sooner than the 2D-shuffling B&B core; several types of steels are expected to perform adequately out to this DPA level (Maloy, 2014).

The disadvantages of the 3D-shuffling strategy identified for the 1250 MWt cores are more pronounced in the 2500 MWt cores – most notably the cycle reactivity swing has risen to 5.2%. This will require either a significantly more extensive burnup reactivity control system than what has been assumed in the design process (which uses 19 independent burnup control assemblies), or an increase in the number of batches and corresponding shortening of the cycle length, or a change in the shuffling scheme or a combination of the above.

Table 7
Results for 2500 MWt cores.

Core type	2D shuffled	3D shuffled
Peak discharge HT9 DPA	483	341
Peak discharge fluence	18.9×10^{23} n/cm^2	13.3×10^{23} n/cm^2
Cycle time	800 days	1100 days
Average discharge burnup	159 MWd/kg	177 MWd/kg
Peak discharge burnup	334 MWd/kg	189 MWd/kg
Axial burnup peaking	2.10	1.06
Reactivity swing	3.2%	5.2%
Neutron leakage probability	1.3%	3.1%
Peak absolute batch power change	41 MW	136 MW
Max/ave radial power peaking factor	2.60/2.50	1.88/1.80
Max/ave axial power peaking factor	2.41/2.11	2.50/2.33

In order to estimate the performance limits of realistic B&B systems, a 3500 MWt design was developed in both 2D and 3D-shuffling version with a lower volumetric power density than the smaller cores, to allow for a really maximized neutron economy. The designs and calculation results for the 3500 MWt cores are given in Tables 8 and 9, respectively.

The lower average power density (72 MW/m^3 compared to 86–88 MW/m^3) allows the 3500 MWt cores to maintain a relatively tight pitch-to-diameter ratio and high fuel volume fraction, even though the radial power peaking factor is significantly higher. The conventional 2D-shuffled core design is able to operate at a very low level of average burnup, but develops a very severe axial power, fluence and DPA peaking factor. The higher peaking nearly eliminates all of the advantage given by the lower average burnup, which results in that the 3500 MWt 2D-shuffled system has a peak DPA level only 2.5% lower (471 vs. 483 DPA) compared to the much smaller and more economically viable 2500 MWt design. There thus appears to be no incentive to go to 2D-shuffled core designs with active core volumes larger than about 30 m^3. For the 3D-shuffling core, the drop in peak DPA is an additional 12%, reducing it from 341 DPA in the 2500 MWt down to 318 DPA in the much larger 3500 MWt core. To achieve this, the fuel mass loading has been increased by over 60%, and the problems suffered by the smaller 3D-shuffling cores have worsened further: for instance the reactivity swing of the 3500 MWt 3D-shuffling core is above 6%. The trends observed indicate that a realistic optimized B&B system cannot operate at a peak discharge radiation damage level below 300 DPA.

The axial distribution of HT9 DPA at discharge for the three core sizes studied is shown in Fig. 18. Increasing the core volume and the active fuel height significantly decreases the average burnup and radiation damage at discharge, but the higher peaking factor means that the reduction in the peak values is more modest.

In contrast, the axial peaking is almost completely eliminated by introducing both axial and radial shuffling of fuel regions (3D-shuffling). By achieving a nearly flat axial radiation damage profile at discharge, the peak DPA values are lowered by 30–35%.

Table 8
Design parameters 3500 MWt cores.

Core type		2D shuffled	3D shuffled
Active fuel height		300 cm	
Equivalent core diameter		453 cm	
Active core volume		48.4 m^3	
Volumetric power density		72.3 MW/m^3	
Fuel assemblies		492	
Total fuel rod(s) length		339 cm	360 cm
		1 cm lower end plug	1 cm lower end plug
		25 cm lower shield	25 cm lower shield
		300 cm fuel	300 cm total fuel
		12 cm expansion space	4 × 3.0 cm expansion space
		1 cm venting	4 × 5.5 cm venting and 3D-connections
Pitch-to-diameter ratio		1.172	1.120
Fuel actinide loading mass		297.2×10^3 kg	328.6×10^3 kg
Core volume fractions (%)	Fuel	32.96	36.34
	Gap	10.99	12.11
	Cladding + wire	11.93	12.23
	Duct	7.15	7.47
	Coolant	36.74	31.85

Table 9
Results for 3500 MWt cores.

Core type	2D shuffled	3D shuffled
Peak discharge HT9 DPA	471	318
Peak discharge fluence	18.5×10^{23} n/cm^2	12.6×10^{23} n/cm^2
Cycle time	750 days	1175 days
Average discharge burnup	117 MWd/kg	160 MWd/kg
Peak discharge burnup	295 MWd/kg	176 MWd/kg
Axial burnup peaking	2.53	1.10
Reactivity swing	3.4%	6.3%
Neutron leakage probability	0.3%	1.6%
Peak absolute batch power change	46 MW	129 MW
Max/ave radial power peaking factor	2.80/2.73	2.12/2.00
Max/ave axial power peaking factor	2.81/2.50	2.79/2.46

The axial distribution of discharge HT9 DPA of the 3D-shuffling cores is shown in Fig. 19.

One could have expected that since the axial peaking factor is nearly halved when going from 2D to 3D-shuffling, the reduction in peak DPA would be closer to 50%. The full potential reduction is not realized because the 3D shuffling core average discharge burnup is higher due to a couple of reason: its neutron leakage probability is higher and all its fuel makes similar contribution to the neutron balance.

In the 2D-shuffling core the discharge burnup of the fuel close to the axial ends is low. Even though the burnup the fuel in the vicinity of the axial center is above 30% – significantly above the infinite medium minimum required burnup, the axial average burnup is lower than the infinite medium minimum required burnup. The under-utilized fuel fraction becomes larger with longer axial fuel, which lowers the average discharge burnup. The higher average discharge burnup implies that the 3D shuffling core offers significantly higher uranium utilization than the 2D shuffling cores. The 3D shuffling scheme used (Fig. 17) results in placing significantly larger concentration of fissile fuel at the axial ends of the core and this significantly increases the neutron leakage probability.

A figure of merit for B&B systems that measures the attainable fuel utilization is the ratio of average discharge burnup to the peak discharge DPA: (the higher the number is, the more economically viable the design is), as defined by Eq. (8).

$$\mathrm{FOM}_{B\&B} = \frac{\text{Average Burnup}}{\text{Peak Irradiation Damage}}\left[\frac{\mathrm{MWd}}{\mathrm{DPA} \times \mathrm{kg}_{\mathrm{fuel}}}\right] \tag{8}$$

The results of Eq. (8) are plotted in Fig. 20, clearly showing the advantage that the 3D-shuffled cores have over the 2D-shuffled cores. For a 3D-shuffled core, one can get about 0.55 MWd/kg of average discharge burnup per 1 DPA of irradiation damage, close to independent of core size and power. For the smaller 2D-shuffled cores, the corresponding number is 1 DPA per every 0.35 MWd/kg (47% lower). Fig. 20 also clearly shows the problem of high axial peaking in the largest 2D-shuffled core. The 3500 MWt 2D-shuffled core has a Burnup/DPA figure of merit value almost exactly half that of the 3D-shuffled core of corresponding size, and about 30% lower than the smaller 2D-shuffled cores.

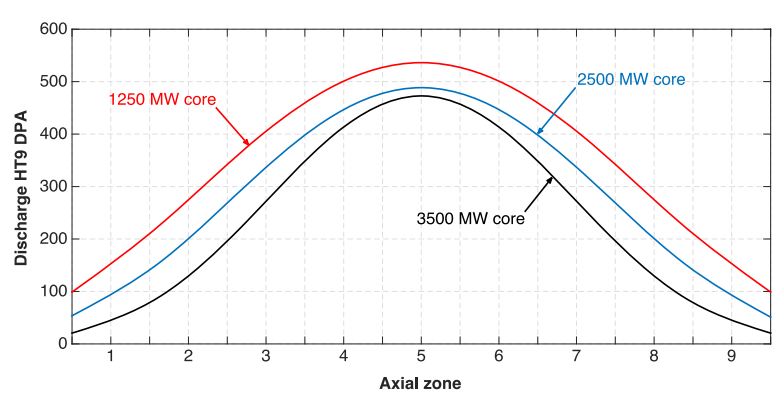

Fig. 18. Axial distribution of HT9 discharge DPA for 2D-shuffled cores.

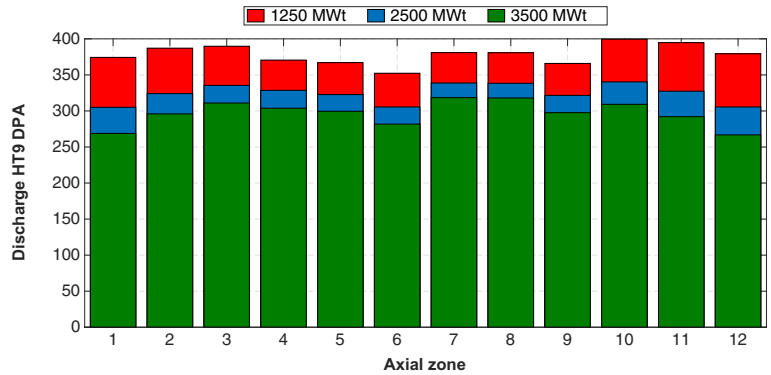

Fig. 19. Axial distribution of HT9 discharge DPA for 3D-shuffling cores.

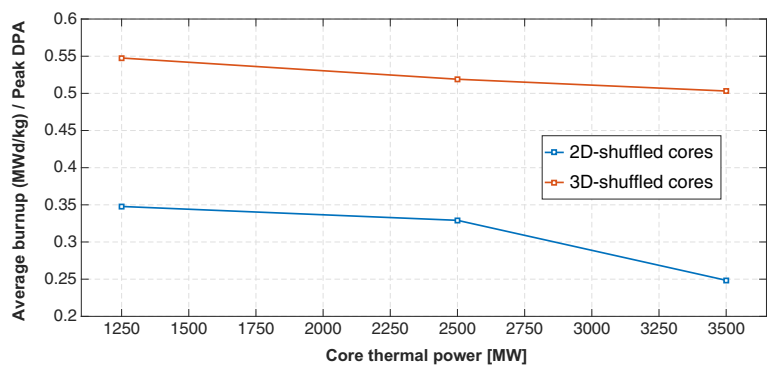

Fig. 20. B&B Burnup/DPA figure of merit (Eq. (8)).

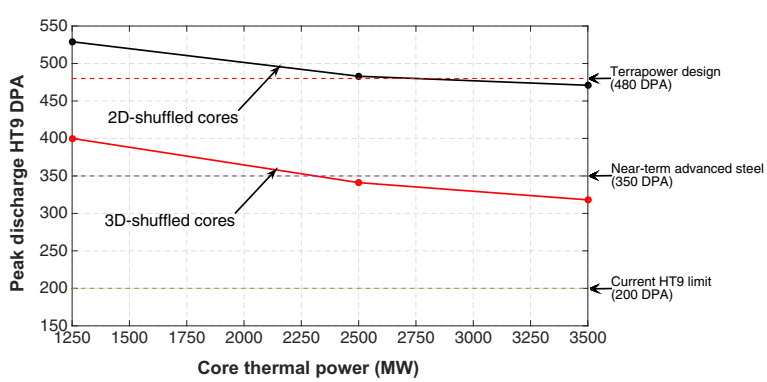

Fig. 21. B&B DPA results and material limits.

The required HT9 DPA levels for equilibrium cycle B&B operation on depleted uranium fuel with 2D and 3D shuffled cores is shown in Fig. 21, along with current (200 DPA), near-term expected (350 DPA) and optimistic (480 DPA) material limits.

11. Conclusions and future work

In this work, we defined and developed the engineering and physical principles of B&B core designs using both 2D and 3D shuffling of fuel. We have shown that it appears possible to design a fully optimized 3D-shuffling system for B&B operation using depleted uranium with a peak irradiation damage at or below 350 DPA. For conventional 2D-shuffled systems, it appears feasible to design systems that can operate on a feed fuel of depleted uranium and suffer a peak irradiation damage below 500 DPA. Little room for further neutron economy improvements exist for the core designs developed in this study. Because of this, all B&B systems will require either periodic replacements of structural materials or steels than can be proven to perform well up to at least 350 DPA. The results also show that no further gain in system performance is obtained for active core volumes in excess of 30 m^3.

The general direction of future work for B&B technology is clear: structural materials such as the steels that make up the cladding, wire and ducts inside the core need to be qualified for significantly higher levels of neutron irradiation damage than has been proven experimentally in the past. For the 3D-shuffling designs introduced in this study, significant focus must be put on the feasibility of the proposed shuffling machine and mechanism. Dimensional changes

to the connecting pieces must be small enough to ensure adequate attachment and detachment of assembly segments throughout the lifetime of the core, without exceeding withdrawal-force limits of the shuffling machine itself. In addition, a safe core response to unprotected transients such as loss of flow, loss of heat sink and transient overpower scenarios (such as the rapid withdrawal of an inserted control assembly) is a difficult challenge. It appears likely that the introduction of Autonomous Reactivity Control (ARC) systems Qvist and Greenspan, 2014 may solve these issues for both 2D and 3D-shuffling B&B systems, but this must be further verified in more detailed time-dependent studies.

B&B systems are the most resource-efficient once-through reactors ever proposed, potentially being able to extract around 20% of the available fission energy out of depleted uranium that is readily available in large quantities as waste material from uranium enrichment facilities. Systems such as the 3D-shuffling 2500 MWt B&B core developed in this study could, if expected performance extensions to advanced fast reactor steels are realized, cover the total current US electricity needs for around 800 years in a once-through cycle (no reprocessing) using only the depleted uranium stockpiles accumulated for fueling the light water reactor fleet and the start-up (first generation) B&B cores. The 40-fold increase in uranium utilization over current LWRs and once-through fast reactors effectively expands the potential for nuclear energy without reprocessing to a technology that is able to supply all of the world's electricity needs for centuries to come, and thus warrants detailed and intense further study.

References

Akhiezer, A.I., Belozorov, D.P., Davydov, L.N., Spolnik, Z.A., 1999. Propagation of a nuclear chain reaction in the diffusion approximation. Phys. At. Nucl. 62 (9), 1474–1481.

Anderson, H.H., Asprey, B.L., 1947. Solvent Extraction Process for Plutonium, US2924506, May 8.

ASME, 2005. Boiler & Pressure Vessel Code, Section VIII, Division 1, Subsection A, Article UG-27. ASME, New York.

Atefi, B., 1980. Evaluation of the Breed/Burn Fast Reactor Concept (Ph.D. thesis). Massachusetts Institute of Technology.

Barthold, W.P., 1974. Constrained Nuclear Design. In: Proc. of ANS meeting on Advanced Reactors; Physics, Design and Economics, Atlanta, Georgia.

Cahalan, J.E., Tentner, A.M., Morris, E.E., 1994. Advanced LMR safety analysis capabilities in the SASSYS-I and SAS4A computer codes. In: International Meeting on Advanced Reactor Safety, Pittsburg, PA, USA.

Chadwick, M.B., 2006. ENDF/B-VII. 0: next generation evaluated nuclear data library for nuclear science and technology. Nucl. Data Sheets 107 (12), 2931–3060.

Chang, Y.I., 2007. Technical rationale for metal fuel in fast reactors. Nucl. Eng. Technol. 39 (3), 161–170.

Chen, X.N., Kiefhaber, E., Maschek, W., 2005. Neutronic model and its solitary wave solutions for a CANDLE reactor. In: Proc. of the 12th International Conference on Emerging Nuclear Energy Systems (ICENES'2005), Brussels, Belgium.

Choi, H., Shleicher, R.W., Gupta, P., 2013. A compact gas-cooled fast reactor with an ultra-long fuel cycle. Sci. Technol. Nucl. Install.

DeVolpi, A., 1986. Fissile materials and nuclear weapons proliferation. Annu. Rev. Nucl. Part. Sci. 36, 83–114.

Di Sanzo, C., Cohen, J. Cisneros, T., Ludewight, B., Greenspan, E., 2011. An accelerator driven energy multiplier for doubling uranium ore utilization. In: Proc. of Accelerator Application Topical Meeting, Knoxville, TN, US.

Farmer, M.T., Hoffman, E.A., Pfeiffer, P.F., 2006. Generation IV Nuclear Energy System Initiative Pin Core Subassembly Design. Nuclear Engineering Division, Argonne National Lab. ANL-GenIV-070.

Feinberg, S.M., Kunegin, E.P., 1958. Discussion comment, Ref. of Proc. Session B-10 ICPUAE 9(2), p. 447.

Feoktistov, L.P., 1988. An Analysis of a Concept of a Physically Safe Reactor. Kurchatov Institute, Moscow, Russia (in Russian, preprint IAE-4605/4).

Fomin, S.P., Mel'nik, Yu, Pilipenko, V., Shul'ga, N., 2005. Investigation of self-organization of the non-linear nuclear burning regime in fast neutron reactors. Ann. Nucl. Energy 32 (13), 1435–1456.

Fuchs, K., Hessel, H., 1961. The possibilities for the operation of a natural uranium breeder reactor without fuel element preparation (in German). Kernenergie (East Germany) 4.

Gaveau, B., Maillard, J., Maurel, G., Silva, J., 2005. Hybrid soliton nuclear reactors: a model and simulation (encapsulated long living accelerator driven system). Nucl. Eng. Des. 235 (15), 1665–1674.

General Atomics, 1974. Gas-cooled fast breeder reactor preliminary environmental report on 300-MW(e) demonstration plant, GA-A12957.

Gilleland, J., 2008. Novel reactor designs to burn non-fissile fuels. In: Proc. Int. Congress Advances in Nuclear Power Plants (ICAPP'08), Anaheim, CA, USA.

Gilleland, J., 2014. Global problems and global solutions. In: Presentation at the University of California Nuclear Engineering Department Colloquium, Terrapower LLC, Berkeley, CA, USA.

Goldin, V., Anistratov, D., 1992. Mathematical Modelling of Neutron-Nuclear Processes in Safe Reactor. Institute of Mathematical Simulation, Russian Academy of Sciences (preprint IMM RAS N. 43).

Greenspan, E., 2012. A phased development of breed-and-burn reactors for enhanced nuclear energy sustainability. Sustainability 4, 2745–2764.

Greenspan, E., Heidet, F., 2011. Energy sustainability and economic stability with breed and burn reactors. Prog. Nucl. Energy 53, 794–799.

Hannum, W.H., Wade, D.C., McFarlane, H.F., 1997. Nonproliferation and safeguards aspects of the IFR. Prog. Nucl. Energy 31 (1–2), 203–217.

Hartanto, D., Kim, Y., 2012. Physics and design studies for a small breed-and-burn reactor. Trans. Am. Nucl. Soc. 107, 1256–1258.

Heidet, F., 2010. Maximum Fuel Utilization in Advanced Fast Reactors without Actinides Separation (Ph.D. thesis). University of California Berkeley, Berkeley, CA, US.

Heidet, F., Greenspan, E., 2010. Breed-and-burn depleted uranium in fast reactors without actinides separation. In: Proc. of PHYSOR 2010, Advances in Reactor Physics to Power the Nuclear Renaissance, Pittsburgh, Pennsylvania, USA.

Heidet, F., Greenspan, E., 2012. Neutron balance analysis for sustainability of breed-and-burn reactors. Nucl. Sci. Eng. 171 (1), 13–31.

Heidet, F., Greenspan, E., 2013a. Superprism-sized breed-and-burn sodium-cooled core performance. Nucl. Technol. 181, 251–273.

Heidet, F., Greenspan, E., 2013b. Performance of large breed-and-burn core. Nucl. Technol. 181 (3), 381–407.

Horak, J.A., Kittel, J.H., Yaggee, F.L., 1962. Irradiation Behavior of Restrained and Vented Uranium-2 w/o Zirconium Alloy. Argonne National Laboratory, Argonne, IL, US (ANL-6431).

Idaho National Laboratory, 2013. Advanced Fuels Campaign 2013 Accomplishments, Idaho Falls, Idaho, US, Technical report.

International Atomic Energy Agency, 1991. LMFBR PLANT PARAMETERS 1991, IAEA, Vienna, Austria, IWGFR/80.

Kaity, S. et al., 2012. Characterization and property evaluation of U-15 wt%Pu alloy for fast reactor. J. Nucl. Mater. 433 (1–3), 206–214.

Keilholtz, G.W., Battle, G.C., 1969. Fission Product Release and Transport in Liquid Metal Fast Breeder Reactors. Oak Ridge National Laboratory, Oak Ridge, TN, US, 0RNL-NSIC-3T.

Khizhnyak, N.A., 2001. On the theory of the initial stage of slow nuclear burning. Probl. Atom. Sci. Technol. 6, 279–282.

Kim, T.K., Taiwo, T., 2010. Fuel Cycle Analysis of Once-Through Nuclear Systems. Argonne National Laboratory, Argonne, IL, US (ANL-FCRD-308).

Kouts, H.J.C., Fischer, G.J., Cerbone, R.J., 1979. Fast Mixed Spectrum Reactor Concept. Brookhaven National Laboratory, BNL-25993.

Leppänen, J., 2010. Serpent Monte Carlo physics code. In: AER Symposium on VVER Reactor Physics and Reactor Safety, Espoo, Finland.

Lewis, E.E., 2008. Fundamentals of Nuclear Reactor Physics. Elsevier Science.

Lipps, A.J., 1968. Evaluation of Vented-to-Coolant Designs for Sodium-Bonded Carbide Fuel Rods: Task I Report, Follow-on Study for a 1000 MWe LMFBR. Westinghouse Electric, Madison, Pennsylvania, WARD-2000-31.

Maloy, S., 2014. Fuel cycle research and development: advances in nuclear fuel and materials. In: Purdue Nuclear Power Workshop, October 16–17.

Martini, M., Gerosa, A., 1973. Venting device for sodium-cooled fast ceramic reactor fuel elements. Nucl. Technol. 19, 96–110.

McNelley, M.J., 1964. Liquid Metal Fast Breeder Reactor Design Study [1000 Mw(electrical)] UO_2–PuO_2 Fueled Plant, General Electric, GEAP-44187 1964.

Medvedev, P., 2012. Fuel Performance Modeling Results for Representative FCRD Irradiation Experiments: Projected Deformation in The Annular AFC-3A U-10Zr Fuel Pins and Comparison to Alternative Designs, Idaho National Laboratory, Idaho Falls, US, Technical report 2012.

Nagata, A., Sekimoto, H., 2007. Analysis of recladding in CANDLE Reactor. In: Proc. of the 15th International Conference on Nuclear Engineering (ICONE15), Nagoya, Japan.

Nagata, A., Takaki, N., Sekimoto, H., 2009. A feasible core design of lead bismuth eutectic cooled CANDLE fast reactor. Ann. Nucl. Energy 36, 562–566.

O'Neill, G.L., 1965. Safety and economic aspects of vented fuel in sodium-cooled reactors. In: Proceedings of the Conference on Safety, Fuels, and Core Design in Large Fast Power Reactors, pp. 540–548.

Osbourne, A.G., Recktenwald, G.D., Deinert, M.R., 2012. Propagation of a solitary fission wave. Chaos 22.

Pavlovich, V.N., Khotyaintseva, E.N., Rusov, V.D., Khotyaintsev, V.N., Yurchenko, A.S., 2007. Reactor operating on a slow wave of nuclear fission. At. Energ. 103 (3), 181–189.

Pilipenko, V.V., Belozorov, D.P., Davydov, L.N., Shul'ga, N.F., 2003. Some aspects of slow nuclear burning (Paper 3169). In: Prof. of the International Congress on Advances in Nuclear Power Plants (ICAPP) 2003, Cordoba, Spain.

Qvist, S., 2013. Safety and Core Design of Large Liquid-Metal Cooled Fast Breeder Reactors (Ph.D. thesis). Nuclear Engineering, University of California Berkeley, Berkeley, CA, USA.

Qvist, S., 2013. Extending serpent. In: Serpent Annual Users Meeting, Berkeley, CA, US.

Qvist, S., 2015. Optimization method for the design of hexagonal fuel assemblies. Ann. Nucl. Energy 75, 498–506.

Qvist, S. Greenspan, E., 2012. Inherent safety of minimum-burnup breed & burn reactors. In: Proc. of ICAPP 2012, Chicago, IL, US.
Qvist, S., Greenspan, E., 2014. 3D shuffling in breed and burn reactors. In: American Nuclear Society Winter Meeting, Anaheim, CA, USA.
Qvist, S., Greenspan, E., 2014. An autonomous reactivity control system for improved fast reactor safety. Prog. Nucl. Energy 77, 32–47.
Qvist, S., Greenspan, E., 2014. The ADOPT code for automated fast reactor design. Ann. Nucl. Energy 71, 23–36.
Qvist, S., Greenspan, E., 2015. Design space analysis for breed-and-burn reactor cores. Nucl. Sci. Eng. (in review)
Rough, F.A., 1955. An evaluation of data on zirconium–uranium alloys, Battelle Memorial Institute, Technical report.
Rusov, V., 2011. Traveling wave reactor and condition of existence of nuclear burning soliton-like wave in neutron-multiplying media. Energies 4 (9), 1337–1361.
Ryu, H., Lee, B.O., Oh, S.J., Kim, J.H., Lee, C.B., 2009. Performance of FCCI barrier foils for U–Zr–Z metallic fuel. J. Nucl. Mater. 392 (2), 206–212.
Sackett, J.I., Grandy, C., 2013. International experience with fast reactor operation & testing. In: International Conference on Fast Reactors and Related Fuel Cycles (FR13), Paris, France.
Schleicher, R.W., Choi, H., Rawls, J., 2013. The energy multiplier module: advancing the nuclear fuel cycle through technology innovations. Nucl. Technol. 184, 169–180.
Schneider, E., Deinert, M., Scopatz, A., 2007. Depleted and recycleable uranium in the United States: inventories and options. In: Proceedings of GLOBAL 07, Boise, Idaho, US.
Seifritz, W., 1995. Non-linear burn-up waves in opaque neutron absorbers. Kerntechnik 60.
Sekimoto, H., Ryu, K., 2000. A new reactor burnup concept "CANDLE". In: Proc. of PHYSOR 2000, Pittsburgh, PA, USA.
Si, S., 2013. Multiphysics model development and the core analysis for in situ breeding and burning reactor. Sci. Technol. Nucl. Install. 2013. http://dx.doi.org/10.1155/2013/154706, 14 pages, Article ID 154706.
Slesarev, J.S., Stukalov, V.A., Subbotin, S.A., 1983. Problems of development of fast reactors self-fuel-provision without fuel reprocessing. Atomkernenergie Kerntechnik 45 (1), 58–60.
Smidt, D., Sommer, W., 1965. Application of the vented fuel concept to a sodium-cooled power breeder with 1000 MWe. In: Proceedings of the Conference on Safety, Fuels, and Core Design in Large Fast Power Reactors, pp. 130–135.
Steward, K.P.,1978. Final summary report on the peach bottom end-of-life program, General Atomics, GA-A14404.
Tak, T., Lee, D., Kim, T.K., 2012. Design of ultralong-cycle fast reactor employing breed-and-burn strategy. Nucl. Technol. 183, 427–435.
Teller, E., Ishikawa, M., Wood, L., 1996. Completely Automated Nuclear Reactors for Long-term Operation. Lawrence Livermore National Laboratory (UCRL-JC–122708).
TerraPower LLC, 2015. About TerraPower <http://terrapower.com/pages/about> (online).
Toloczko, M.B., Garner, F.A., Eiholzer, C.R., 1994. Irradiation creep and swelling of the US fusion heats of HT9 and 9Cr-1Mo to 208 dpa at ~400°C. J. Nucl. Mater. 212–215, 604–607.
Toshinsky, G.I., 1997. LMFBR operation in the nuclear cycle without fuel reprocessing. In: Proceedings of the International Topical Meeting on Advanced Reactors Safety, vol. 1, Orlando, FL, USA, pp. 39–44.
Toshinsky, V.G., Sekimoto, H., Toshinsky, G.I., 1999. Multiobjective fuel management optimization for self-fuel-providing LMFBR using genetic algorithms. Ann. Nucl. Energy 26, 783–802.
Toshinsky, V.G., Sekimoto, H., Toshinsky, G.I., 2000. A method to improve multiobjective genetic algorithm optimization of a self-fuel-providing LMFBR by niche induction among nondominated solutions. Ann. Nucl. Energy 27, 397–410.
Van Dam, H., 1998. Burnup waves. Ann. Nucl. Energy 25, 1409–1417.
Van Dam, H., 2000. Self-stabilizing criticality waves. Ann. Nucl. Energy 27 (16), 1505–1521.
Wade, D.C., Fujita, E.K., 1987. Trends vs. reactor size of passive reactivity shutdown and control performance. In: Proc. of the International Fast Reactor Physics Conference, Jackson Hole, WY, US.
Waltar, A.E., Todd, D.R., Tsvetkov, P.V., 2012. Fast Spectrum Reactors. Springer, New York.
Walters, L.C., 2011. Sheathed, Annular metallic nuclear fuel, US Patent 13/004,974, Aug. 11.
Yarsky, P., 2005. Core Design and Reactor Physics of a Breed and Burn Gas-cooled Fast Reactor (Ph.D. thesis). Massachusetts Institute of Technology.
Yu, K., Driscoll, M.J., Hejzlar, P., 2002. Neutronic limits of breed-and-burn fast reactor performance. In: ANS Annual Meeting, Hollywood, FL, USA.

Appendix B

J. Hou, S. Qvist, R. Kellogg and E. Greenspan, “3D In-core Fuel Management Optimization for Breed-and-Burn Reactors," *Progress in Nuclear Energy*, vol 88, pp. 58-74 (2016).

Progress in Nuclear Energy 88 (2016) 58–74

Contents lists available at ScienceDirect

Progress in Nuclear Energy

journal homepage: www.elsevier.com/locate/pnucene

3D in-core fuel management optimization for breed-and-burn reactors

Jason (Jia) Hou [a, *], Staffan Qvist [b], Roger Kellogg [c], Ehud Greenspan [a]

[a] Department of Nuclear Engineering, University of California, Berkeley, Berkeley, CA, 94720, USA
[b] Department of Physics and Astronomy, Uppsala University, Sweden, Ångström Lab, Lägerhyddsvägen 1, 752 37, Uppsala, Sweden
[c] Nuclear Engineering Division, Argonne National Laboratory, Argonne, IL, 60439, USA

ARTICLE INFO

Article history:
Received 11 July 2015
Received in revised form
26 September 2015
Accepted 7 December 2015
Available online xxx

Keywords:
Breed-and-burn reactor
Peak radiation damage
3D fuel shuffling optimization
Simulated annealing
Optimal core design

ABSTRACT

Breed-and-burn (B&B) reactors are a special class of fast reactors that are designed to utilize low grade fuel such as depleted uranium without fuel reprocessing. One of the most challenging practical design feasibility issues faced by B&B reactors is the high level of radiation damage their fuel cladding has to withstand in order to sustain the B&B mode of operation – more than twice the maximum radiation damage cladding materials were exposed to so far in fast reactors. This study explores the possibility of reducing the minimum required peak radiation damage by employment of 3-dimensional (3D) fuel shuffling that enables a significant reduction in the peak-to-average axial burnup, that is, more uniform fuel utilization. A new conceptual design of a B&B core made of axially segmented fuel assemblies was adopted to facilitate the 3D shuffling. Also developed is a Simulated Annealing (SA) algorithm to automate the search for the optimal 3D shuffling pattern (SP). The primary objective of the SA optimization is to minimize the peak radiation damage while its secondary objective is to minimize the burnup reactivity swing, radial power peaking factor and maximum change of fuel assembly power over the cycle. Also studied is the sensitivity of the 3D shuffled core performance to the number of axially stacked subassemblies, core height and power level.

It was found that compared with the optimal 2-dimensional (2D) shuffled core, the optimal 3D shuffled B&B core made of four 70 cm long axially stacked sub-assemblies and 12 radial shuffling batches offers a 1/3 reduction of the peak radiation damage level – from 534 down to 351 displacements per atom (dpa), along with a 45% increase in the average fuel discharge burnup, and hence, the depleted uranium utilization, while satisfying all major neutronics and thermal-hydraulics design constraints. For the same peak dpa level, the 3D shuffling offers more than double the uranium utilization and the cycle length relative to 2D shuffling. The minimum peak radiation damage is increased to 360 or to 403 dpa if the core is made of, respectively, three – 70 cm or two – 140 cm long axially stacked subassemblies. Reducing the length of the subassemblies of B&B cores made of three-segment assemblies from 70 cm to 60 or 50 cm results in an increase in the peak radiation damage from 360 dpa to, respectively, 368 and 397 dpa.

© 2015 Elsevier Ltd. All rights reserved.

1. Introduction and research objective

Present day commercial Light Water Reactors (LWRs) can extract only ~0.6% of the potential energy that is available in the natural uranium mined for making LWR fuel. Approximately 90% of the unused uranium goes to the depleted uranium (DU) stream of the enrichment process and ~95% of the enriched uranium is left in the used nuclear fuel (UNF). Fast Breeder Reactors (FBRs) can, in principle, fission almost all the DU "waste", although high uranium utilization cannot be achieved in a single irradiation campaign because the radiation damage accumulated by the fuel and cladding challenges the mechanical integrity of the fuel rod. Consequently, the approach that enables attaining high uranium utilization also involves multiple fuel recycling. Fuel recycling includes removal of the fuel cladding, removal of the fission products, addition of some DU make up fuel, fabrication of new fuel

* Corresponding author. 3115 B&AA Etcheverry Hall, University of California, Berkeley, Berkeley, CA 74720, USA.
E-mail address: jasonhou@berkeley.edu (J. Hou).

http://dx.doi.org/10.1016/j.pnucene.2015.12.002
0149-1970/© 2015 Elsevier Ltd. All rights reserved.

assemblies and reloading them into the reactor core for another irradiation cycle. Such recycling is commonly required for every 10%–15% fissions per initial heavy metal atom (FIMA), depending on the core neutron spectrum and fuel enrichment. Although technically feasible, the fuel recycling was not acceptable to many U.S. administrations and by other countries due to economic viability and proliferation concerns.

FBRs could, in principle, also operate without fuel recycling. That is, using a once-through fuel cycle as do the majority of LWRs. Although the standard FBR discharge burnup of 10%–15% FIMA is two to three times higher than that of LWRs, the uranium utilization of a once-through FBR is not significantly different from that of a once-through LWR because the level of uranium enrichment required to achieve criticality in the FBR is often three times that required to fuel the LWR.

To achieve significant uranium utilization without resorting to fuel recycling, special class of fast reactors known as Breed-and-Burn (B&B) reactors has been proposed and studied since the 1950s. The unique feature of a B&B reactor is that it can breed plutonium in depleted or natural uranium feed fuel and then fission a significant fraction of the bred plutonium without having to reprocess the fuel. Once the initial criticality is established with the assistant of either enriched uranium (EU) or plutonium with or without minor actinides, the B&B reactor is capable of continuing its operation fed only with fertile fuel such as DU or natural uranium.

There are two basic variants of B&B reactors: Traveling Wave Reactors (TWRs) and Stationary (or Standing) Wave Reactors (SWRs). In TWRs, like the CANDLE reactor concept (Sekimoto and Ryu, 2000) and the one proposed by Teller et al. (1996), the breeding and burning wave travels axially through the long core from one end to the other. In SWRs, like the one presently being pursued by TerraPower (Ahlfeld et al., 2011; Hejzlar et al., 2013), the location of the fission reaction in the core is maintained nearly stationary by adequate radial, i.e., 2-dimensional (2D) shuffling of fuel assemblies. The TWR concept is considered difficult to implement due to its poor neutron economy and excessive level of radiation damage. Therefore, this study focuses on the SWR type of B&B reactor and its fuel shuffling strategy.

In order to sustain the B&B mode of operation by feeding the core with fertile fuel such as DU, the burnup the fuel needs to accumulate has to exceed a certain threshold, which strongly depends on the core neutron balance. In a sodium-cooled metallic-fueled B&B core featuring high fuel volume fraction and low-leakage, the minimum required peak burnup is above 20% FIMA and the corresponding peak radiation damage of the fuel cladding is in the vicinity of 500 displacements per atom (dpa). (Hou et al., 2015) The maximum radiation damage cladding materials were exposed to so far in fast reactors is 200 dpa, experienced by the ferritic-martensitic steel HT-9 in the Fast Flux Test Facility (FFTF) (Toloczko et al., 1994). This means that the SWRs cladding material must withstand a radiation damage more than double the level that has been proven feasible. A combination of development of advanced structural and fuel materials and irradiation experiments are likely to increase the permissible clad radiation damage beyond 200 dpa but proving the practicality and licenceability of cladding material up to ~500 dpa may take significant time and resources.

Three approaches for operation in the B&B mode without exceeding the 200 dpa constraint had recently been investigated: (1) reconditioning the fuel whenever the cladding reaches 200 dpa. The function of the reconditioning is to remove the cladding, remove the gaseous and some volatile fission products, and load the fuel into a new cladding (Greenspan and Heidet, 2011). (2) Double-clad the fuel (Di Sanzo et al., 2011) after removal of the gaseous fission products. (3) Using excess neutrons from transmutation of trans-uranium elements from LWR UNF to drive a subcritical B&B blanket up to 200 dpa (Zhang et al., 2015).

The overall objective of this paper is to investigate a different approach for reducing the peak minimum required radiation damage level – use of 3-dimensional (3D) in-core fuel management strategy to reduce the axial variation of the discharge burnup and, thereby, reduce the peak burnup and corresponding peak radiation damage. In the 2D shuffled system, as the plutonium builds up near the axial center faster than at the bottom and top of the fuel assembly, the axial power and burnup distribution in B&B cores is significantly more centrally peaked than in conventional (uniform axial composition) sodium-cooled fast reactor (SFR) cores. In a typical low-leakage B&B core the peak-to-axially average discharge burnup can far exceed 2.0. If the axial profile of burnup or fast fluence can be flattened down to close to 1.0, the peak dpa level may be reduced significantly. An engineering approach to facilitate 3D fuel shuffling has been proposed in a previous study. (Qvist and Greenspan, 2014a; Qvist et al., 2015) That preliminary study concluded that the optimal 3D shuffling pattern (SP) offers an approximately 30% reduction in the peak radiation damage while increasing the fuel utilization relative to a 2D shuffling.

However, the previous study was based on a user specified trial-and-error approach and was limited to few trials applied to a single core. The 3D SP optimization presents a large decision space – for the reference core given in Hou et al. (2015) that features 12-batches and 4 axially stacked subassemblies there are on the order of 10^{61} SP combinations. Hence, an exhaustive search is not feasible since it is extremely computationally expensive. Moreover, the optimal core design should meet several constraints including the burnup reactivity swing, radial power peaking factor and relative assembly power change over the cycle. This makes a manual selection of SP impractical. In addition, the optimal SP is highly sensitive to the core dimensions and number of radial and axial shuffling zones. Thus, an automated optimization capability that is able to account for all the constraints is desirable.

The first objective of this study was to develop an automated methodology for the optimization of in-core fuel management for B&B reactors, for both 2D and 3D shuffling strategies that is able to account for multiple design constraints. Generic Algorithm (GA) has been successfully applied to in-core fuel management optimization of, primarily, light water reactors (Poon and Parks, 1993; DeChaine and Feltus, 1995; Parks, 1996) as well as for a self-sustaining LMFBR design. (Toshinsky et al., 1999; Toshinsky et al., 2000) Simulated Annealing (SA), a close relative to GA, is another stochastic approach to large-scale combinatorial optimization and has proven to be extremely robust in determining families of near-optimum decision variables in the in-core fuel management problems. (Turinsky and Parks, 1999; Stevens et al., 1995; Park et al., 2009) Although SA and GA are often viewed as separate, competing paradigms in the field of modern heuristics, the key difference between the two methods is the mechanism of generating a new solution from an existing one. While GA generates a new solution guess by combining several prior solutions, SA creates a new solution by modifying only the most recent solution with a local move. In the current optimization problem, the decision variable – the SP, is based on the shuffling of fuel batches rather than of individual assemblies. As a typical B&B core batch contains tens of fuel assemblies, the impact of SP modification on the core characteristics is much larger than that with single assembly-based SP, creating a much more nonlinear decision space. As a result, the "crossover" between different solutions in GA becomes less important in the generation of new solutions. The SA algorithm was adopted as the optimization method for this study.

The second objective of this study was to quantify the improvements in B&B core performance made possible by 3D fuel

shuffling and to investigate the dependence of these improvements on the number of axially stacked subassemblies, core power level and core dimensions.

Section 2 provides a detailed description of the reference B&B core design that features 2D shuffling, the engineering solution to implement the 3D shuffling in B&B cores, and the modeling methodology used in this work. The stochastic SP optimization methodology based on SA and the improvements of the core performance resulting from its application to the 2D/3D shuffled B&B core are then discussed in Section 3 and 4, respectively. Section 5 explores the 3D shuffled core performance sensitivity to the SP simplification, core power, and core size. Last, the general conclusion of the study and future work are provided in Section 6.

2. Breed-and-burn reactor with 3D fuel shuffling

2.1. Reference 2D shuffled core description

The reference B&B core concept upon which the 3D shuffled core were developed in this study is a large SFR fed with DU with 0.25% ^{235}U. The unirradiated nominal fuel density is 18.66 g/cm^3 at 800 K, and a smear density of 75% is assumed to accommodate the fuel swelling with burnup. The cladding material, which is the ferritic-martensitic alloy HT-9, and the coolant have densities of 7.87 and 0.830 g/cm^3, respectively, both at 800 K. The effective core height is 300 cm and equivalent diameter of the simulated core is ~493 cm, giving a total active core volume of 57.19 m^3, and a volumetric power density of 52.45 MW/m^3 for a total core thermal power of 3000 MW. This reference design adopts the vented fuel rod concept (O'Neill, 1965). The diving bell type ventilating device allows the release of the fission gas, but prevents the reverse-flow of the coolant into the fuel pin. (O'Neill, 1965) Venting the released fission gases from the fuel pin into the primary reactor coolant will maintain cladding stresses at low levels to high burnup. The fraction of core volume that is required for the control system was not accounted for in the preliminary core design because the required number of control assemblies cannot be estimated before detailed calculation for safety parameters is performed. The general characteristics and assumed volume fraction of the active core ingredients are presented in Table 1.

In fast reactors, the mean free path for absorption of the large majority of the neutrons far exceeds the dimension of the unit cell. Consequently, it is common to model the core as homogenized; that is, compositions of fuel, coolant, gap and structural materials are mixed together within the fuel assembly by volume weighting.

In order to further reduce the modeling effort of this feasibility study, the assembly-based hexagonal B&B core is represented in *R-Z* geometry, which consists of a number of equal-volume concentric fuel batches, each made of several axial regions to account for axial power and burnup variation. A schematic side view of the 2D shuffled core is given in Fig. 1, where the center of the core is at the left edge of the figure and fuel batches are separated by vertical lines in the active core region. It was estimated in previous studies that the relative errors in the multiplication factor k_{eff} introduced by the cylindrical modeling of the B&B core is between 0.02% and 0.2% $\Delta k/k$, when compared with the assembly-level core model. (Heidet and Greenspan, 2013) This error partially stems from the radial power distribution differences between the two models – in the cylindrical core model all the assemblies of a given batch are depleted with the same power level while in the assembly-based core model, a different power level is assigned to each fuel assembly. This approximation is considered acceptable for a study aimed at estimating the relative differences between 3D and 2D fuel shuffling on B&B core characteristics.

2.2. Engineering solution for 3D fuel shuffling

This section introduces the perceived design of the fuel rods and fuel assemblies to facilitate the 3D shuffling. In the original solution

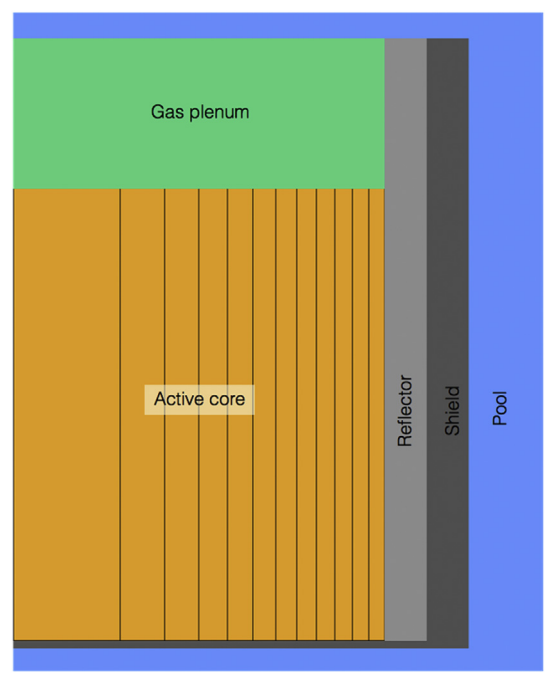

Fig. 1. Schematic layout of cylindrical 2D shuffled reference B&B core.

Table 1
Main parameters of reference B&B core.

Thermal power (MW)		3000
Core equivalent radius (cm)		246.34
Active fuel length (cm)		300
Gas plenum height (cm)		100
Feed fuel		DU (0.25%^{235}U) with 75% smear density
Coolant		Sodium
Inlet/outlet coolant temperature (°C)		355.0/506.8
Structural material (cladding, duct, wire-wrap, reflector pin)		HT-9
Fuel assembly volume fraction (%)	Fuel	40.70
	Gap	13.57
	Cladding + wire	13.04
	Duct	6.28
	Coolant	26.41
Density (g/cc)	Fuel (theoretical)	18.99
	Cladding	7.87
	Coolant	0.83

(Qvist et al., 2015), assembly segments are axially connected with upper and lower connecting grapplers to form a full-length assembly, while the segment at the bottom of the core is connected to a shielding and flow orificing block that is designed to remain in a fixed location in the reactor for the lifetime of the core. This design was later carefully evaluated and modified especially for the connecting mechanism to ensure the core stability under all operating conditions and the reliability when moving fuel assembles in the sodium coolant.

Assembly segments are composed of conventional rod-type fuel. In the updated fuel segment design, a nesting tapered conic interface is proposed for the segment–segment interface, as can be seen in Fig. 2. The top cap (blue) has a protruding hexagonal cone, and the bottom cap (green) has a re-entrant hexagonal cone. The generous tapered hexagonal cone provides a self-centering zone that is larger than the resolution limits of the refueling machine, ensuring consistently robust fuel segment movements. Adequate passages are provided on the conic surface for coolant flow.

Centering buttons on the side of the top and bottom cap provide consistent lateral positioning of the assembly segment in the core and maintain consistent gaps between segments, as shown in Fig. 3. Two buttons are provided at the bottom of the segment in order to maintain rotational registry with the core grid, while a single button at the top is adequate to maintain the position of the top of the segment. This arrangement minimizes the dragging of one segment against its neighbors when being inserted or removed. These centering buttons also provide a measure of tolerance for bowing or twisting of fuel assemblies over their service life.

Fig. 4 demonstrates the design of the fuel handling gripper with 3 jaws, which is positioned at the end of the refueling mast. A robust reinforcing ring is placed in the top of the fuel segment to distribute gripper forces and provide adequate wear surfaces for the life of the segment. A central rod actuator can actuate 3 jaws equally. During the refueling process, the refueling mast is positioned over the assembly segment and extended downwards to reach the segment. The segment is then attached with the handling gripper and lifted up. The gripper is smaller than the footprint of a segment, thus allowing it to reach a fuel segment on the lowest course without removing neighboring segments.

The full-length fuel assembly of the first design of 3D shuffled core investigated in this study, named as Design I, is made of four 77 cm long sub-assemblies making a 301 cm active core height. This core has three 7 cm thick fuel-free layers at the top of each of the three lower sub-assemblies due to the design of the sub-assembly fuel rods illustrated in Fig. 5. The effective fuel volume fraction of the resulting core is lower than the 2D shuffled core. The total power of the Design I core with segmented fuel assemblies is the same as of the 2D reference core.

All the fuel rods are assumed to be vented and allow for continuous release of gaseous fission products through a thin porous filter followed by small openings in the upper end cap as illustrated in Fig. 5. In order to minimize the fuel-free volume at the top of the rod, sodium bonding is eliminated. Instead, the metallic

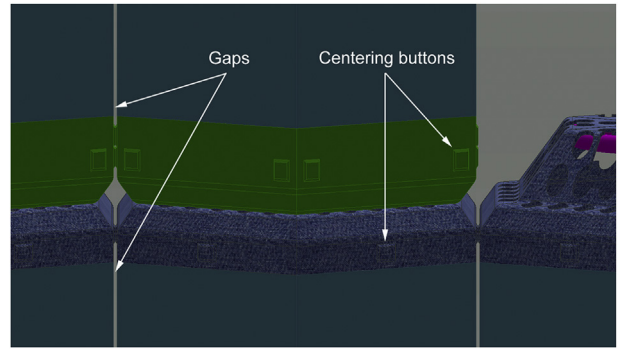

Fig. 3. Stacked fuel assembly segments with demonstration of centering buttons at the top and bottom of the segment and the gaps between segments.

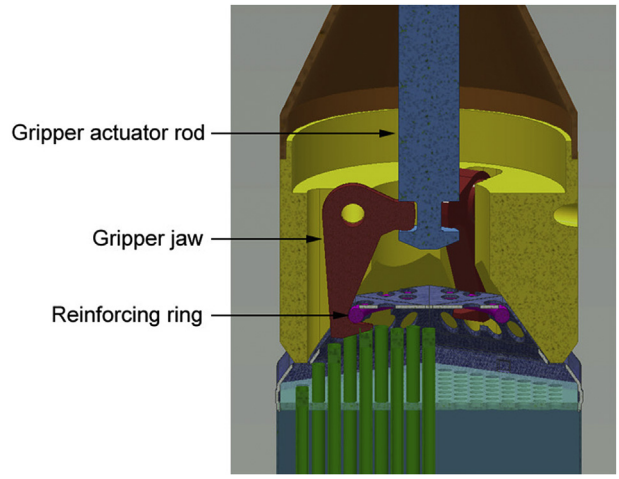

Fig. 4. Section view of the fuel gripper mechanism.

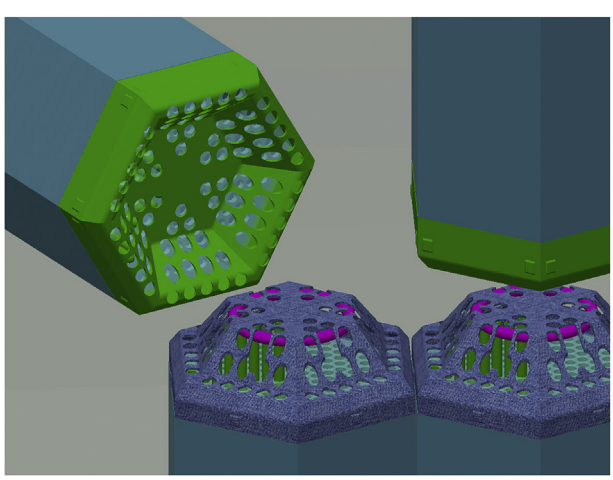

Fig. 2. Top and bottom cap of the proposed fuel segment design for 3D fuel shuffling.

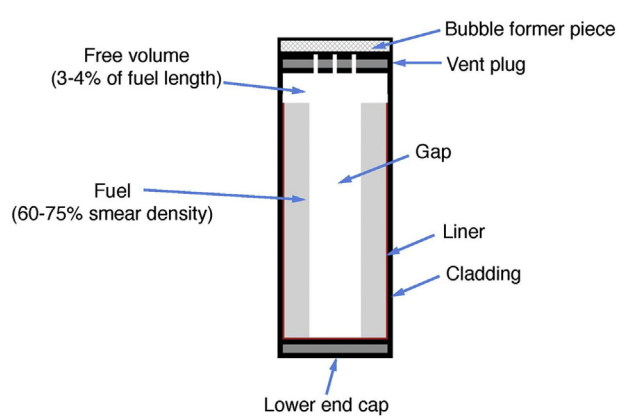

Fig. 5. Axially segmented fuel rod design for 3D fuel shuffling.

fuel is annular and mechanically bonded to a 30 μm vanadium liner (Ryu et al., 2009; Horak et al., 1962), which acts as a diffusion barrier to avoid fuel/cladding chemical interaction. The fuel swelling with burnup is accommodated by the central gap. The mechanical bonding to the cladding restrains the fuel axial swelling thus enabling to minimize the length of the fuel-free section at the top of the fuel rod.

2.3. Core design methodology

2.3.1. Neutronics model

The core characteristics compared in this study pertain to the critical equilibrium cycle. The search for the equilibrium cycle was performed using the DIF3D/REBUS-3 codes (Derstine, 1984; Toppel, 1983) which are part of the Argonne Reactor Computation (ARC) system from the Argonne National Laboratory (ANL). The finite difference diffusion method was employed in the flux and eigenvalue solver DIF3D as it is the only available option for *R-Z* geometry. The variable mesh structure can be defined in both radial and axial direction provide a higher resolution of the results, including flux and power etc. The fuel shuffling was modelled explicitly on a fuel batch basis in REBUS-3 calculations. For a given core geometry and constituents volume fraction, the design variables are the shuffling pattern and cycle length.

Burnup region-dependent 33-group cross section sets were generated from the ENDF/B-VII.0 data library using the ETOE-2/MC2-3/TWODANT sequence of codes of the ARC package. (Lee and Yang, 2013; Alcouffe et al., 1990) Specifically, the MC2-3 code first calculates 0-dimensional (0-D) neutron spectra and condenses point-wise cross sections prepared by ETOE-2 into an ultrafine group structure (~2000 groups). For non-multiplying regions such as reflectors and shield, leaking spectra from the fueled region is used for the condensation. Then, a 2-D ultrafine group transport calculation is conducted by TWODANT to take into account realistic leakage and the calculated spectra are fed back to MC2-3 for the final cross section condensation. It was found in previous studies that in order to accurately account for spectral variation in the B&B core, the best approach is to use burnup and location dependent group constants for the core simulation. (Hou et al., 2014) However, it is impossible to generate cross sections without knowing the zone-wise equilibrium composition beforehand. It is also difficult to assign cross sections to burnup zones while performing fuel shuffling in REBUS-3. Therefore, the preliminary core calculation was carried out using a cross section set generated for the fuel composition pertaining to intermediate burnup (~10% FIMA). This approximation is acceptable for the initial exploration of the effects to be expected from the newly proposed B&B core design and fuel management.

An external module has been developed to post-process REBUS-3 simulation results and produce key performance characteristics for the equilibrium core such as the zone-wise fuel burnup, infinite multiplication factor, power, and leakage. In particular, the radiation damage accumulated by HT-9 cladding is evaluated by folding cell averaged multi-group flux from REBUS-3 results with the isotopic neutron dpa cross sections. Based on the widely used Norgett–Robinson–Torrens (NRT) model (Norgett, 1975), the isotopic dpa cross section is given by the following formula:

$$\sigma_{DPA} = \kappa \frac{\sigma_d}{2E_d} \tag{1}$$

where σ_d is the damage cross section, which is included in the standard nuclear data in ENDF/B format (MT = 444 on the PENDF tape) and is available in MCNP libraries for most nuclides below 20 MeV. In this study, σ_d is collapsed into ANL 33-group structure using the same neutron spectrum as in the cross section preparation as described above. κ is the displacement efficiency compensating for forward scattering and is usually set to be 0.8. E_d, known as the displacement energy, is the minimum energy required to create a stable interstice and vacancy pair (Frankel pair). A constant value is used for each element in the compound, which is available in the ANL computer code SPECOMP (Greenwood, 1987). The dpa cross section of compound materials $\overline{\sigma}_{dpa}$ takes the form of a weighted average of isotopic-wise values, calculated by Eq. (1). The accumulated dpa of HT-9 cladding over the equilibrium cycle is obtained by

$$R = \sum_{j=1}^{4}\left(\sum_{g=1}^{33}\overline{\sigma}_{dpa,g}\phi_{g,t}\right)\Delta T_j \tag{2}$$

where $\phi_{g,t}$ is the burnup zone averaged neutron flux of group g during burnup step j, and ΔT_j is the corresponding burnup step interval. In REBUS-3, the maximum allowable number of burnup steps in the equilibrium cycle is 4.

In previous studies, (Hou et al., 2015) the capability of the simplified DIF3D/REBUS-3 model for determining equilibrium composition of B&B cores has been verified by comparing against a continuous energy Monte Carlo (MC) code Serpent. (Leppänen, 2010) Both deterministic and MC calculations used the ENDF/B-VII.0 cross section library and assumed uniformity of temperature distribution for fuel/clad (800 K) and coolant (600 K) in the active core to have consistency between the two models. They differ, however, in the depletion calculations – whereas Serpent uses a detailed burnup chain, the REBUS-3 calculations use a pre-stored plutonium–uranium burnup chain to simplify the input preparation in two ways. First, it does not include all the heavy metal nuclides prepared in the cross section library. Second, the effect of fission products was accounted for using lumped fission product (LFP) cross sections for 4 different fissionable isotopes that were created from cross sections of 137 individual fission products using fission yields for ^{235}U, ^{238}U, ^{239}Pu, and ^{241}Pu. It was found (Hou et al., 2015) that the relative difference of the core characteristics such as cycle length, discharge burnup, reactivity swing, and power peaking factor, is within 4%, indicating that the deterministic approach is adequate for quantifying the relative difference in the performance of B&B cores designed using 3D versus 2D fuel shuffling. The computational time for an equilibrium cycle search using REBUS-3 is ~12 min on the UNIX cluster at UCB, which is a significant reduction when compared with ~23 h using Serpent.

2.3.2. Coupled neutronics/thermal-hydraulics approach

The abovementioned standalone neutronics study of the equilibrium performance of the B&B core assumes that the core can operate at the designed power level without violating any thermal-hydraulics constraints. However, the peak assembly power depends on the radial power distribution which depends on the fuel shuffling scheme. Therefore, thermal-hydraulics calculations are incorporated into the core optimization process through coupling with neutronics calculations using the ADOPT code (Qvist and Greenspan, 2014b). ADOPT aims to automatically search for the optimal fuel assembly design that maximizes the fuel volume fraction while adhering to set constraints for all component temperatures, pressure drop, coolant velocity and structural integrity limits, subjected to a specified peak assembly power level. The coupling scheme used to converge on thermal-hydraulic and neutronics solutions for critical equilibrium cycle B&B cores is given in Fig. 6. A separate module – PyRebus, was developed to prepare the input files, control data exchange, and check the convergence of the iterative process. For a given core specification (defined by

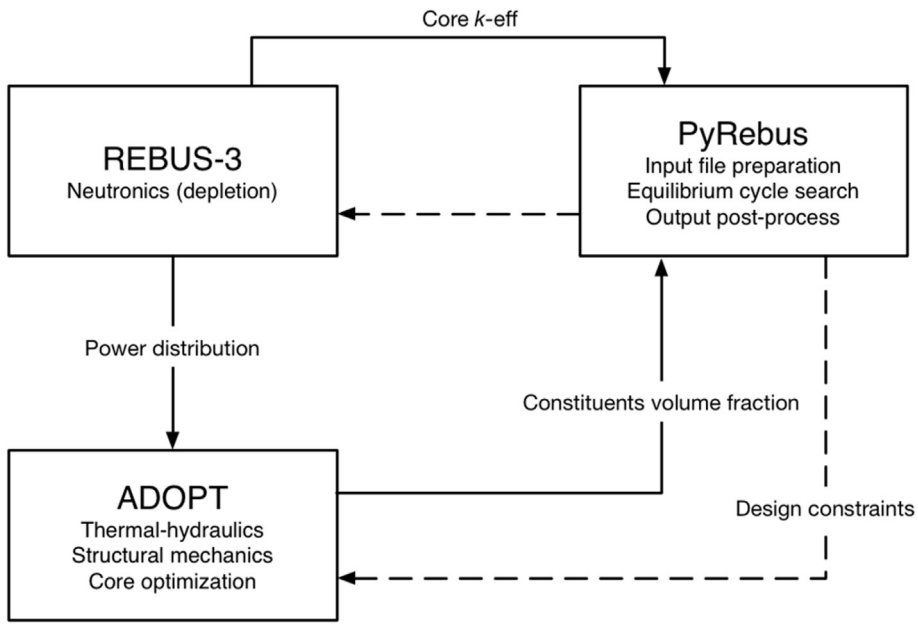

Fig. 6. Coupled neutronics-TH calculation scheme for equilibrium B&B core search.

geometry, material, SP, etc.), the process starts with REBUS by searching for the equilibrium critical cycle and calculating its performance parameters. Then, the power distribution is sent to the ADOPT model, which has the identical core specification as in REBUS, to generate the volume fraction of all constituents that will enable the peak power assembly to meet all the design constraints. If different from the previous iteration, this information is fed back to REBUS to repeat the search for equilibrium core until a converged critical core design has been found. The fuel volume fraction and the maximum cycle radial power peaking factor require 4–5 iterations to converge to an error less than 2%.

The thermal-hydraulics constraints accounted for in this study are:

(1) maximum core pressure drop: 0.9 MPa, (Qvist et al., 2015).
(2) maximum sodium velocity across the core: 12 m/s, (Fast Reactor Database 20, 2006).
(3) maximum fuel-cladding interface temperature: 650 °C, (Suspluagas and Greenspan, 2005) and
(4) maximum peak fuel temperature: 1000 °C. (Bleise et al., 2003).

3. Shuffling pattern optimization using simulated annealing method

3.1. Simulated annealing method

Simulated Annealing (SA) is a stochastic optimization technique motivated by an analogy to annealing in metallurgy, which involves repeatedly heating and cooling of a material to increase the crystal size and remove defects so as to alter its physical properties. The principal fundamental of SA was first introduced by Metropolis et al. (1953) as a tool of finding equilibrium configuration of a system of particles at a given temperature. Kirkpatrick and Vecchi (1983) later proposed and applied it to combinatorial optimization problems, in which a family of candidate solutions to minimize the objective function is generated following a Markov chain sampling. Its major advantage over other methods is an ability to avoid being trapped at local minima, because the random search not only accepts changes that improve the solution performance but also some changes that worsen it.

In the general implementation of the SA method (Dowsland and Reeves, 1995), a control parameter T is introduced for system temperature, and the energy difference between the two states of the material is replaced by the difference between the current objective function value $F(X_i)$ and the proposed objective function value $F(X_j)$, with X denoting the solution to the optimization problem. The algorithm begins with an initial guess at the optimal solution and then seeks successively improved solutions through a continuing examination of randomly generated solutions in the neighborhood of the ever-changing optimum. For a minimization problem, the probability of acceptance for a new solution $F(X_j)$ is given by

$$p(\Delta F, T) = \min\left\{1, \exp\left(-\frac{F(X_j) - F(X_i)}{T}\right)\right\} \tag{3}$$

As such, candidates that decrease F are, of course, accepted, while candidates that increase F by $\Delta F = F(X_j) - F(X_i)$ are accepted as new solutions with the probability calculated in Eq. (3).

The control parameter T usually decreases in a series of discrete steps over time. In principle, the initial temperature must be high enough to allow shuffling to more neighborhood states. The annealing process continues until the temperature reaches the final temperature, or until some other conditions are met. The most widely used temperature decrement strategy is the exponential multiplicative schedule or geometric schedule, where the temperature decrease is achieved by multiplying the initial temperature T_0 by a factor that decreases exponentially with respect to the k-th simulation cycle:

$$T_k = T_0\alpha^k \tag{4}$$

where $\alpha(0 < \alpha < 1)$ is called the cooling parameter. The cooling parameter is the significant search controller. If α is too small, then cooling is too fast, and the search quickly terminates near a local optimum. If α is too large, then cooling is slow, and the search degenerates to an expensive enumeration.

While convergence on the global optimum solution is generally not guaranteed, empirical evidence shows that for many problems, the SA algorithm converges on a family of solutions in the neighborhood of the global optimum and overcomes convergence to local optimum solutions. (Aarts and Korst, 1989).

3.2. Optimization model

3.2.1. Formulation of objective functions

The primary objective of the SP optimization is to reduce the peak minimum required radiation damage as much as possible. However, it is desirable to account for other design constraints including:

(1) Reactivity swing during burnup cycle: $\Delta\rho \le \Delta\rho^{lim}$
(2) Change of batch power over the cycle: $\Delta P_B \le \Delta P_B^{lim}$
(3) Radial power peaking factor: $F_R \le F_B^{lim}$

The burnup reactivity swing FBRs are usually designed to have does not exceed 3.5%. A smaller reactivity swing implies a smaller number of required control assemblies or smaller worth of each control assemblies. The former leads to a higher core average fuel volume fraction and therefore a better neutron economy, while the latter can reduce consequences of a transient overpower accident (UTOP). The minimization of the maximum relative change in the batch power will result in maximum core average coolant exit temperature and, hence, highest possible energy conversion efficiency. This is because the radial coolant flow distribution must be designed, via orificing, for the peak-power conditions and cannot be adjusted over the cycle. Minimization of the radial peaking factor results in minimization of the peak assembly power and maximization of the fuel volume fraction and, hence, of the neutron economy.

These constraints can be handled in SA as "hard" limits, meaning that any solution that violates them is rejected. For an optimization viewpoint, the disadvantage of this approach is that trapping in local minima can occur, thus preventing an optimal SP from being found. (Turinsky and Parks, 1999) An alternative is to define an augmented objective function, in which the main objective function is augmented by the penalty terms reflecting the extent of violation of the active constraints:

$$\overline{F} = \gamma R^* + \sum_{i=1}^{I} \lambda_i \Omega_i \tag{5}$$

where the first term on the right side of Eq. (5) is the main objective function corresponding to the evaluation of peak radiation damage, and each penalty term in the summation represents the contribution of one of the constraint related objectives to the augmented objective function. The violation functions Ω, taking the forms given in Table 2, are the relative differences of current value of the parameter from the pre-defined design constraints, of which the values in the 3rd column of the same table were adopted in this study. The impact factor λ are introduced to adjust the importance of each objective; for example, in the case where reactivity swing minimization takes the priority in SP optimization, all that must be done for the objective function transition is to increase the impact factor associated to Ω_1. γ is a multiplication constant used to adjust R^* to the same order of magnitude of the penalty terms in Eq. (5); a value of 0.01 is used in this study.

Table 2
Elements and constraints of augmented objective function.

Description	Violation function	Constraint
Reactivity swing during burnup cycle	$\Omega_1(\Delta\rho) = \frac{\Delta\rho}{\rho^{lim}} - 1$	$\Delta\rho^{lim} = 7.0$
Max change of batch power	$\Omega_2(\Delta P_b) = \frac{\Delta P_b}{\Delta P_b^{lim}} - 1$	$\Delta P_B^{lim} = \frac{P_{th}}{N_b}$[a]
Radial power peaking factor	$\Omega_3(F_R) = \frac{F_R}{F_R^{lim}} - 1$	$F_R^{lim} = 2.5$

[a] P_{th} refers to the core thermal power; N_b denotes the number of radial fuel batches in the core.

3.2.2. Solution update and cooling scheme

The variable of the optimization problems considered in this work is the SP, which can be visualized as a 2D array of burnup zones. Given as an example of SP map in Fig. 7, four layers of zones indicate that a fuel assembly is constituted of four axially stacked segments, and the radial zones correspond to fuel batches. The lower left corner on the map is the center of the core lower boundary. In the 3D shuffling, the content of one sub-assembly or burnup zone can be relocated to any other zone on the SP map at the refueling stage before discharged from the core. The tracking of the fuel content creates a fuel management path, which represents a unique shuffling sequence of this sub-assembly. In a 12-batch core using the current assembly design, there exist four independent fuel paths, each consisting of 12 burnup stages. In the 2D shuffling, the SP map is reduced to 1D array of 12 burnup zones, because the fuel assembly is only shuffled in radial direction.

The mechanism for generating a candidate SP from the current solution is based on binary fuel exchange, which involves the exchange of burnup cycle numbers of two randomly selected fuel zones from the SP map. In the 3D shuffled case, an additional exchange is required for another two zones, whose positions are axially symmetric with those in the first operation, so that the symmetry of the SP can be preserved. The normal and dashed lines in Fig. 7 demonstrate these two executive operations in a SP with four axial assembly segments (as in Design I core). This type of SP is later referred to as "unconstrained" SP, because it imposes no restrictions on the choice of four sub-assemblies for reconstituting new fuel assemblies. In a 2D shuffled case, the exchange is performed only once for two randomly selected batches, or equivalently two columns in the 3D shuffling map. The binary exchange update scheme is designed in such a way that the perturbation to the accepted SP is small enough to ensure the desirable attributes can be carried forward.

For the purpose of expediting the optimization, the randomly generated SP goes through a screening process for additional restrictions before the performance evaluation. For example, the fresh fuel loading is restricted to the core radially outermost batch. This is primarily to minimize the radial leakage probability, but can also significantly reduce the search space of the optimization process. In 3D shuffled case, discharging fuel from axial boundary zones is avoided because previous studies show that the loading of high reactivity fuel in boundary zones introduces strong axial leakage and imposes detrimental impact on the neutron economy.

As shown in Eq. (3), the probability of accepting worse SPs is also reduced with the control parameter T as the optimization proceeds. The value of T has no physical meaning and its scale is highly dependent on the problem under consideration such as the initial guess of the SP. The determination of the initial value of T is then transferred to the determination of the initial acceptance probability, because the latter defines the optimization process in a more direct way and has little problem dependence, as pointed out in Stevens et al. (1995) Once the initial probability threshold P_0 is input by the user, several trial-and-error runs are conducted to estimate the average change in the objective function outcome $\overline{\Delta F}$. Based on Eq. (3), the value of T_0 can be determined as

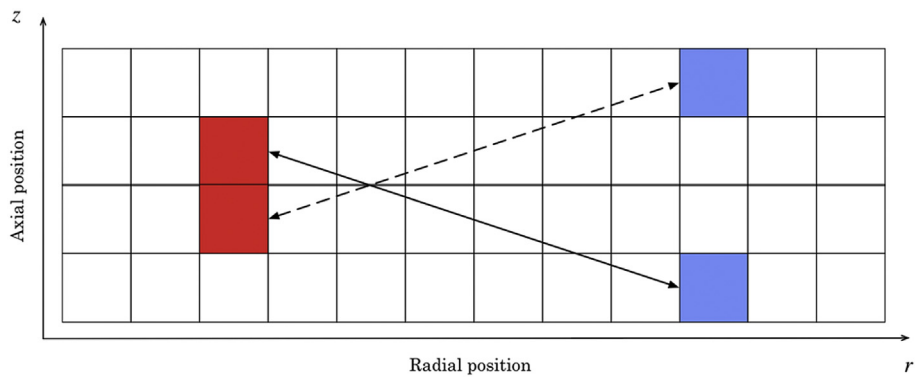

Fig. 7. Shuffling pattern update scheme: binary fuel exchange.

$$T_0 = -\frac{\overline{\Delta F}}{\ln P_0} \tag{6}$$

A value of P_0 usually selected is ≈ 8.2 as it was found to ensure early acceptance of solutions between local minima. The selection of the cooling parameter value α is usually arrived at based on the experience, but typically it is between 0.80 and 0.99. (Aarts and Korst, 1989) A number at the higher end of this range is preferred as the design space for this problem is highly nonlinear. The final value of T can be determined by its initial value, the total number of cooling stages and the cooling parameter α.

In summary, the SA optimization proceeds by performing a perturbation to the initial guess of SP, based on a single binary fuel exchange, and calculating the initial probability of acceptance. The SA algorithm then chooses whether or not to preserve or replace the current SP. More binary exchanges are then performed, producing improved evaluations of the objective function at decreasing values of the control parameter T until the maximum number of cooling stages specified by the user is reached. A strategy flowchart of the optimization process is displayed in Fig. 8, in which the term "evaluate SP" refers to the estimation of the augmented objective function outcome for a specific SP using REBUS.

4. Simulation results and analyses

The performance of the SA algorithm was first examined by optimizing the SP for both the 2D shuffled reference core and the 3D shuffled Design I core; both using 12-radial batches. The "out-in" SP was selected as the initial guess, where the fresh fuel is loaded at the outmost radial batch, sequentially shuffled inwards at the end of cycle and finally discharged from the central core batch. The reason for choosing this SP, which inevitably leads to an extreme radial power peaking, rather than using some already optimized SP otherwise as the initial SP is to avoid trapping in the local minima and enable deeper exploration of the new methodology and design space.

In the 2D shuffling, each assembly was subdivided into 8 equal volume axial burnup zones, while in the 3D shuffling each of the four sub-assemblies was subdivided into two burnup zones so that

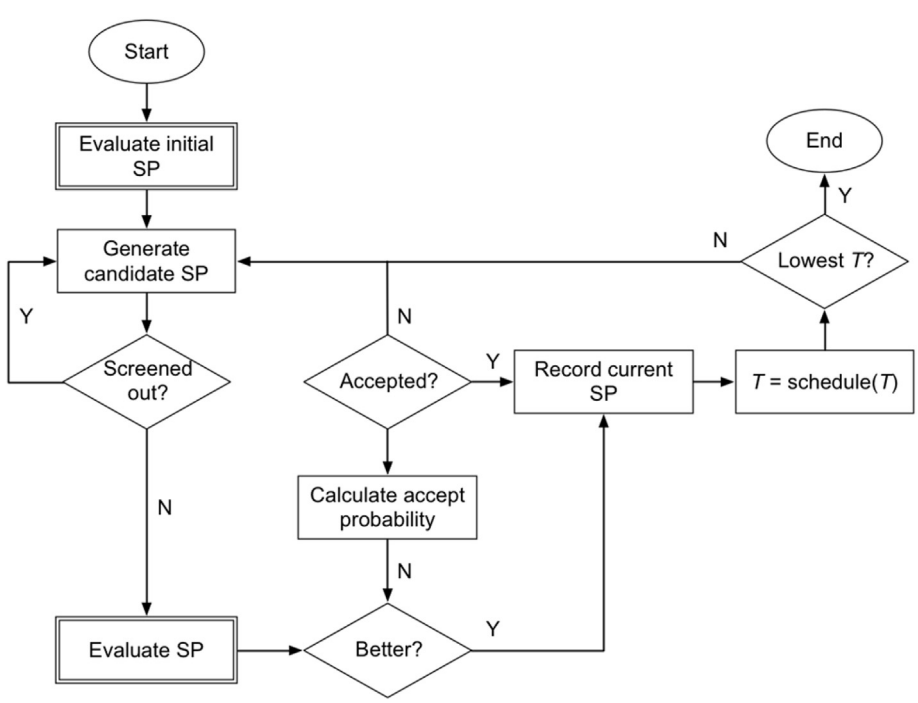

Fig. 8. Flow diagram of shuffling pattern optimization using simulated annealing.

a consistent comparison of core performance can be performed for the two cases. The path dependent burnup and radiation damage were calculated based on these eight burnup zones.

The behavior of the augmented objective function, defined by Eq. (5), as well as of its components, in the 3D shuffled case is displayed in Fig. 9 as a function of cooling stage. The radial power peaking factor or the peak assembly power was considered as a thermal-hydraulics constraint and is not included in the neutronics optimization. It was later on taken into account separately in the thermal-hydraulics validations, as described in Section 2.3.2, to adjust the achievable fuel inventory for a selected SP. All other active constraints were considered equally important, so 1.0 was adopted for all impact factors λ. As a result, the current problem is considered as the multi-objective optimization problem aiming at finding the best SP to have the lowest possible peak radiation damage (R^*), the smallest burnup reactivity swing ($\Delta\rho$) and the least relative change of batch power (ΔP_B). The initial and final temperatures of this case were determined to be 6.15 and 0.22, respectively, based on the approach described in Section 3.2.2.

In the first 500 cooling stages in the optimization history, all components of the augmented objective function clearly exhibit a decreasing trend, with larger oscillations at the early stage and smaller towards the end. It implies that the SA algorithm allows a wide exploration of the design space by accepting solutions degrading the core performance, and tightens the acceptance criterion as the simulation proceeds. It could also be seen that penalty terms reached their minima at different rates, and the minimum value of the augmented objective function is found at cooling stage 464. In this case, most of the SPs generated after the 400 simulation cycle are preferred from the neutronics point of view, among which four SPs with low radial power peaking factor were selected for thermal-hydraulics evaluation. For each of the SPs, it took no more than five iterations for the REBUS-ADOPT approach to arrive at converged volume fractions and radial power peaking factor, and generate the best 3D SP that can meet all thermal-hydraulics constraints.

The same SP optimization was conducted for the 2D SP, and the actual optimum SP is depicted at the top of Fig. 10. The fresh fuel is loaded at the core periphery, then shuffled to the center, before starting to "bounce" between the outer and inner region of the core and finally discharged from the 8th radial location. The optimum 3D SP, as shown in the bottom of Fig. 10, uses four independent fuel paths. The colors of the 3D SP distinguish those shuffling paths, while the numbers indicate the burnup cycle of the relocation (1 where the fuel is loaded and 12 where the fuel is discharged). It can be seen that the fuel is shuffled to the high reactivity worth regions after the first irradiation cycle and discharged from the core axial center from the 10th and 11th radial positions. The axial discretization of each full-length assembly in 3D shuffling is shown in Fig. 11.

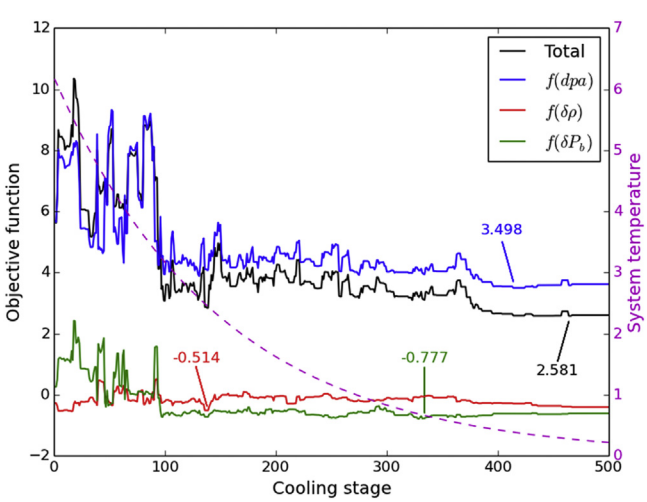

Fig. 9. Convergence history of SP optimization with SA algorithm.

Table 3 compares the equilibrium core performance using the optimal 2D and 3D SP described above. The 3D shuffling enables a 34% reduction of the peak radiation damage – from 534.2 dpa in 2D shuffling case to 351.0 dpa for the 3D case. The equilibrium cycle length was increased from 1083 for 2D to 1566 effective full power days (EFPD) for 3D shuffled systems. The corresponding average discharge burnup increased from 9.91% to 14.49% FIMA. This implies an approximately 45% increase in the fuel utilization. If normalized to the same dpa level, the average discharge burnup of the 3D shuffled core is 2.23 times that of the 2D shuffled core; this corresponds to a relative increase in the fuel utilization of nearly 120%. Although 351 dpa is still beyond the proven radiation damage limit for HT-9 cladding, it is expected that ongoing and future irradiation experiments and new material development will enable to reach this dpa value much sooner and with higher certainty than the >500 dpa required for 2D shuffling cores.

The thermal-hydraulics corrected fuel volume fraction was 40.16% and 39.77%, corresponding to the fuel pin pitch-to-diameter (P/D) ratio of 1.065 and 1.070, for 2D and 3D shuffled system, respectively, due to the somewhat higher radial power peaking factor of the 3D shuffled core. The radial and axial power distributions of the 2D and 3D shuffled cores, shown in Figs. 12 and 13, are quite similar. The radial power distribution peaks at the 8th radial batch since a large portion of the high burnup and, therefore, high k_∞ fuel is located in radial batches 8 through 10. Over the cycle the radial power distribution tends to shift towards the core center as the fissile contents builds up steeply with burnup at the low burnup fuel that is loaded at the inner region of the core. Due to the axial shuffling of the segmented assemblies, the axial peaking factor was brought down from 2.35 in 2D to 2.00 in 3D shuffled core. As a result, the leakage probability from the 3D shuffled core is 17% higher.

It should be noted that a relatively fine computational mesh has been applied to the finite-difference calculation of the equilibrium core using DIF3D with the mesh size always smaller than 5 cm everywhere in the active core in both radial and axial direction. This is considered adequate for the fast reactor simulation. The fine-mesh output of power and flux were then averaged within each burnup zone to obtain the corresponding distribution in a coarser discretization, from which the peak and average value of some of the key performance characteristics were interpreted, such as power and radiation damage. Despite the simplified cylindrical geometry, this spatial mesh structure (as seen in Figs. 12 and 13) is considered adequate to represent the actual core performance. This is because the B&B core has to be designed sufficiently large to improve the neutron economy and each fuel batch consists of a large number of assemblies, which leads to many possible ways to reduce the peaking factor in each batch to nearly 1.0 by carefully choosing the new location and rotation for each assembly during fuel shuffling. This is especially the case for 3D shuffling where the axial movement of the fuel segment is realized. However, the development of the explicit assembly-based SP and its optimization were not included in the current study and will be pursued when a hexagonal assembly-by-assembly model is available.

The neutron balance analysis described in Heidet et al. (2009) and Heidet and Greenspan (2012) can be used to estimate the net number of excess neutrons generated by a unit volume of fuel, N_{ex}, as a function of burnup as follows:

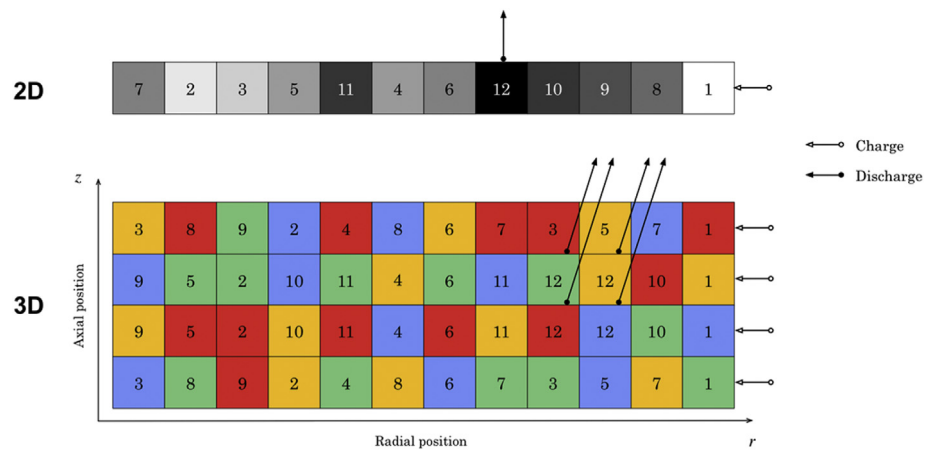

Fig. 10. Optimal 2D (top) and 3D (bottom) shuffling pattern for Design I B&B core.

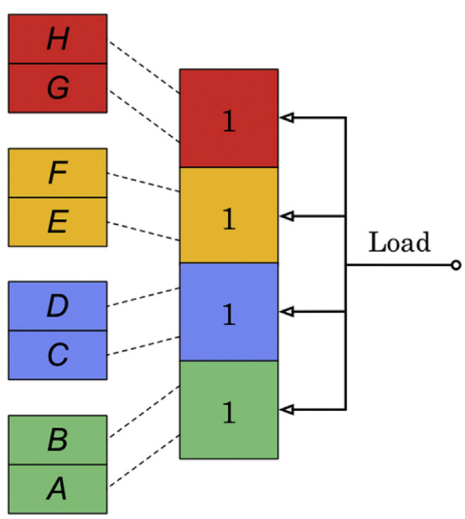

Fig. 11. Axial discretization of fuel zones.

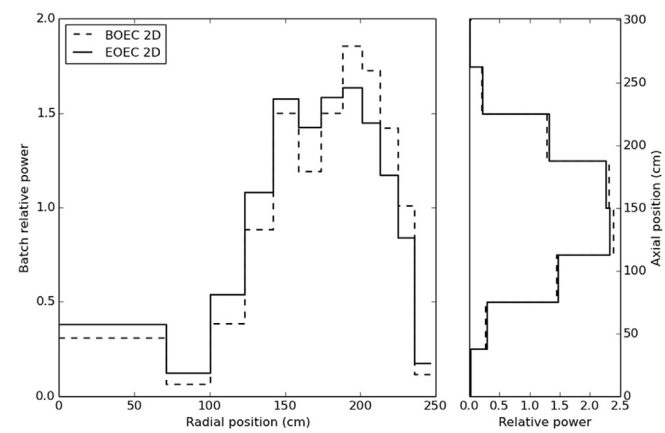

Fig. 12. Radial and axial power distribution for 2D shuffled Design I core.

Table 3
Results for Design I B&B core (3000 MW).

Equilibrium parameter		2D shuffled	3D shuffled
Burn cycle time (EFPD)		1083	1566
Burnup reactivity swing (% Δk/k)		2.81	4.66
Average discharge BU (% FIMA)		9.91	14.49
Peak discharge BU (% FIMA)		23.62	15.69
Peak radiation damage (dpa)		534.2	351.0
Peak fast fluence (n/cm^2)		1.28E+24	9.88E+23
Axial/radial leakage probability (%)		1.00/2.67	1.56/2.75
Axial/radial power peaking factor		2.35/1.64	2.00/1.70
Peak batch power change (%)		17.07	22.14
Pitch-to-diameter ratio		1.065	1.070
Core volume fractions (%)	Fuel	40.16	39.77
	Gap	13.39	13.26
	Cladding + wire	12.85	12.77
	Duct	6.59	6.57
	Coolant	27.03	27.63

$$N_{ex} = N_{HM}\int_0^{BU}\left[1-\frac{1}{k(BU)\times P_{NL}\times P_{NRC}}\right]\bar{\nu}(BU)dBU \qquad (7)$$

In the above, $k(BU)$ refers to the k_∞ evolution with burnup in the control volume. Although in practice fuel is shuffled in the reactor core and thus depleted with variable power density during its lifetime, the k_∞ evolution curve in the infinite medium with fixed power density can be used to understand its behavior as a function of burnup, as illustrated in Fig. 14. It can be seen that k_∞ increases rapidly with burnup before it reaches 1.0 and the change slows down in the vicinity of its maximum value.

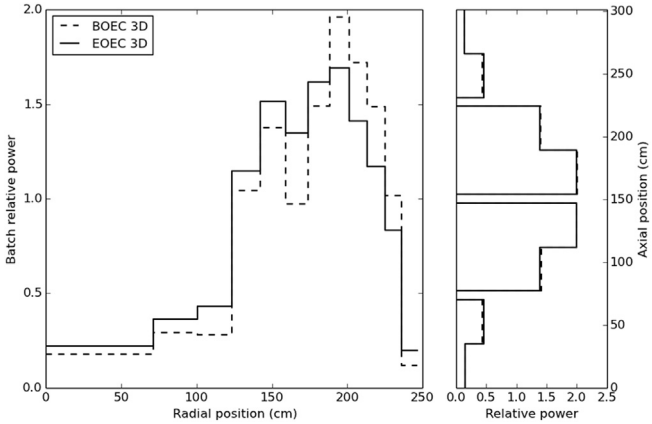

Fig. 13. Radial and axial power distribution for 3D shuffled Design I core.

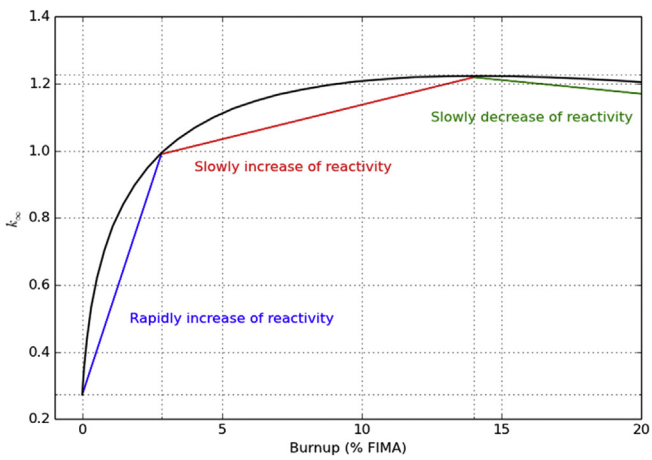

Fig. 14. k_∞ evolution with burnup of metallic DU fuel (Qvist et al., 2015).

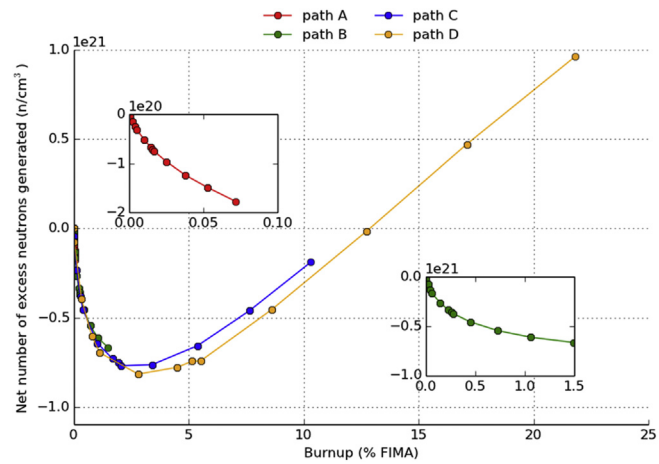

Fig. 15. Fuel path dependent neutron balance of 2D shuffling for Design I core.

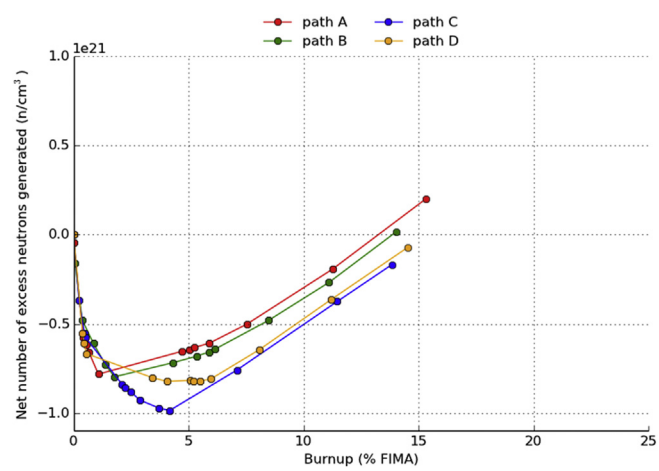

Fig. 16. Fuel path dependent neutron balance of 3D shuffling for Design I core.

In Eq. (7), N_{HM} is the Heavy Metal (HM) atom density, BU is the burnup expressed in FIMA, $\bar{\nu}$(BU) is the average number of neutrons released per fission, P_{NL} (=1 − P_L) is the non-leakage probability and P_{NRC} (=1 − P_{RC}) is the probability that a fission-born neutron will escape capture in the control elements used to compensate for the burnup reactivity swing over the equilibrium cycle. The minimum burnup required for sustaining a B&B operation is that burnup for which $N_{ex} = 0$.

A neutron balance analysis is carried out for each of the 8 axial equal burnup fuel batches as they traverse the core from loading to discharge. The burnup dependent infinite multiplication factor of each of these fuel batches is calculated as the ratio of neutron production rate to neutron absorption rate. The neutron production from (n, 2n) and (n, 3n) reactions is assumed negligible. It is assumed that the neutron loss is constant throughout the cycle and equals to the average of its BOEC and EOEC values. Fig. 15 and Fig. 16 plot the neutron balance curves of 4 out of the 8 axial fuel burnup batches, also referred to as "fuel paths", for the optimal 2D and 3D shuffled cores following each batch shuffling path as defined in Figs. 8 and 9. Because of near axial symmetry, the neutron balance of the other four axial fuel burnup paths is very similar. The turning point of the neutron balance plots from a negative to a positive slope corresponds to k_∞ of 1.0; at smaller burnups the fuel is a net neutron consumer – i.e., it absorbs more neutrons than it generates, while at higher burnups the rate of fission neutrons the fuel generates exceeds the rate of neutrons it absorbs. A negative sign in the neutron balance implies that there is a net cumulative neutron loss, whereas a positive sign pertains to burnup over which a net excess of neutrons has been generated by a unit fuel volume.

In the 2D shuffled reference core, The fuel of path A and B remained a net neutron absorber throughout its residence in the core; the neutron balance of these burnup batches did not even reach the turning point implying that their discharge $k_\infty < 1.0$. The fuel of path C, although becoming a net neutron producer, did not manage to pay back the number of neutrons it absorbed. Only the axially central fuel path D (and its counterpart E) exceeded the zero balance line and by a large extent as it has to make up for the neutron deficiency of the other three fuel paths.

In the 3D shuffled Design I core on the other hand, the fuel of each of the paths has paid back all or most of the neutrons it absorbed; it's neutron balance at discharge is in the vicinity of zero, as can be seen in Fig. 16. This is because the 3D fuel shuffling significantly flattens the burnup distribution of the discharged fuel as can be deduced from the burnup corresponding to the end point of the neutron balance curve of each of the fuel paths shown in Fig. 16. The 3D fuel shuffling also significantly increases the average discharge burnup and therefore also the cycle length. The longer cycle increases the positive burnup reactivity swing from 2.81% of the 2D to 4.66% of the 3D shuffled and therefore also of the fraction of neutrons that are absorbed in the reactivity control system. However, per unit time or given amount of energy generated, the

burnup reactivity swing is comparable: 1.09% versus 0.95% $\Delta k/k$ per effective full power year (EFPY).

The peak dpa of the fuel discharged from each of the 8 fuel management paths of the 2D and 3D shuffled cores is displayed in Fig. 17. In the 2D shuffled core the dpa strongly peaks at the core axial center (Paths D and E) while with 3D fuel shuffling the peak discharge dpa is within ±3% of the average.

In summary, 3D shuffling offers an increase of 45% in the average discharge burnup, and hence the fuel utilization, along with a 34% reduction in the minimum required peak HT-9 dpa – from 534.2 to 351.0 dpa. The 3D shuffled Design I core therefore far outperforms the 2D shuffled reference core on both economics (average burnup and cycle time) and radiation damage. However, the 2D shuffled core provides a less severe reactivity swing over the cycle and a smaller power change within one batch, both of which are direct results of the difference in the SPs.

5. Sensitivity of core performance to core design simplification

The implementation of the 3D fuel shuffling strategy considered in the previous section will require significantly longer refueling time, more complicated refueling machine and, possibly, two separate refueling machines to cut down the total refueling time, (Qvist et al., 2015) and larger workspace above the core to disassemble and reassemble the fuel assemblies relative to 2D fuel shuffling. Therefore, a number of design approaches for 3D shuffling simplifications were examined and their effect on the core performance improvements relative to 2D fuel shuffling was quantified.

The first approach to reduce the refueling effort is to avoid shuffling sub-assemblies between fuel assemblies; that is, to restrict the shuffling of sub-assemblies to axial shuffling within the same fuel assembly. (Dubberley) Radial shuffling will be performed for entire fuel assemblies as in a 2D shuffling strategy. More specifically, at the refueling outage, a fuel assembly is lifted from the core segment by segment, then reassembled in a different radial location using the same sub-assemblies but in a different axial order. This shuffling strategy will greatly reduce the workspace and time required for refueling. The performance of Design I core using this restricted SP is compared with the reference 3D shuffling strategy in Section 4.

The second approach is to reduce the number of segmented assemblies used to constitute one fuel assembly. Two variants of Design I core were studied; their design parameters are given in Table 4. Design II core is loaded with fuel assemblies made of 3 axially stacked sub-assemblies, each having identical dimensions as of Design I. The active core height is 228 cm (consisting of 3 segmented rods and 2 volumes of fuel-free space in the axial direction), giving a core volume of 42.70 m^3. As will be shown in Section 5.2, the core thermal power of Design II was adjusted to achieve the same fuel specific power as of Design I, which was 7.22 kW/kg. The resulting core power was 2340 MW, corresponding to a volumetric power density of 54.80 MW/m^3, which is slightly lower than that of Design I.

Design III core further reduces the number of sub-assemblies to two per assembly while preserving Design I active fuel length. The fuel length of each sub-assembly was doubled to 140 cm followed by 7 cm for fuel axial expansion and venting. The resulting core height is 287 cm–14 cm shorter of Design I core. Again, the core power of 2935 MW was determined by matching the fuel specific power of Design I and III. This yields a slightly lower core volume of 54.71 m^3 and volumetric power density of 54.83 MW/m^3. The performance of Design II and III cores is given in Section 5.2 and 5.3, respectively.

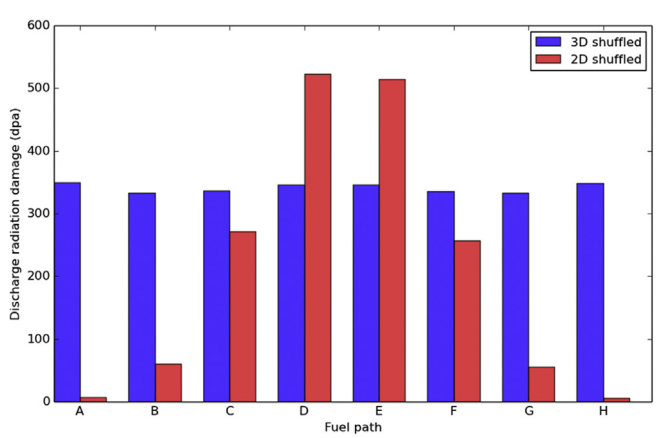

Fig. 17. HT-9 discharge dpa for Design I core.

5.1. Design I core with constrained axial shuffling

SA algorithm was employed to search for the optimal 3D SP for Design I B&B core while restricting the axial shuffling to interchanges in the axial location of the sub-assemblies within the same fuel assembly. The radial shuffling of entire assemblies follows the strategy of the optimal 2D SP for the reference core, as shown in Fig. 10, to take advantage of the already improved core performance in addition to further reducing the optimization effort. The optimal SP arrives at is shown in Fig. 18. Comparing with the 2D shuffled core, each fuel assembly in this case was reassembled using the same sub-assemblies but in a different order, which helps flatten the axial profile of burnup and power.

The resulting optimal core performance using axially-constrained fuel shuffling is compared with the unconstrained result in Table 5. The equilibrium cycle length and discharge burnup are 1728 EFPD and 16.02% FIMA respectively, both slightly larger than those of the unconstrained case. By placing high burnup fuel (e.g. batch 11 and 12) at the axial periphery of the core, this shuffling strategy is able to flatten the axial power peaking factor to 1.37, but inevitably causes a higher axial leakage probability of 3.84%. The radial power peaking factor of 1.78 is slightly higher than the 1.70 of the unrestricted 3D shuffled core. This required to reduce the fuel volume fraction from 39.77% to 39.27% in order to meet the thermal-hydraulic constraints. This increase of core leakage and the reduction of fuel volume fraction are the major contributors to the 25 dpa increase in the minimum required peak radiation damage to the HT-9 cladding, when compared with the 3D SP introduced in Section 4 for the same core design.

5.2. Design II core characteristics

The SP optimization procedure for Design II core was similar to

Table 4
Design parameters of alternative B&B core designs with 3D fuel shuffling.

Design parameter	Design I	Design II	Design III
Number of sub-assemblies per assembly	4	3	2
Total fuel length in assembly (cm)	280	210	280
Core thermal power (MW)	3000	2340	2935
Active core height (cm)	301	224	287
Equivalent core radius (cm)	246.34	246.34	246.34
Active core volume (m^3)	57.38	42.70	54.71
Power density (MW/m^3)	56.20	54.80	53.64

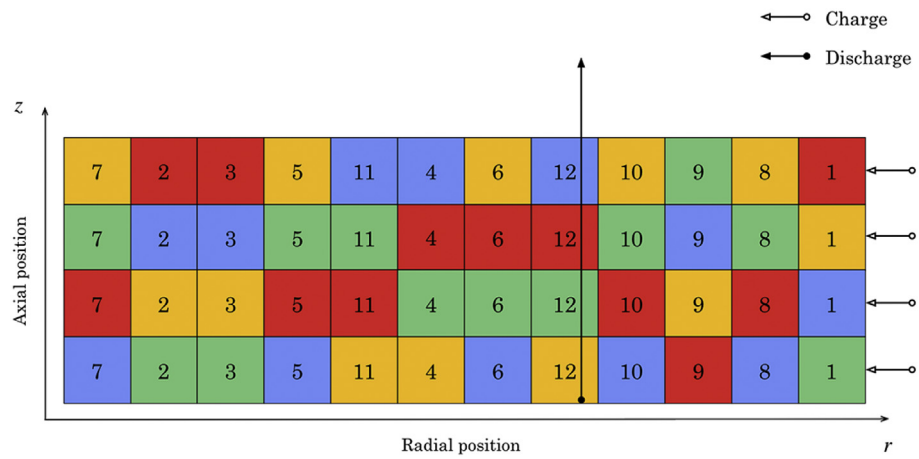

Fig. 18. Optimal 3D shuffling pattern for Design I B&B core with constrained axial shuffling.

Table 5
Performance of optimal Design I B&B core with axially-constrained shuffling.

Shuffling type		3D axially-constrained	3D unconstrained
Core thermal power (MW)		3000	3000
Burn cycle time (EFPD)		1728	1566
Burnup reactivity swing (% $\Delta k/k$)		3.26	4.66
Average discharge BU (% FIMA)		16.02	14.49
Peak discharge BU (% FIMA)		17.16	15.69
Peak radiation damage (dpa)		375.8	351.0
Peak fast fluence (n/cm^2)		9.85E+23	9.88E+23
Axial/radial leakage probability (%)		3.84/3.05	1.56/2.75
Axial/radial power peaking factor		1.37/1.78	2.00/1.70
Peak batch power change (%)		16.28	22.14
Pitch-to-diameter ratio		1.076	1.070
Core volume fractions (%)	Fuel	39.27	39.77
	Gap	13.09	13.26
	Cladding + wire	12.66	12.77
	Duct	6.56	6.57
	Coolant	28.42	27.63

that described in Section 4, except for the solution update scheme, because the axial symmetry is lost with three segments per fuel assembly. Thus, the preservation of symmetry was removed from the binary fuel exchange strategy. The optimal 3D SP found is given in Fig. 19 and the core characteristics are summarized in Table 6 left column of results. The core thermal power of 2340 MW was determined by matching the fuel specific power to that of Design I, which is 7.22 kW/kg. Therefore, in addition to the fuel volume fraction and radial power peaking factor, the coupled neutronics and thermal-hydraulics calculation scheme as shown in Fig. 6 also iterates on specific power in this case. It took four iterations for this case to converge.

As can be seen by comparing Table 6 with Table 3, the reduction of the number of axially stacked sub-assemblies from 4 to 3 along with a 25% reduction in the total active fuel length does not significantly penalize the core performance except for the total core power. The minimum required peak radiation damage is 359.8 dpa – only about 2.5% higher than of the optimal 3D shuffled Design I

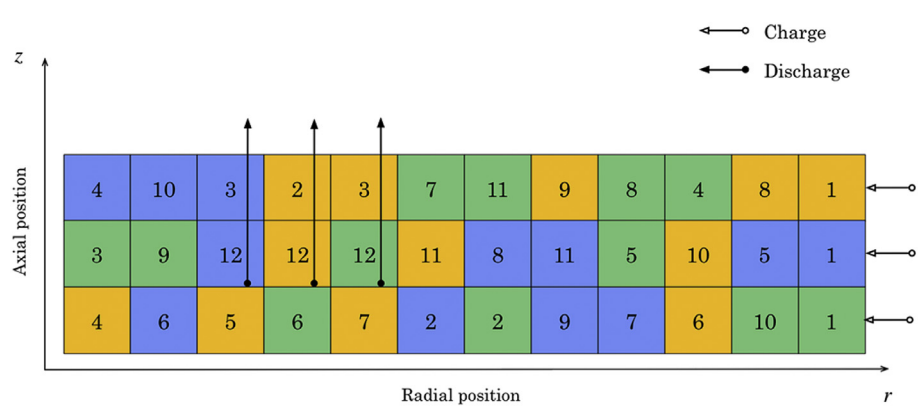

Fig. 19. Optimal 3D shuffling pattern for Design II B&B core.

Table 6
Performance of Optimal Design II B&B core with various sub-assembly lengths.

Active fuel length (cm)		210	180	150
Core thermal power (MW)		2340	2078	1794
Burn cycle time (EFPD)		1598	1628	1756
Burnup reactivity swing (% $\Delta k/k$)		4.85	4.44	3.96
Average discharge BU (% FIMA)		14.64	14.91	16.03
Peak discharge BU (% FIMA)		14.95	15.31	16.58
Peak fast fluence (n/cm^2)		1.19E+24	1.19E+24	1.19E+24
Axial/radial leakage probability (%)		1.72/0.89	2.63/0.92	4.17/0.98
Peak radiation damage (dpa)		359.8	367.9	397.1
Axial/radial power peaking factor		2.18/1.85	2.02/1.76	1.85/1.63
Peak batch power change (%)		12.19	10.45	9.27
Pitch-to-diameter ratio		1.055	1.034	1.017
Core volume fractions (%)	Fuel	41.45	42.92	44.52
	Gap	13.82	14.31	14.84
	Cladding + wire	13.13	13.50	13.94
	Duct	6.63	6.69	6.77
	Coolant	24.96	22.58	19.93

core even though the average power density is similar. Due to the reduced core height and therefore reduced pressure drop, the fuel volume fraction could be increased to 41.45%.

A trade-off between the height and performance of the 3-subassebly core was studied by designing two additional cores the sub-assembly length of which was reduced from the original 70 cm–60 cm and 50 cm, respectively. All three cases have the same fuel specific power. The results are compared in Table 6.

It was found that shortening of the effective core height from 210 to 150 cm results in an increase of the fuel volume fraction from 41.45% to 44.52% which could not provide enough excess neutrons to fully compensate for the increase of the axial leakage probability from 1.72% to 4.17%. As a result, the averaged discharge burnup had to be raised from 14.64% to 16.03%, corresponding to an increase in the equilibrium cycle length from 1598 to 1756 EFPD, and the peak radiation damage has increased by 37.3 dpa. However, the intermediate 180-cm core design presents a well-balanced performance; the peak radiation damage is 367.9 dpa – only 2.3% increase from the 210-cm core.

5.3. Design III core characteristics

In Design III core where fuel assemblies were constituted by only 2 segments, any 3D SP can technically be considered as an axially-constrained shuffling scheme as shown in Section 5.1 due to the core symmetry in axial direction. Therefore, the same optimization strategy was applied and the optimal 3D SP is shown in Fig. 20. It can be seen that the radial movement of the fuel assemblies follows that of the optimal 2D SP shown in Fig. 10, and the axial locations of the sub-assemblies switch when necessary. In fact, only 4 switches are required for each of the fuel assemblies (at the end of cycle 4, 5, 8, and 10). Provided the refueling machine can handle complete assemblies, it means 2/3 of the shuffling operations does not involve disassembling and reassembling of the fuel assembly, which provides a significant reduction in refueling time and effort, when compared with any of the designs investigated so far.

A core thermal power of 2935 MW is required to maintain the fuel specific power of 7.22 kW/kg. Each sub-assembly has been split into 4 burnup zones so as to have comparable axial burnup resolution as of the previously considered core designs. It was expected that the axial burnup flattening is more challenging in this core design because its sub-assemblies are twice as long.

As a result of the limited axial shuffling, the performance of this core, summarized in Table 7, is degraded as compared to the previous two designs. The peak radiation damage is 402.6 dpa – almost 15% higher than that of Design I. This is due primarily to the large peak to average peak discharge dpa of 1.20 as compared to ~1.03 in Design I cores (for both unconstrained and axially-constrained shuffling cases), as can be seen in Fig. 21. Also contributing to increase in minimum required dpa is the relatively high radial power peaking that is forcing a decrease of the fuel inventory resulting in a negative impact on the neutron economy.

A variation of Design III in which the length of the assembly segment was reduced from 140 cm to 105 cm was then investigated. As can be seen in Table 7, the overall performance of the shorter core is not much degraded relative to the original design, where the peak radiation damage was only 2.3 dpa higher. This is because the reduced pressure drop enables a higher fuel inventory (or smaller P/D ratio) that can partially compensate for the neutron leakage probability – primarily in the axial direction, which increases from 2.66% to 3.82%. This also results in a slightly larger

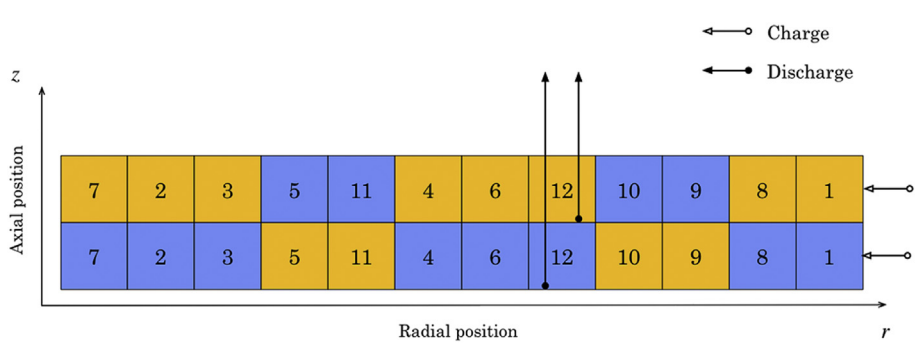

Fig. 20. Optimal 3D shuffling pattern for Design III B&B core.

Table 7
Design III B&B core performance with 3D shuffling.

Core thermal power (MW)		2935	2338
Active fuel length (cm)		280	210
Burn cycle time (EFPD)		1584	1650
Burnup reactivity swing (% Δk/k)		3.88	3.90
Average discharge BU (% FIMA)		14.49	15.09
Peak discharge BU (% FIMA)		17.50	17.39
Peak radiation damage (dpa)		402.6	404.9
Peak fast fluence (n/cm^2)		9.89E+23	1.02E+24
Axial/radial leakage probability (%)		2.66/3.26	3.82/2.97
Axial/radial power peaking factor		1.31/1.86	1.31/1.85
Peak batch power change (%)		16.61	18.38
Pitch-to-diameter ratio		1.083	1.050
Core volume fractions (%)	Fuel	38.97	41.45
	Gap	12.99	13.82
	Cladding + wire	12.61	13.14
	Duct	6.55	6.63
	Coolant	28.89	24.95

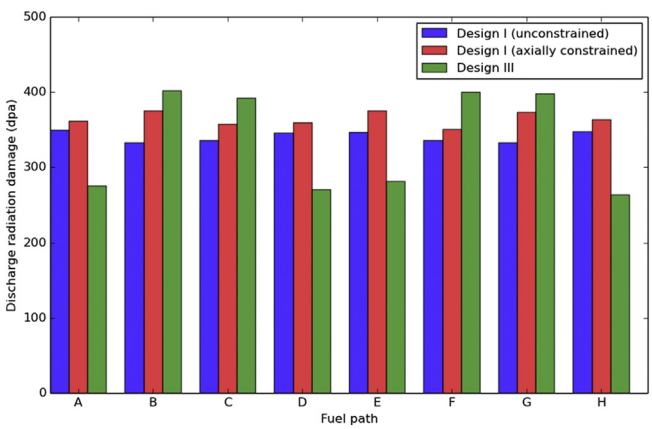

Fig. 21. HT-9 discharge dpa for Design III core in comparison with Design I.

average discharge burnup in the shorter core. In comparison with the standard Design II core, which has the same active fuel length (210 cm), the peak radiation damage has increased by 45.1 dpa in the shorter core of Design III; however, it is still ~25% lower than that of the reference 2D shuffled core while offering significantly simpler shuffling strategy and less refueling effort, when compared with the previously studies 3D shuffled cores.

5.4. Effect of power density on optimal core performance

The core designs developed so far are characterized by low power density, which is typical to B&B cores. The sensitivity of the core performance, especially the peak radiation damage, to the core power density was investigated for Design II core. The results are presented in Table 8 for 2500 MW, 3000 MW and 3500 MW Design II-like cores as compared to the original 2340 MW core. All three cores adopt the same core geometric configuration and optimal SP depicted in Fig. 19.

As the core power increases from 2340 MW to 3500 MW, a larger coolant flow area is required to meet the thermal hydraulic constraints – in particular the pressure drop, leading to an increase of P/D ratio and decrease of fuel inventory, which harms the neutron economy. As a result of the impaired neutron economy higher fuel burnup is required to sustain the B&B mode of operation, and consequently, the minimum required peak radiation damage increases with an increase in the core power level. Since in the vicinity of the discharge burnup the reactivity increase with burnup is much smaller than in the low burnup range, the increase of overall fuel burnup when going to a higher power level results in a decrease in the burnup reactivity swing. The impact of core power level on some of the design parameters is illustrated in Fig. 22. It can be seen that except for the peak dpa level, all other parameters are slightly improved with power upgrade. Overall it appears desirable to increase the core power level – a ~50% increase in the power level will result in an additional 10% increase in fuel utilization and incur a penalty of only a ~6% increase in the dpa the cladding will have to accommodate.

6. Conclusions

This paper presents the development and implementation of a combinatorial optimization search methodology of 3D shuffling pattern (SP) based on the Simulated Annealing (SA) algorithm for self-sustaining B&B reactors. The automated search for the optimal SP was performed using coupled neutronics and thermal-hydraulics code system consisting of the deterministic neutronics ARC code package developed by ANL coupled with the in-house developed ADOPT code for the thermal-hydraulics and structural design of fuel assemblies. The developed methodology was found to be very effective in identifying optimal SP some of which were counterintuitive – for example, featuring a relatively large neutron leakage probability – a performance characteristics that we tried to minimize when using a trial-and-error search (Hou et al., 2015). Moreover, in addition to minimizing the peak dpa level the SA-based optimization search methodology was found capable of improving a number of performance characteristics including reducing the burnup reactivity swing, the radial power peaking factor and the relative change in the assembly power over a cycle.

Compared with the optimal conventional 2D fuel shuffling, the optimal 3D SP offers a 34% reduction of the peak radiation damage level, down to ~350 dpa; a 45% increase in the average fuel discharge burnup, and hence the uranium utilization, without violating all major neutronics and thermal-hydraulics constraints. For the same peak dpa level, the average discharge burnup of the 3D shuffled core is 2.23 times that of the 2D shuffled core; this corresponds to a ~120% relative increase in the fuel utilization. These significant improvements may enable an earlier commercialization of B&B reactors than otherwise. In the long term, the successful deployment of the B&B core along with optimal 3D shuffling of fuel could provide at least 25-fold increase in uranium utilization over current once-through LWRs, and hence significantly improve the sustainability of the once-through nuclear fuel cycle.

The introduction of the axially segmented fuel assembly design

Table 8
Sensitivity of Design II B&B core performance to power density.

Core design		2500 MW	3000 MW	3500 MW
Burn cycle time (EFPD)		1488	1236	1062
Burnup reactivity swing (% Δk/k)		4.66	4.30	3.97
Average discharge BU (% FIMA)		14.87	15.41	16.02
Peak discharge BU (% FIMA)		15.23	15.87	16.57
Peak radiation damage (dpa)		362.84	370.93	381.35
Peak fast fluence (n/cm^2)		1.18E+24	1.19E+24	1.20E+24
Axial/radial leakage probability (%)		1.84/0.96	2.07/1.09	2.30/1.21
Axial/radial power peaking factor		2.15/1.81	2.10/1.75	2.04/1.69
Peak batch power change (%)		12.08	11.92	11.37
Pitch-to-diameter ratio		1.055	1.074	1.093
Core volume fractions (%)	Fuel	40.99	39.44	37.99
	Gap	13.66	13.15	12.66
	Cladding + wire	13.03	12.69	12.42
	Duct	6.61	6.56	6.52
	Coolant	25.71	28.16	30.41

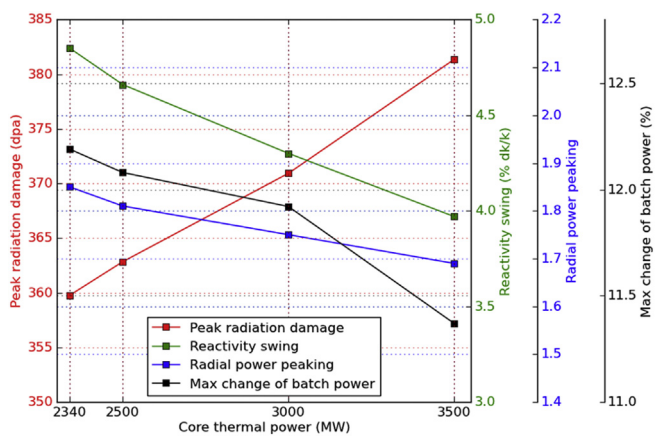

Fig. 22. Optimal core performance of Design II as a function of core power.

will inevitably increase the complexity of refueling strategy, and will increase refueling time. A number of variations of the standard 3D shuffled design approach to alleviate these drawbacks were examined. The first approach was to restrict the shuffling of sub-assemblies to axial shuffling within the same fuel assembly. It was found that this approach can flatten the radiation damage distribution of the discharge fuel to the same level of the unconstrained 3D shuffling, but it also increases the core leakage and therefore causes an increase in the peak radiation damage from 351 to 376 dpa.

The second approach is to reduce the number of sub-assemblies used to constitute a single fuel assembly. It was found that by reducing the number of segments from 4 to 3, i.e., reducing the active fuel length by 25%, the core performance was not significantly degraded except for the core power. The minimum required peak radiation damage was increased by only 2.5%, while other performance parameters were similar, when compared with the 4-segments fuel assembly design with unconstrained 3D fuel shuffling. When the number of fuel segments in each fuel assembly was reduced to 2, the core designs were challenged for the ability to flatten the axial burnup distribution of the discharge fuel. As a result, the peak radiation damage level was ~400 dpa, which is nearly 15% higher than that of the 4 subassembly per assembly core but still offers ~25% reduction compared with the optimal 2D shuffling case. More importantly, a much simpler shuffling strategy and significantly less refueling effort could be achieved using this design approach.

The impact of power level increase on the minimum required peak dpa level was investigated for Design II core. It was found that a 50% increase in the power level (or power density) will require only a ~6% increase in the peak dpa the cladding will have to accommodate.

While offering significant improvements of the B&B core performance as discussed above, the 3D fuel shuffling also gives rise to a number of mechanical feasibility issues. First, the segmented fuel assembly design requires further evaluation and optimization. The venting fixtures on top of the sub-assembly has to be carefully designed and the gaseous fission products vented into the reactor primary loop has to be properly handled. Dimensional changes to the connecting pieces must be small enough to ensure adequate attachment and detachment of assembly segments throughout the lifetime of the core, without exceeding withdrawal-force limits of the shuffling machine itself.

Second, a refueling machine and strategies have to be designed for disconnecting sub-assemblies and reconnecting them to make new assemblies. Even using only 2 segmented assemblies will cause a considerable increase in the time and workspace required for fuel handling. Thus, a cost/benefit analysis must be performed in order to assess the tradeoff between the improved core performance versus the complexity in fuel handling devices and increased reactor down time and a corresponding decrease in the nuclear plant capacity factor. A refueling machine with the capability of transferring more than one assembly segments at a time can be a potential solution to reduce the down time associated with fuel shuffling. (Meuschke and Malandra, 1997) Another possible approach currently under study is to increase the lateral dimension of the fuel segment while decreasing the number of segments required to constitute a full-length assembly, as such the quantity of fuel segments in the core can be significantly reduced.

Another important feasibility issue is to design a B&B core to be passively safe; the large low-leakage core features a larger positive coolant temperature reactivity coefficient and coolant voiding reactivity feedback (Qvist and Greenspan, 2012) than conventional fast reactor cores. Novel negative reactivity insertion systems passively actuated by coolant temperature increase may be required to compensate for the low-leakage reactivity effects. (Qvist and Greenspan, 2014c).

The stochastic optimization method based on the SA algorithm can be further improved: the cooling schedule used in the current study is based on the exponential multiplicative schedule, which is somewhat simplified and may not be the most effective one for this type of problem. An optimal cooling schedule will be selected for future studies from a problem dependent comparative study of different schedules and used in future SP optimizations.

Acknowledgments

This research is being performed using funding received from the DOE Office of Nuclear Energy's Nuclear Energy University Programs (NEUP 13-5144). The technical assistance and feedback of experts at the Argonne National Laboratory (ANL) is highly appreciated. In particular, the authors would like to thank Dr. Florent Heidet for his assistance.

References

Aarts, E., Korst, J., 1989. Simulated Annealing and Boltzmann Machines: a Stochastic Approach to Combinatorial Optimization and Neural Computing. John Wiley & Sons, Chichester.
Ahlfeld, C., Burke, T., Ellis, T., Hejzlar, P., Weaver, K., Whitmer, C., Gilleland, J., 2011. Conceptual design of a 500 MWe traveling wave demonstrator reactor plant. In: Proc. ICAPP 2011, Nice, France.
Alcouffe, R.E., Brinkley, F.W., Marr, D.R., O'Dell, R.D., 1990. User's Guide for TWODANT: a Code Package for Two-dimensional, Diffusion-accelerated, Neutral Particle Transport.
Bleise, A., Danesi, P., Burkart, W., 2003. Properties, use and health effects of depleted uranium (DU): a general overview. J. Environ. Radioact. 64 (2–3), 93–112.
DeChaine, M., Feltus, M., 1995. Nuclear fuel management optimization using genetic algorithms. Nucl. Tech. 111, 109–114.
Derstine, K.L., 1984. DIF3D: a Code to Solve One-, Two-, and Three-dimensional Finite Difference Diffusion Theory Problems.
Di Sanzo, C., Cohen, J., Cisneros, T., Ludewight, B., Greenspan, E., 2011. An accelerator driven energy multiplier for doubling uranium ore utilization. In: Proc. of Accelerator Application Topical Meeting, Knoxville, TN, US.
Dowsland, K.A., Reeves, C.R., 1995. Morden Heuristic Techniques for Combinatorial Problems. McGraw-Hill.
Dubberley, A., Private Communication.
Fast Reactor Database 2006 Update, 2006.
Greenspan, E., Heidet, F., 2011. Energy sustainability and economic stability with breed and burn reactors. Prog. Nucl. Energy 53, 794–799.
Greenwood, L., 1987. SPECOMP calculations of radiation damage in compounds. In: Sixth ASTM-EURATOM Symposium on Reactor Dosimetry, Jackson Hole, WY.
Heidet, F., Greenspan, E., 2012. Neutron balance analysis for sustainability of breed-and-burn reactors. Nucl. Sci. Eng. 171 (1), 13–31.
Heidet, F., Greenspan, E., 2013. Performance of large breed-and-burn core. Nucl. Technol. 181, 381.
Heidet, F., Petroski, R., Greenspan, E., 2009. Minimum burnup required for sustainable operation of fast reactors without recycling. In: Proceedings International Conference on Fast Reactors and Related Fuel Cycles: Challenges and Opportunities-FR09, Kyoto, Japan.
Hejzlar, P., Petroski, R., Cheatham, J., Touran, N., Cohen, M., Truong, B., Latta, R., Werner, M., Burke, T., Tandy, J., Garrett, M., Johnson, B., Ellis, T., McWhirter, J., Odedra, A., Schweiger, P., Adkisson, D., Gilleland, J., 2013. TerraPower, LLC traveling wave reactor development program overview. In: Proceedings of ICAPP 2013, Jeju Island, Korea.
Horak, J.A., Kittel, J.H., Yaggee, F.L., 1962. Irradiation Behavior of Restrained and Vented Uranium-2 w/o Zirconium Alloy. Argonne, IL, US.
Hou, J., Heidet, F., Gorman, P., Greenspan, E., 2014. On multi-group cross sections for breed-and-burn reactors. In: Transaction of the American Nuclear Society, Anaheim, CA.
Hou, J., Qvist, S., Greenspan, E., 2015. 3-D fuel shuffling for reduced peak burnup and increased uranium utilization of breed-and-burn reactors. In: Proceedings of ICAPP 2015, Nice, France.
Kirkpatrick, S., Vecchi, M.P., 1983. Optimization by simmulated annealing. Science 220 (4598), 671–680.
Lee, C.H., Yang, W.S., 2013. MC2–3: Multigroup Cross Section Generation Code for Fast Reactor Analysis.
Leppänen, J., 2010. Serpent Monte Carlo physics code. In: AER Symposium on VVER Reactor Physics and Reactor Safety, Espoo, Finland.
Metropolis, N., Rosenbluth, A., Rosenbluth, M., Teller, A., Teller, E., 1953. Equation of state calculations by fast computing machines. J. Chem. Phys. 21, 1087.
Meuschke, R., Malandra, L. Refueling machine. US Patent 5,687,207, 11 1997.
Norgett, M.R.I.T.M.J., 1975. A proposed method of calculating displacement dos rates. Nucl. Eng. Des. 33, 50–54.
O'Neill, G.L., 1965. Safety and economic aspects of vented fuel in sodium-cooled reactors. In: Proceedings of the Conference on Safety, Fuels, and Core Design in Large Fast Power Reactors.
Park, T.K., Joo, H.G., Kim, C.H., Lee, H.C., 2009. Multiobjective loading pattern optimization by simulated annealing employing discontinuous penalty function and screening technique. Nucl. Sci. Eng. 162 (2), 134–147.
Parks, G., 1996. Multiobjective pressurized water reactor reload core design by nondominated genetic algorithm search. Nucl. Sci. Eng. 124, 178–187.
Poon, P., Parks, G., 1993. Application of genetic algorithms to in-core nuclear management optimization. In: Proc. Joint Int. Conf. Mathematical Methods Supercomputing Nuclear Applications, Karlsruhe, Germany.
Qvist, S., Greenspan, E., 2012. Inherent safety of minimum-burnup breed & burn reactors. In: Proc. of ICAPP 2012, Chicago, IL, US.
Qvist, S., Greenspan, E., 2014. 3D shuffling in breed and burn reactors. In: American Nuclear Society Winter Meeting, Anaheim, CA, USA.
Qvist, S., Greenspan, E., 2014. The ADOPT code for automated fast reactor design. Ann. Nucl. Energy 71, 23–36.
Qvist, S., Greenspan, E., 2014. An autonomous reactivity control system for improved fast reactor safety. Prog. Nucl. Energy 77, 32–47.
Qvist, S., Hou, J., Greenspan, E., 2015. Design and performance of breed-and-burn reactors. Ann. Nucl. Energy 85, 93–114.
Ryu, H., Lee, B.O., Oh, S.J., Kim, J.H., Lee, C.B., 2009. Performance of FCCI barrier foils for U–Zr–Z metallic fuel. J. Nucl. Mater. 392 (2), 206–212.
Sekimoto, H., Ryu, K., 2000. A new reactor burnup concept "CANDLE". In: Proc. of PHYSOR 2000, Pittsburgh, PA, USA.
Stevens, J.G., Smith, K.S., Rempe, K.R., Downar, T.J., 1995. Optimization of pressurized water reactor shuffling by simulated annealing with heuristics. Nucl. Sci. Eng. 121 (1), 67–88.
Suspluagas, A., Greenspan, E., 2005. Implementation of the ENHS Thermal Hydraulic Optimization Code for Recent ENHS Design Improvement. University of California, Berkeley.
Teller, E., Ishikawa, M., Wood, L., 1996. Completely automated nuclear reactors for long-term operation II. In: Proceeding of ICENES'96, International Conference on Emerging Nuclear Energy Systems, Obninsk, Russia.
Toloczko, M.B., Garner, F.A., Eiholzer, C.R., 1994. Irradiation creep and swelling of the US fusion heats of HT9 and 9Cr–1Mo to 208 dpa at ~400 °C. J. Nucl Mater. 21C2–215, 604–607.
Toppel, B.L., 1983. A User's Guide to the REBUS-3 Fuel Cycle Analysis Capability.
Toshinsky, V.G., Sekimoto, H., Toshinsky, G.I., 1999. Multiobjective fuel management optimization for self-fuel-providing LMFBR using genetic algorithms. Ann. Nucl. Energy 26 (9), 783–802.
Toshinsky, V., Sekimoto, H., Toshinsky, G., 2000. A method to improve multiobjective genetic algorithm optimization of a self-fuel-providing LMFBR by niche induction among nondominated solutions. Ann. Nucl. Energy 27, 397–410.
Turinsky, P.J., Parks, G.T., 1999. Advances in nuclear fuel management for light water reactors. Adv. Nucl. Sci. Technol. 137–165.
Zhang, G., Greenspan, E., Jolodosky, A., Vujic, J., July 2015. SFR with once-through depleted uranium breed & burn blanket. Prog. Nucl. Energy 82, 2–6.

Appendix C

J. Hou, F. Heidet, P. Gorman and E. Greenspan, “On Multi-Group Cross Sections for Breed-and-Burn Reactors,” Transaction of the American Nuclear Society, Anaheim, CA, November 2014.

On Multi-Group Cross Sections for Breed-and-Burn Reactors

Jason Hou[1], Florent Heidet[2], Phillip Gorman[1] and Ehud Greenspan[1]

[1]*Department of Nuclear Engineering, University of California, Berkeley, Berkeley, CA, 94720-1730*
[2]*Nuclear Engineering Division, Argonne National Laboratory, Argonne, IL 60439-4842*
jasonhou@berkeley.edu

INTRODUCTION

The main motivation of the Breed-and-burn (B&B) reactors proposed [1-3] is to achieve significant uranium utilization without resorting to fuel reprocessing. After establishing initial criticality, B&B reactors are only fed with fertile fuel such as depleted uranium (DU).

Sustaining the B&B mode of operation requires a minimum burnup of ~20% FIMA (fissions per initial metal atoms) [3] in order to convert enough feed fuel to plutonium and make the fuel a net producer of neutrons. Unlike the conventional Fast Breeder Reactor (FBR), which uses separate seed and blanket fuel assemblies, all the B&B fuel assemblies are identical and will fill the function of both blanket and seed during their residence in the core.

In FBR neutronics analysis it is customary to use burnup-independent pre-prepared multi-group cross sections. [4] This paper investigates whether or not it is justified to use this approach for the analysis of B&B cores.

METHODOLOGY

Reference Code Design

The B&B core designed in [5] is used as the reference for this study. The radial side-view of this core is given in Fig. 1. It is a large low-leakage sodium-cooled fast reactor that uses metallic fuel U-6Zr with 6% zirconium. The fuel nominal density is taken to be 15.85 g/cm^3, and a smear factor of 75% is assumed to accommodate the fuel swelling with burnup. The main design parameters and volume fractions of the core are presented in Table I and II, respectively.

Table I. Main Parameters of Reference Core

Thermal power (MW_{th})	2750
Coolant	Sodium
Feed fuel	DU-6%Zr
Cladding, duct & wire-wrap	HT-9
Inter/outlet coolant temperature (ºC)	350/500
Core radius (cm)	197.2
Active core height (cm)	200
Gas plenum height (cm)	100

Table II. Reference B&B Core Volume Fraction (%)

Fuel	40.3
Gap	13.4
Structural material	20.1
Coolant	26.2

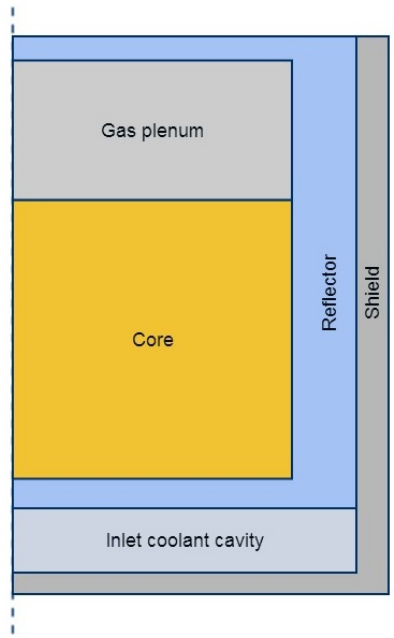

Fig. 1. Radial side-view of B&B core design.

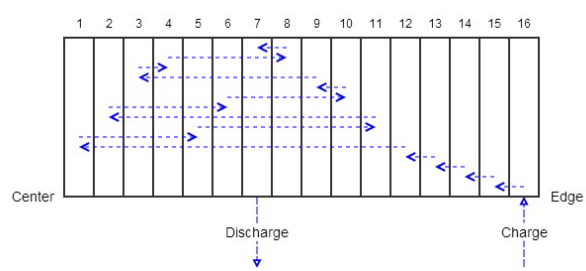

Fig. 2. Schematic of shuffling scheme used for the B&B core.

Neutronics Modeling

The active core is divided into 16 equal volume concentric burnup zones, each representing a fuel batch. Each batch is subdivided into 7 axial regions to account for the axial variation of the neutron flux and therefore burnup rate. It was estimated in previous studies that the relative errors in batch multiplication factor k_{eff} introduced by the cylindrical modeling of the B&B core is between -0.4% and 0.4% $\Delta k/k$, when compared with assembly-level core model [2]. This approximation is considered acceptable in this preliminary study.

An optimized shuffling scheme, depicted in Fig. 2, was chosen to minimize the discharge burnup, radial power peaking, and burnup reactivity swing [6]. The fresh DU batch is loaded at the outermost location (16) and then shuffled inward and outward a couple of times, before being discharged from location 5.

In this study, the whole core calculation was performed using Monte Carlo transport code Serpent [7] using the ENDF/B-VII.0 nuclear data at 600 K. Except for the feed fuel, which is DU with 0.2%w ^{235}U, the material composition of each burnup zone is obtained at the beginning of equilibrium cycle (BOEC) of the reference core. [8] The unresolved resonance probability tables were not used in Serpent calculation to shorten the computational time.

RESULTS

The calculated core k_{eff} at BOEC is 1.0115±0.0001. The neutron spectra of selected fuel batches are normalized using 1000 energy bins with equal lethargy and depicted in Fig. 3. Relatively large statistical errors in flux values were found for energy lower than 0.149 keV due to the very low number of tally scores, that is, low flux. It is observed that the spectrum becomes harder as burnup increases; in particular in burnup range below 1% FIMA. This spectrum hardening observed in Fig. 3 is space and composition dependent. The outermost batches have very low plutonium content and low k_∞. Most of the neutrons observed in these batches are the fission neutrons originating in the inner fuel region and leaking into the outer regions. Those neutrons undergo many scattering reactions that slow them down, resulting in a slightly softer spectrum. In addition, depletion of ^{238}U and buildup of transuranic (TRU) inventory with burnup results in changes in the neutron spectrum in, primarily, the MeV and resonance energy ranges.

In order to understand the impact of spectrum change on cross section values within each energy group, cross sections for selected nuclides are condensed into a 33-group structure. The upper bound of each group is listed in Table III. This energy structure is commonly used in the lattice calculation module ECCO of ERANOS code [9] for fast reactor simulation. Due to large statistical errors in the reaction rate and flux at low energy, group cross sections below 0.149 keV are not considered in this analysis.

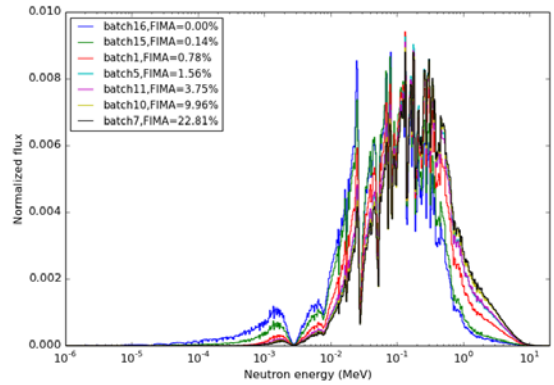

Fig.3. Neutron spectra at BOEC for selected fuel batches.

Table III. ECCO 33-group energy structure

Group	E(MeV)	Group	E(MeV)	Group	E(MeV)
1	1.96E+1	12	6.74E-2	23	3.04E-4
2	1.00E+1	13	4.09E-2	24	1.49E-4
3	6.07E+0	14	2.48E-2	25	9.17E-5
4	3.68E+0	15	1.50E-2	26	6.79E-5
5	2.23E+0	16	9.12E-3	27	4.02E-5
6	1.35E+0	17	5.53E-3	28	2.26E-5
7	8.21E-1	18	3.35E-3	29	1.37E-5
8	4.98E-1	19	2.03E-3	30	8.32E-6
9	3.02E-1	20	1.23E-3	31	4.00E-6
10	1.83E-1	21	7.49E-4	32	5.40E-7
11	1.11E-1	22	4.54E-4	33	1.00E-7

The change in the cross section value with burnup for Group 6 (0.821 to 1.353 MeV) is presented in Fig. 4 and 5 for ^{238}U capture and ^{239}Pu fission, respectively. It is observed that the ^{238}U fission cross section decreases by ~1% at the early stage of burnup and reaches an asymptotic value thereafter. In contrast, ^{239}Pu fission cross section increases before it converges to an asymptotic value. Similarly the change mostly takes place during the initial 0.78% FIMA. This phenomenon can be understood by comparing the normalized point-wise neutron spectra at different burnup within Group 6, as shown in Fig. 6. At low burnup, the point-wise spectrum peaks at lower energies, while it tends toward a more uniform distribution beyond 0.78% FIMA. As ^{238}U capture cross section decreases and ^{239}Pu fission cross section increases with energy within this group, spectrum hardening leads to opposite trend of cross section evolution with burnup. The similar asymptotic trend is found for energy range above 24.8 keV (Group 1 to 13), which does not contain significant resonances of cross section.

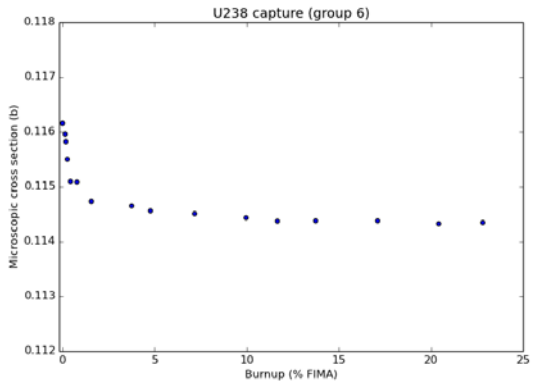

Fig. 4. ^{238}U capture cross section vs. burnup in Group 6.

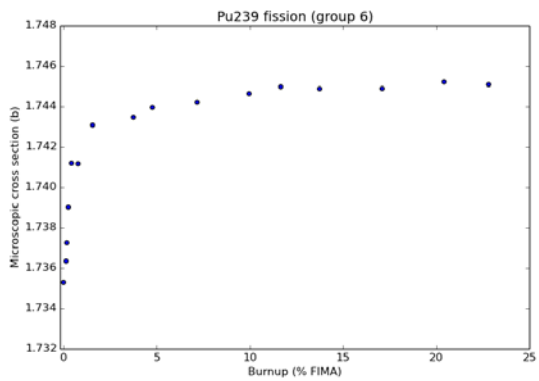

Fig. 5. ^{239}Pu fission cross section vs. burnup in Group 6.

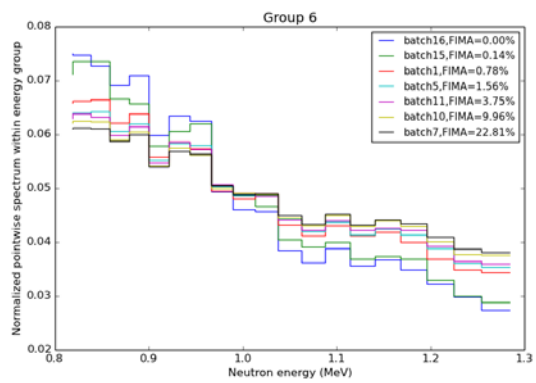

Fig. 6. Normalized point-wise spectrum in Group 6.

A slightly different trend is observed for energy range below 24.8 keV. In Group 19 (1.23 to 2.03 keV), for example, after the initial drop, the cross section rises and continuously increases almost linearly with burnup for ^{238}U capture, as seen in Fig. 7. This is consistent with the non-converging normalized flux distribution in the group (Fig. 9). It is primarily because Group 19 is within the resonance range of ^{238}U capture cross section and the depletion of ^{238}U reduces the self-shielding effect and increases the effective group cross section. For ^{239}Pu fission shown in Fig. 8, on the other hand, the cross section is reaching an asymptotic value with burnup, because it has no resonances in this energy range.

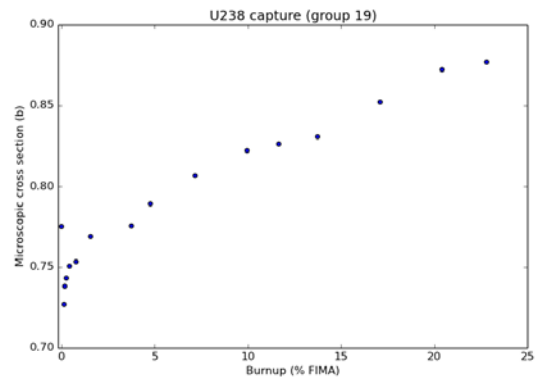

Fig. 7. ^{238}U capture cross section vs. burnup in Group 19.

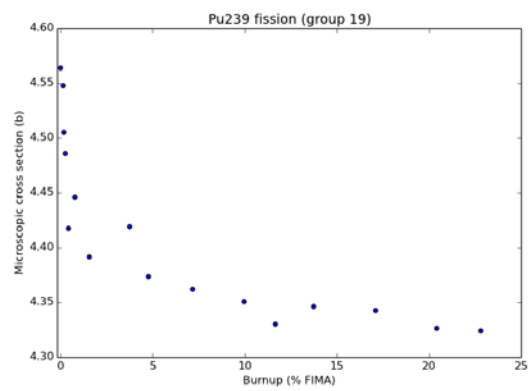

Fig. 8. ^{239}Pu fission cross section vs. burnup in Group 19.

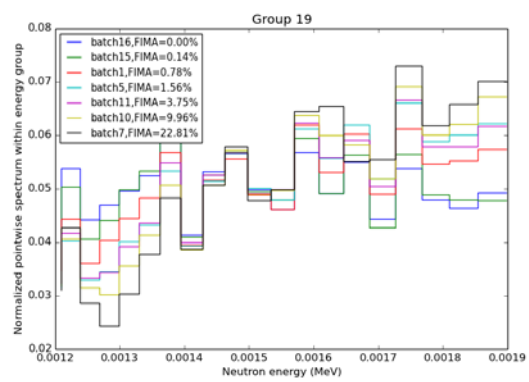

Fig. 9. Normalized point-wise spectrum in Group 14.

The relative difference of the group cross section compared to the values at intermediate burnup (9.96% FIMA) is plotted in Fig. 10 for ^{238}U capture and in Fig. 11 for ^{239}Pu fission. In general, good agreement is found for both cases in the MeV energy range, but the deviation becomes larger in the resonance energy range. As shown in Table IV, the maximum absolute difference is always below 2.5% for energy range above 24.8 keV (above Group 14), where the cross section variation is the reflection of the spectrum hardening. In the resonance energy range, self-shielding effects dominate the evaluation of the group cross section, leading to the opposite trend of the cross section change with burnup. It is believed that the adequate resonance treatment during the flux calculation will reduce the degree of cross section change with burnup, and the quantification study will be carried out in the future work.

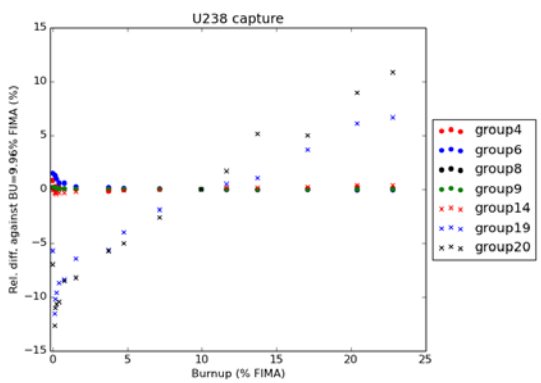

Fig. 10. Relative difference of ^{238}U capture cross section to its value at burnup of 9.96% FIMA.

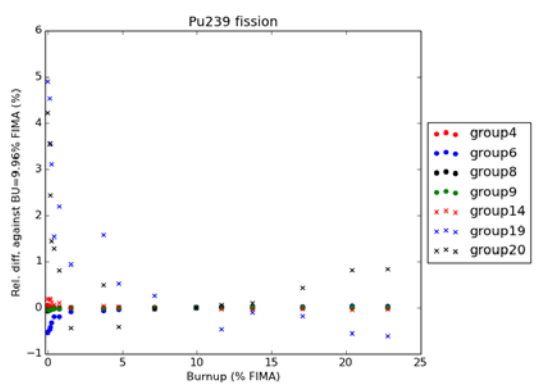

Fig. 11. Relative difference of ^{239}Pu fission cross section to its value at burnup of 9.96% FIMA.

CONCLUSIONS

The results of this study indicate that in order to accurately account for spectral variations in large B&B cores, it would be preferable to use burnup and location dependent group constants. The degree of inaccuracy that will be introduced by using a single pre-generated multi-group library will be quantified in a follow-up study.

Table IV. Maximum difference (%) of group cross section to its value at burnup of 9.96% FIMA

Group	^{238}U σ_c	^{239}Pu σ_f	Group	^{238}U σ_c	^{239}Pu σ_f
1	0.9	0.2	12	0.6	0.0
2	0.5	0.3	13	0.5	0.0
3	1.8	0.1	14	0.4	0.2
4	0.8	0.1	15	1.7	0.1
5	2.1	0.1	16	2.4	0.0
6	1.5	0.5	17	3.2	0.6
7	0.5	0.4	18	5.4	0.9
8	0.2	0.1	19	11.6	4.9
9	0.1	0.1	20	12.7	4.2
10	0.6	0.1	21	16.5	35.6
11	1.0	0.0	22	25.2	13.6

ACKNOWLEDGEMENTS

This study has been supported by funding received from the U. S. Department of Energy Office of Nuclear Energy's Nuclear Energy University Programs.

REFERENCES

1. E. Greenspan, "A Phased Development of Breed-and-Burn Reactors for Enhanced Nuclear Energy Sustainability," *Sustainability*, **4**, 2745 (2012).
2. F. Heidet and E. Greenspan. "Performance of large breed-and-burn core," *Nucl. Tech.*, **181**, 381 (2013).
3. F. Heidet and E. Greenspan, "SuperPRISM-sized Breed-and-Burn Sodium-cooled Core Performance," *Nucl. Tech.*, **181**, 381 (2013).
4. W. S. Yang, "Fast Reactor Physics and Computation Methods," Nuclear Engineering and Technology, Vol **44**, 177 (2012).
5. F. Heidet and E. Greenspan, "Neutron Balance Analysis for Sustainability of Breed-and-Burn Reactors," Nuclear Science and Engineering **171**, 13 (2012).
6. S. Qvist, "Safety and Core Design of Large Liquid-Metal Cooled Fast Breeder Reactors," PhD thesis, University of California, Berkeley (2013).
7. J. Leppänen, "Serpent-a Continuous-energy Monte Carlo Reactor Physics Burnup Calculation Code," VTT Technical Research Centre of Finland (2012).
8. S. Qvist and E. Greenspan, "Inherent Safety of Minimum Burnup Breed-and-Burn Reactors", Proceedings of International Conference of Advanced Power Plants: ICAPP-12', Chicago, IL, USA, 24–28 June (2012).
9. Ruggieri, J. M., et al. "ERANOS 2.1: International Code System for GEN IV Fast Reactor Analysis," American Nuclear Society (2006).

Appendix D

S. Qvist and E. Greenspan, “3D shuffling in Breed and Burn reactors,” *in American Nuclear Society Winter Meeting*, Anaheim, CA, USA, 2014.

3D shuffling in Breed and Burn Reactors

Staffan Qvist[a] and Ehud Greenspan[b]

[a)] *Department of Physics and Astronomy, Uppsala University, Sweden*
Ångström Lab, Lägerhyddsvägen 1, 752 37 Uppsala, Sweden, 1

[b)] *Department of Nuclear Engineering, University of California Berkeley, US*

INTRODUCTION

To enable a high utilization of uranium while using a once-through fuel cycle, a special class of fast nuclear reactors collectively known as "breed-and-burn" (B&B) reactors have been under theoretical development since the late 1950s [1]. The unique feature of a B&B reactor is that it can breed plutonium in fertile fuel such as depleted uranium (DU) and then fission a significant fraction of the bred plutonium without having to reprocess the fuel. In order to initiate the chain reaction, the initial loading of the B&B core has to have an adequate amount of fissile fuel – either enriched uranium (EU) or plutonium with or without minor actinides. Thereafter, the B&B core is capable of continued operation while being fed with DU only. Eventually, the uranium utilization will approach the fraction of the loaded uranium that has been fissioned.om conventional two-dimensional to three-dimensional shuffling strategies.

B&B reactors come in two basic flavors: Traveling Wave Reactors (TWR) and Standing (or Stationary) Wave Reactors (SWR). SWRs can use the neutrons more effectively, and therefore require a lower amount of neutron fluence to operate in B&B equilibrium. The limit of neutron irradiation experience for current fast reactor steels is a fast fluence of 3.9×10^{23} n/cm^2 (E>0.1 MeV), corresponding to an irradiation damage of ~200 DPA (displacements per atom) [2]. The minimum peak fast fluence required to sustain SWR B&B-type operation with DU feed fuel is around 1.2×10^{24} n/cm^2 (E>0.1 MeV), or 550-600 DPA [3]. While this is significantly lower than what is required for TWRs, it still requires a threefold increase of the current irradiation damage limit.

In this paper, we study the potential to introduce three-dimensional fuel shuffling in SWR cores in order to minimize the peak DPA. The axial peaking-factor (maximum value divided by the average value) for fluence, burnup and DPA in a typical SWR is on the order of 1.8-2.0. If the axial dpa-profile could be flattened down to a peaking-factor of ~1.1-1.2, peak DPA levels could theoretically be brought down below 350 DPA.

The ambition of this paper is to define engineering solutions to actualize 3D shuffling in SWR cores, as well as to give indicative calculations of the attainable reduction in peak DPA going from conventional two-dimensional to three-dimensional shuffling strategies.

ENGINEERING SOLUTIONS FOR THREE-DIMENSIONAL SHUFFLING

There is inherent difficulty designing for 3D shuffling using solid cylindrical fuel rods, since high burnup fuel elements require a large fission gas plenum to contain the large production of gaseous fission products. In a standard fuel assembly, this poses no problem to the neutron economy since the fission gas plenum is above (or below) the active core. If the fuel rod is subdivided axially, individual fuel rod segments would need to have a volume for fission gas within the active core, effectively neutronically de-coupling fuel regions with a detrimental impact on the neutron economy. Thus, the only identified option to having high actinide-density axially segmented solid fuel rods is to vent the gaseous fission product to the coolant and in this way avoid in-core fission gas plena.

A very extensive study on the research and development of fission gas venting devices was carried out, which ended in the conclusion that any type of hydrostatic venting device would take up too much space axially inside of the core. The only applicable option for a 3D-shuffled system is to continuously vent the fission gas directly to the coolant using small holes in the upper end caps of the fuel rods.

Fuel rod design

To enable the use of axially segmented solid fuel rods in B&B SWR, a number of unique design characteristics are required:

- Fission gas venting to the flowing coolant via a minimum-length venting device
- Minimized axial fuel swelling (and accommodation within the pin for such swelling)
- Maximized actinide density

The resulting fuel rod design concept is shown from the top and side in Figure 1 respectively.

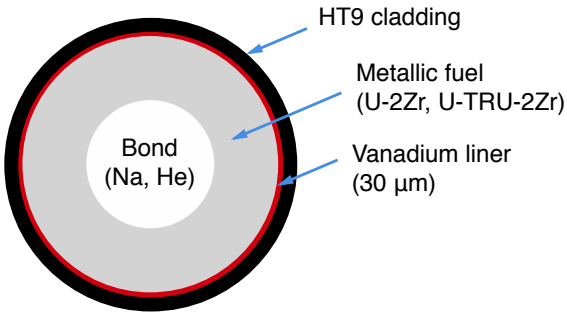

Figure 1, To-scale model of a 3D-shuffled B&B fuel rod with 75% fuel smear density as seen from above

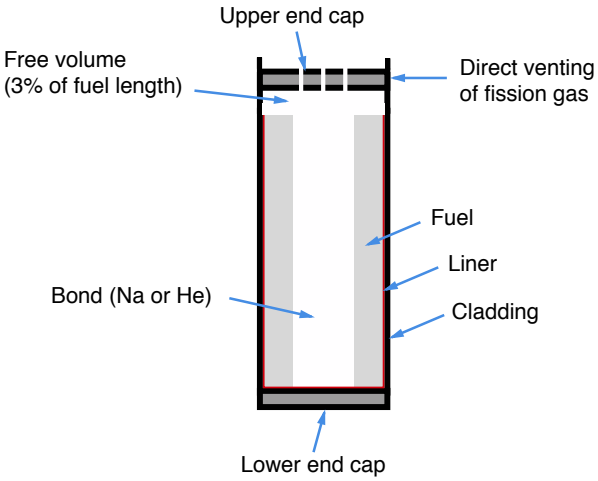

Figure 2, 3D-shuffled SWR B&B fuel rod design with direct fission gas venting seen from the side (not to scale)

The only realistic fuel option for a B&B system is metallic fuel with a maximized actinide density and a minimized fraction of alloying components (2 w.% Zr rather than the conventional 10 w.%). Such fuel is known to swell axially by up to 10%, and due to the low melting temperature, require a liquid bond [4]. If axially segmented, the space allotted to allow for axial swelling and the displacement of liquid bond as the fuel swells radially will axially de-couple the core segments to the point detrimental to the neutron economy. Because of this, an annular fuel rod design was worked out to avoid both of these issues simultaneously. The annular fuel is mechanically bonded to a 30-µm vanadium liner [5], which acts as a diffusion barrier to avoid fuel/cladding chemical interaction (FCCI). While the fuel is swelling inwards as burnup progresses, the bonding restrains the fuel from swelling axially.

Fuel assembly segment design

The assembly-segment design, assuming a 3-zone axial split and a total fueled length of 210 cm, is shown from the side is shown in. Each assembly segment has a total length of 77 cm, made up of the following components:

- Fuel: 70 cm
- Lower end cap: 3 mm
- Upper end cap (including vent-holes): 5 mm
- Upper connector grappler: 2 cm
- Lower connector grappler: 2 cm
- Fuel expansion volume: 2.2 cm (3% of fuel length)

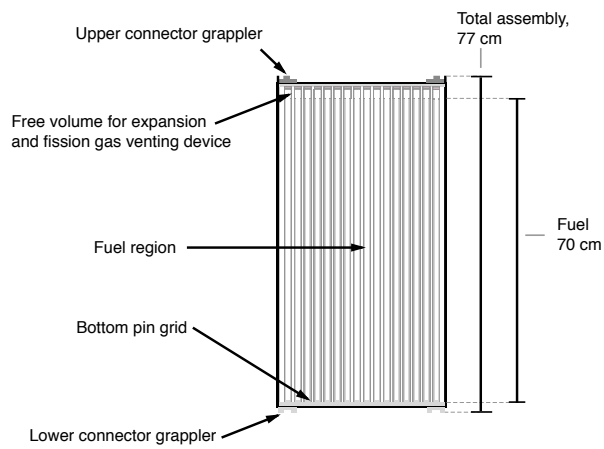

Figure 3, Axially segmented fuel assembly design

The axially segmented fuel assemblies are connected with upper and lower connecting grapplers, the design of which have not been worked out in any detail. The concept of axially connecting pieces and the method of shuffling is shown in Figure 4.

The bottom assembly piece connects to an inlet orificing and shielding piece that ensures the correct coolant flow distribution to the specific radial region of the core. The single most challenging part of this design concept is the operation of the shuffling machine mechanism. A large computational study will have to be undertaken to find the optimal set of operations to move each fuel assembly segment. A large SWR B&B core may have as many as 400-600 fuel assemblies, meaning a total of 1200-1800 fuel assembly segments to be moved. In order to finish a complete fuel shuffling (every assembly segment relocated to a new position) within 1 month, the average time spent moving each assembly to its new location must be on the order of ~30 min.

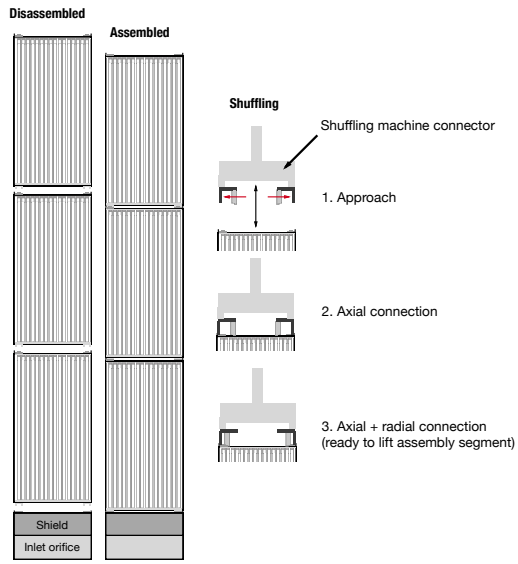

Figure 4, Axial connection between segments and shuffling method

Core structures

New concepts for core assembly "spacers" were developed specifically for the axially segmented 3D-shuffled core, both relying on solid structures inside of the core connected to the lower grid plate, that keep the connected fuel assembly segments in a well-defined shape. The spacers guide the shuffling machine to place the assembly segmented in their predetermined precise locations. The structural design of such a core is shown from the side in Figure 5.

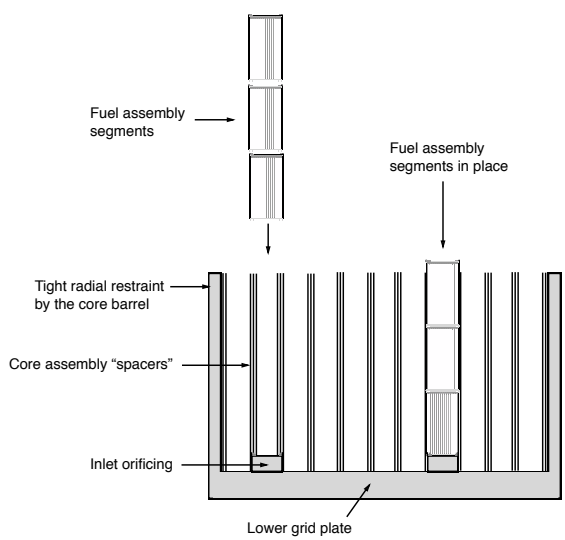

Figure 5, 3D-shuffled SWR B&B general core structural design (not to scale)

An assembly spacer design based on triangle spoke wall structures is shown from the top and side in Figure 6.

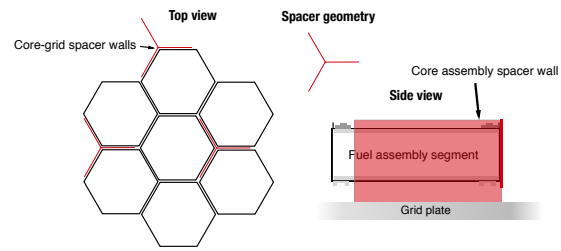

Figure 6, Wall-type assembly spacer design

PRELIMINARY SIMULATION RESULTS

A core design using the fuel rods, assemblies and core structures presented in the previous section was developed using the ADOPT code [6]. The fuel assembly segments used in the simulations were however lengthened to 110 cm (compared to the 77 cm of Figure 3). The diameter of the simulated core is 492 cm, giving a total active core volume of 57 m^3, and a volumetric power density for a 3000 MWt system of 52.5 MW/m^3. The volume fraction of fuel within the fuel assembly segments is 40.7%. A shuffling scheme using 12 radial and 3 axial zones (for a total of 36 batches) was defined, but no optimization of the shuffling path has been made. The radial shuffling path results in radial power peaking factor of 2.1. The feed-fuel for the equilibrium cycle analysis is depleted uranium with 0.25% ^{235}U.

Neutron transport calculations were performed using the Serpent neutron transport code with the ENDF/B-VII.0 cross-section library [7] [8]. To speed up calculations, the active core regions were modeled as 108 equi-volume cells with smeared homogenized materials – 3 burnable zones per fuel assembly segment.

Preliminary simulation results indicate that, similar to conventional 2D shuffled SWR B&B systems, the average discharge burnup required for a critical equilibrium system is 16-17% FIMA (Fission of Initial Metal Atom). The axial movement and short length of assembly segments eliminate most of the axial peaking.

The preliminary calculations indicate that an optimized 3D shuffled SWR B&B system can operate at equilibrium mode with a peak discharge burnup of ~350 DPA, a reduction of about 40% as compared to conventional 2D-shuffled systems. The results of these simulations are showed in Figure 7.

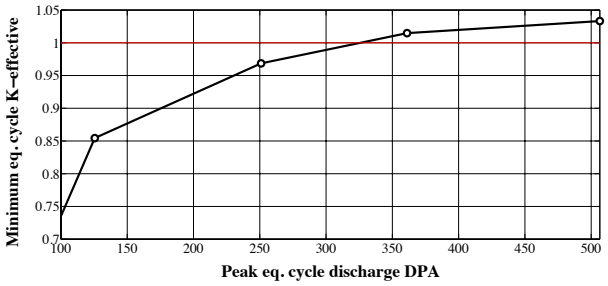

Figure 7, Minimum eq. cycle effective multiplication factor vs. peak cycle dpa for 3D shuffled B&B system

Future studies will serve to refine and validate these initial findings. With further optimization studies of the shuffling strategy, it may be possible to further reduce the peak equilibrium cycle discharge DPA.

REFERENCES

1. S. M. FEINBERG, E. P. KUNEGIN, "Discussion Comment," Prof. of Session B-10, ICPUAE, United Nations, Geneva, Switzerland (1958).
2. M. B. TOLOCZKO, F.A. GARNER, C. EIHOLZER, "Irradiation creep and swelling of the US fusion heats of HT9 and 9Cr-1Mo to 208 dpa at ~400°C", *Journal of Nuclear Materials,* **212,** 604-607 (1994).
3. S. QVIST, "Safety and core design of large liquid-metal cooled fast breeder reactors", *PhD. Thesis*, University of California Berkeley. Berkeley, CA, USA (2013).
4. Y.I. CHANG, "Technical rationale for metal fuel in fast reactors", *Nuclear Engineering and Technology*, **39**, 161-170 (2007)
5. H. RYU et al. "Performance of FCCI barrier foils for U-Zr-Z metallic fuel". *Journal of Nuclear Materials*, **392**, 206-212 (2009)
8. S. QVIST, E. GREENSPAN, "The ADOPT code for automated fast reactor design," *Annals of Nuclear Energy*, **71**, 23-36 (2014)
7. J. LEPPÄNÄN, "Serpent – a Continuous-energy Monte Carlo Reactor Physics Burnup Calculation Code", *AER Symposium on VVER Reactor Physics and Reactor Safety*, Espoo, Finland (2010)
8. M.B CHADWICK et. al, "ENDF/B-VII. 0: Next generation evaluated nuclear data library for nuclear science and technology", Nuclear Data Sheets, **107**, 2931-3060 (2006)

Appendix E

J. Hou, S. Qvist and E. Greenspan, “3-D Fuel Shuffling for Reduced Peak Burnup and Increased Uranium Utilization of Breed-and-Burn Reactors,” ICAPP 2015 - Nuclear Innovations for a Low-carbon Future, May 03-06, 2015, Nice, France.

Proceedings of ICAPP 2015
May 03-06, 2015 - Nice (France)
Paper 15144

3-D fuel shuffling for reduced peak burnup and increased uranium utilization of breed-and-burn reactors

Jason Hou,[a] Staffan Qvist,[b] and Ehud Greenspan[a]
[a]*Department of Nuclear Engineering, University of California, Berkeley, Berkeley, CA 94720, USA*
[b]*Department of Physics and Astronomy, Uppsala University, Sweden, Ångström Lab, Lägerhyddsvägen 1, 752 37 Uppsala, Sweden, 1*
Email:jasonhou@berkeley.edu

Abstract – *This paper assesses the feasibility of improving the performance of a large breed-and-burn (B&B) reactor by using the 3-dimensional (3-D) in-core fuel management strategy. A preliminary conceptual design of a core made of segmented fuel assemblies is outlined. Each fuel assembly is made of 4 subassemblies that are axially stacked in a way that enabled disconnecting subassemblies and reconstituting new assemblies from any four subassemblies in any desirable order. Each subassembly is made of short vented fuel pins. The REBUS-3 fuel cycle analysis code was used to search for the 3-D shuffling strategy that will result in optimal equilibrium core performance. Preliminary simulation results show that, compared with the optimal 2-D shuffling scheme, the optimal 3-D shuffling scheme offers an approximately 30% reduction in the peak radiation damage, from 539 to 378 displacement per atom (dpa); a 88% increase in the average discharge burnup and, therefore, fuel utilization; and a 35% reduction in the radial power peaking factor.*

I. INTRODUCTION

Present day commercial nuclear power reactors, mostly Light Water Reactors (LWRs), can extract only less than 1% of the potential energy that is available in the uranium fuel. The remainder of the potential energy is left wasted in the used nuclear fuel (UNF) and in the depleted uranium (DU) that remains from the enrichment process. The primary motivation for the Breed-and-Burn (B&B) reactors under development is to utilize feed fuel with low uranium enrichment and achieve significant uranium utilization without resorting to fuel reprocessing. The self-sustaining B&B reactors are designed in such a way that once the initial criticality is established, it can be fed with only fertile fuel such as DU, breed plutonium from DU then fission a significant fraction of the bred plutonium.

There are two basic variants of B&B reactors: one is the Travelling Wave Reactor (TWR) like CANDLE concept[1] and the one initially pursued by Terra-Power;[2] the other is the Stationary-Wave-Reactor (SWR) in which the location of the fission reaction in the core is maintained nearly stationary by adequate radial, or 2-dimensional (2-D) shuffling of fuel assemblies. This study focuses on the SWR type of B&B reactor and its fuel shuffling strategy.

In order to sustain the B&B mode of operation, the burnup the DU feed fuel needs to accumulate has to exceed a certain threshold, which strongly depends on the core neutron balance. In a high fuel volume fraction, hard spectrum low-leakage sodium-cooled metallic-fueled B&B core, the minimum required peak burnup is ~30% FIMA (Fissions per Initial heavy Metal Atom).[3] This corresponds to a peak radiation damage of the fuel cladding in the vicinity of 500 dpa (displacements per atom), which far exceeds the presently demonstrated clad radiation damage limit of 200 dpa. As the plutonium builds up near the axial center of the fuel faster than closer to the bottom and top of the fuel, the axial power and burnup distribution in B&B cores is significantly more centrally peaked than in conventional (uniform axial composition) SFR cores. In a typical low-leakage B&B core the peak-to-axially average discharge burnup can exceed 2.

The objective of this study is to investigate the feasibility of reducing the axial variation of the discharge burnup and, thereby, reducing the peak burnup and corresponding radiation damage required for sustaining the B&B mode of operation along with an increase in the overall fuel utilization by introducing three-dimensional (3-D) in-core fuel management strategy.

Section II provides a detailed description of the reference B&B core design and the modeling methodology used in this work. The REBUS-3 results of equilibrium cycle calculation are presented and compared with that of the Monte Carlo code Serpent. In Section III, a conceptual design of fuel rod and assembly is introduced to actualize the 3-D fuel shuffling, followed by the basic strategy for shuffling scheme optimization. The improvement of the core performance using 3-D shuffling is then discussed. The general conclusion of the study and future work are provided in Section V.

II. B&B CORE MODELING METHODOLOGY

II.A. B&B Core Description

The B&B core concept considered in this study is a large sodium-cooled fast reactor fed with DU with 0.25% ^{235}U. The nominal fuel density is 18.66 g/cm^3, and a smear density of 75% is assumed to accommodate the fuel swelling with burnup. The effective core height is 300 cm and equivalent diameter of the simulated core is ~493 cm, giving a total active core volume of 57.19 m^3, and a volumetric power density of 52.46 MW/m^3 for a total core power of 3000 MW (thermal). The general characteristics and volume fraction of the active core are presented in Table I and II, respectively.

TABLE I

Main Parameters of Reference Core

Thermal power (MW$_{th}$)	3000
Coolant	Sodium
Feed fuel	DU (0.25% ^{235}U)
Cladding, duct & wire-wrap	HT-9
Inlet/outlet coolant temperature (ºC)	355.0/506.8
Equivalent core radius (cm)	246.34
Active fuel length (cm)	300
Gas plenum height (cm)	100

TABLE II

Constituents Volume Fractions of the B&B Fuel Assembly

Constituents	Volume Fraction (%)
Fuel	40.70
Gap	13.57
Cladding	12.73
Wire	0.31
Active coolant	22.75
Duct	6.28
Inter-assembly coolant	3.66

II.B. Numerical Modeling of B&B Core

In fast reactors, the large neutron mean free path effectively masks details of the heterogeneous fuel assembly geometry owing to the average fast neutron track length typically far exceeding the dimension of repeating lattices. Consequently, it is common that the core is modeled as homogenized; that is, compositions of fuel, coolant, bonding and structural materials are mixed together within the fuel assembly by volume weighting. In order to further reduce the modeling effort, the assembly-based hexagonal B&B core is simplified into *R-Z* geometry, which consists of 12 equal-volume concentric fuel batches, each made of 4 axial sub-batches. The core is divided into 12 equal volume radial and 8 axial for a total of 96 burnup zones – each sub-batch is axially divided into 2 burnup zones. It was estimated in previous studies that the relative errors in batch multiplication factor k_{eff} introduced by the cylindrical modeling of the B&B core is between -0.4% and 0.4% $\delta k/k$, when compared with the assembly-level core model.[3] This approximation is considered acceptable for scoping studies. A schematic side view of the core is given in Fig. 1, where the center of the core is at the left edge of the figure and fuel batches are separated by vertical lines in the active core region.

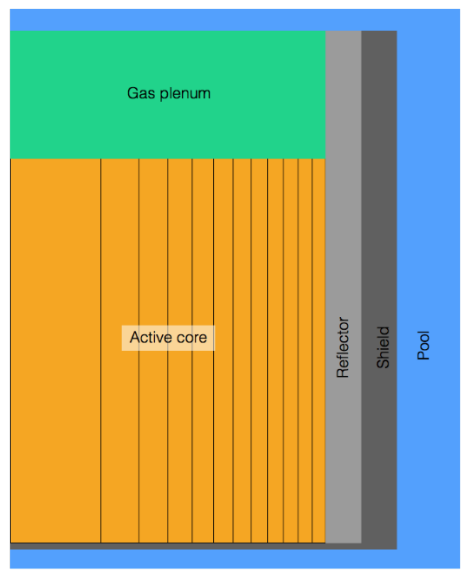

Fig. 1. Schematic layout of cylindrical B&B core.

An optimal radial shuffling scheme identified in a previous study was adopted; it minimized the average discharge burnup, radial power peaking, and burnup reactivity swing.[3] As depicted in Fig. 2, colors distinguish the 4 sub-batch in one fuel batch, and numbers indicate how many cycles the fuel has gone through before it is relocated. The fresh DU batch is loaded at the outermost location and then shuffled inward and outward a couple of times, before being discharged from the 5th radial location from the core center. Note that the schematic only illustrates the relative location and shuffling sequence of fuel batches, other than their thickness in the *R-Z* model.

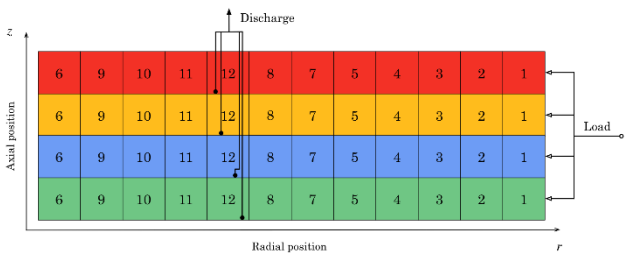

Fig. 2. Schematic of an optimal 2-D shuffling scheme for reference B&B core.

The search for the equilibrium cycle was performed using the DIF3D/REBUS-3 codes,[4,5] which are part of the Argonne Reactor Computation (ARC) system from the Argonne National Laboratory (ANL). In this study, the finite difference diffusion method was employed in the flux and eigenvalue solver DIF3D, because it is the only available option for *R-Z* geometry. The fuel shuffling was modeled explicitly in REBUS-3 calculations. An external module has been developed to post-process REBUS-3 simulation results and produce key characteristic parameters for the equilibrium core, such as the zone-wise fuel burnup, infinite multiplication factor, power, and leakage. The calculation of the displacement per atom (dpa) was also incorporated using the multi-group flux obtained in REBUS-3 results and the microscopic dpa cross section of each isotope contained in the structural material.

Based on the ENDF/B-VII.0 data, region-dependent 33-group cross section sets were generated with the ETOE-2/MC2-3/TWODANT approach.[6,7] Specifically, the MC2-3 code first calculates 0-dimensional (0-D) neutron spectra and condenses point-wise cross sections prepared by ETOE-2 into a ultrafine group structure (~2000 groups). For non-multiplying regions such as reflectors and shield, leaking spectra from the fueled region is used for the condensation. Then, a 2-D ultrafine group transport calculation is conducted by TWODANT to take into account realistic leakage and the calculated spectra are fed back to MC2-3 for the final cross section condensation. It was found in previous studies that in order to accurately account for spectral variation in the B&B core, the best approach is to use burnup and location dependent group constants in the core simulation.[8] However, it is impossible to generate cross sections without knowing the zone-wise equilibrium composition. It is also difficult to assign cross sections to burnup zones while performing fuel shuffling in REBUS-3. Therefore, the preliminary core calculation was carried out using a cross section set generated for the fuel composition pertaining to intermediate burnup (~10% FIMA). This approximation is acceptable for the initial exploration of the effects to be expected from the newly proposed B&B core design and fuel management.

The adequacy of the simplified DIF3D/REBUS-3 model was checked by comparing against a continuous energy Monte Carlo (MC) code Serpent.[9] Both deterministic and MC calculations the ENDF/B-VII.0 cross section library and assume uniformity of temperature distribution for fuel/clad (900 K) and coolant (600 K) in the active core to keep the consistency between two models. They differ, however, in the depletion calculations – whereas Serpent uses a detailed burnup chain, the REBUS-3 calculations use a pre-stored plutonium-uranium burnup chain to simplify the input preparation in two ways. First, it does not include all the heavy metal nuclides prepared in the cross section library. Second, the effect of fission products was accounted for using lumped fission product (LFP) cross sections for 4 different fissionable isotopes, that is, the lumps were created from cross sections for 137 individual isotopes using fission yields for ^{235}U, ^{238}U, ^{239}Pu, and ^{241}Pu.

II.C. Verification Results

First, the 33-group cross sections were generated by MC2-3 using the material composition pertaining to fuel composition of burnup at 10% FIMA, which was extracted from the Serpent full core calculation. They were then utilized in the REBUS-3 burnup calculation of 0-D unit cell made of the B&B fuel assembly average composition, using the average power density derived from the full core model. Fig. 3 shows the k_∞ evolution with burnup and the comparison with that of Serpent results. It can be seen that the REBUS-3 overestimates k_∞ initially and underestimates it when burnup exceeds 8.8% FIMA. The relative error constantly increases in magnitude with burnup, up to a difference of -3.6% at burnup of 40% FIMA. It has been reported that this trend is due to the use of LFPs in REBUS-3, and the discrepancy of the model using LFPSs is approximately -3% at burnup of 40% FIMA, when compared with that using explicit fission products.[10] Since the fuel peak discharge burnup is below 30% FIMA (as will be shown next) in the reference core design, the relative error is judged acceptable for the scoping study.

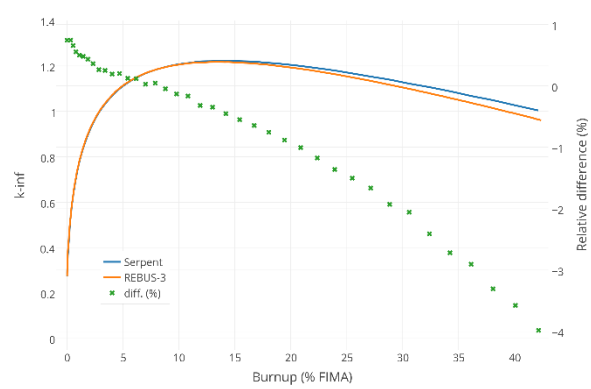

Fig. 3. k_∞ evolution of a B&B core unit cell. Initial fuel composition is depleted uranium.

The k_∞ evolution in a 0-D unit cell as a function of burnup can be used to estimate the minimum burnup required for sustaining the B&B mode of operation using the neutron balance analysis, which counts the number of neutrons that are absorbed and that are generated by fissions in a unit volume of fuel as a function of burnup, starting from the fresh feed fuel.[11] The minimum required burnup, is the lowest burnup for which Eq. (1) is satisfied.

$$N_{HM} \int_0^{BU} \left[P_{NL} \times P_{NRC} - \frac{1}{k(BU)} \right] \bar{\nu}(BU) \times dBU = 0 \quad (1)$$

In the above, N_{HM} is the Heavy Metal (HM) atom density, BU (burnup) is expressed in FIMA, $\bar{\nu}$(BU) is the average number of neutrons released per fission, P_{NL} (= 1 − P_L) is the non-leakage probability and P_{NRC} (= 1 − P_{RC}) is the probability that a fission-born neutron will escape capture in the control elements used to compensate for the burnup reactivity swing over the equilibrium cycle. In the 0-D analysis, the values of P_L and P_{RC} are assumed to be 0. The estimated minimum required burnup is 11.1% and 11.0% FIMA for Serpent and REBUS-3, respectively. The slightly smaller value calculated for REBUS-3 is primarily due to the overestimation of k_∞ at lower burnup.

Next, the modeling capability of REBUS-3 for B&B cores was checked against Serpent for key parameter of the reference core under consideration. Each of the codes was set to search for the minimum equilibrium cycle length that will provide criticality at the beginning of equilibrium cycle (BOEC). 500 active cycles with 10000 neutron histories per cycle were used in Serpent calculation resulting in ~36 pcm statistical uncertainty in k_{eff}. A convergence criterion of 0.5% was applied to the material concentration of each burnup zone in the Serpent calculation. The computational time required by REBUS-3 and Serpent calculations on the UNIX cluster at the University of California, Berkeley was ~12 min and ~23 hr, respectively.

TABLE III

Verification of REBUS-3 Calculation of B&B core

Core parameter	Serpent	REBUS-3
Cycle length (EFPD)	955	955
Reactivity swing (% $\delta k/k$)	4.78	4.83
Average discharge burnup (% FIMA)	8.35	8.08
Peak discharge burnup (% FIMA)	25.1	22.4
Power peaking factor (EOEC)		
Radial	3.05	3.03
Axial	2.66	2.69

As shown in Table III, a good agreement was found in the comparison. The required equilibrium cycle length predicted by the two codes is identical. The REBUS-3 overestimates the reactivity swing and axial power peaking factors at the end of equilibrium cycle (EOEC), while it underestimates the discharge burnup and radial power peaking factor. Overall, the MC2-3/REBUS-3 approach is found adequate for quantifying the relative difference in the characteristics of B&B cores designed using 3-D versus a 2-D shuffling.

The large peak-to-axially average discharge burnup ratio reported in Table III is primarily due to the fact that the fuel is shuffled only in the radial direction. The probability for neutrons born at the high power density region, or the core axial center, to reach the fuel at the core periphery and build up its fissile content is small, especially in a large size core. As a result, the fuel discharged from the core edge never becomes a net neutron producer and its low burnup significantly brings down the average discharge burnup.

III. THE DESIGN OF A B&B CORE WITH 3-D FUEL SHUFFLING

The radiation damage limit to HT-9 cladding proven by the current technology is ~200 dpa, corresponding to an average burnup of ~10% FIMA; further irradiation experiments and/or development of new materials may push these limits above 20% FIMA or 400 dpa. In the high fuel volume fraction, large size and low leakage sodium cooled metallic-fuelled B&B reference core examined above, the minimum peak radiation damage accumulated in the HT-9 fuel clad is 538 dpa, corresponding to the peak discharge burnup of 22.4% FIMA. A large gap exists between this peak radiation damage level and the present constraint, which may delay the commercialization of B&B reactors.

This study assesses the feasibility of reducing the peak radiation damage in a B&B reactor core by axially relocating the fuel, that is, by performing 3-dimensional (3-D) fuel shuffling. As the axial peak-to-average dpa ratio of the fuel discharged from the reference core is 2.64, there is significant potential for peak dpa reduction. The circulation of pebble fuel in a pebble-bed or use of stationary pebbles within fuel sub-assemblies to perform 3-D shuffling have been examined previously.[12,13] It was found difficult to get high enough fuel volume fraction and reach high power density without excessive coolant pressure drop. Consequently, the current study adopted the segmented rod-type fuel assembly design that is free of the above limitations.[14]

III.A. Engineering Solution for 3-D Shuffling

Large volume of plena is required if the B&B fuel is designed to store the gaseous fission products released the fuel. The use of un-vented fuel makes the segmentation of the fuel assemblies impractical because the gas plenum at

the top of the fuel sub-assembly will have significant negative impact on the neutron economy. The only identified option to design high actinide-density axially segmented solid fuel rods is to vent the gaseous fission products directly to the coolant. Because of the relatively large space required for accommodating any type of hydrostatic venting devices, continuous release of fission gas through small openings in the upper end cap is assumed in this study.

The depleted uranium metal fuel, which was selected as the feed fuel for the purpose of maximizing the actinide density, is known to swell axially in the range of 8-10% at burnup of ~20% FIMA caused by the internal pressure of fission gas bubbles, and requires a liquid bond due to low melting temperature.[15] In a segmented fuel rod design, the free volume reserved for fuel swelling and the displacement of the bonding liquid will also have detrimental effects on the neutron economy. As a result, an annular fuel rod design was adopted to avoid both of these issues. The annular fuel is mechanically bonded to a 30-μm vanadium liner[16], which acts as a diffusion barrier to avoid fuel/cladding chemical interaction (FCCI). When the fuel swells inwards with burnup, the bonding restrains the fuel from swelling axially.

In the preliminary design of the axially segmented fuel rod shown in Fig. 4, the height of the fuel region and the additional volume for venting device and fuel expansion is 70 cm and 7 cm, respectively. For the reference B&B core with the height of 300 cm, four sub-assemblies are axially connected with upper and lower connecting grapplers to form a single segmented assembly, as depicted in Fig. 5. The length of fuel rods in the active core is 301 cm, and it includes three internal free volume spaces taking a combined length of 21 cm, leading to a lower effective fuel volume fraction. The total power of the B&B core with segmented fuel assemblies remains the nominal.

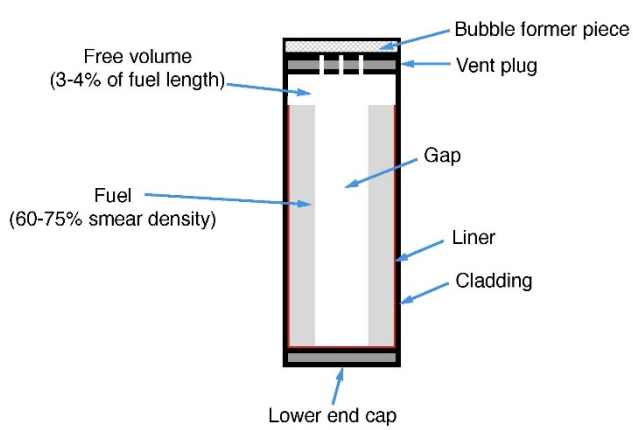

Fig. 4. Axially segmented fuel rod design (not to scale).

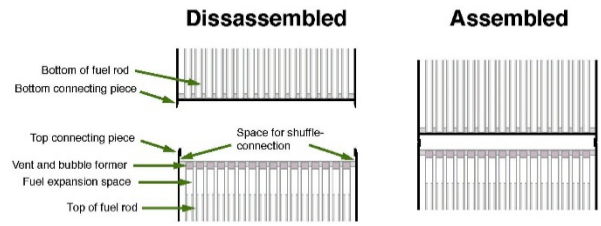

Fig. 5. Axial connection of segmented assemblies.

III.B. Optimization of shuffling scheme

The primary objective of the 3-D fuel shuffling scheme optimization is to reduce the fuel radiation damage as close as possible to a level of recent technology experience, which effectively requires minimizing the peak fuel discharge burnup, owing to the strong correlation between the two quantities.

The peak fuel discharge burnup can be minimized by: 1) flattening the power distribution across the core, as burnup is time-integrated power, and 2) reducing of core leakage, since the minimum required discharge burnup demonstrates high sensitivity to the efficient use of neutrons based on the neutron balance analysis from previous studies. However, the two goals cannot be achieved simultaneously because the tradeoff between the decreased peak-to-average power ratio and decreased neutron leakage would have a large impact on the performance of a shuffling scheme. On one hand, a small power peaking factor requires locating active fuel in the core periphery, which results in stronger neutron leakage effect. On the other hand, the reduced leakage rate demands the outer region of the core maintains very low power density, i.e., the fuel close to core boundary having low fissile content, which in turn leads to higher rate of burnup accumulation at the core center.

Aiming to maintain the low core leakage while minimizing the power peaking, the search for an optimal 3-D shuffling scheme is guided by the following considerations:

- Fresh depleted uranium fuel is loaded at the core outermost radial zone so as to minimize neutron loss via leakage in the radial direction. Considering the small thickness of the outer radial zones, once or twice burned fuel should also be loaded in the adjacent regions.
- A low burnup and, hence, a low fissile content fuel should be loaded at top and bottom zones to avoid strong axial leakage. Although the top and bottom locations are interchangeable because of the core near symmetry, it is desirable to keep axial burnup gradient

outward (such that the more burned fuel is in the axial center) in order to reduce the leakage.

- A high burnup fuel batch with largest reactivity worth should be loaded at the axially middle zones, but not in radial innermost location to avoid large radial power peaking, or outer locations to prevent high neutron leakage.
- Intermediate burnup fuel is loaded in the rest of the locations in the axial core center.
- The burnup zones should be shuffled between the upper and lower halves of the core during their residence time to minimize the axial burnup gradient within subassemblies. This is particularly important for high fissile content fuel, since its reactivity worth is high and the burnup accumulates much faster within the burnup zone.

Some of the considerations, such as reducing the leakage and the burnup gradient of the fuel zones at axial boundaries, cannot be satisfied at the same time. In this case, decisions should be made based on the quantified burnup distribution within each boundary zone, which requires axial refinement of the fuel region in the numerical model. In the current study, each subassembly is divided into 2 axial sub-zones to account for the burnup variation, i.e., there are totally 8 burnup sub-zones when the fresh fuel is loaded, labeled as *A*, *B*, *C*…, *H* from the bottom to the top of the core, as seen in Fig. 6. A fuel management path is defined as the track of the specific sequence of positions and motions of one sub-zone. The accumulated burnup and radiation damage are calculated for each path for the evaluation of the shuffling scheme.

The optimization of the shuffling scheme is an iterative procedure. Starting from an initial fuel management strategy, any modification made by combining the low burnup fuel and high leakage locations, as described in the second consideration above, will inevitably lead to different profiles of burnup, power, and fluence in the equilibrium cycle, which introduces the demand for another modification. After the average discharge burnup has been decreased to a certain level, it is necessary to make fine adjustments to the shuffling scheme further to eliminate the already minimized peaking of the discharge fuel burnup. One of the approaches, for example, is switching locations of fuel zones in the low reactivity fuel batch. Fig. 7 shows one of the optimized 3-D shuffling schemes for the reference core, which will be used in the later analysis.

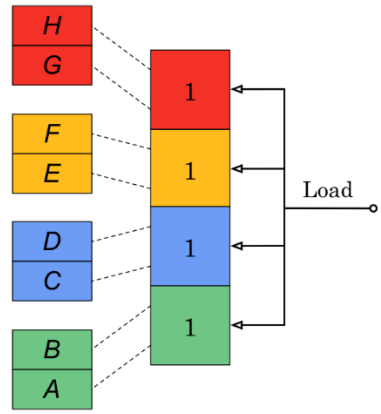

Fig. 6. Axial discretization of fuel zones.

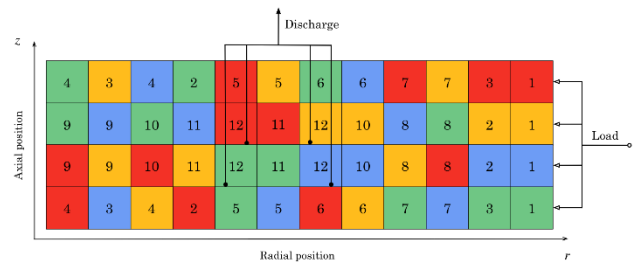

Fig. 7. Schematic of the optimized 3-D shuffling scheme pattern for reference B&B core.

III.C. Simulation Results

The equilibrium core results using the optimal 3-D shuffling scheme given in Fig. 7 were obtained using REBUS-3 and compared in Table IV with those using the 2-D shuffling scheme. It can be seen that the peak radiation damage has been reduced by 29.8% -- from 538.63 to 378.40 dpa. Among all 8 fuel management paths, as illustrated in Fig. 8, the dpa of discharge fuel in the 2-D shuffling case was strongly peaked at the core axial center (Paths *D* and *E*) with a peaking factor of 2.67; while with 3-D fuel shuffling, the peaking factor has been brought down to 1.03, allowing the discharge burnup distributed almost evenly over all the fuel. Although the radiation damage level is still beyond the proven damage limit for HT-9 cladding (~200 dpa), it is much more realistic to expect that further experimental test or new material under development will be able to reach this value than the one required for the 2-D shuffling core.

It is worth noting that the vanadium liner between the fuel and cladding has been taken into account in the 3-D shuffling core model. The liner, taking up ~0.44% of the active core volume under the current segmented rod design, results in a lower fissile material breeding rate and a smaller core leakage. Additional calculations suggest that the negative impact of the liner on the neutron economy is negligible: the current design requires an increase on both

average and peak discharge burnup by ~1%, and the resulting increase on peak radiation damage is within 2 DPA, when compared with the case without liner.

Fig. 9 compares the zone-wise burnup distribution at EOEC of the two cores. A very large axial burnup gradient is observed in Fig. 9 (a) for batch 5 fuel. In contrast, 3-D fuel shuffling offers a significantly smaller gradient of burnup as seen in Fig. 9 (b) and the peak discharge burnup is 15.9% FIMA versus 22.4% for 2-D shuffling. The 3-D discharge burnup peaking factor is only 1.05 versus 2.64 with 2-D shuffling.

TABLE IV

B&B Core Parameters Using 2-D and 3-D Fuel Shuffling

Core parameter	2-D	3-D
Cycle length (EFPD)	955	1675
Reactivity swing (% $\delta k/k$)	4.83	6.96
Average discharge burnup (% FIMA)	8.08	15.19
Peak discharge burnup (% FIMA)	22.44	15.91
Peak radiation damage (DPA)	538.63	378.40
Leakage probability (%)		
Radial	0.059	0.610
Axial	0.054	0.515
Total	0.113	1.125
Power peaking factor (EOEC)		
Radial	3.03	1.97
Axial	2.69	2.35

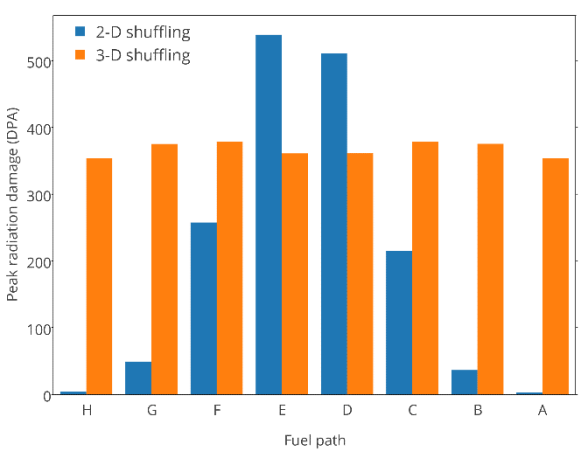

Fig. 8. Discharge radiation damage of 8 half-subassemblies. A and B are two halves of one subassembly, etc.

Table IV also indicates that the axial fuel shuffling increases the average discharge burnup from 8.08 to 15.19% FIMA; that is, the fuel utilization is increased by 88%. The resulting longer cycle length will also increase the capacity factor because of less frequent shuffling. However, the 3-D fuel shuffling also increases the core leakage probability, especially in the axial direction. The neutron loss due to leakage must be compensated by some more source neutrons, from a neutron balance perspective, contributing somewhat to an increase in the minimum required discharge burnup. Future studies will attempt to reduce this leakage probability.

In addition, a significant reduction of both the radial and axial power peaking was observed - the radial power peaking is only ~65% of the optimal 2-D shuffling core. This may enable increasing the average power density and specific power of the 3-D B&B core.

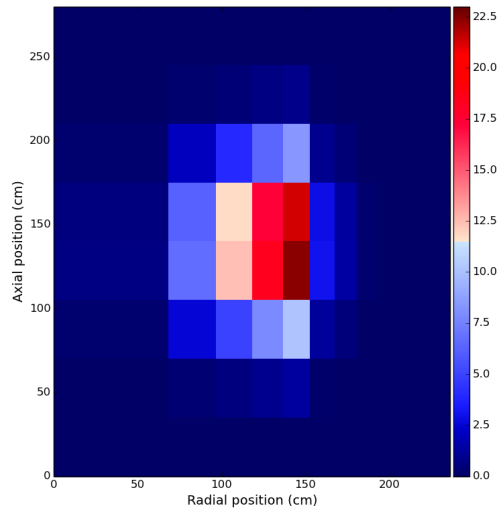

(a)

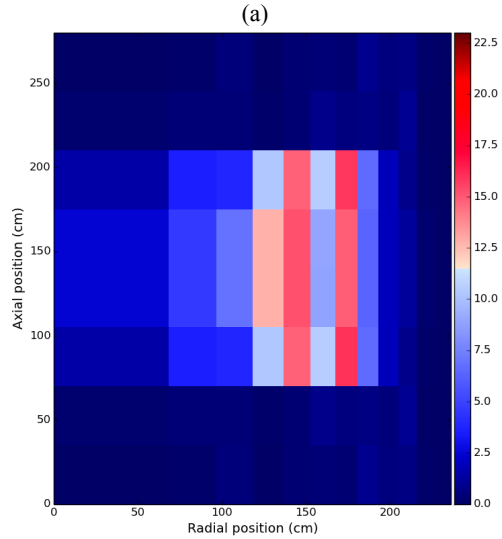

(b)

Fig. 9. Fuel sub-zone average burnup distribution at EOEC for B&B core with 2-D (a) and 3-D (b) fuel shuffling.

A drawback of the 3-D versus the 2-D shuffled core is a larger burnup reactivity swing: 6.96 versus 4.83 % $\delta k/k$ (Table IV). However, the 3-D core cycle is significantly longer and the burnup reactivity swing per unit time or give amount of energy generated is actually smaller: 1.52% versus 1.85% $\delta k/k$ per EFPY. It is possible to reduce the cycle burnup reactivity swing by increasing the number of

radial batches and, to some extent, optimizing the fuel shuffling strategy.

IV. DISCUSSION

While providing significant improvements of the B&B core performance as discussed above, 3-D fuel shuffling also gives rise to some realistic design challenges. First, reliable designs of segmented fuel assemblies need be developed as well as of a refueling machine and strategies for disconnecting subassemblies and reconnecting them to make new assemblies. One of the challenges of the subassembly design is the design of its venting fixtures. Safe handling of the fission products vented into the reactor primary loop is another challenge. The use of segmented fuel assembly will also significantly increase the refueling time.

V. CONCLUSIONS AND FUTURE WORK

A three-dimensional in-core fuel management strategy was identified for the large sodium cooled B&B reactor that can greatly improve this core performance compared with the reference 2-D fuel shuffling case -- a 30% reduction of the minimum required peak burnup and, hence, radiation damage along with an 88% increase in the uranium utilization and a 35% reduction in the radial power peaking factor. The latter is likely to enable an increase in the core power. An increase in the core power and in the uranium utilization may enable an improvement in the B&B reactors economic viability. The reduction of the minimum required peak radiation damage to below 400 dpa is likely to enable a sooner commercialization of B&B reactors than otherwise.

There is a slight difference in the B&B core performance predicted by the MC2-3/REBUS-3 analysis approach versus Serpent. Although the inconsistency between the two computational tools is not expected to affect the above conclusions, effort will be expanded to identify the source of discrepancies.

Future studies will apply the ADOPT code[17] to identify the maximum power level the B&B core with 3-D shuffling could safely operate at. Design variables of the thermal-hydraulic optimization will include the number of fuel rods per assembly and fuel rod dimensions. Once the assembly design is determined, the cylindrical geometry model will be converted to a hexagonal assembly-by-assembly model for more realistic simulation of the B&B core.

The optimization process used so far is based on a trial-and-error approach. The use of an automated fuel management optimization algorithm such as the genetic algorithm for further improving the B&B core performance will be explored.

A sound mechanical design needs to be developed of segmented fuel assemblies made of axially stacked subassemblies made of short vented fuel pins, as well as of a refueling machine that can efficiently perform the 3-D fuel shuffling. Effective means for handling the fission products that will be vented into the primary loop need be developed as well.

ACKNOWLEGEMENTS

This work has been performed under the auspices of the Department of Energy Nuclear Energy University Programs (NEUP).

REFERENCE

1. H. SEKIMOTO and K. RYU, “A New Reactor Burnup Concept CANDLE,” *Proc. of PHYSOR 2000*, Pittsburgh, PA, US (2000).

2. J. GILLELAND, C. AHLFELD, D. DADIOMOV, R. HYDE, Y. ISHIKAWA, D. MCALEES, J. MCWHIRTER, N. MYHRVOLD, J. NUCKOLLS, and A. ODEDRA, “Novel Reactor Designs to Burn Non-Fissile Fuels,” *Proc. Int. Congress on Advances in Nuclear Power Plants (ICAPP ’08),* Anaheim, CA, USA, June 8-12, American Nuclear Society (2008) (CD-ROM).

3. F. HEIDET and E. GREENSPAN. “Performance of large breed-and-burn core,” *Nucl. Tech.,* **181**, 381 (2013).

4. K. L. DERSTINE, “DIF3D: A Code to Solve One-, Two-, and Three-Dimensional Finite Difference Diffusion Theory Problems,” ANL-82-64, Argonne National Laboratory (1984).

5. B. J. TOPPEL, “A User’s Guide to the REBUS-3 Fuel Cycle Analysis Capability,” ANL-83-2, Argonne National Laboratory (1983).

6. C. H. LEE and W. S. YANG, “MC2-3: Multigroup Cross Section Generation Code for Fast Reactor Analysis,” ANL/NE-11-41, Argonne National Laboratory (2013).

7. R. E. ALCOUFFE, F. W. BRINKLEY, D. R. MARR, and R. D. O’DELL, “User’s Guide for TWODANT: A Code Package for Two-Dimensional, Diffusion-Accelerated, Neutral Particle Transport,” LA-10049-M, Los Alamos National Laboratory (1990).

8. J. HOU, F. HEIDET, P. GORMAN and E. GREENSPAN, "On Multi-Group Cross Sections for Breed-and-Burn Reactors," *Transaction of the American Nuclear Society,* Anaheim, CA, November (2014).

9. J. LEPPÄNEN, "Serpent - a Continuous-energy Monte Carlo Reactor Physics Burnup Calculation Code," VTT Technical Research Centre of Finland (2012).

10. F. HEIDET, private communication.

11. F. HEIDET and E. GREENSPAN, "Neutron Balance Analysis for Sustainability of Breed-and-Burn Reactors," *Nuclear Science and Engineering*, **171**, 1 13-31 (2012).

12. D. FRAZER, P. GAURAV, P. GORMAN, K. ROWLAND, and D. WOOTEN, "A Pebble Based Breed & Burn Reactor Capable of 3-D Shuffling," NE 265 Course Project, University of California, Berkeley (2013)

13. S. GONZALES, "Study of the feasibility of a Pebble Bed Breed & Burn Reactor," Master Report, Department of Nuclear Engineering, University of California, Berkeley (2012)

14. S. QVIST and E. GREENSPAN, "3D shuffling in Breed and Burn Reactors", *Transaction of the American Nuclear Society,* Anaheim, CA, November (2014).

15. Y. I. CHANG, "Technical rationale for metal fuel in fast reactors", *Nuclear Engineering and Technology,* **39**, 3, 161 (2007).

16. H. RYU et al. "Performance of FCCI barrier foils for U-Zr-Z metallic fuel," *Journal of Nuclear Materials,* **392**, 206-212 (2009)

17. S. QVIST and E. GREENSPAN, "The ADOPT Code for Automated Fast Reactor Core Design," *Annals of Nuclear Energy*, **71**, 23-36 (2014).

Appendix F

J. Hou, S. Qvist, R. Kellogg and E. Greenspan, “In-core Fuel Management Optimization for Breed-and-Burn Reactors with 3D Fuel Shuffling,” *PHYSOR 2016 - Unifying Theory and Experiments in the 21st Century*, Sun Valley, Idaho, May 2016 (accepted).

IN-CORE FUEL MANAGEMENT OPTIMIZATION FOR BREED-AND-BURN REACTORS WITH 3D FUEL SHUFFLING

Jason Hou, Staffan Qvist, Ehud Greenspan
Department of Nuclear Engineering
University of California, Berkeley, Berkeley, CA 94720 USA
jasonhou@berkeley.edu

Roger Kellogg
Nuclear Engineering Division
Argonne National Laboratory, Argonne, IL 60439, USA

ABSTRACT

This paper describes the continuing effort to employ the 3-dimensional (3D) in-core fuel management strategy in Breed-and-Burn (B&B) reactors to reduce the axial variation of the discharge burnup and, thereby, reduce the peak burnup and corresponding minimum required peak radiation damage. A more robust design of the segmented fuel assembly has been identified. A combinatorial optimization search methodology of the 3D shuffling pattern (SP) based on the Simulated Annealing (SA) algorithm has been developed and implemented; it aims to minimize the peak radiation damage while reducing the burnup reactivity swing, radial power peaking factor and maximum change of assembly power over a cycle. It was found that compared with the optimal 2-dimensional (2D) shuffled core, the optimal 3D shuffling pattern offers a 1/3 reduction of the peak radiation damage level – from 534 down to 351 displacements per atom (dpa), along with a 45% increase in the average fuel discharge burnup. Also studied are a number of potential approaches aiming to minimize the complexity of the 3D shuffling strategy and the associated refueling time without significantly penalizing the improvements of the core performance.

Key Words: **breed-and-burn reactor, peak radiation damage, 3D fuel shuffling optimization, simulated annealing, optimal core design**

1. INTRODUCTION

Present day commercial nuclear power reactors, mostly Light Water Reactors (LWRs), can extract only less than 1% of the potential energy of the natural uranium. The remainder of the potential energy is left wasted in the used nuclear fuel (UNF) and in the depleted uranium (DU) that remains from the enrichment process. The primary motivation for the Breed-and-Burn (B&B) reactors under study is to utilize low grade fuel with low fissile uranium content, such as DU, and achieve significant uranium utilization without resorting to fuel reprocessing. The self-sustaining B&B reactor is designed in such

a way that once the initial criticality is established, it can be fed with only fertile fuel such as DU, breed plutonium from DU then fission a significant fraction of the bred plutonium.

There are two basic variants of B&B reactors: Traveling Wave Reactors (TWRs) and Stationary (or Standing) Wave Reactors (SWRs). In TWRs, the breeding and burning wave travels axially through the long core from one end to the other. [1, 2] In SWRs, like the one presently being pursued by TerraPower [3, 4], the location of the fission reaction in the core is maintained nearly stationary by adequate radial, i.e., 2-dimensional (2D) shuffling of fuel assemblies. This study focuses on the SWR type of B&B reactor and its fuel shuffling strategy, because relative to TWR it features higher efficiency of neutron utilization and lower level of radiation damage required to establish B&B equilibrium.

In order to sustain the B&B mode of operation by feeding the core with fertile fuel such as DU, the burnup the fuel needs to accumulate must exceed a certain threshold, which strongly depends on the core neutron balance. In a sodium-cooled metallic-fueled B&B core featuring high fuel volume fraction and low-leakage, the minimum required peak burnup is about 20% fission per initial heavy metal atom (FIMA) and the corresponding peak radiation damage of the fuel cladding is in the vicinity of 500 displacements per atom (dpa) [5], which far exceeds the presently demonstrated cladding radiation damage limit of 200 dpa [6]. In the 2D shuffled system, as the plutonium builds up near the axial center faster than at the top and bottom of the fuel assembly, the axial power and burnup distribution in B&B cores is significantly more centrally peaked than in conventional (uniform axial composition) sodium-cooled fast reactor (SFR) cores. It is expected that the peak dpa level will be reduced significantly, if the axial profile of the discharge burnup and dpa level could be flattened down to a peaking factor close to 1.0.

Previous studies have been carried out to investigate the feasibility of achieving this objective by introducing 3-dimensional (3D) in-core fuel management strategy. [7, 8] An axially segmented fuel rod and assembly design has been proposed to facilitate 3D fuel shuffling and preliminary results suggested show that the optimal 3D shuffling pattern (SP) can offer an approximately 30% reduction in the peak radiation damage while increasing the fuel utilization relative to a 2D shuffling. However, the optimal SP search was based on a user intuitively specified trial-and-error approach. A practical limit exists on its optimization capability, especially for the identification of the optimal core design that should meet additional constraints such as the burnup reactivity swing, radial power peaking factor and relative assembly power change over the cycle. Thus, an automated optimization capability that is able to account for all the constraints is desirable.

The first objective of this study was to identify a mechanical design of the segmented assembly with improved robustness and practicality. The second objective was to develop an automated methodology for the optimization of in-core fuel management for B&B reactors, for both 2D and 3D shuffling strategies that is able to account for multiple design constraints. The third objective was to quantify the improvements in B&B core performance made possible by 3D fuel shuffling and to investigate the dependence of these improvements on the number of axially stacked sub-assemblies, core power level and core dimensions.

2. BREED-AND-BURN CORE DESIGN WITH 3D FUEL SHUFFLING

2.1. Generic B&B Core Design

A generic B&B core concept OBB (*Optimized B&B*) has been developed and used as the reference core, upon which the optimal 3D shuffling were searched in this study. It is a large SFR fed with DU having an unirradiated nominal fuel density of 18.66 g/cm^3 at 800 K. A smear density of 75% is assumed to accommodate the fuel swelling with burnup. The cladding material, which is the ferritic-martensitic alloy HT-9, and the coolant have densities of 7.87 and 0.83 g/cm^3, respectively, both at 800 K. The effective core height is 300 cm and its equivalent diameter is $\sim$493 cm, giving a total active core volume of 57.19 m^3 and a volumetric power density of 52.45 MW/m^3 for a total core thermal power of 3000 MW. This reference design uses vented fuel rods that allow the release of the fission gas, but prevent the reverse-flow of the coolant into the fuel pins. [9] The general characteristics and assumed volume fraction of the active core constituents are presented in Table I.

Table I. Main characteristics of the reference B&B core.

Thermal power (MW)		3000
Core equivalent radius (cm)		246.34
Active fuel length (cm)		300
Gas plenum height (cm)		100
Feed fuel		DU (0.25% ^{235}U)
Coolant		Sodium
Structual material		HT-9
Inlet/outlet coolant temperature (°C)		355.0/506.8
Fuel assembly volume fraction (%)	Fuel	40.70
	Gap	13.57
	Cladding+Wire	13.04
	Duct	6.28
	Coolant	26.41

2.2. Engineering Solution for 3D Fuel Shuffling

In the original design concept, assembly segments are axially connected with connecting grapplers to form a full-length assembly, while the segment at the bottom of the core is connected to a shielding and flow orificing block that is designed to remain in a fixed location in the reactor for the lifetime of the core. [8] A recent mechanical concept review identified a number of mechanical engineering challenges associated with the original design including difficulties to provide core stability under all operating conditions and to move fuel segments reliably in the sodium coolant. Both of these challenges must be met in a manner that introduces as little as possible non-fuel volume to the assembly; therefore, the original design has been modified and the upgraded design arrived at is described below.

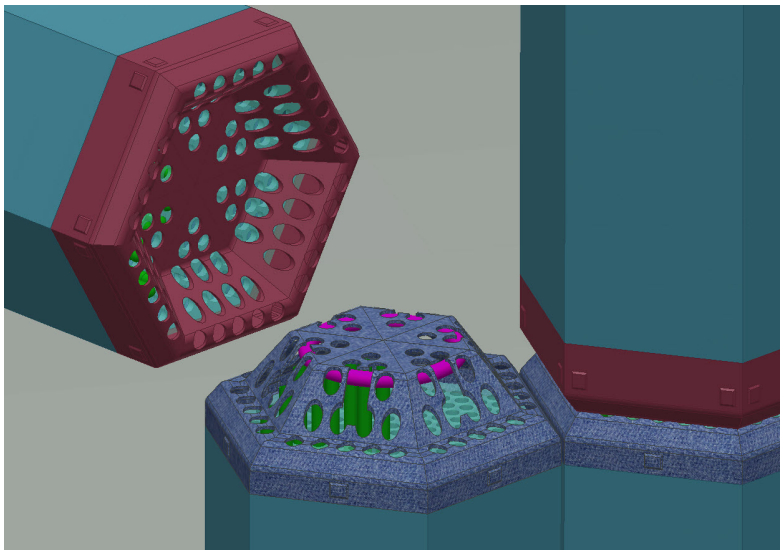

Figure 1. Top and bottom cap of the newly proposed fuel assembly segment design for 3D fuel shuffling.

An important guiding principle is that assembly segments should be free stacking without axial joining connections to avoid penalties on fuel-free volume and the introduction of a reliability weakness. As a result, a nesting tapered conic interface is proposed for the segment-segment interface, as illustrated in Figure 1. The top cap (blue) has a protruding hexagonal cone, while the bottom cap (red) has a re-entrant hexagonal cone, which provides a self-centering zone that is larger than the resolution limits of the refueling machine. Adequate passages for coolant flow are provided through aligned coolant holes on the conic surface.

Upper and lower external edges of the assembly segments have bevels to provide additional self-centering and resistance to snagging on adjacent fuel assemblies. This contributes significantly to eliminating difficulties with placing segments in the core, especially the last few segments placed in the array, as neighboring ones that tend to lean toward the open space can be pushed back into proper position as the new assembly segment is inserted. Centering buttons on the side of the top and bottom cap provide consistent rotational and lateral positioning of the assembly segment in the core and maintain consistent gaps between segments. This arrangement minimizes the dragging of one segment against its neighbors when being inserted or removed. These centering buttons can also provide a measure of tolerance for bowing or twisting of fuel assemblies over their service life.

Figure 2 (left) depicts the design of the fuel handling gripper with 3 jaws, which is positioned at the end of the refueling mast. A robust reinforcing ring (also shown in Figure 1) is placed in the top of the assembly segment to distribute gripper forces and provide adequate wear surfaces for the life of the segment. A central rod actuator can actuate 3 jaws equally. During the refueling process, the refueling mast is positioned over the assembly segment and extended downwards to reach the segment. The segment is then attached with the handling gripper and lifted up. The gripper is smaller than the footprint of a segment, thus allowing it to reach an assembly segment on the lowest course without

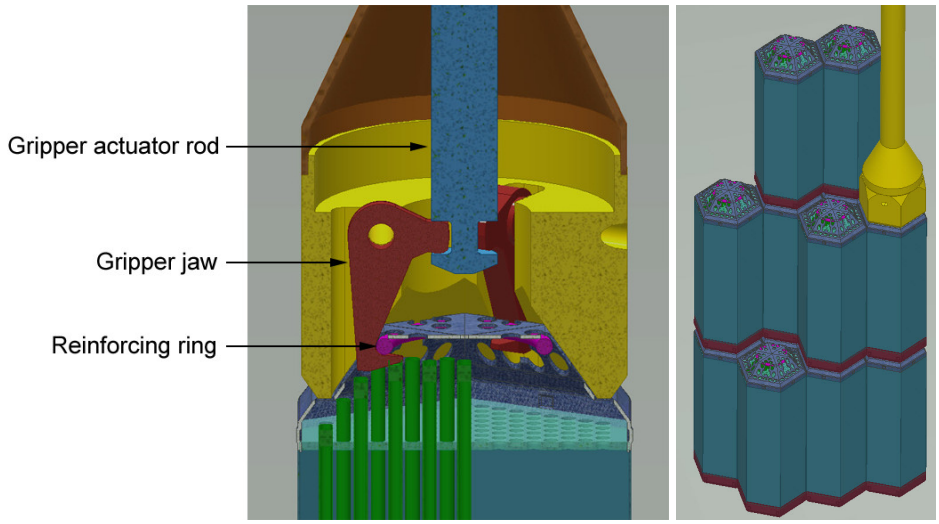

Figure 2. Section view of the assembly segment gripper mechanism (left); and stacked fuel segments, representing a portion of a core (right).

removing neighboring segments. Figure 2 (right) shows the attachment of the gripper to one of the sub-assemblies sitting on top of the stacked segments during the refueling process.

The assembly segments are constituted of rod-type fuel, which are designed to allow for continuous release of gaseous fission products through a thin porous filter followed by small openings in the upper end cap. The annular metal fuel is mechanically bonded to a 30 μm vanadium liner to avoid fuel-cladding chemical interaction. Both of these features are described in the original design paper [8]. The full-length fuel assembly of the first design of 3D shuffled core investigated in this study, referred to as OBB-I, is made of four 77 cm long sub-assemblies (an alternative term for assembly segment) making a 301 cm active core height. This core has three 7 cm thick fuel-free layers at the top of each of the three lower sub-assemblies due to the design of the sub-assembly fuel rods. The total power of the OBB-I core with segmented fuel assemblies is the same as of the 2D shuffled reference core.

2.3. Core Modeling Methodology

The core characteristics compared in this study pertain to the critical equilibrium cycle. The search for the equilibrium cycle was performed using the DIF3D/REBUS-3 codes [10, 11] which are part of the Argonne Reactor Computation (ARC) system developed at the Argonne National Laboratory (ANL). The finite difference diffusion method was employed in the flux and eigenvalue solver DIF3D. The batch-wise fuel shuffling was modeled explicitly with REBUS-3. For a given core geometry and constituents volume fraction, the design variables are the shuffling pattern and cycle length. Burnup independent 33-group cross section sets were generated for the fuel composition pertaining to intermediate burnup ($\sim$10% FIMA) based on the ENDF/B-VII.0 data library using the MC2-3 code of the

ARC package. [12] Thermal-hydraulics calculations are incorporated into the core optimization process through coupling with neutronics calculations using the ADOPT code [13]. ADOPT is designed to search for the optimal number of fuel rods and lattice pitch in a fuel assembly that will maximize the permissible power density while abiding by the thermal-hydraulic and structural design constraint – most if not all based on first principles. The thermal-hydraulics constraints accounted for in this study are:

- maximum core pressure drop: 0.9 MPa,
- maximum sodium velocity across the core: 12 m/s,
- maximum fuel-cladding interface temperature: $650\,^{\circ}\mathrm{C}$, and
- maximum peak fuel temperature: $1000\,^{\circ}\mathrm{C}$.

3. SHUFFLING PATTERN OPTIMIZATION

Simulated Annealing (SA) is a stochastic optimization technique inspired by an analogy to annealing in metallurgy, which involves repeatedly heating and cooling of a material to increase the crystal size and remove defects so as to alter its physical properties. It was first introduced as a tool of finding equilibrium configuration of a system of particles at a given temperature, and then applied to combinatorial optimization problems, in which a family of candidate solutions to minimize the objective function is generated following a Markov chain sampling. [14, 15] Its major advantage over other methods is the ability to avoid being trapped at local minima, because the random search not only accepts changes that improve the solution performance but also some changes that worsen it.

In this study, the primary objective of the SP optimization is to reduce the peak minimum required radiation damage (R^*) as much as possible while its second objective is to minimize other design constraints, including the reactivity swing ($\Delta\rho$), change of batch power over the cycle (ΔP_B) and the radial power peaking factor (F_R). Optimization of the decision variable, the fuel shuffling pattern can, therefore, be characterized as a combinatorial minimization problem expressed in the following augmented objective function:

$$\bar{F} = \gamma R^* + \sum_{i=1}^{I} \lambda_i \Omega_i \tag{1}$$

where the first term on the right side of Equation (1) is the main objective function corresponding to the evaluation of peak radiation damage, and each penalty term in the summation represents the contribution of one of the constraint related objectives to the augmented objective function. The violation functions Ω, taking the forms given in Table II, are the relative differences of current value of the parameter from the pre-defined design constraints, of which the values in the 3rd column of the same table were adopted in this study. The impact factor λ are introduced to adjust the importance of each objective; for example, in the case where reactivity swing minimization takes the priority in SP optimization, all that must be done for the objective function transition is to increase the impact factor

Table II. Elements and constraints of augmented objective function.

Description	Violation function	Constraint
Burnup reactivity swing	$\Omega_1 = \Delta\rho/\rho^{\text{lim}} - 1$	$\rho^{\text{lim}} = 3.5$
Max change of batch power	$\Omega_2 = \Delta P_B/P_B^{\text{lim}} - 1$	$P_B^{\text{lim}} = P_{th}/B_b$ [a]
Radial power peaking factor	$\Omega_3 = F_R/F_R^{\text{lim}} - 1$	$F_R^{\text{lim}} = 2.5$

[a] P_{th} refers to the core thermal power; N_b denotes the number of radial fuel batches in the core.

associated to Ω_1. γ is a multiplication constant used to adjust R^* to the same order of magnitude of the penalty terms in Equation (1) ; a value of 0.01 is used in this study.

In the general implementation of the SA method [16], a control parameter T is introduced as system temperature, and the energy difference between the two states of the material is replaced by the difference between the current objective function value $F(X_i)$ and the proposed objective function value $F(X_j)$, with X denoting the solution to the optimization problem. The algorithm begins with an initial guess at the optimal solution and then seeks successively improved solutions through a continuing examination of randomly generated solutions in the neighborhood of the ever-changing optimum. For a minimization problem, the probability of acceptance of a new solution $F(X_j)$ is given by

$$p(\Delta F, T) = \min\left\{1, \exp\left(-\frac{F(X_j) - F(X_i)}{T}\right)\right\} \tag{2}$$

Candidates that decrease F are, of course, accepted, while candidates that increase F by $\Delta F = F(X_j) - F(X_i)$ are accepted as new solutions with the probability calculated in Equation (2). The usually decreases in a series of discrete steps over time. In the current implementation, the decrease of the control parameter T is achieved by the exponential multiplicative schedule, where the initial temperature is multiplied by a positive factor less than 1, so that the temperature decreases exponentially with respect to the simulation cycle. The value of this multiplication factor, also known as the cooling parameter, is chosen between 0.80 and 0.99 for various optimization problems shown in this study, because the design space for this problem is highly nonlinear. [17]

The SA optimization proceeds by performing a perturbation to the initial guess of SP and calculating the initial probability of acceptance. The SA algorithm then chooses whether or not to preserve or replace the current SP. More perturbations are then performed, producing improved values of the objective function at decreasing values of the control parameter T until the maximum number of simultaion cycles specified by the user is reached. A strategy flowchart of the optimization process is displayed in Figure 3, in which the term "evaluate SP" refers to the estimation of the augmented objective function outcome for a specific SP using REBUS.

Since the SP optimization is expected to involve a large number of equilibrium core calculations, it is desirable to further reduce the core modeling effort even using deterministic codes. Therefore, the assembly-based hexagonal B&B core is represented in R-Z geometry, which consists of a number of

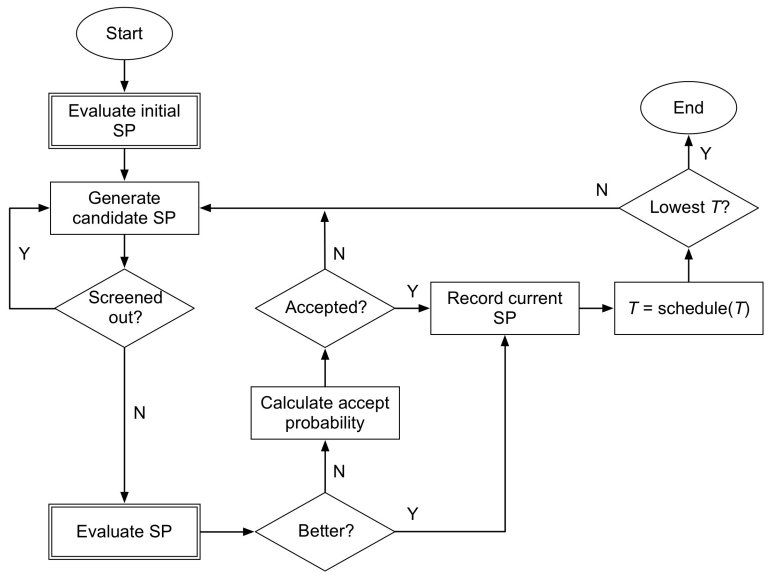

Figure 3. Flow diagram of shuffling pattern optimization using simulated annealing.

equal-volume concentric fuel batches. The discrepancy of using the simplified R-Z model, which primarily stems from depleting all the assemblies of a given batch with the same power level, is considered acceptable for a study aimed at estimating the relative differences between 3D and 2D fuel shuffling on B&B core characteristics as will be shown in the later sections. The R-Z model enables a 70-80% reduction in the computational time of the neutronics calculations and thus expedite the optimization process.

4. SIMULATION RESULTS

The performance of the SA algorithm was first examined by optimizing the SP for both 2D and 3D shuffled OBB-I core; both consisting of 12-radial batches. In the 2D shuffling, each assembly was subdivided into 8 equal volume axial burnup zones, while in the 3D shuffling each of the four sub-assemblies was subdivided into two burnup zones, so that a consistent comparison of the performance of the two cores can be performed.

The SP optimization process was completed after 500 cycles and the optimum SPs found are depicted in Figure 4. For the 2D SP (top), the fresh fuel is loaded at the core periphery, then shuffled to the center, before starting to "bounce" between the outer and inner region of the core and finally discharged from the 8th radial location. The optimum 3D SP, shown at the bottom of Figure 4, features 4 independent "fuel paths", each corresponding to one of the 4 segments used to constitute the full-length assembly. The colors of the 3D SP distinguish those shuffling paths, while the numbers indicate the burnup cycle of the relocation (1 where the fuel is loaded and 12 where the fuel is discharged). It can be seen that the

fuel is shuffled to the high reactivity worth regions after the first irradiation cycle and discharged from the core axial center from the 10th and 11th radial positions. The axial discretization of each full-length assembly in 3D shuffling is shown to the right of the optimal SP map.

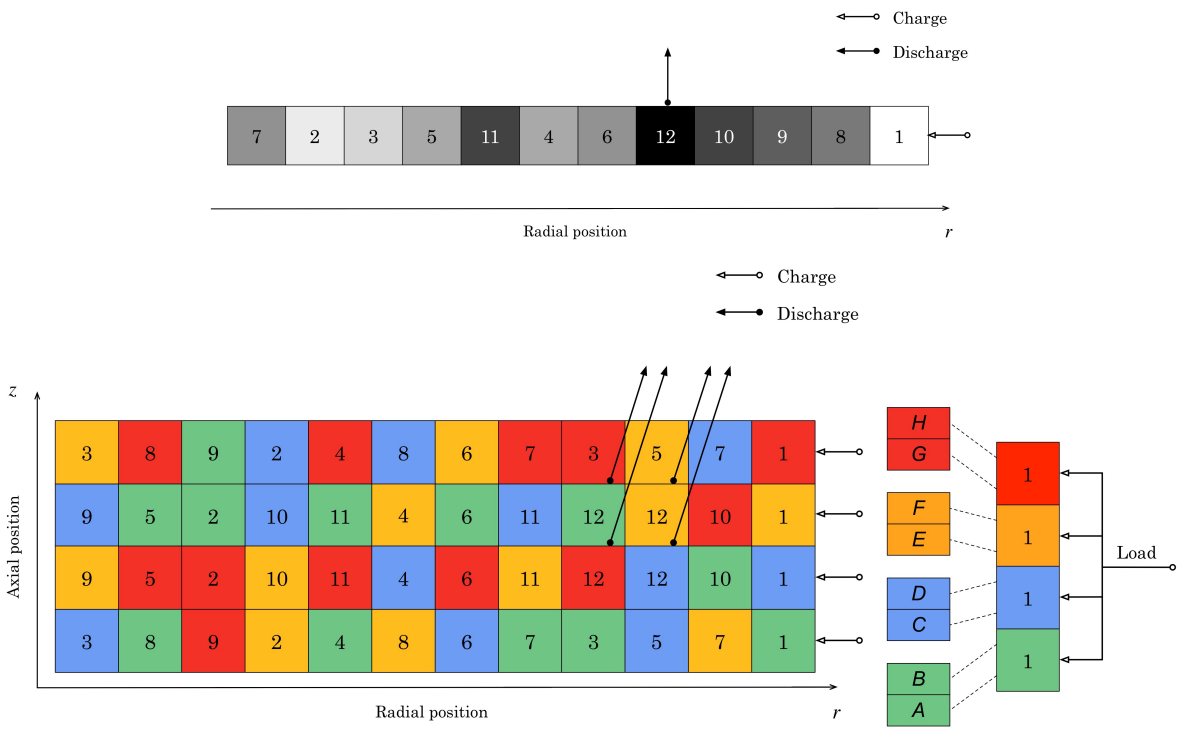

Figure 4. Optimal 2D (top) and 3D (bottom) shuffling pattern for OBB-I core.

Columns 2 and 3 in Table III compare the equilibrium core performance using the optimal 2D and 3D SP in R-Z geometry. It can be seen that the 3D shuffling enables a 34% reduction of the peak radiation damage – from 534.2 dpa in 2D shuffling case to 351.0 dpa for the 3D case. Even though the peak burnup was reduced proportionally, the corresponding average discharge burnup increased from 9.91% to 14.49% FIMA, which implies an approximately 45% increase in the fuel utilization. This is despite of the higher neutron leakage probability from the 3D shuffled core. If normalized to the same dpa level, the average discharge burnup of the 3D shuffled core is 2.23 times that of the 2D shuffled core; this corresponds to a relative increase in the fuel utilization of nearly 120%. As a result of the higher average burnup, the equilibrium cycle length was increased from 1083 for 2D to 1566 effective full power days (EFPD) for 3D shuffled systems. Correspondingly, the burnup reactivity swing increases from 2.81% of the 2D to 4.66% of the 3D shuffled system and therefore also of the fraction of neutrons that are absorbed in the reactivity control system. However, per unit time or given amount of energy generated, the burnup reactivity swing is comparable: 1.09% versus 0.95% $\Delta k/k$ per effective full power year (EFPY).

Although 351 dpa is still beyond the proven radiation damage limit for HT-9 cladding, it is expected that ongoing and future irradiation experiments and new material development will enable to reach this

Table III. Comparison of performance of optimal 2D and 3D shuffled OBB-I core.

Equilibrium parameter		2D shuffled (R-Z)	3D shuffled (R-Z)	3D shuffled (Hex-Z)
Burn cycle time (EFPD)		1083	1566	1647
Burnup reactivity swing (% $\Delta k/k$)		2.81	4.66	4.41
Peak/average discharge BU (% FIMA)		23.62/9.91	15.69/14.49	15.94/14.88
Peak radiation damage (dpa)		534.2	351.0	357.7
Axial/radial leakage probability (%)		1.00/2.67	1.56/2.75	1.72/3.15
Axial/radial power peaking factor		2.35/1.64	2.00/1.70	1.93/1.67
Peak batch power change (%)		17.07	22.14	20.73
Pitch-to-diameter ratio		1.065	1.070	1.068
Core volume fractions (%)	Fuel	40.16	39.77	40.31
	Gap	13.39	13.26	13.44
	Cladding+Wire	12.85	12.77	12.92
	Duct	6.59	6.57	6.46
	Coolant	27.03	27.63	26.88

dpa value much sooner and with higher certainty than the >500 dpa required for 2D shuffling cores. The thermal-hydraulics corrected fuel volume fraction was 40.16% and 39.77%, corresponding to the fuel pin pitch-to-diameter (P/D) ratio of 1.065 and 1.070, for 2D and 3D shuffled system, respectively, due to the somewhat higher radial power peaking factor of the 3D shuffled core.

The neutron balance analysis described in [18] can be used to estimate the net number of excess neutrons generated by a unit volume of fuel, N_{ex}, as a function of burnup as follows:

$$N_{ex} = N_{HM} \int_0^{BU} \left[1 - \frac{1}{k(BU) \times P_{NL} \times P_{NRC}} \right] \bar{\nu}(BU) dBU \tag{3}$$

where $k(BU)$ refers to the k_∞ evolution with burnup in the control volume, N_{HM} is the Heavy Metal (HM) atom density, BU is the burnup expressed in FIMA, $\bar{\nu}(BU)$ is the average number of neutrons released per fission, $P_{NL}(= 1 - P_L)$ is the non-leakage probability and $P_{NRC}(= 1 - P_{RC})$ is the probability that a fission-born neutron will escape capture in the control elements used to compensate for the burnup reactivity swing over the equilibrium cycle. The minimum burnup required for sustaining a B&B operation is that burnup for which $N_{ex} = 0$. A neutron balance analysis is carried out for each of the 8 axial equal burnup fuel batches as they traverse the core from loading to discharge. Figure 5 plot the neutron balance curves of 4 out of the 8 these batches due to near axial symmetry for the optimal 2D (left) and 3D (right) shuffled cores. Fuel path A corresponds to the lowest 1/8, while fuel path H corresponds to the highest 1/8 of the fuel assembly when first loaded. The turning point of the neutron balance plots from a negative to a positive slope corresponds to k_∞ of 1.0; at smaller burnups the fuel is a net neutron consumer - i.e., it absorbs more neutrons than it generates, while at higher burnups the rate of fission neutrons the fuel generates exceeds the rate of neutrons it absorbs. A negative sign in the neutron balance implies that there is a net cumulative neutron loss, whereas a positive sign pertains to burnup over which a net excess of neutrons has been generated by a unit fuel volume.

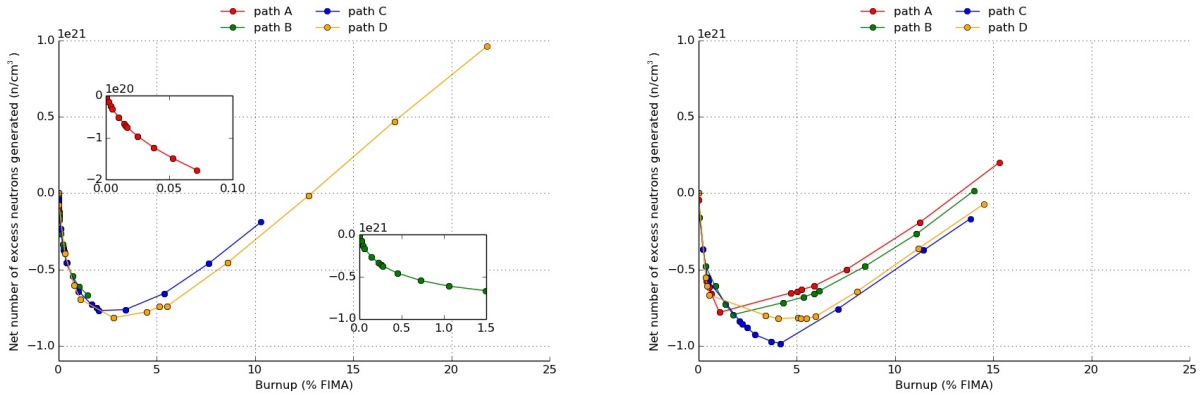

Figure 5. Fuel path neutron balance of optimal 2D (left) and 3D (right) shuffled OBB-I core.

In the 2D shuffled OBB-I core, The fuel of path A and B remained a net neutron absorber throughout its residence in the core; the neutron balance of these burnup batches did not even reach the turning point implying that their discharge $k_\infty < 1.0$. The fuel of path C, although becoming a net neutron producer, did not manage to pay back the number of neutrons it absorbed. Only the axially central fuel path D (and its counterpart E) exceeded the zero balance line and by a large extent as it has to make up for the neutron deficiency of the other three fuel paths. In the 3D shuffled core on the other hand, the fuel of each of the paths has paid back all or most of the neutrons it absorbed; it's neutron balance at discharge is in the vicinity of zero. This is because the 3D fuel shuffling significantly flattens the burnup distribution of the discharged fuel as can be deduced from the burnup corresponding to the end point of the neutron balance curve of each of the fuel paths. When comparing the peak dpa of the fuel discharged from each of the 8 fuel paths, as shown in Figure 6, it can be seen that in the 2D shuffled core the dpa strongly peaks at the core axial center while with 3D fuel shuffling the peak discharge dpa is within $\pm 3\%$ of the average.

The 3D shuffled core that was optimized using the R-Z geometry was simulated using hexagonal assembly-based geometry. A comparison of the core characteristics obtained using the two simulations is given in the two rightmost columns of Table III. The Hex-Z core has a slightly longer equilibrium cycle length and average discharge fuel burnup, primarily due to larger core leakage in both radial and axial direction. This is because the outmost batch filled with the fresh fuel does not have enough assemblies to enclose the inner core in the Hex-Z model, and thus increases the probability of neutrons leaking out of the core. However, the corresponding increase in the peak discharge burnup and peak radiation damage is only 1.6% and 1.9%, respectively, and the peak radiation damage is 357.7 dpa. It can be concluded that the B&B core performance predicted using both geometries is close enough, so that it is adequate to optimize the shuffling pattern using R-Z geometry and later simulate the optimal core using the hexagonal model and thereby improve the spatial resolution of the results.

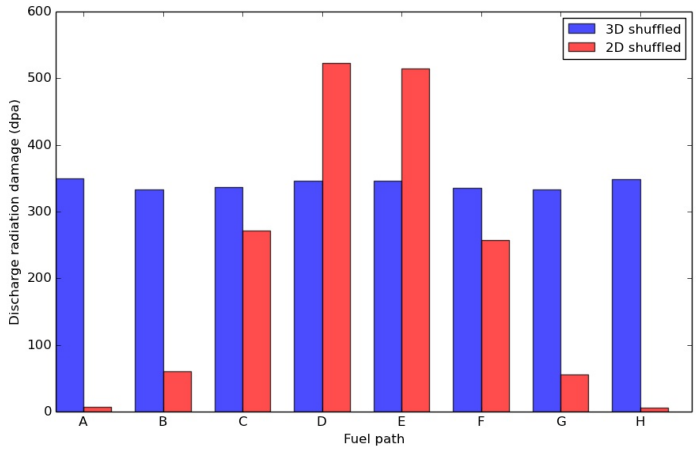

Figure 6. HT-9 discharge dpa for OBB-I core.

5. CORE DESIGN SIMPLIFICATION

The implementation of the 3D fuel shuffling strategy considered in the previous section will require significantly longer refueling time, more complicated refueling machine and, possibly, two separate refueling machines to cut down the total refueling time. It will also require larger workspace above the core to disassemble and reassemble the fuel assemblies relative to 2D fuel shuffling. Therefore, a number of design approaches for 3D shuffling simplifications were examined and their effect on the core performance improvements from 2D fuel shuffling was quantified.

The first approach was to restrict the shuffling of sub-assemblies to axial shuffling within the same fuel assembly in OBB-I without changing the design parameters of the core, so that radial shuffling will be performed for entire fuel assemblies as in a 2D shuffling strategy. More specifically, at the refueling outage, a fuel assembly is lifted from the core segment by segment, then reassembled in a different radial location using the same segments but in a different axial order. This shuffling strategy will greatly reduce the workspace and time required for refueling, because the relocation of one full-length assembly does not affect the rest of the core except for the assembly at the targeting location - as is the case in 2D shuffling.

The second approach was to reduce the number of segmented assemblies used to constitute one fuel assembly. This design, called OBB-II core, is loaded with fuel assemblies made of 3 axially stacked segments, each having identical dimensions as of OBB-I. The active core height is 228 cm (consisting of 3 segmented rods and 2 volumes of fuel-free space in the axial direction), giving a core volume of 42.70 m^3. The core thermal power of OBB-II is adjusted to achieve the same fuel specific power as of OBB-I, which is 7.22 kW/kg, and the resulting core power is 2340 MW.

The third approach attempts to reduce both the number of fuel batches and the number of segmented

Table IV. Design parameters of alternative B&B core designs with 3D fuel shuffling.

Design Parameter	OBB-I	OBB-II	OBB-III
Number of radial fuel batch	12	12	8
Number of sub-assemblies per assembly	4	3	3
Total fuel length in assembly (cm)	280	210	210
Active core height (cm)	301	224	224
Equivalent core radius (cm)	246.34	246.34	246.34
Active core volume (m^3)	57.38	42.70	42.70
Core thermal power (MW)	3000	2340	2335
Power density (MW/m^3)	56.20	54.80	54.68

assemblies used to constitute one fuel assembly. Based on the OBB-II core, the assembly pitch in this OBB-III core is increased to 18.78 cm while maintaining the number of full-length assemblies within each batch and total core cross-sectional area. As a result, the number of assembly segments contained in OBB-III core is further reduced to only half of that in OBB-I core. Determined by matching the fuel specific power as of OBB-I, the core power of OBB-III is 2335 MW with volumetric power of 54.68 MW/m^3. The design parameters and the resulting performance characteristics of the alternative cores are presented in Table IV and V, respectively.

As shown in Table V, the equilibrium cycle length and discharge burnup of the OBB-I core with axially-constrained shuffling (3rd column) are 1728 EFPD and 16.02% FIMA, respectively - both slightly larger than those of the unconstrained case (2nd column). By placing segments with high burnup fuel at the axial periphery of the core before the discharge, this shuffling strategy is able to flatten the axial power peaking factor to 1.37, but inevitably causes a higher axial leakage probability of 3.84%. The radial power peaking factor of 1.78 is slightly higher than the 1.70 of the unrestricted 3D shuffled core; it is required to reduce the fuel volume fraction from 39.77% to 39.27% in order to meet the thermal-hydraulic constraints. The increase of core leakage and the reduction of fuel volume fraction are the major contributors to the 25 dpa increase in the minimum required peak radiation damage to the HT-9 cladding, when compared with the unconstrained core design.

The OBB-II core performance is summarized in the 4th column of Table V. The reduction of the number of axially stacked sub-assemblies from 4 to 3 along with a 25% reduction in the total active fuel length does not significantly penalize the core performance. The minimum required peak radiation damage is 359.8 dpa – only 2.5% higher than of the optimal 3D shuffled OBB-I core. Due to the reduced core height and therefore reduced pressure drop, the fuel volume fraction could be increased to 41.45%.

The peak radiation damage of the OBB-III core, shown in the rightmost column of Table V, is 376.3 dpa – only about 4.6% higher than of the optimal 3D shuffled OBB-II core while the average discharge burnup and, hence, fuel utilization, is even slightly higher. When compared with OBB-I core with 2D shuffling (Table III), the OBB-III core enables a $\sim$30% reduction in peak radiation damage, from 534.2 to 376.3 dpa, while providing a $\sim$131% increase in cycle length, primarily due to the increased DU loading per batch. The number of shuffling operations this core requires is only approximately doubled,

assuming this number is directly proportional to the number of assembly segments in the core. With the significantly extended cycle length, the number of shuffling operations required per year in OBB-III core is even $\sim 14\%$ less than that in the 2D shuffled OBB-I core. However, the burnup reactivity swing of this core is significantly higher and this may force an increase in the number of batches that will enable to shorten the cycle. A search for alternative SP that features a smaller burnup reactivity swing is worth trying as well.

Table V. Performance of optimal 3D shuffled B&B core of various designs.

Shuffling type	OBB-I unconstrained	OBB-I axially constrained	OBB-II	OBB-III
Core thermal power (MW)	3000	3000	2340	2335
Burn cycle time (EFPD)	1566	1728	1598	2506
Burnup reactivity swing (% $\delta k/k$)	4.66	3.26	4.85	5.52
Peak/ave. discharge BU (% FIMA)	15.69/14.49	17.16/16.02	14.95/14.64	15.78/15.36
Peak radiation damage (dpa)	351.0	375.8	359.8	376.3
Axial/radial leakage probability (%)	1.56/2.75	3.84/3.05	1.72/0.89	1.83/1.31
Axial/radial power peaking factor	2.00/1.70	1.37/1.78	2.18/1.85	2.02/1.89
Peak batch power change (%)	22.14	16.28	12.19	14.00
Pitch-to-diameter ratio	1.070	1.076	1.055	1.052
Fuel volume fraction (%)	39.77	39.27	41.45	41.27

6. CONCLUSIONS

This paper presents the development and implementation of a automated search methodology of the optimal 3D shuffling pattern (SP) based on Simulated Annealing (SA) algorithm for self-sustaining B&B reactors. The SP optimization was performed using a coupled neutronics and thermal-hydraulics calculation scheme. In addition to minimizing the peak dpa level the SA-based optimization search methodology was found capable of improving multiple performance characteristics.

Compared with the optimal conventional 2D fuel shuffling, the optimal 3D SP offers a 34% reduction of the peak radiation damage level, down to ~ 350 dpa; a 45% increase in the average fuel discharge burnup, and hence the uranium utilization, without violating all major neutronics and thermal-hydraulics constraints. For the same peak dpa level, the 3D shuffled core enables a $\sim 120\%$ increase in the fuel utilization when compared to 2D shuffled core.

In order to minimize the increased demand for refueling effort and workspace introduced by the axially segmented fuel assembly design, a number of variations of the standard 3D shuffled design approach to alleviate these drawbacks were examined. It was found possible to reduce by 50% the number of refueling operations in 3D shuffling while extending the cycle length and thereby reducing the number of shuffling operations required per unit reactor operation time when compared with 2D shuffling.

Future studies should perform a cost/benefit analysis in order to assess the tradeoff between the improved core performance versus the complexity in the fuel assembly design, the fuel handling devices and increased reactor downtime and a corresponding decrease in the nuclear plant capability factor. In addition, detailed safety analysis need also be performed.

ACKNOWLEDGMENTS

The current study has been supported by funding from the U. S. Department of Energy Nuclear Energy University Programs (NEUP). Useful collaboration with Dr. Taek Kyum Kim and others at ANL is acknowledged.

REFERENCES

[1] H. Sekimoto and K. Ryu. "A new reactor burnup concept candle." *Proc. of PHYSOR2000*, (pp. 1–9). Pittsburgh, PA, USA (2000).

[2] E. Teller *et al.* "Completely automated nuclear reactors for long-term operation." In: *Proceedings of ICENES*, volume 96, (pp. 24–28). Obninsk, Russia (1996).

[3] C. Ahlfeld *et al.* "Conceptual design of a 500 MWe traveling wave demonstrator reactor plant." In: *Proceedings of ICAPP 2011*. Nice, France (2011).

[4] P. Hejzlar *et al.* "Terrapower, LLC traveling wave reactor development program overview." *Nuclear Engineering and Technology*, **45(6)**: pp. 731–744 (2013).

[5] J. Hou, S. Qvist, and E. Greenspan. "3-D fuel shuffling for reduced peak burnup and increased uranium utilization of breed-and-burn reactors." In: *Proceedings of ICAPP 2015*. Nice, France (2015).

[6] M. Toloczko, F. Garner, and C. Eiholzer. "Irradiation creep and swelling of the US fusion heats of HT9 and 9Cr-1Mo to 208 dpa at $\sim$400 °C." *Journal of Nuclear Materials*, **212**: pp. 604–607 (1994).

[7] S. Qvist and E. Greenspan. "3D shuffling in Breed and Burn reactors." In: *American Nuclear Society Winter Meeting*. Anaheim, CA, USA (2014).

[8] S. Qvist, J. Hou, and E. Greenspan. "Design and performance of breed-and-burn reactors." *Annal of Nuclear Energy*, **85**: pp. 93–114 (2015).

[9] G. O'Neill *et al.* "Safety and economic aspects of vented fuel in sodium-cooled reactors." In: *Proceedings of the Conference on Safety, Fuels, and Core Design in Large Fast Power Reactors*, (pp. 11–14). Argonne National Laboratory, Illinois, October (1965).

[10] K. Derstine. *DIF3D: a code to solve one-, two-, and three-dimensional finite-difference diffusion theory problems.[LMFBR]. Technical report*, Argonne National Lab., IL (USA) (1984).

[11] B. Toppel. *User's guide for the REBUS-3 fuel cycle analysis capability*. Argonne National Laboratory (1983).

[12] C. Lee and W. Yang. "MC2-3: multigroup cross section generation code for fast reactor analysis." *Argonne National Laboratory, ANL/NE-11-41* (2012).

[13] S. Qvist and E. Greenspan. "The ADOPT code for automated fast reactor core design." *Annals of Nuclear Energy*, **71**: pp. 23–36 (2014).

[14] N. Metropolis *et al.* "Equation of state calculations by fast computing machines." *The Journal of Chemical Physics*, **21(6)**: pp. 1087–1092 (1953).

[15] S. Kirkpatrick *et al.* "Optimization by simulated annealing." *Science*, **220(4598)**: pp. 671–680 (1983).

[16] C. R. Reeves. *Modern heuristic techniques for combinatorial problems*. John Wiley & Sons, Inc. (1993).

[17] E. H. L. Aarts and J. H. M. Korst. *Simulated annealing and Boltzmann machines - a stochastic approach to combinatorial optimization and neural computing*, volume 55 (1990).

[18] F. Heidet and E. Greenspan. "Neutron balance analysis for sustainability of breed-and-burn reactors." *Nuclear Science and Engineering*, **171(1)**: pp. 13–31 (2012).

Appendix G

R. Kelloge, “Mechanical Concept Review of 3D Fuel Shuffling in Breed-and-Burn Reactors,” Nuclear Engineering Division, Argonne National Laboratory Technical Memo, 2015.

Mechanical Concept Review

3D Fuel Shuffling in Breed-and-Burn Reactors

Roger Kellogg, PE, Nuclear Engineering Division, Argonne National Laboratory

2015 September 02

Foreword

This mechanical concept review is based on documents developed by Staffan Qvist, Jason Hou, and Ehud Greenspan of Uppsala University, Sweden, and UC Berkeley, USA.

Concept Outline

The 3D Shuffle Breed- and-Burn (3D B&B) reactor concept applies to a sodium cooled reactor. Fuel elements are one quarter of the length of conventional fuel elements and are stacked four deep to create a full height core. It is necessary to minimize non-fuel headspace at the top and bottom of the fuel elements in order to conserve neutron flux between upper and lower fuel elements. Since there are four layers of fuel elements, it is possible to reposition fuel elements in three dimensions in order to attain uniform burn-up and DPA damage in the fuel elements. Fuel elements are composed of conventional cladding tubes containing fuel.

Mechanical Engineering Challenges

Some of the mechanical engineering challenges in creating a 3D B&B reactor will include providing core stability under all operating conditions and moving fuel elements reliably under the molten sodium coolant. Both of these challenges must be met in a manner that does not introduce non-reactive volume to the fuel elements or core.

Core stability must be maintained so that a fuel element (FE) can be removed from the core without the neighboring elements collapsing into the void space left behind. Additionally, adequate gaps must be engineered into the core to prevent binding and snagging of neighboring FE during fuel moves. Consideration must be made for swelling and thermal expansion of the FE over their functional lifetime.

Fuel element movement challenges arise from the need to reliably place fuel elements with a fuel handling machine that has limited resolution under liquid sodium. A robust means of gripping individual fuel elements will be required.

Additional Boundary Conditions

The B&B fuel elements must allow adequate flow of sodium coolant.

Fuel elements must accommodate swelling of metallic fuel.

Fission gas production must be handled with an appropriate engineered solution.

A segmented hold-down mechanism will be provided on top of the core to prevent FE from drifting upward in the coolant flow. The hold-down mechanism must be removed to provide fuel handling access.

Fuel elements will be stacked within a core barrel frame which provides lateral support at the periphery of the core assembly.

Fuel Element Stacking

The 3-D Shuffling concept presented appears to provide inadequate self-centering capability. Images provided show very limited tapering of top / bottom interfaces. Additionally, there is no clear method to prevent a moved fuel element from snagging on neighboring fuel elements when being inserted or removed from the core assembly.

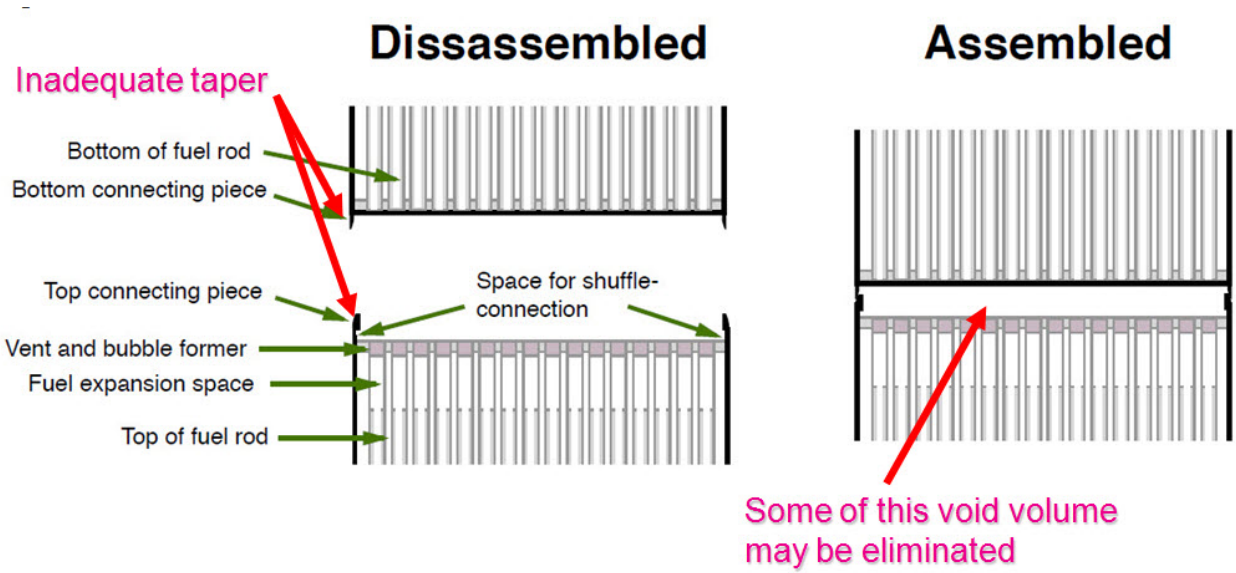

Figure 1. Concept illustration of fuel element interface. Very small tapers will not provide adequate centering for remote manipulation under sodium. Sharp square corners will snag neighboring elements during insertion / removal operations and are damage-prone.

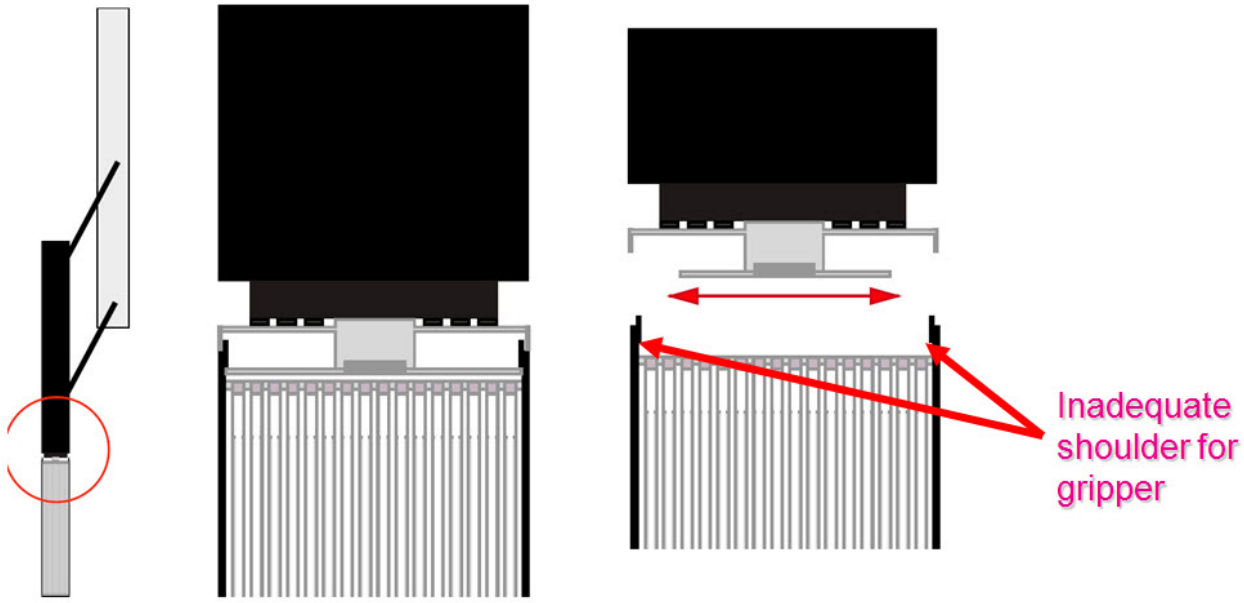

Figure 2. Illustration of concept for gripping fuel elelment. The shoulder provided is not adequate for robust engagement of gripper with the fuel element.

Suggested Fuel Element Configuration

A nesting tapered hexagonal conic interface is proposed for the FE / FE interface. The generous tapered hexagonal cone provides a self-centering zone that is larger than the resolution limits of the fuel handling machine, ensuring consistently robust fuel element movements. Figures 3 and 4 illustrate the conic interface. The fuel clad tubes will follow the profiles of the top and bottom caps, minimizing non-reactive volume in the core. It may be necessary to provide various length clad tubes to accommodate edge bevels and gripper features.

Upper and lower external edges of the fuel elements have generous bevels to provide additional self-centering and resistance to snagging on adjacent fuel elements. This contributes significantly to eliminating difficulties with placing FE in the core, especially the last few elements placed in the array, as neighboring elements that tend to lean toward the open space can be pushed back into proper position as the new fuel element is placed. These bevels are robust against damage from minor handling impacts.

The fuel element end caps are designed so that horizontal surfaces control the axial position of stacked fuel elements. This requires that a small gap exist at the conic interface when nested. Horizontal contact surfaces provide a straighter stack and are less likely to stick together.

Centering buttons at the top and bottom of the fuel elements provide consistent lateral positioning of the FE in the core. Two buttons are provided at the bottom of the FE in order to maintain rotational

registry with the core grid. A single button at the top of the FE is adequate to maintain position of the top of the FE. This arrangement minimizes the dragging of one FE against its neighbors when being inserted or removed. These centering buttons provide a measure of tolerance for bowing or twisting of fuel elements over their service life. The centering buttons have bevels at their periphery. If the centering buttons of a lower course FE snag the buttons of a higher neighboring FE, additional clearance will be automatically created as the neighbor is lifted past its adjacent neighbors, allowing the snagged FE to drop back into proper position.

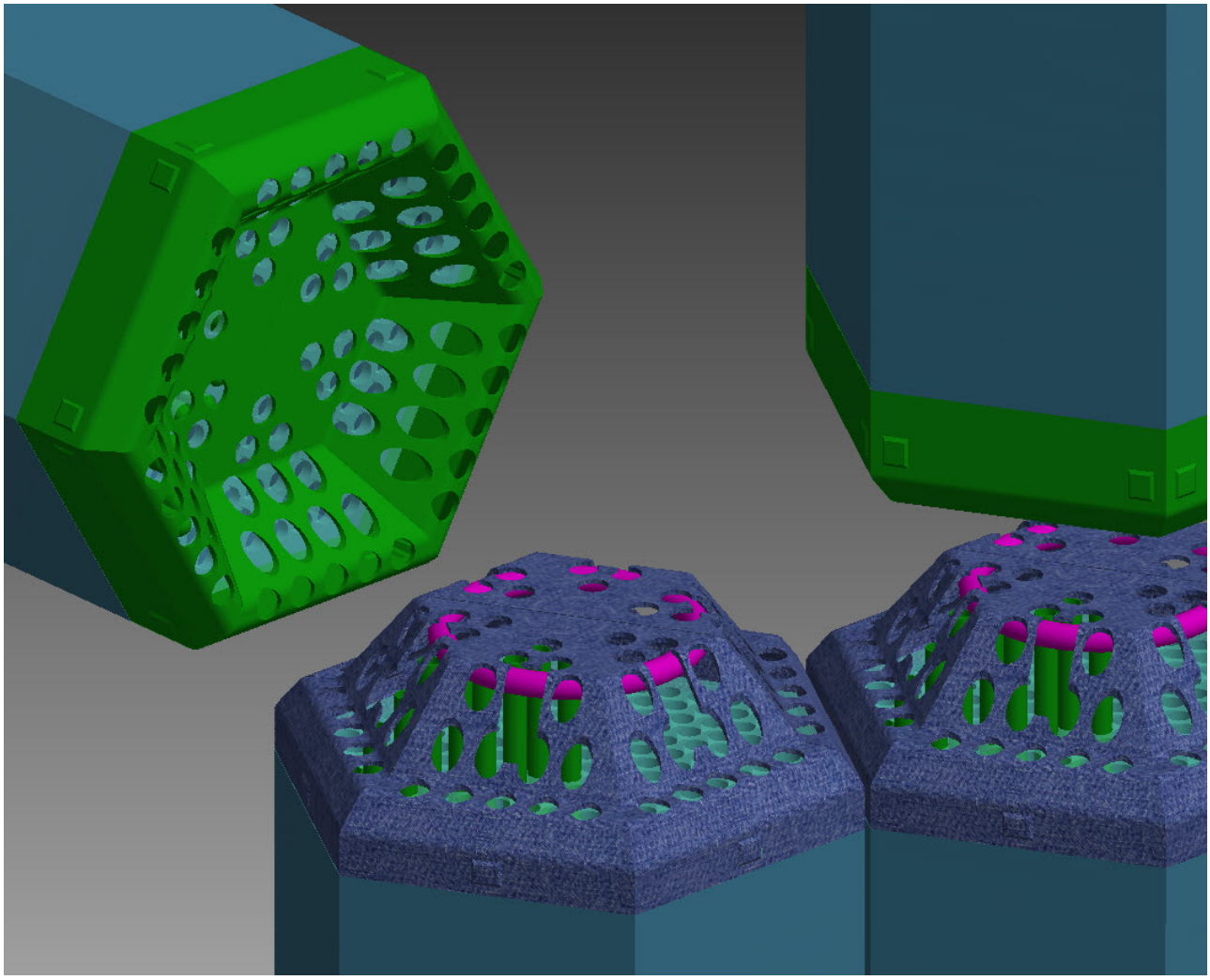

Figure 3. Proposed fuel element configuration. The top cap (blue) has a protruding hexagonal cone, and the bottom cap (green) has a re-entrant hexagonal cone.

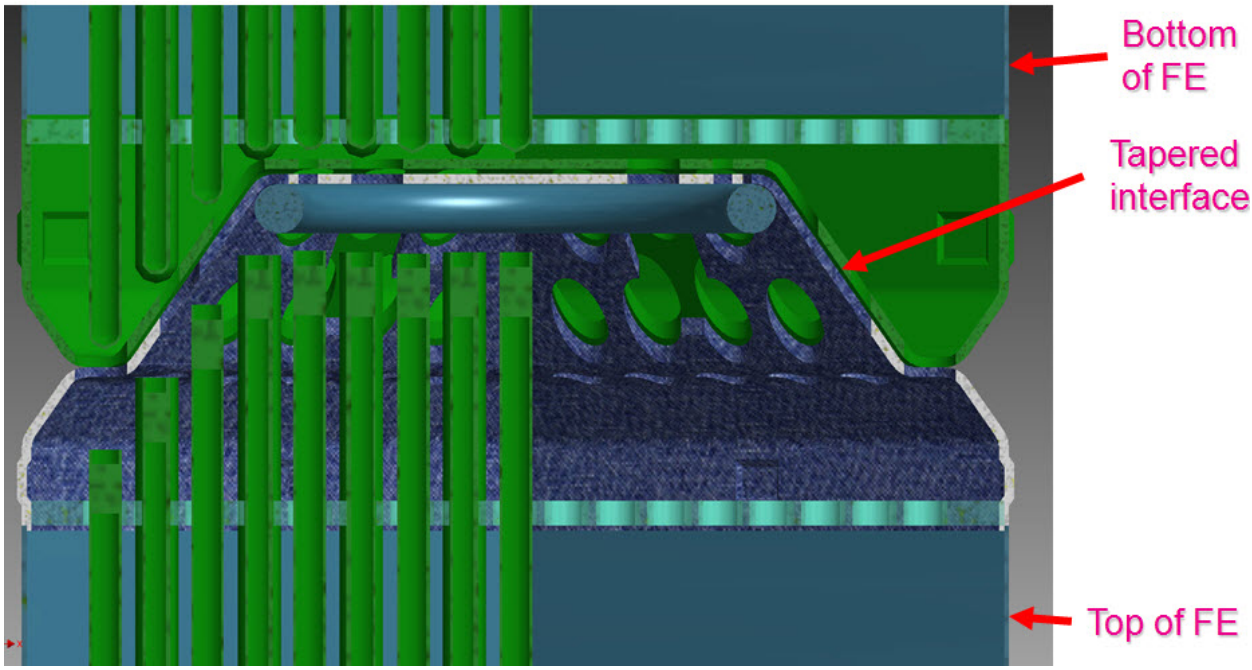

Figure 4. Suggested fuel element interface includes generous tapered hexagonal cone, providing generous self-centering range. Fuel clad tubes follow the taper of the interface, minimizing the volume fraction loss.

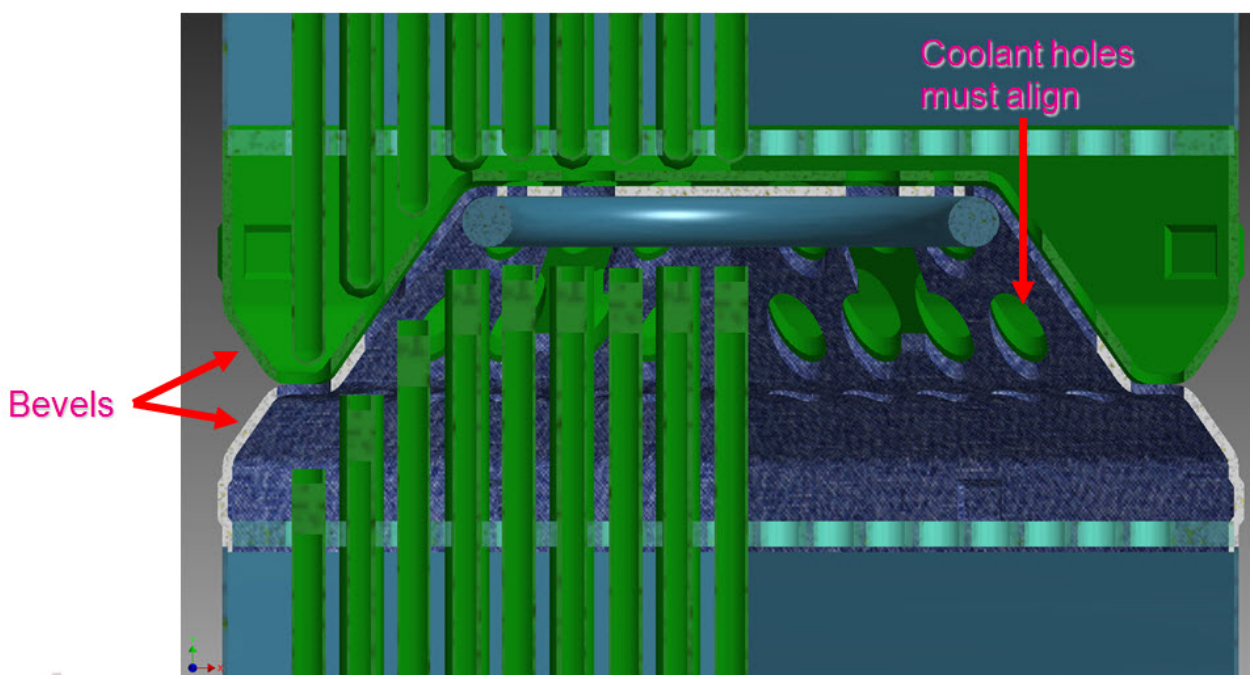

Figure 5. Fuel elements have generous bevels at edges to maximize self-centering and minimize snagging. Adequate passages are provided for coolant flow.

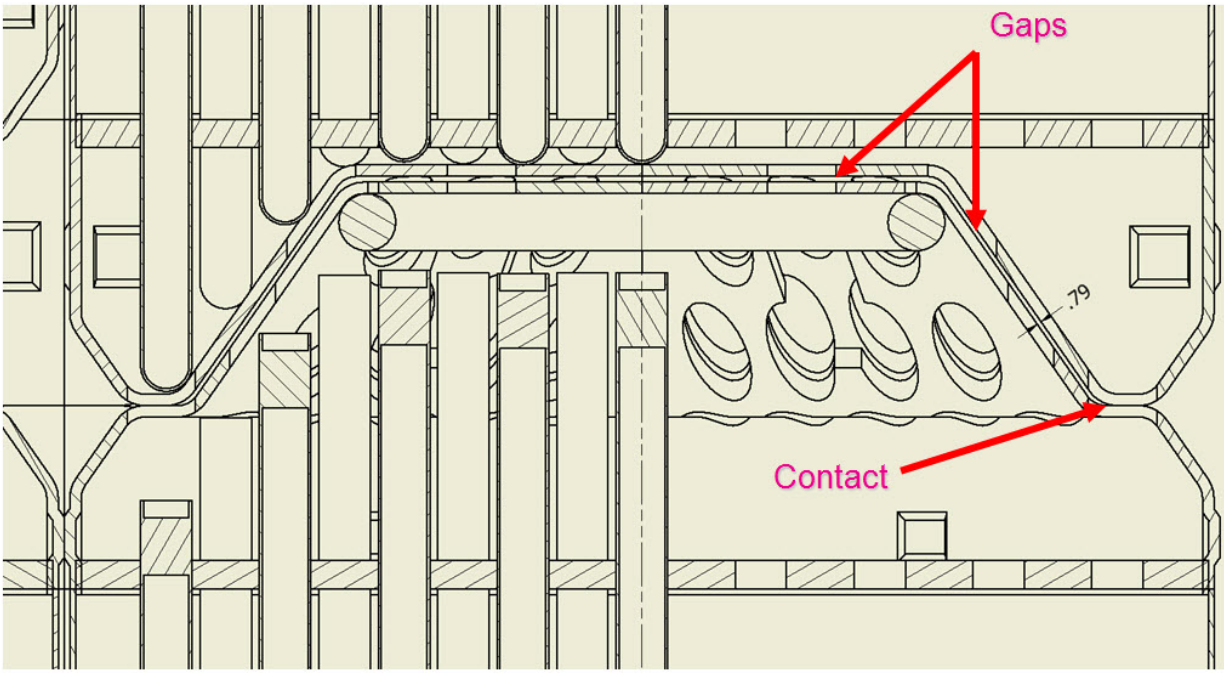

Figure 6. In order to maximize stack stability, fuel emenents touch at the broadest horizontal surface, not on tapers. Contact at horizontal surfaces is less likely to wedge and inadvertenly jam two elements together.

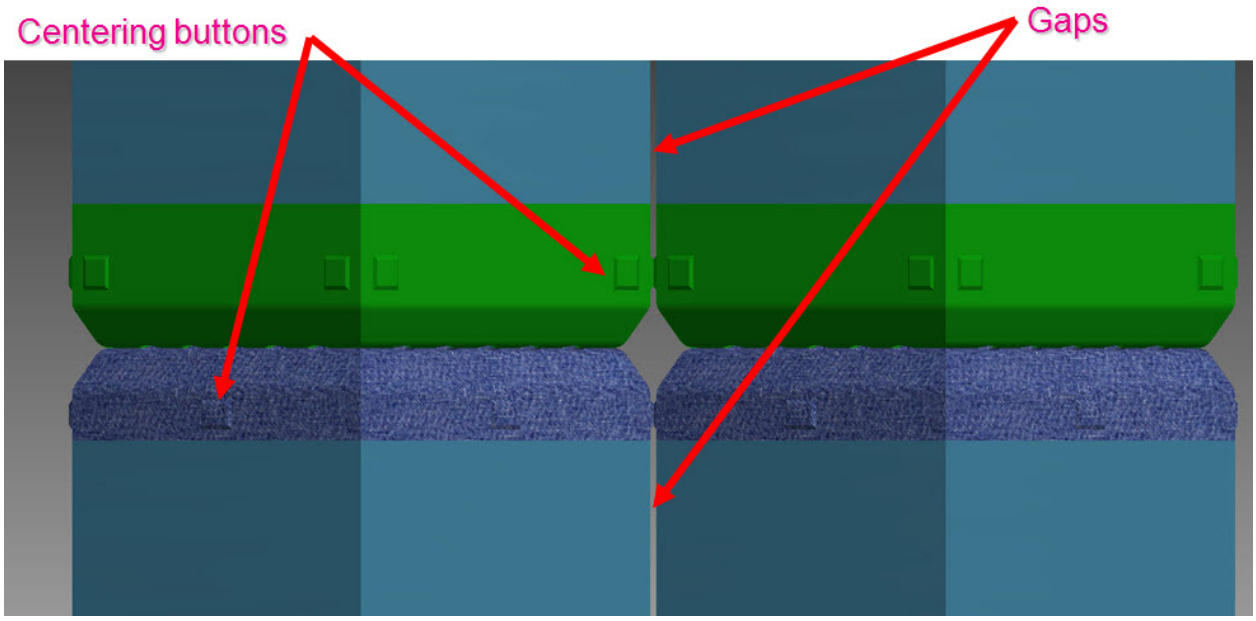

Figure 7. In order to consistently remove fuel elements from the core, it will be necessary to have a finite gap between any two ajacent emements. Centering buttons maintain consistent gaps between elements, and provide clearance after a very short lift distance.

Fuel Element Gripper

Suggest fuel handling gripper with three jaws. A reinforcing ring in the top of the fuel element provides strength and robust performance over the life of the FE. A central rod actuates 3 jaws equally. The actuator is placed above the sodium surface. The gripper is smaller than the footprint of a FE, thus allowing it to reach past a course of FE to lift a FE from a lower course.

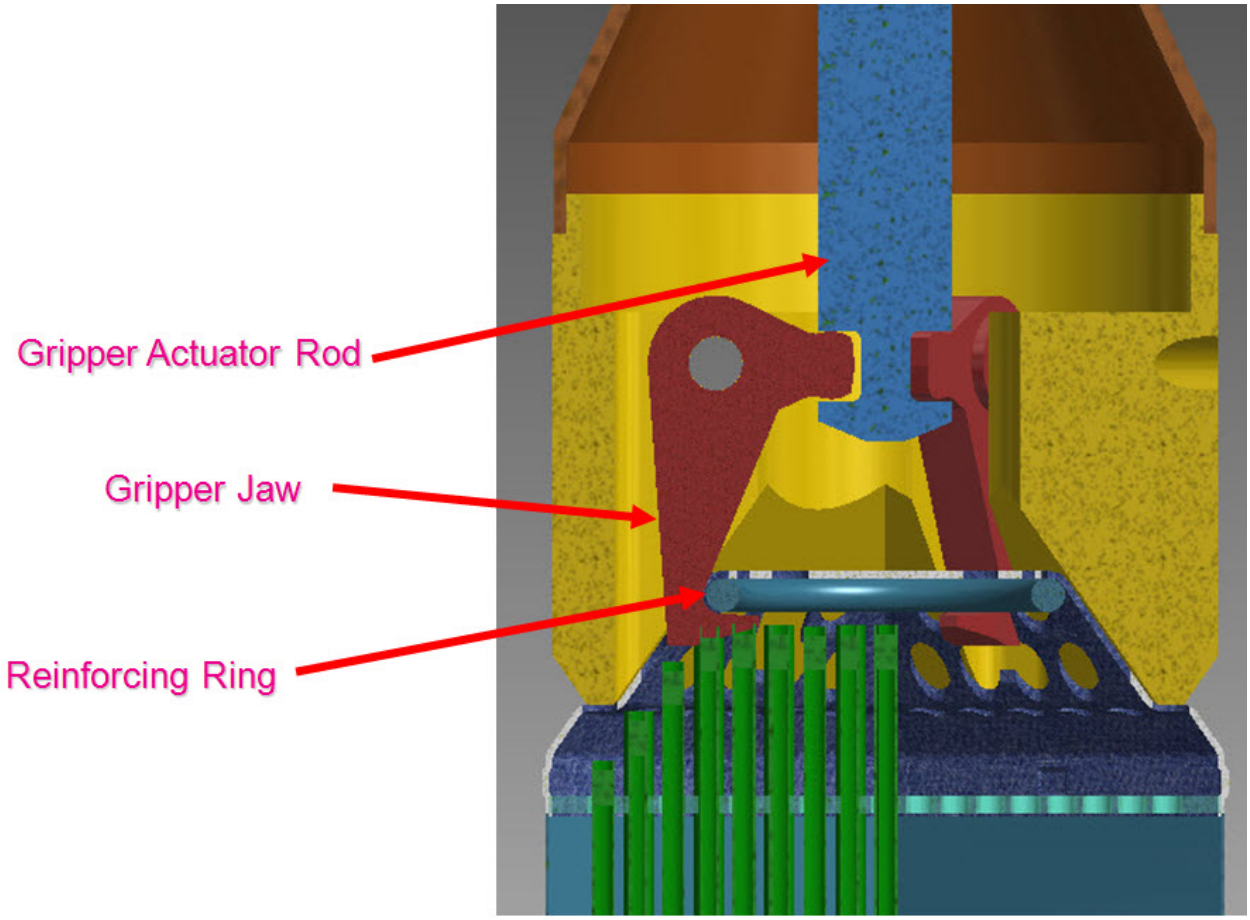

Figure 8. Fuel gripper shown interfacing with fuel element. A robust reinforcing ring is placed in the top of the fuel element to distribute gripper forces and provide adequate wear surfaces for the life of the fuel element.

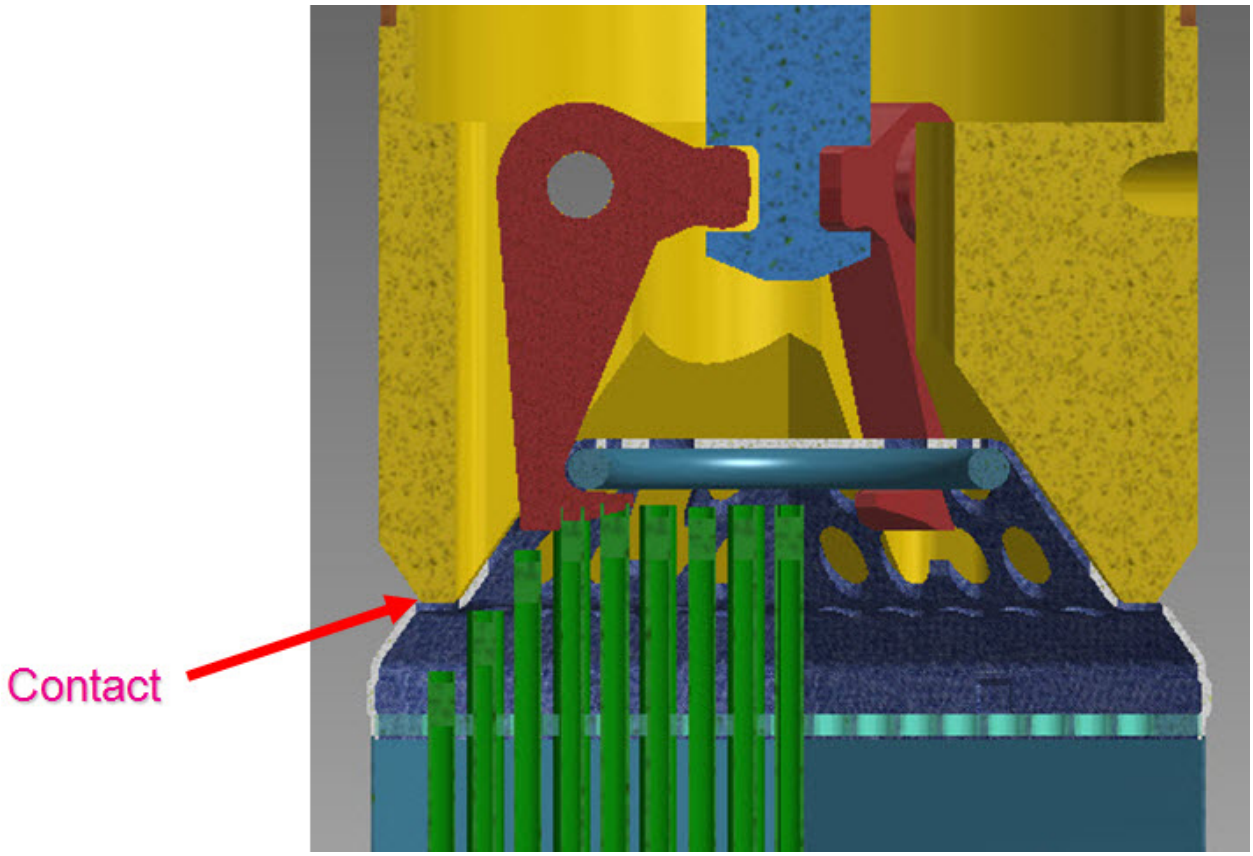

Figure 9. Gripper contacts element at horizontal surface, providing maximum control. Gripper can reach a fuel element on the lowest course without removing neighboring elements.

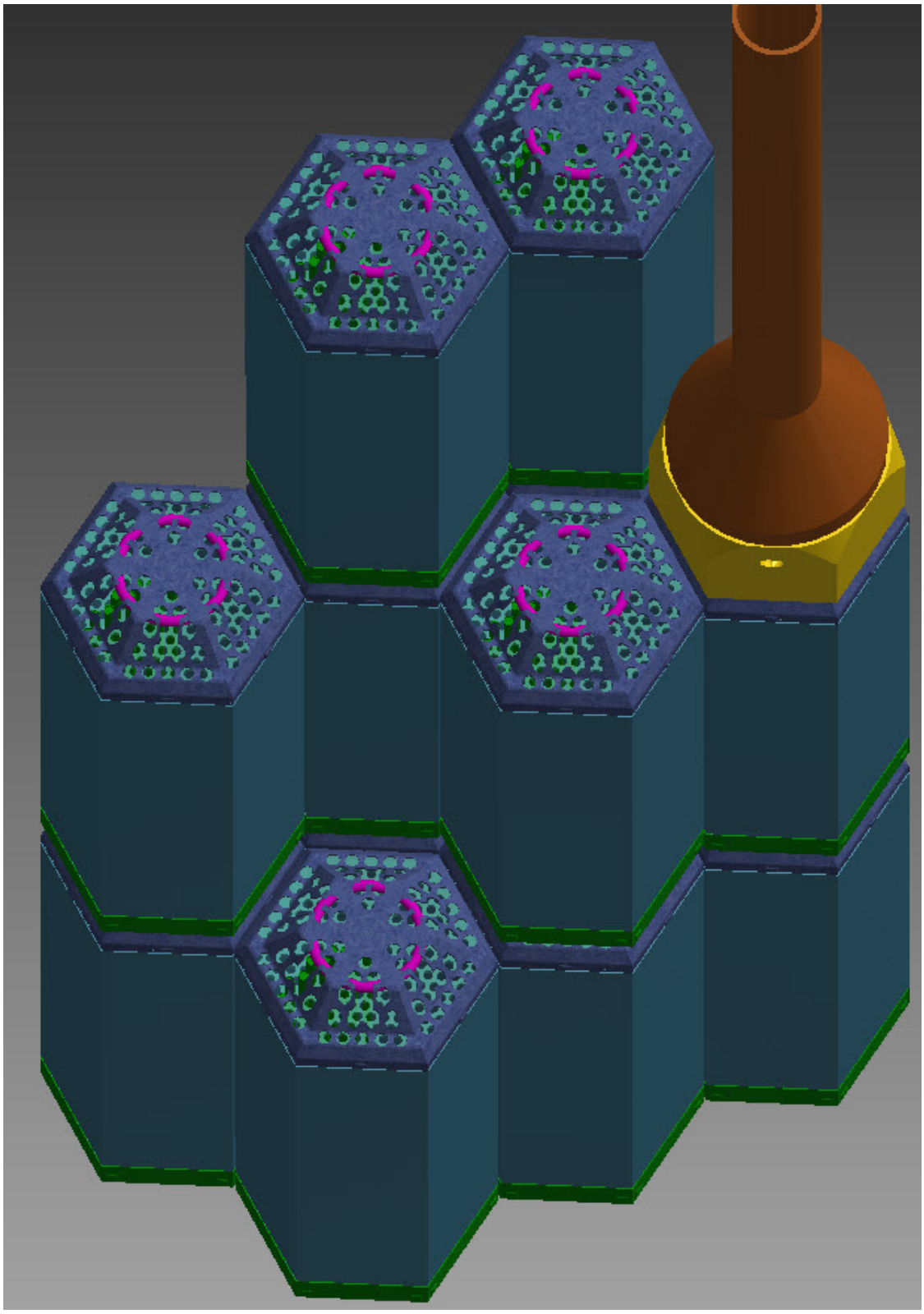

Figure 10. Stacked fuel elements, representing a portion of a core. The gripper is shown attached to one element.

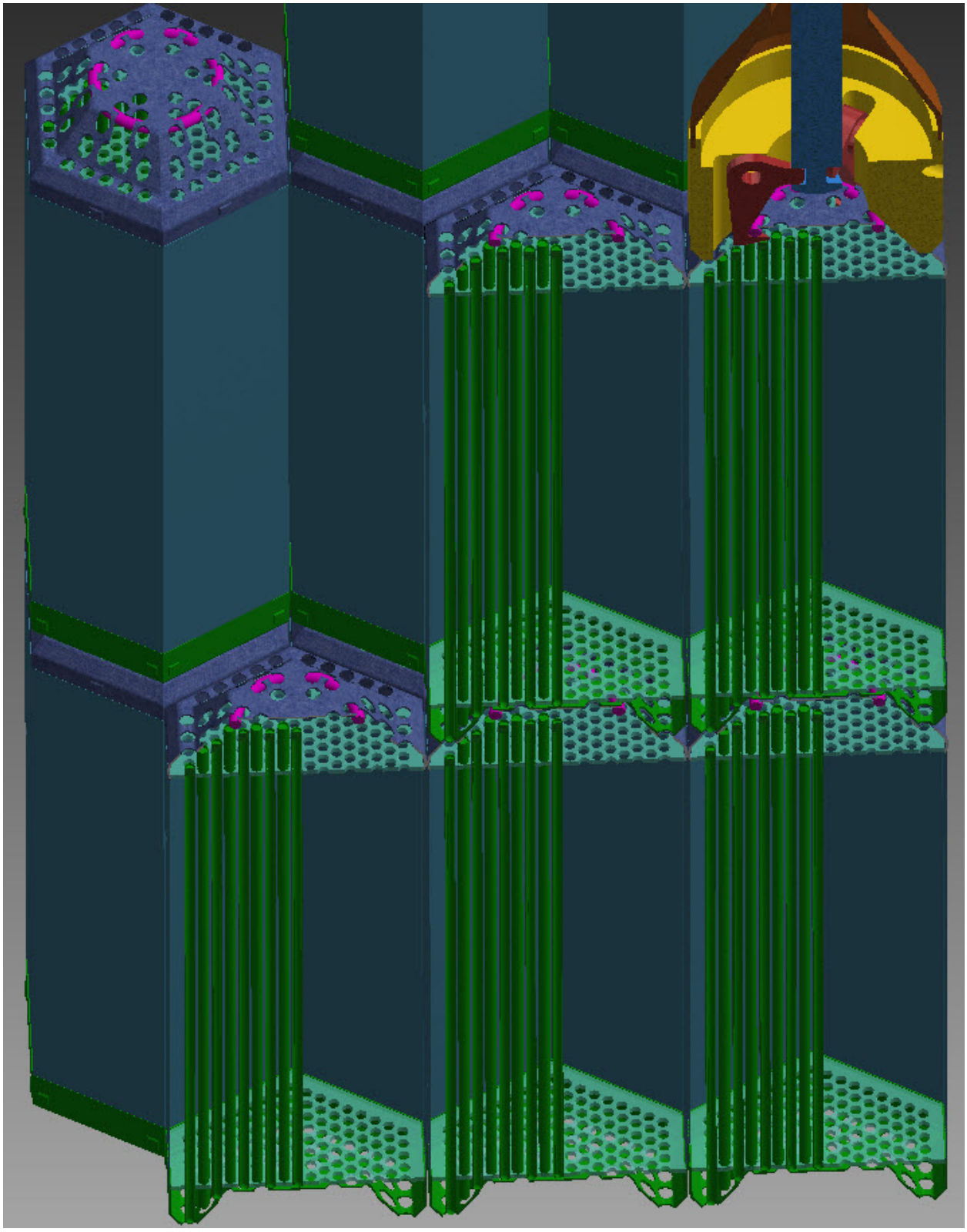

Figure 11. Section view through a stack of fuel elements. Gripper is shown at upper right.

Additional Considerations

The 3D B&B concept dramatically increases the quantity of fuel elements in the core, and effectively managing fuel burn / DPA will require a significant number of fuel moves. Reducing the quantity of fuel elements in the core will reduce the down time associated with fuel shuffling, improving economic viability.

Increasing the plan area of the fuel element will reduce the quantity of FEs. Doubling the width of the FE reduces the quantity of FE by 75 %. Rotating the FE about a vertical axis in addition to 3-D shuffling provides additional means to maintain uniform burn-up and DPA.

Increasing the height of the FE while maintaining core height will reduce the quantity of fuel elements and associated shuffle time. A fuel element that is half of the core height might sustain consistent burn-up after an equal amount of time in upper and lower positions.

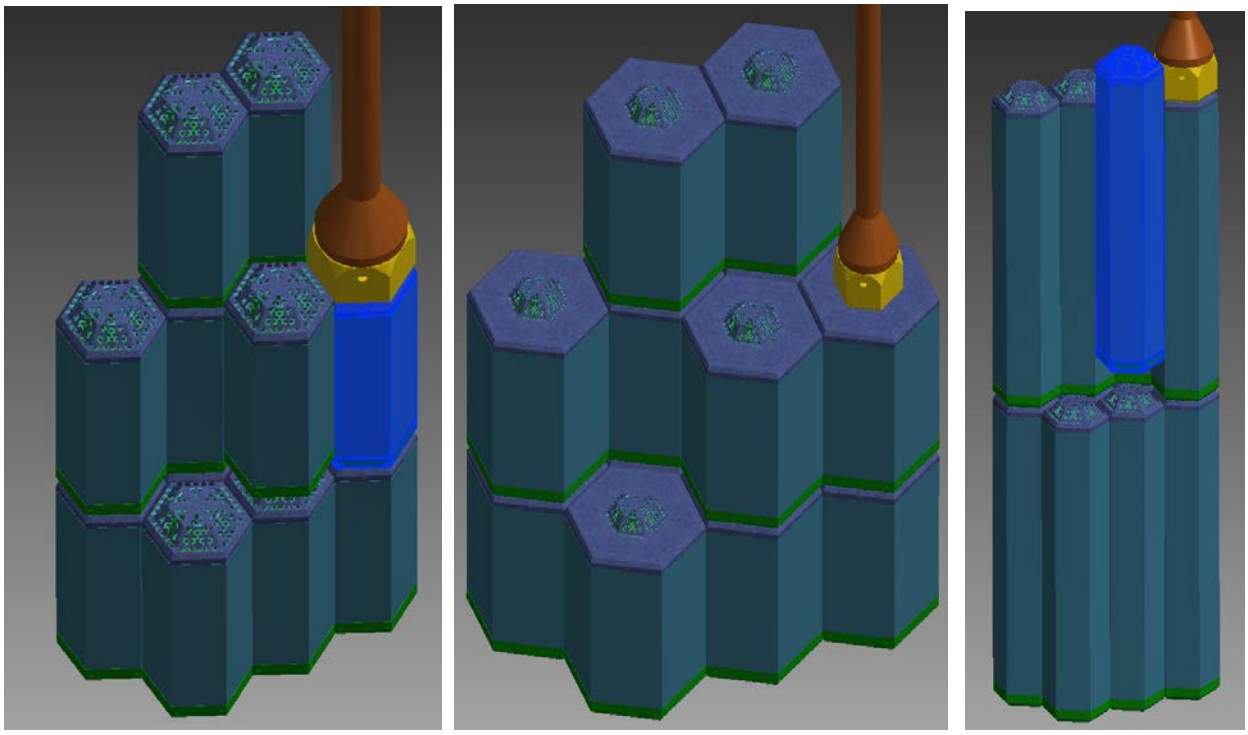

Figure 12. Standard, double-wide (twice as wide), and tall (twice as tall) fuel elements.

Conclusions

Preliminary review indicates that adequate mechanical engineering solutions exist to allow implementation of the 3D Shuffle Breed-and-Burn strategy, including:

- Structure of fuel element with high fuel volume fraction.
- Stable stacking of FE within the core.
- Tolerant placement of FE by fuel handling machine in liquid sodium environment.
- Robust gripping / handling of FE.

Ideas for Consideration

- Fuel elements should be free stacking, without axial joining connections. Any latching mechanism is likely to create a significant volume penalty and introduce a reliability weakness. An external guide tube or tube frame will introduces significant non-fuel volume and tolerance issues. A machine to re-shuffle fuel super-assemblies is an additional complexity. Re-shuffling fuel super-assembly complicates logistics of shuffle operations. Individual fuel elements appear to offer a simpler overall implementation.
- The fuel handling machine should be able to reach lowest course of fuel elements in core without disturbing neighboring FE.
- "Double-wide" fuel elements reduce the number of FE moves by 75%. May interfere with placement of control rods.
- "Half-height" fuel elements reduce the number of FE moves by 50%, provide uniform burn-up.
- Finite gaps will be required between adjacent fuel elements to accommodate part variation and component swelling. These gaps should be included in reactivity calculations.
- Will need an operational strategy to know/guarantee that a second FE is not stuck to the bottom of a FE that is being lifted from the core. Such a "hitch-hiker" could subsequently fall and become a retrieval problem within the vessel. Perhaps a deliberate lateral move as the FE has just cleared the top of the adjacent course could verify the absence of hitch-hikers.

**** End of File ****

Appendix H

A Pebble Based Breed & Burn Reactor Capable of 3-D Shuffling

David Frazer, Priyanka Gaurav, Phil Gorman, Kelly Rowland, Daniel Wooten

University of California Nuclear Engineering Department

Berkeley, CA, 94720

NE-265 Project Report (partial) to Ehud Greenspan

December 2013

1. Introduction

This appendix details the technical issues behind the pebble-based ordered bed design with 3-D shuffling. Section 2 details the issues pertaining to the materials performance, while Section 3 details the thermal hydraulic characteristics of the design. Section 4 concludes this study.

The pebbles were arranged into hexagonal assemblies using a hexagonal close-packed scheme. The fresh fuel pebbles consisted of metallic depleted uranium (DU) with 6 wt% to inhibit swelling, clad with HT-9 steel. Although typical rod-type fuel has a sodium bond which is pushed out into the coolant, it was assumed that the fuel portion would be porous in order to provide space for the fission gases and for swelling.

1.1. Reference core description

The core that was taken as a starting reference point is a 2750 MW_{th}/1100 MW_e SFR B&B reactor, obtained from [1]. It uses metallic DU-6wt%Zr fuel in a pin configuration, with HT9 as the cladding material. The design is summarized below.

Table 1.1. Summary of key parameters from the reference B&B core.

Parameter	Value
Thermal power	2750 [MW]
Fuel smear density	75%
Core diameter	4.0 [m]
Active core height	2.0 [m]
Coolant inlet/outlet temperature	355/510 [°C]
Radial fuel batches	16
Assembly type	Hexagonal
# of active fuel assemblies	336
# of control assemblies	12
Assembly pitch	23.25 [cm]
Duct wall thickness	4.00 [mm]
Inter-assembly gap	4.50 [mm]

During the project, it was noted that there was a bug within the ADOPT code [6] that caused the intra-assembly geometry to be nonphysical. Since the focus on this project is to use pebbles instead of rods, the intra-assembly geometry was discarded anyway. However, the results for each of the cases were compared against analogous cases using the volume fractions from the reference case, which are shown in Table 1.2.

Table 1.2. Volume fraction summary for the reference core.

Component	Assembly unit cell volume fractions	Full-core volume fractions
Fuel	44.95%	43.40%
Cladding (including wire)	8.95%	8.29%
Duct	6.63%	6.63%

Inter-assembly coolant	3.83%	3.83%
Active coolant	20.30%	19.60%
Bond	14.98%	14.47%
ARC expansion volume (void)	0.69%	0.69%
Control assembly internals	0%	3.09%

1.2. Description of the Pebble Bed Core

Many features of the reference core were maintained for the pebble bed core, particularly regarding the material specification for each component and the core-wide geometry. The number of fuel assemblies and control assemblies was kept constant. Additionally, the assemblies were hexagonal. The core size was variable, although the core diameter was kept close to the reference diameter. As the pebble size was changed, the packing factor formed a sawtooth function based off of the assembly pitch (and, therefore, the core diameter). Therefore, the diameter was allowed to vary such that the packing factor was at (or nearly at) a local peak for a given pebble size.

However, the geometry within the assemblies was completely different from the reference design. The fuel was shaped into pebbles, with a metallic core wrapped in an HT9 shell. Pebbles were preferred over rods for this project due to the better ability of spheres to distribute stresses. For conservatism, it was assumed that the metallic fuel kernel was "spongey" (i.e. voids were distributed evenly among the fuel). The pebbles were organized into an ordered lattice: either a close packed lattice (HCP) or a simple stacked lattice (SC). Any extra passive safety systems (such as the ARC system [1]) were moved to the control assemblies.

2. Materials Analysis

2.1. Metal Fuel

It was desired to investigate how the fuel material properties changed under irradiation. The main issues that are of concern due to irradiation are the swelling of the fuel and the production of fission products especially the fission gas build up build up. The swelling and buildup of fission gas products will induce a stress in the cladding of the fuel. In this core design the cladding was chosen to be HT-9, a ferretic/martensitic material. Most metallic fuel is not fully dense when loaded in a reactor to allow volume for the swelling of the fuel under irradiation. This initial void space reduces the Fuel Clad Mechanical Interactions (FCMI) by allowing the fuel to initially swell into the void space, reducing stress on the cladding material [2, 3]. Figure 2.1 which shows the swelling of a Zr10% U alloy fuel vs. burnup, buildup of internal pressure due to fission gases vs. burnup and FCMI vs. burnup for different smear densities of fuel.

Figure 2.1 shows that the swelling of the fuel is from three main parts: solid fission products, gas bubbles, and open pore. The solid fission products are from when fission occurs and a uranium atom splits into two or three atoms and releases energy. Those product atoms take more space than the single uranium atom, causing the fuel to swell. From Figure 2.1 it appears that the solid fission product swelling rate is linear with burnup at 1.5% dv/v per 1% burnup. The

other two swelling mechanisms are gas bubbles and open pore. During fission, gas atoms can be produced that initially start to form gas bubbles in the fuel. As additional burnup of the fuel occurs, the gas bubbles start to connect with each other, forming pathways in the fuel. These pathways allow the gas atoms to escape the fuel and, in modern pin assemblies, collect in a gas plenum at the top of the fuel rod. The escaping gas leaves open pores in the fuel which initially cause swelling but begin to reduce in size because of the swelling from solid fission products, reducing this void volume. There are some gas bubbles that never get large enough or never become part of the pathways that allow the gas to escape in the plenum. These remaining gas bubbles cause the fuel to swell. Experiments conducted on a variety of U, Zr and U, Zr, Pu alloys show that about 80% of the fission gas produced in the fuel escapes and is collected in the gas plenum which is shown in Figure 2.2.

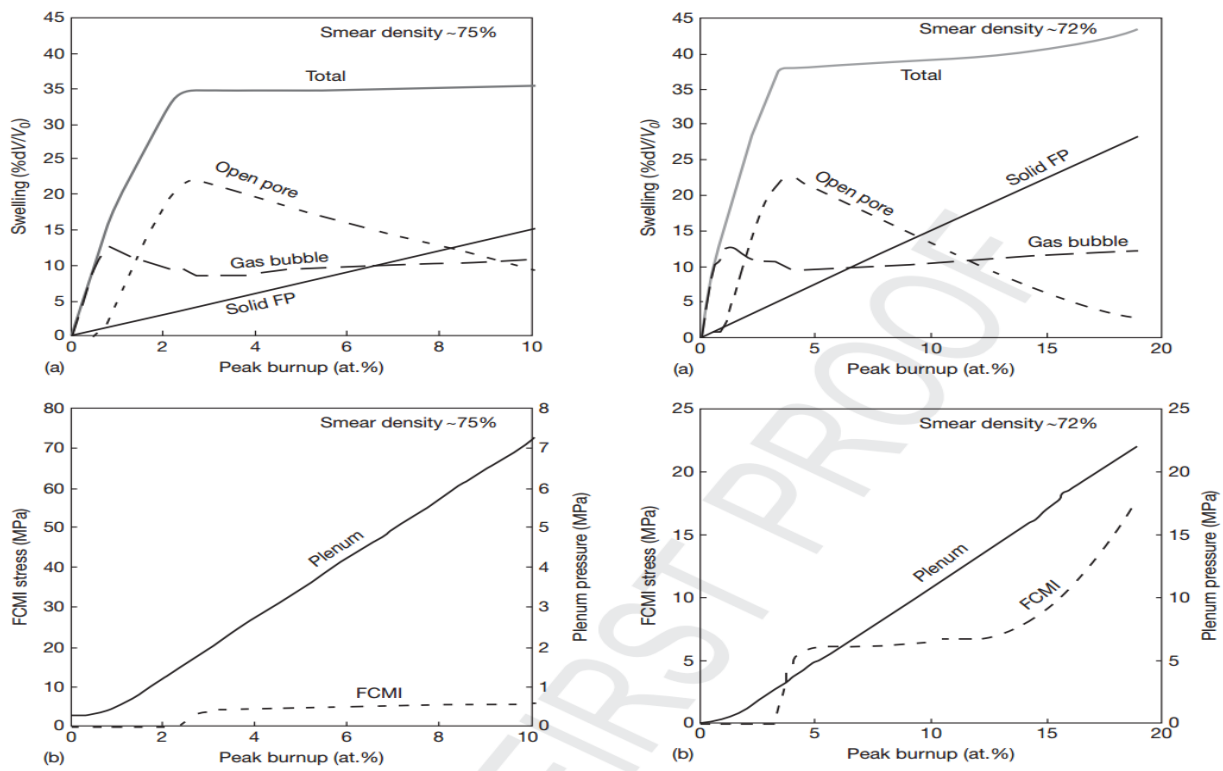

Figure 2.1. Swelling of Zr10% U alloy fuel vs. burnup, buildup of internal pressure due to fission gases vs. burnup and FCMI vs. burnup for different smear densities of fuel [3].

The bottom plots of Figure 2.2 show the FCMI and internal pressure buildup vs. burnup of the cladding. It can be seen that initially, because of the void fraction of the fuel when the fuel swells, it swells into the voids and does not produce a stress on the cladding. However, when that void space is taken up by the swelling of the fuel, a stress on the cladding is produced. The stress on the cladding stays relativity low because fission gas escapes into the plenum and forms voids that allow the fuel to swell into them. It is seen in the lower right hand graph that once all of the open pore voids have been reduced from the swelling of the fuel, the FCMI produce stress in the clad starts to increase rapidly. These processes are significant for this design because a pebble does not have a gas plenum for the fission gases to be collected which means that the gases will have to stay inside the fuel.

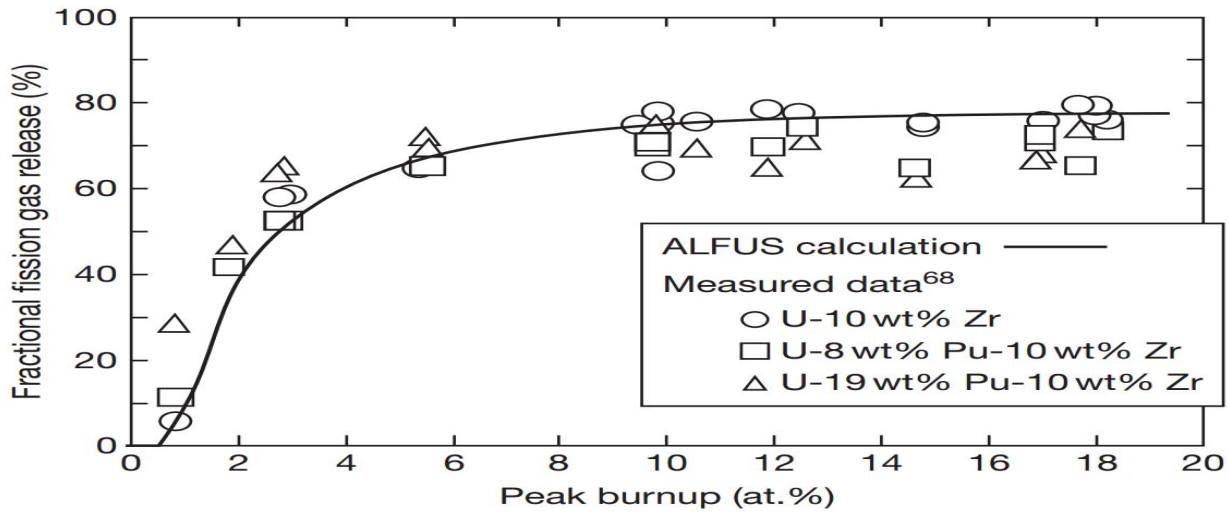

Figure 2.2. Fraction of fission gas release to the plenum vs. burnup for a variety of different fuel alloys [3].

2.2. Fuel Geometry

Since it is believed that the peak burnup and the radial and axial peaking factors can be reduced by having the ability to both axial and radial shuffle the fuel (3-D shuffling), the design uses pebble shaped fuel instead of rod- or pin-type fuel. Having pebble fuel allows for 3-D shuffling by putting the fuel in baskets or sectioned assemblies. The basic shapes and fuel placement are shown on the following page in Figure 2.3. The fuel inside the spherical pebble fuel shape is spread though out the entire inner volume of the pebble, whereas the cylindrical fuel shape has the fuel in the bottom of the pin and has a large space above the fuel for the collection of fission gas products. The spherical shape of the pebble however is stronger and has a lower stress in the cladding material by a factor of two. This would allow the pebble to have higher internal pressures, which would offset some of the challenges of not having a gas plenum for the fission gases produced. Since there is no gas plenum in the pebble, the initial fuel will have to have a lower smear density to provide a volume for the fission gases to collect in.

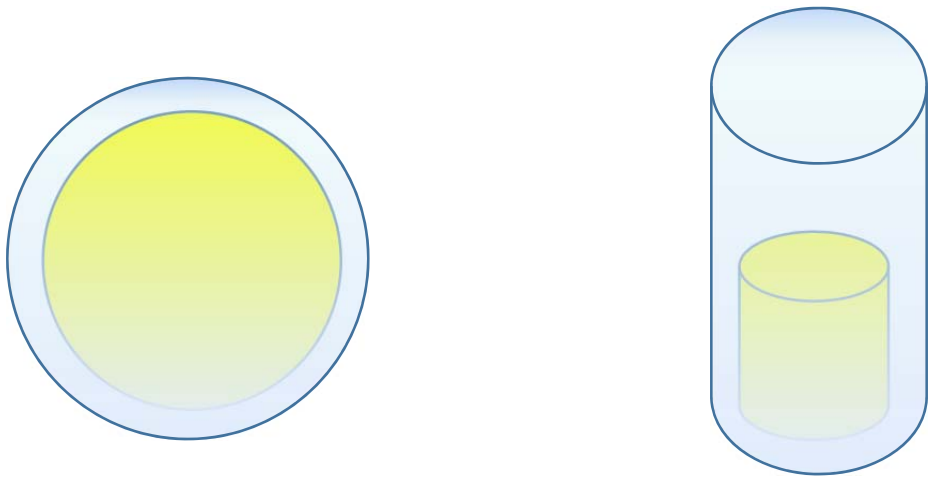

Figure 2.3. Geometry and placement of fuel in a pebble versus a pin.

2.3. Cladding Material

The material chosen for the cladding and in-core components of this reactor design is HT-9. HT-9 is a high-Cr (~12%) ferritic/martensitic steel that has gained popularity as the material of choice for Generation IV reactors [4,5]. The increased Cr content of the steel provides superb resistance to corrosion. The crystal structure of this steel is BCC [5]. A nominal composition of HT-9 is shown below in Table 2.1.

Table 2.1. Composition of HT-9 in w% [5].

Element	Weight Percent
C	0.20
Si	0.21
Mn	0.50
P	0.008
S	0.003
Cr	11.800
Mo	1.030
Ni	0.510
V	0.330
W	0.240
N	0.006
Al	0.030
Ti	< 0.010
Fe	Bal.

Many B&B reactors require that the cladding and in-core components experience greater than 300 dpa, with most in the range of roughly 550 dpa [6,7]. This amount of damage has caused

many problems because the materials used lose their structural integrity and ductility and swell under irradiation [8-12]. Due to the microstructure of HT-9, the material has a very low swelling rate and appears to be stable up to hundreds of dpa [13-16]. These properties of HT-9 make it an excellent material for use in fast reactors. Some additional properties of HT-9 are shown in Table 2.2.

Table 2.2. Physical and Thermal Properties of HT-9 [17].

Physical and Thermal Properties of HT-9	**Property Value**
Thermal Conductivity	28 W/m*K
Modulus of Elasticity	160 GPa
Poisson's Ratio	0.33
Coefficient of Thermal Expansion	$12.5 * 10^{-6}$ per ºC

2.3.1. Cladding Stress

Since there is no gas plenum in the spherical geometry, all gaseous fission products produced will have to be contained in the pebble unless the fuel pebbles are to be vented. Since all gaseous fission products have to remain in the sphere, the smear density will have to be reduced to allow room for the gaseous fission products. The thick sphere model, shown in Equation 2.1, was used to calculate the stress in the cladding, while the Redlich–Kwong real gas law was used to calculate the internal pressures of the pebble. The Redlich—Kwong real gas law equation is shown below in Equation 2.2. Equations 2.3 and 2.4, which follow, are used to calculate the constants a and b in the Redlich—Kwong real gas law.

$$\sigma = \frac{PR_i^3}{\left(2R_i^3(R_o^3 - R_i^3)\right)}(R_o^3 + 2R_i^3) \qquad \text{Equation 2.1}$$

$$RT = P(V_m - b) + \frac{a}{V_m(V_m + b)T^{\frac{1}{2}}}(V_m - b) \qquad \text{Equation 2.2}$$

$$a = 0.4275\frac{R^2T_c^{2.5}}{P_c} \qquad \text{Equation 2.3}$$

$$b = 0.0867\frac{RT_c}{P_c} \qquad \text{Equation 2.4}$$

In Equation 2.1, P is the internal pressure of the sphere, R_0 is the outer radius of the hollow sphere, and R_i is the inner radius of the hollow sphere. In Equation 2.2, R is the gas constant, T is the temperature, P is the pressure, V_m is the molar volume of the gas, and a and b are constants. In Equations 2.3 and 2.4, R is the gas constant, T_c is the critical temperature of the

gas, and P_c is the critical pressure of the gas. Since xenon is the main component of the fission gas that is produced, the values used for the critical pressure and temperature are those of xenon.

The other assumptions made in the analysis of the stress in the pebbles was 1.5% dv/v per 1% burnup from solid fission products, 80% of fission gas escapes to void, the other 20% of gas forms bubbles causing the fuel to swell, and the pebble is a perfect hollow spherical shape [3]. These assumptions are consistent with Section 2.1. From References [2,3] it was assumed that the other 20% of fission gas would form bubbles in the material and cause a 13% volume increase in the fuel. The amount of fission gas that was produced was calculated using the Equation 2.5, shown as function of fissions per metal atom (FIMA).

$$N_{gas} = V_{fuel}\rho(\%U)\left(\frac{6.022 * 10^{23}}{238}\right)(FIMA).26_{gasatoms/fission} \qquad \text{Equation 2.5}$$

In Equation 2.5, %U is the percentage of the fuel that is uranium, ρ is the overall density of the fuel, and V_{fuel} is the volume of fuel which is the volume made available for fuel multiplied by the smear density of the fuel.

2.3.2.Material Degradation

There are many possible ways to evaluate the degradation of the materials while in service. In order to determine if the stresses on the cladding were acceptable, it was decided to evaluate are the yield stress and tensile strength thermal creep, and irradiation-induced creep and damage.

2.3.2.1. Yield Stress and Tensile Strength

The yield stress and tensile strength of a material are measured by performing a tensile test of the material. In a tensile test, a material is pulled apart until failure of the material. The yield stress of the material is the point at which plastic deformation begins to occur and the tensile strength is when necking of the sample begins to occur. Stress/strain curves from tensile tests performed by Los Alamos National Laboratory are shown on the following page in Figure 2.4.

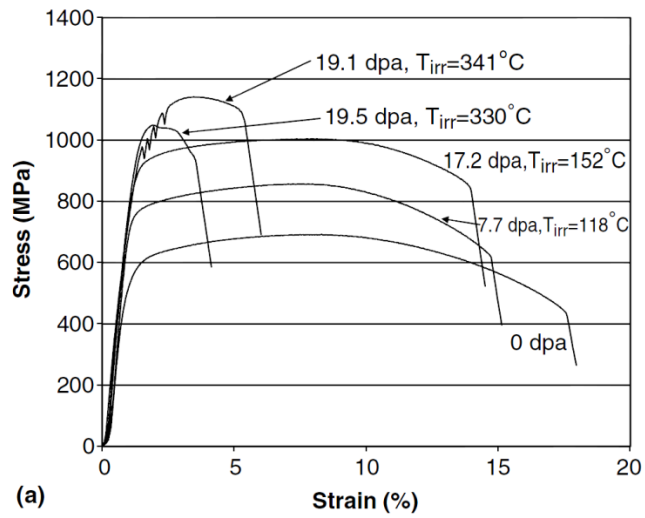

Figure 2.4. Stress/strain curves from tensile tests performed on HT-9 at 400ºC [18].

From the tensile curves shown above, there is an elastic region at the beginning of the test that is linear. The yield stress is found by taking the slope of this region and then offsetting 0.2% and seeing at what stress that line intercepts the stress/strain curve. When this procedure was completed with the data gathered from the tensile tests from [18], it produced the plot shown below in Figure 2.5.

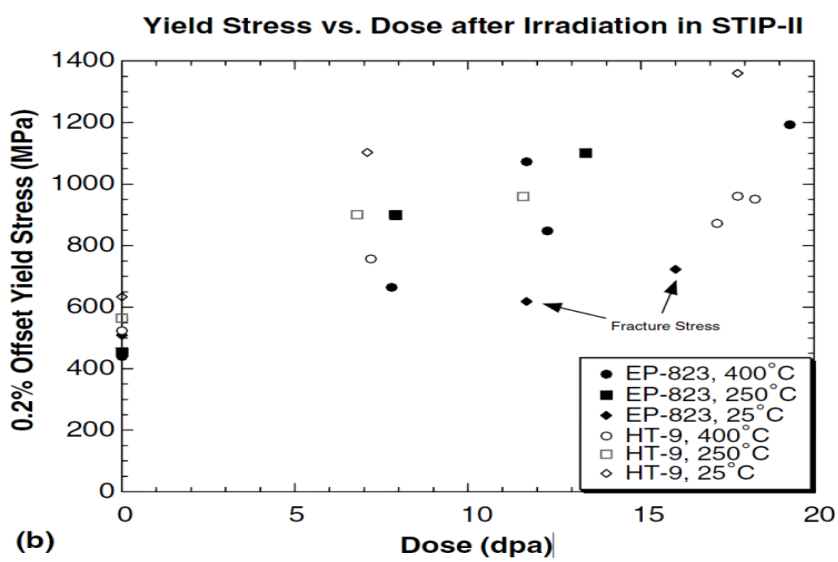

Figure 2.5. Yield stress of HT-9 at variety of temperature and doses [18].

From Reference [19], the maximum allowable stress in the material for cladding or in-core components of a reactor is 2/3 the specified minimum yield stress of the material at room temperature. Taking 25ºC to be room temperature and using the 0 dpa information gives a yield

stress of ~640 MPa. Thus, the allowable stress in the material evaluated from the yield stress would be 426 MPa.

2.3.2.2.Cladding Strain

From Reference [19], the allowable strain in the material during operation is 1% over its lifetime in the core. The two major contributors to strain are irradiation-enhanced creep and thermal creep of the material. Irradiation creep will be examined first. There have been a few studies of the irradiation creep of HT-9 [20,21]. There was a study done at the Fast Flux Test Facility (FFTF) to study the irradiation creep of HT-9 to high dpa under stress. The study manufactured tubes of HT-9 that were sealed and pressurized with helium gas to cause different hoop stress in the material. The tubes were then placed in the FFTF and irradiated up to 208 dpa. In Figure 2.6, the plots of diametral strain vs. hoop stress for a variety of different dpa are shown. The diametral strain is the strain of the diameter of a circle.

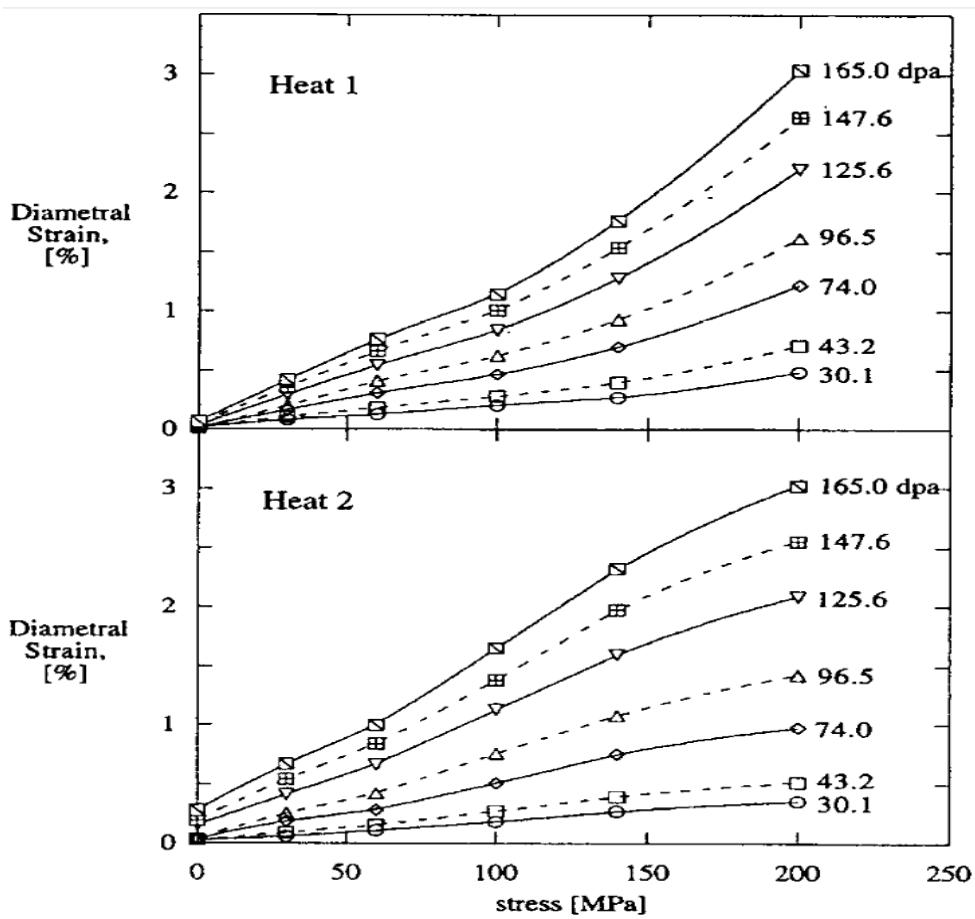

Figure 2.6. Plots of the diametral strain vs. hoop stress for cylinders that were irradiated to a variety of dpa at FFTF on two different heats of HT-9 [2.20].

The irradiation temperature was between 380ºC and 400ºC, which is in the operation temperature of the core. The study also produced Equation 2.6 to predict the strain of a material based on stress in the material and dpa seen by the material.

$$\frac{\varepsilon_{eff}}{\sigma_{eff}[MPa]} = B_0[MPa^{-1}\ dpa^{-1}] + D[MPa^{-1}]S[\frac{\%}{dpa}] \qquad \text{Equation 2.6}$$

In Equation 2.6, ε_{eff} is the effective strain per dpa of material, σ_{eff} is the effective stress in the material, B_0 is the creep compliance, D is the creep-swelling coupling coefficient, and S is the instantaneous swelling rate per dpa. From Reference [20], B_0 has a value of $0.9*10^{-6}$ [$MPa^{-1}dpa^{-1}$], D has a value of $0.51*10^{-2}$ [MPa^{-1}], and S has a value of 0.00595%/dpa. From early analyses, the allowable strain of 0.01 and design constraints limit the material to 300 dpa, and so this was used in the calculation of the allowable stress in cladding. If Equation 2.6 is rearranged to solve for the stress level in the HT-9 and dpa, we arrive at Equation 2.9.

$$\frac{\varepsilon_{eff}}{B_0[MPa^{-1}\ dpa^{-1}] + D[MPa^{-1}]S[\frac{\%}{dpa}]}(dpa) = \sigma_{eff}[MPa] \qquad \text{Equation 2.9}$$

When Equation 2.9 is evaluated with the values mentioned previously, the effective stress in the material can be 106.68 MPa. A plot of the stress allowed in a material vs. dpa for the constraint of 1% strain is shown below in Figure 2.7.

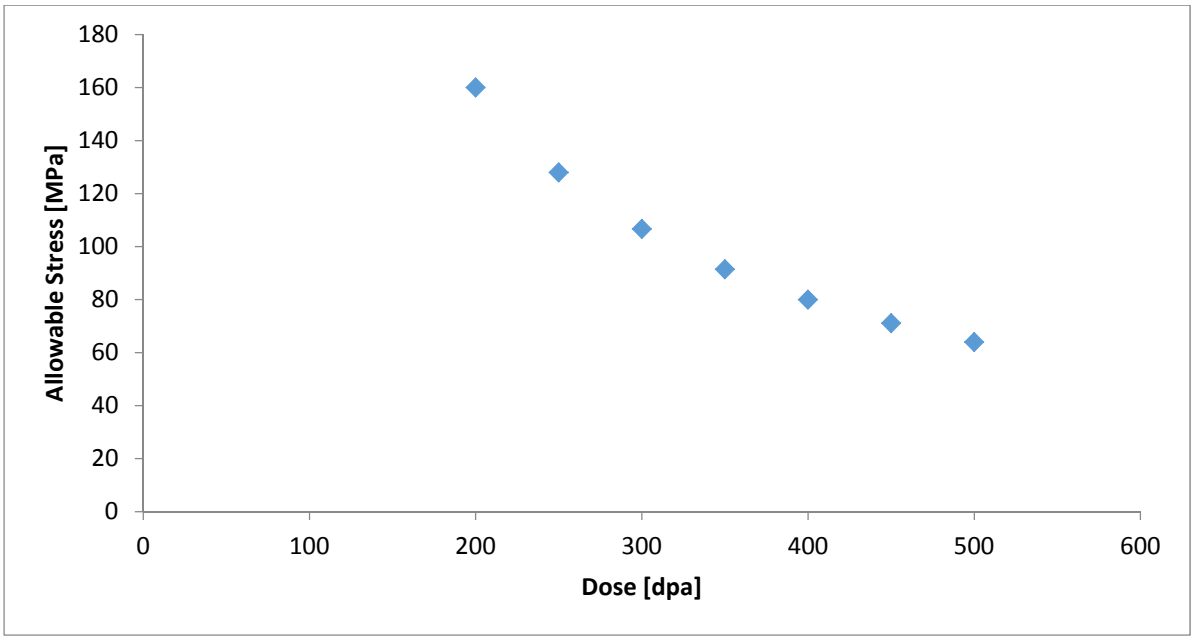

Figure 2.7. Allowable stress vs. dpa for HT-9 limiting the strain in the material to 1%.

The points in plot in Figure 2.7 are from extrapolating the equation given in the report to higher doses than actually studied in the report, so they should be used cautiously. Also, in the study, the irradiation only happened in a small temperature range between 380ºC and 400ºC, which means that data should only be used to evaluate systems in the temperature range and if a system was not in this temperature range then values recorded here would not be representative of the system. For our core since the operation window is 355ºC to 510ºC this evaluation is not comprehensive and these values may not represent what would actually happen in the core; however, due to lack of data on the strain of HT-9 irradiated to high dose under stress this is best representation and prediction of the core possible.

2.3.2.3.Thermal Creep

Since the pebbles spend a lengthy time in the core at elevated temperatures, the thermal creep of the pebbles was evaluated. There have been many studies of the thermal creep of HT-9 for the nuclear community [22-24]. The thermal creep strain was evaluated two different ways: one was the time to rupture and the other examined the steady state creep rate and limiting the creep to 1% [19].

The creep to rupture was a quick evaluation to see the stress limits that would be placed on the clad. Since this is the creep to rupture time, it is the extreme upper limit of the stress allowed in the material. A plot of the creep to rupture times for HT-9 vs. stress in the material is shown below.

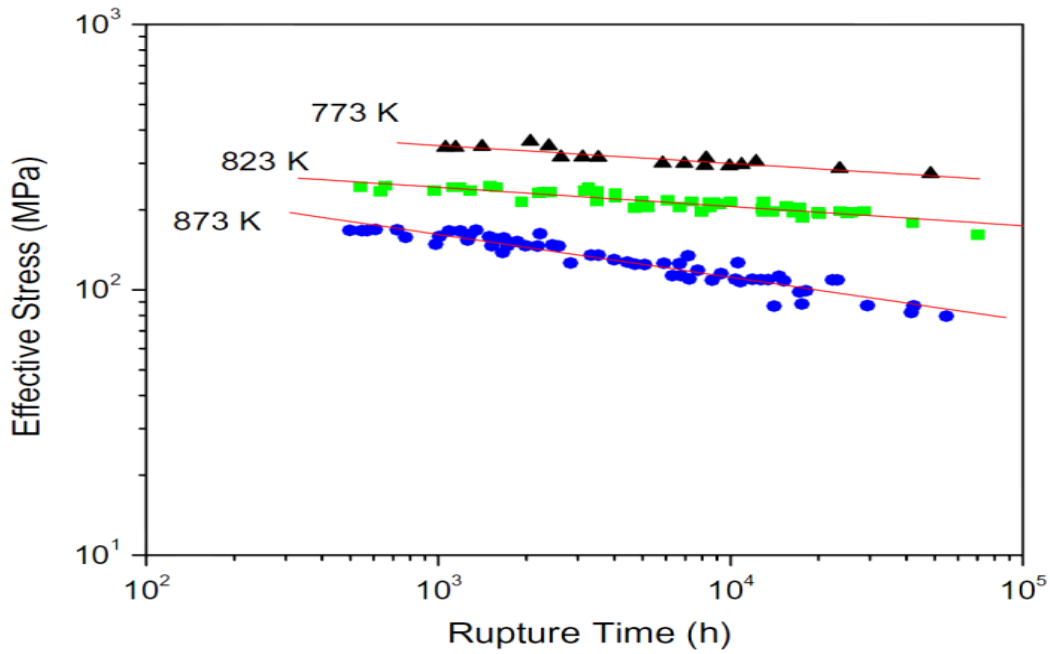

Figure 2.8. Rupture time vs. stress for HT-9 for a variety of temperatures [24].

From the initial neutronics analysis, the core had a cycle length of 700 to 2000 days. Our design had twelve batches in the core, meaning that a pebble would spend 8400 to 24000 days in the core. These two time lengths were used as the time to rupture of the material. The temperature that this analysis was performed at was 510ºC (783 K). The time to rupture equation [24] is stated below as Equation 2.10, where $R_0(T)$ is given by Equation 2.11, $R_1(T)$ is given by Equation 2.12, t_r is time to rupture in hours, and σ_r is rupture stress in MPa. In both Equations 2.11 and 2.12, T is the temperature in Kelvin.

$$\mathrm{Log}_{10}\,\sigma_r = R_0\,(T) + R_1\,(T)\log_{10} t_r \qquad \text{Equation 2.10}$$

$$R_0(T) = 32.65 - \frac{49039}{T} + \frac{2004800}{T^2} \qquad \text{Equation 2.11}$$

$$R_1(T) = -12.97 + \frac{20373}{T} - \frac{8041900}{T^2} \qquad \text{Equation 2.12}$$

Evaluating for the two different cycle lengths at 783 K gave stress of 230MPa for the 700 day cycle and 213 MPa for 2000 day cycle.

Next, the steady state creep rates were evaluated. Figure 2.9, below shows the steady state creep rates vs. stress for variety of temperatures.

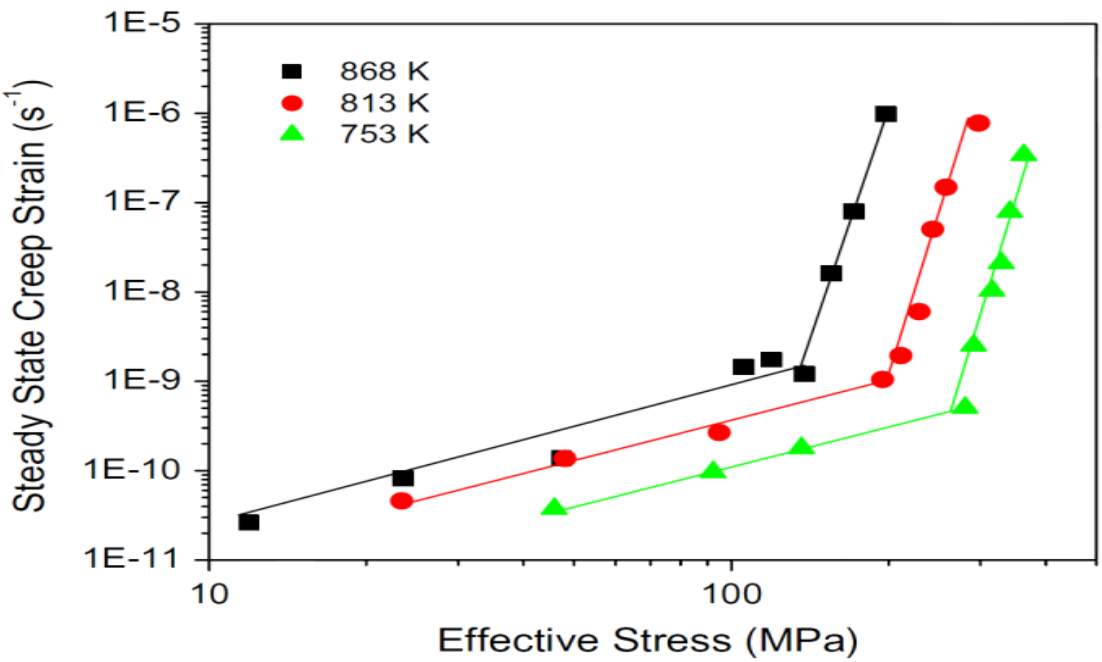

Figure 2.9. Steady state creep rate vs. effective stress for HT-9 at an assortment of temperatures [24].

The 1% limit is placed on the system which gives strain rates of $1.4*10^{-11}$ s^{-1} for the 700 day cycle and $5*10^{-12}$ s^{-1} for the 2000 day cycle. Using Equation 2.13 given in Reference [24] can provide the allowable stress in the material.

$$\log_{10} \varepsilon\ [S^{-1}] = S(T) + 1.5 \log_{10} \sigma\ [MPa] \qquad \text{Equation 2.13}$$

$$S(T) = -5.58 - \frac{5562.28}{T} \qquad \text{Equation 2.14}$$

In Equation 2.13, ε is the strain rate, S(T) is given by Equation 2.15 where T is in K, and σ is the stress in the material. The evaluation of the material was performed at an average temperature of the core which is 432.5ºC (705.5 K), resulting in stresses of 53.13 MPa for the 700 day cycle and 26.74 MPa for the 2000 day cycle length. These are unacceptably low values. Since most of the fission products are produced in the last 1/3 of the pebble life in the core, it was decided to calculate the strain for groups of similar conditions and add it together. Approximate values for a typical pebble are shown in Table 2.4.

Table 2.4. Evaluation of the steady-state creep strain of the HT-9 pebbles.

FIMA	# of cycles (700 day cycle length)	Temperature ºC
0.006	6	432.5

0.03	3	432.5
0.09	1	510
0.13	1	510
0.20	1	510

Table 2.4 shows the more in-depth and realistic of the life of the pebble. In Table 2.4 it is seen that the first 6 cycles are evaluated at 432.5ºC and 0.006 FIMA, the next 3 cycles are at 432.5ºC but 0.03 FIMA, and then the last 3 cycles are all evaluated at 510ºC at 0.09, 0.13, and 0.20 FIMA, respectively. To find the optimum smear density and clad thickness, a selection of clad thicknesses and smear densities were evaluated. The results can be seen on the following page in Figure 2.11. The % is the percentage of the radius of the pebble that is clad. This works because it is the stress in the material, which is independent of the pebble radius. Thus, all pebbles with 10% of radius being cladding and the fuel having a smear density of 30% have the same stress in the material. From the plot, it can be seen that pebbles cannot have a very high smear density; this will reduce the amount of fuel that can be loaded into the reactor and may cause the reactor to not reach criticality.

The plot in Figure 2.10 was used to produce Table 2.5, which shows the largest smear density of fuel for the different % of the radius that is clad.

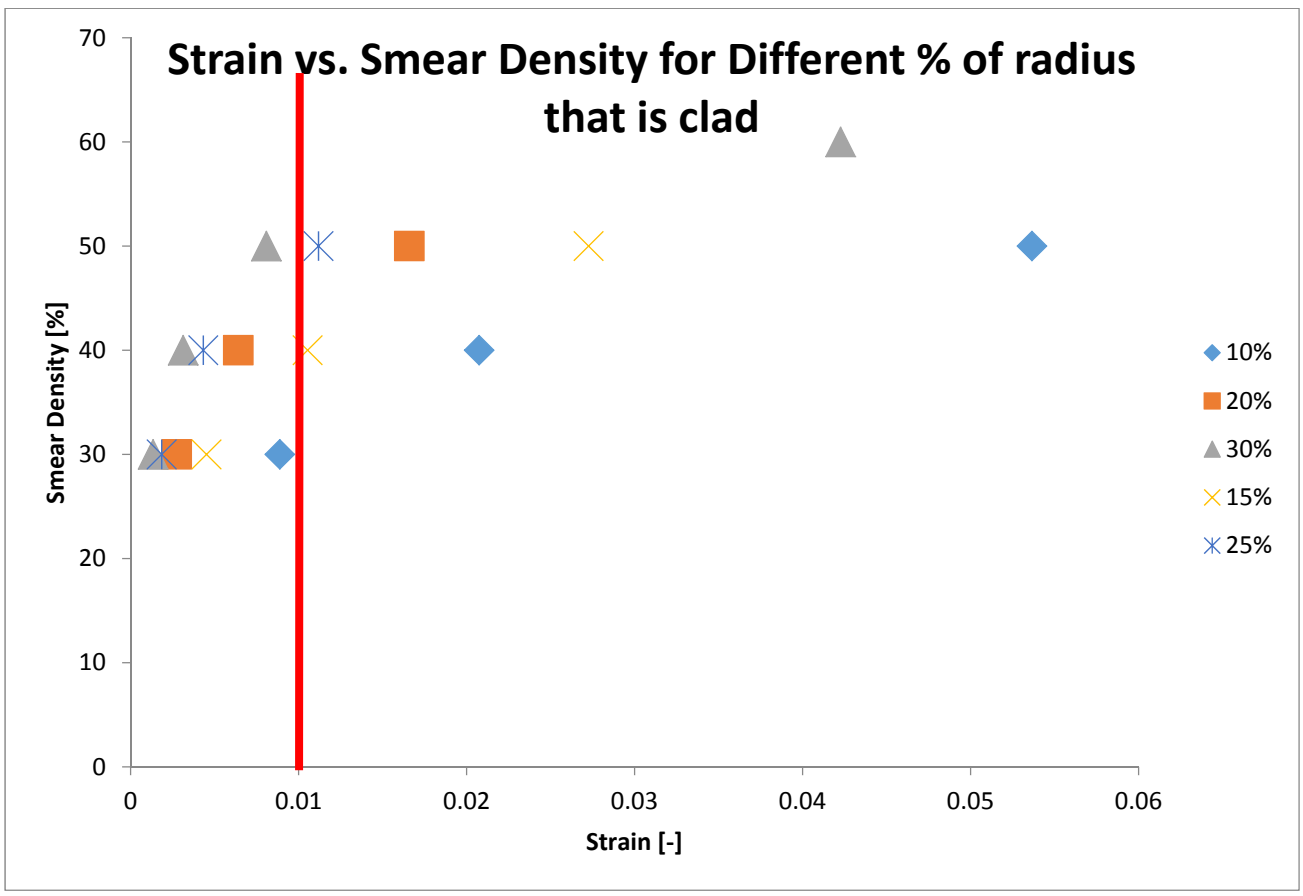

Figure 2.10. Strain vs. smear density of the fuel for a different % of radius of the pebble that is clad. The red line is 1% strain.

Table 2.5. Largest smear density for different % of the radius that is clad and fraction of the pebble that is fuel.

% of radius clad	Largest smear density	Fraction of pebble fuel
10	31 %	0.23
15	39%	0.24
20	45%	0.23
25	49%	0.21
30	51%	0.17

From Table 2.5 it appears that the best combination for pebble would be 15% of the radius clad and smear density of 39%, which would give pebble with a fuel fraction of 0.24. The analysis of the pebbles in the reactor have shown that due to the long cycle lengths and amount of time spent in the reactor, the limiting factor for the pebbles is the thermal creep. With such low fuel volumes, the reactor would not be able to attain breed and burn mode of operation with depleted uranium being the fuel.

Additional analysis was done to determine the strain of the sphere or pebble from the internal pressure build up. The equation for the strain from internal pressure for a hollow sphere is shown below in Equation 2.15, where P is the internal pressure, r is the outer radius of the sphere, v is Poisson's ratio, t is the thickness of the sphere, and E is the modulus of elasticity. If the equation is rearranged to solve for the maximum pressure for a given strain, Equation 2.16 is produced.

$$\frac{Pr(1-v)}{2tE} = \varepsilon \qquad \text{Equation 2.15}$$

$$\frac{2tE\varepsilon}{r(1-v)} = P \qquad \text{Equation 2.16}$$

Solving this for a 1% strain gives an internal pressure of 60 MPa, which is not reached for steady-state operation so the internal pressure buildup should not be a problem.

2.4. Fuel Clad Chemical Interactions (FCCI) and Diffusion

After the mechanical integrity of the pebbles analysis, the next major concern to be addressed is the fuel clad chemical interactions and diffusion between the two metals. When two metals or alloys are in contact at elevated temperature for extended periods of time, the materials can diffuse into each other, causing the formation of intermetallics and wastage of the cladding material [3,26]. These intermetallics are often brittle and may have different mechanical and thermal properties. In Figures 2.11 and 2.12, the diffusion of the uranium metal into the HT-9 (mostly Fe and Cr) has caused wastages of clad and the formation of new phases in this diffusion region.

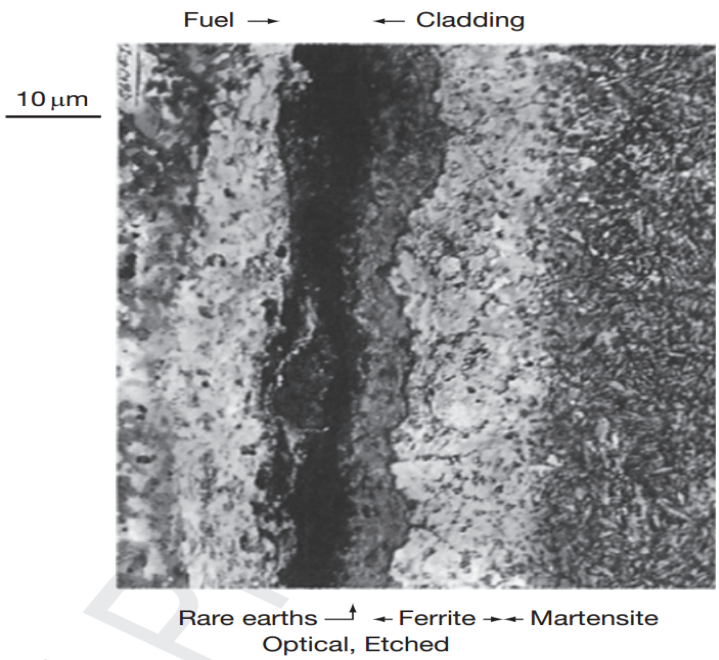

Figure 2.11. Diffusion of Uranium Zr alloy into the HT-9 cladding [3].

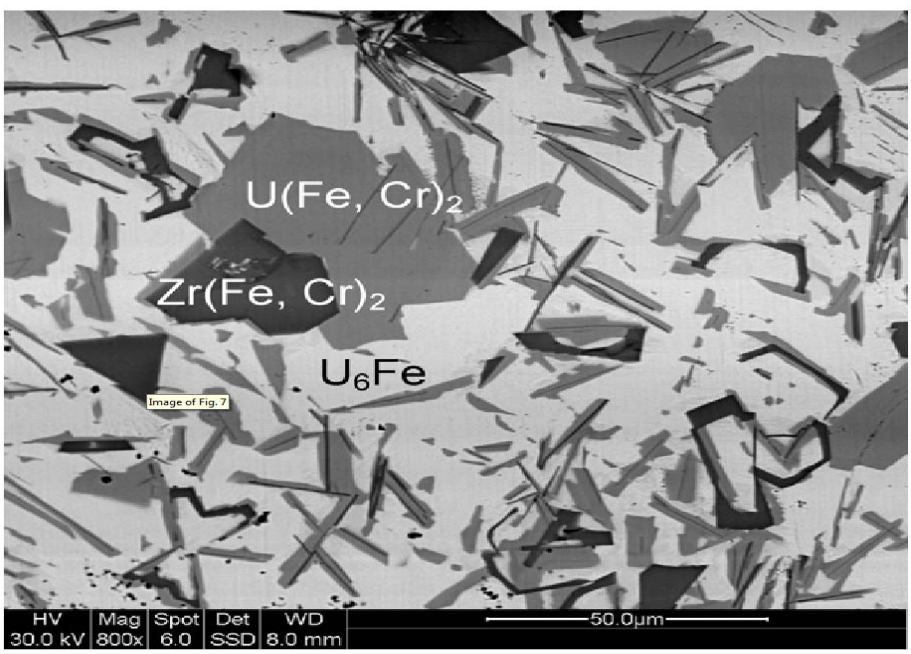

Figure 2.12. Scanning electron microscopy image showing the different phases that form when a U,Zr alloy (fuel) diffuses with HT-9 clad (Fe and Cr) [26].

Another concern is the FCCI during operation. FCCI in metallic fuel can be characterized by two stages of interaction [3]. The first stage is prior to the accumulation of lanthanide fission products at the fuel-cladding interface (from fission product immigration); FCCI is characterized by a ferretic layer formation. This layer can be a result of Ni depletion in autenitic cladding or

decarburization of the martensitic cladding [3]. This type of interaction has solid-state diffusion type time and temperature dependence. However, in the rare-earth fission products (lanthanides) that ultimately controls the FCCI as they migrate to the fuel-cladding interface [2]. Reference [2] gave us an equation to calculate the wastage rate of the cladding material due to FCCI; this is shown in Equation 2.17.

$$\frac{dw_x}{dt} = \frac{1}{2}\frac{C_{0L} - C_{\alpha L}}{C_{\beta L} - C_{\alpha L}}\sqrt{\frac{D_L}{t}} \qquad \text{Equation 2.17}$$

C_{0L} is the concentration of lanthanides atom, $C_{\alpha L}$ is the solubility limit of the lanthanides in the fuel which, from the literature, is assumed to be 0 [2], $C_{\beta L}$ is the solubility limit of the lanthanides in the clad which has a value of 0.1 [2], D_L is the diffusion coefficient for the lanthanides which is calculated from Equation 2.18, t is the time, and dw_x/dt is the wastage rate.

$$D_L = D_{0L}e^{\frac{-Q}{Rt}} \qquad \text{Equation 2.18}$$

In Equation 2.19, D_{0L} is the initial diffusion coefficient, R is the gas constant, t is temperature in K, and Q is the activation energy. In the calculation, D_{0L} is 1350 m^2/s, Q is 300 kJ/mol, R is 8.315 J/(mol*K), and t is 783 K (510ºC). This gives a value of D_L of $1.314*10^{-17}$ m^2/s. Now the concentration of the lanthanides in the fuel needs to the calculated. The major constituents of lanthanides accumulate in the fuel with yields of 0.18 for Nd, 0.17 for Ce, 0.06 for La, and 0.05 for Pr per fission. Adding all of those yields together gives a total yield per fission for lanthanides of 0.46. Using Equation 2.19 gives an accumulation of $8.4*10^{20}$ atoms for the lifetime of the pebble.

$$N_{lanthanides} = V_{fuel}\rho(\%U)\left(\frac{6.022 * 10^{23}}{238}\right)(FIMA)0.46\frac{lanthanide\ atoms}{fission} \qquad \text{Eq. 2.19}$$

In the pebble there are $4.1*10^{22}$ atoms of uranium which would give a concentration of lanthanides atoms of 0.0204. Using equation 2.19 and plugging in all the numbers and taking the integral of both sides to find the wastage, we arrive at Equation 2.20.

$$\int dw_x = \int_0^{2.1*10^9} 0.102\sqrt{\frac{1.314^{-17}}{t}}\,dt \qquad \text{Equation 2.20}$$

This calculation gives us a wastage amount over the lifetime of the pebble of 34 microns of material. This is an extreme overestimation of the wastage because it was assumed that pebble had that high of concentration of lanthanides and was at 783 K for the entire time; however, this still small amount of wastage illustrates that FCCI should not be a major concern for cladding material. If it is instead assumed that the pebble has that concentration of lanthanides for half the time of its life in the core the wastage becomes 24 microns of material which again is a slight overestimation of the wastage of the clad. The FCCI should not be a major concern but still needs to be addressed in the analysis of the pebble especially since the core design requires long cycle lengths.

Another issue that diffusion causes is the formation of ternary phases at the fuel clad interface that have low melting points. The major one in this core is Pu, U, Fe phases that are liquid at 590ºC. This is illustrated in on the next page in Figure 2.14. These liquid phases limit the peak clad temperature to below this temperature in order to prevent the formation of liquid and clad degradation during operation. The steady-state operation temperature of the clad for this design is 510ºC which is below the melting temperature of the liquids region on the phase diagrams.

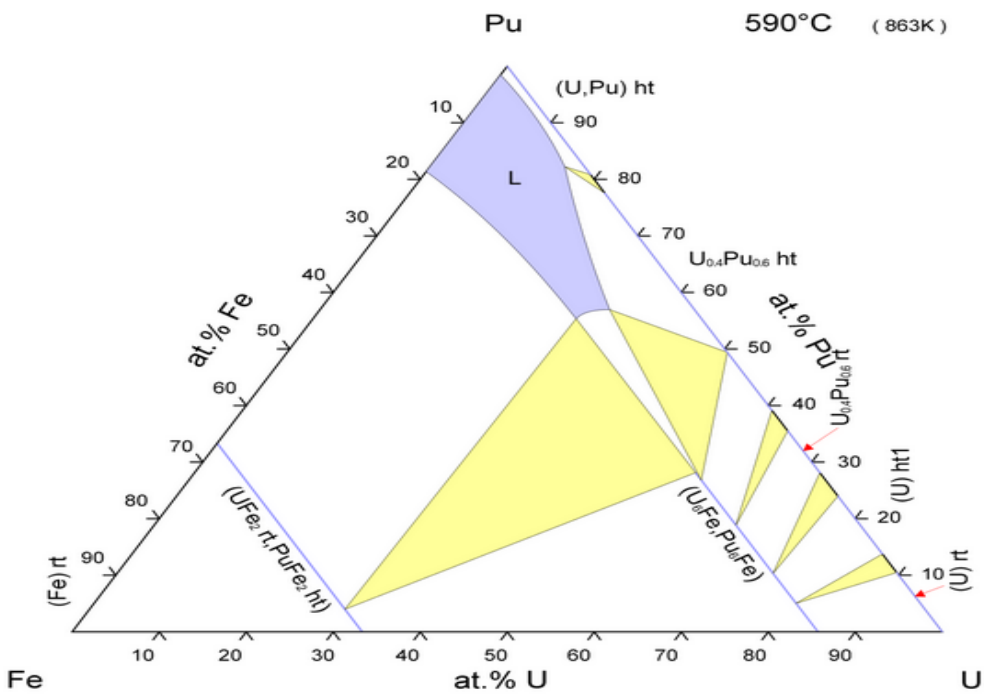

Figure 2.14. Ternary phase diagram for Fe, Pu, U showing a liquid phase at 590ºC which limits clad temperature [27].

An additional consideration to evaluate and be aware of is the reconstitution of the elements in the fuel during operation. During operation, the Zr in the fuel migrates towards the center of the fuel, causing there to be a Zr-rich and U-depleted center zone and Zr-depleted and U-rich middle zone. This is shown with energy dispersive X-ray spectroscopy (EDS) lines scans on irradiated fuel alloys in Figure 2.15. This is not a major concern and actually helps because a

high Zr concentration actually increases the melting temperature, which is good for the center of the pebble since that is the region will the highest temperature (see Figure 2.1). The EDS line scans show that the Pu concentration in the fuel stays relatively constant, illustrating that Pu does migrate to any region in the fuel. It was also stated that most of the other actinides were similar to Pu and did not migrate to any region in the fuel [3]. It was also stated that the saturation of the Zr and U migration happened within the first few percent burnup of the fuel [2,3].

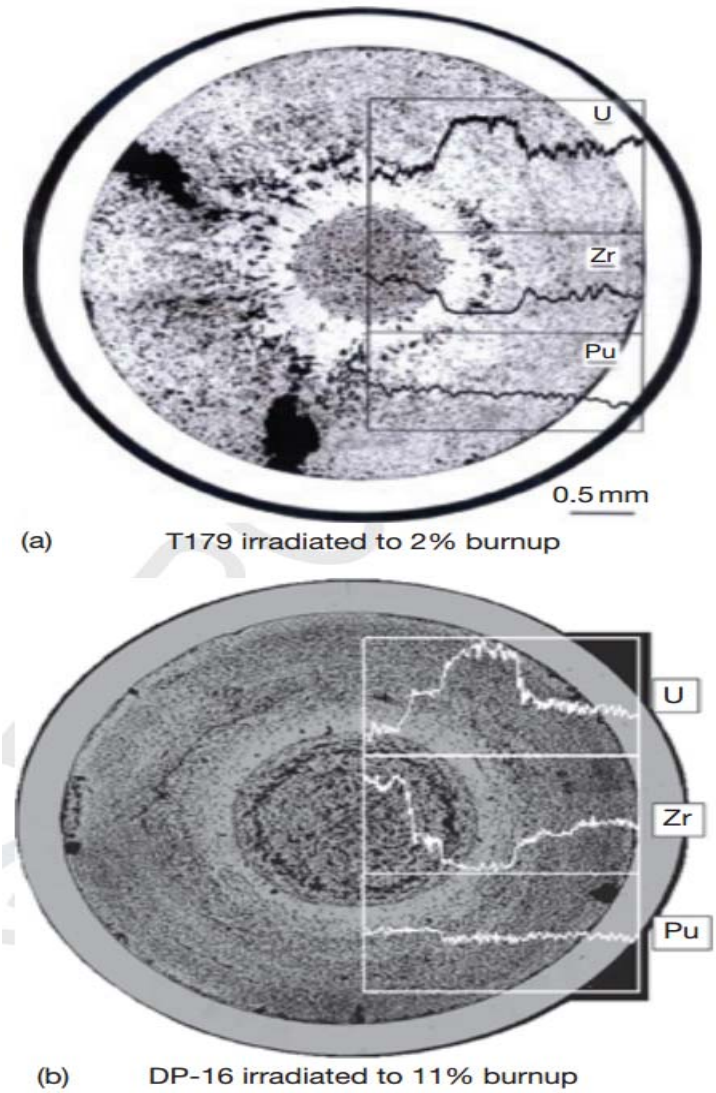

Figure 2.15. Cross section EDS lines cans on irradiated metallic fuel alloys of Zr,U showing the migration of the Zr to the center of the fuel [3].

2.5. Thermal Expansion of Pebbles and In-core Components

The thermal expansion of the pebbles was analyzed to discover how much they would expand and to investigate the ability of the fuel assemblies to withstand this expansion and still maintain structural and geometrical integrity. The fuel assemblies need to maintain geometrical integrity to allow coolant flow through them. The largest number of pebbles in any one direction

was calculated to be 25. This direction was the first to be examined and since an HCP lattice is being used, the close-packed direction is analyzed. It is assumed that the pebbles are 25 rings of diameter 1.44 cm lined up. A representation of this can be seen in Figure 2.16.

Figure 2.16. A representation of the pebbles as rings in the assembly.

The formula for the expansion of the diameter of a ring is shown below.

$$D_1 = D_0(\Delta T * \alpha + 1) \qquad \text{Equation 2.22}$$

D_1 is the new diameter, D_0 is the initial diameter, ΔT is the change in temperature, and α is the linear expansion coefficient. The linear expansion coefficient was found to $12.5*10^{-6}$ per ºC [17] and ΔT used was 485 ºC which is room temperature to 510 ºC. The expansion of one ring is approximately 0.00873 cm; multiplied by 25 pebbles, this gives 0.21825 cm.

After the expansion of the longest row of pebbles was calculated, the expansion of the hexagonal fuel assembly was calculated to evaluate whether there would be space for the expansion of the pebbles. The expansion was calculated the same way as the rings were and the apothem of the hexagonal assembly expanded 0.0625 cm which meant that half of the diagonal of the hexagon expanded 0.0722 cm and the total expansion along the length of the 25 pebbles for the assembly was 0.144 cm. This shows that the assembly will expand less than the pebbles will which is an issue; this will put a stress on the pebble and would cause the pebbles to start to neck. An illustration of necking is shown below in Figure 2.17.

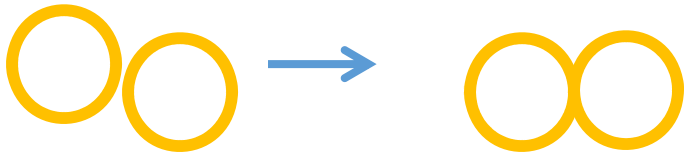

Figure 2.17. A representation of two pebbles necking.

Necking is when instead of the pebbles touching a point it starts to become a circle of contact. The necking of the pebble is a concern because this is a deformation of the shape of the cladding and fuel. This necking would also start to block coolant path in the coolant, inhibiting the ability to cool the pebbles. To prevent necking of the pebbles, it is advisable to leave space in between the pebbles to allow space for the thermal expansion of the pebbles. The minimum amount of space was calculated to be 28 microns. This value came from that there are 26 spaces in between the 25 pebbles and the assembly will expand 0.144 cm and the pebble 0.218 cm. The differences between the two expansions are 0.074 cm which divides by 26 spaces between the pebbles leaving 28 microns per space.

2.6. Conclusions

The large stress that would be produced in the pebble cladding from the containment of the fission gases greatly reduces the smear density fuel in the pebble. To load enough heavy metal into core and reach equilibrium would cause large stress in the pebble and possible failure during operation of the reactor. The major factor limiting the smear density of the fuel is the thermal creep strain of the cladding. Since the cycle lengths are extremely long, the pebbles spend a significant amount of time at elevated temperatures which means that pebbles have to have a small steady state creep rate in order to only experience 1% strain during their lifetime in the reactor. The venting of the pebbles will allow high smear density of fuel in the pebbles but a mechanism needs to be developed to allow venting but prevent ingress of Na coolant. FCCI was determined to not be an issue, but necking could be problematic.

3. Thermal Hydraulics

For the thermal hydraulics analysis, the goal was to find the largest core height that would meet all of the constraints while still provide a reasonable power density. A larger height reduces the core leakage and therefore the peak burnup, but it also increases the pressure drop.

3.1. Design Variables

The primary design variables are the pebble diameter and the core height. The coolant flow rate is uniquely set by the core area, pebble packing fraction, and inlet and output temperatures, so it is not an independent variable. To some degree, the lattice structure is a design variable, but it was obvious from early in the design that a close packed lattice would be required to achieve reasonable fuel volume fractions. The core power is also a design variable in a sense, but it was always maximized for a given combination of pebble diameter and core height so that the constraints were barely met.

3.2. Assumptions and Constraints

Several necessary assumptions were made in this analysis. No temperature drop is assumed between the clad and the fuel; this is effectively saying that there is no gap. This is a reasonable assumption, since the highest powered pebbles are the most burned, and the fuel swells to eliminate the gap within a few percent FIMA. It is also assumed that the fuel is completely smeared within the cladding (i.e. all voids are homogeneously distributed, and there is no central void). This is conservative, because a central void would reduce the center temperature. Lastly, it is assumed that the BOEC thermal conductivity for the highest power subassembly applies for the whole cycle. The thermal conductivity starts off small, due to the high porosity of the fuel, but recovers somewhat as solid fission products build up. For the parametric studies, it was assumed that the power shape was sinusoidal, which was a reasonable assumption for the 3-D fuel shuffling.

The thermal hydraulic constraints are summarized in Table 3.1. The melting temperature of U-6%Zr is 1150°C, so the temperature constraint provides a 350°C margin. The cladding temperature limit is set by the formation of a Pu-Zr-Fe eutectic at 590°C, which can cause the cladding to melt. The 12 m/s sodium flow rate limit is due to vibration concerns. The pressure

drop is larger than in the reference B&B core using 2-D shuffling [1], but that is due to the fact that the pressure drop correlations for the pebble bed include the core inlet and exit form loss pressure drops, while the reference core does not.

Table 3.1. Thermal hydraulic constraints.

Constraint	Value [units]	Reason
Pressure Drop	< 1.3 [MPa]	Pump size
Max Fuel Temperature	< 800 [°C]	Melting
Sodium Velocity	<12 [m/s]	Vibration
Max Clad Temperature	< 590 [°C]	Pu-Fe Eutectic Formation
Coolant Inlet/Outlet Temperature	355/510 [°C]	Design point

3.3. Nomenclature

The following table was included due to the obscure nature of some of the variables used. Additionally, there is a large overlap in typical nomenclature used for some things (for example, "k" is typically used for thermal conductivity and permeability). Commonly used variables that are not ambiguous (such as "C_p" for specific heat) are not included.

Table 3.2. Nomenclature.

Variable	Meaning
ε	porosity (1- [packing factor])
u_0	superficial velocity (velocity before reaching the pebble bed)
ρ_0	mean sodium density
p	pressure
P	power
D_p	pebble diameter
U	mean sodium velocity (within bed)
U_{in}	inlet sodium velocity (within bed)
U_{out}	outlet sodium velocity (within bed)
L, H	core length, core height (used interchangeably)
k_{perm}	permeability, $\frac{\varepsilon^3 D_p^2}{180(1-\varepsilon)^2}$
k	thermal conductivity
f	Fanning friction factor
s	Assembly unit cell pitch
D_h	Hydraulic diameter
F_r	Radial power peaking factor
Pe	Péclet number = $Re_D Pr$
q'''	Power density (average power per unit core volume)
$\dot{q}$	Volumetric heat generation rate (power per unit fuel volume)
F_t	Overall power peaking factor

3.4. Models Used

3.4.1.Thermal Conductivity

As shown in Section 3.01.2.1.5 of Reference [35], the initial nominal density thermal conductivity for metallic uranium-zirconium alloys. For our reactor, a value of 24 W/m-K was determined to be a somewhat conservative yet reasonable estimate.

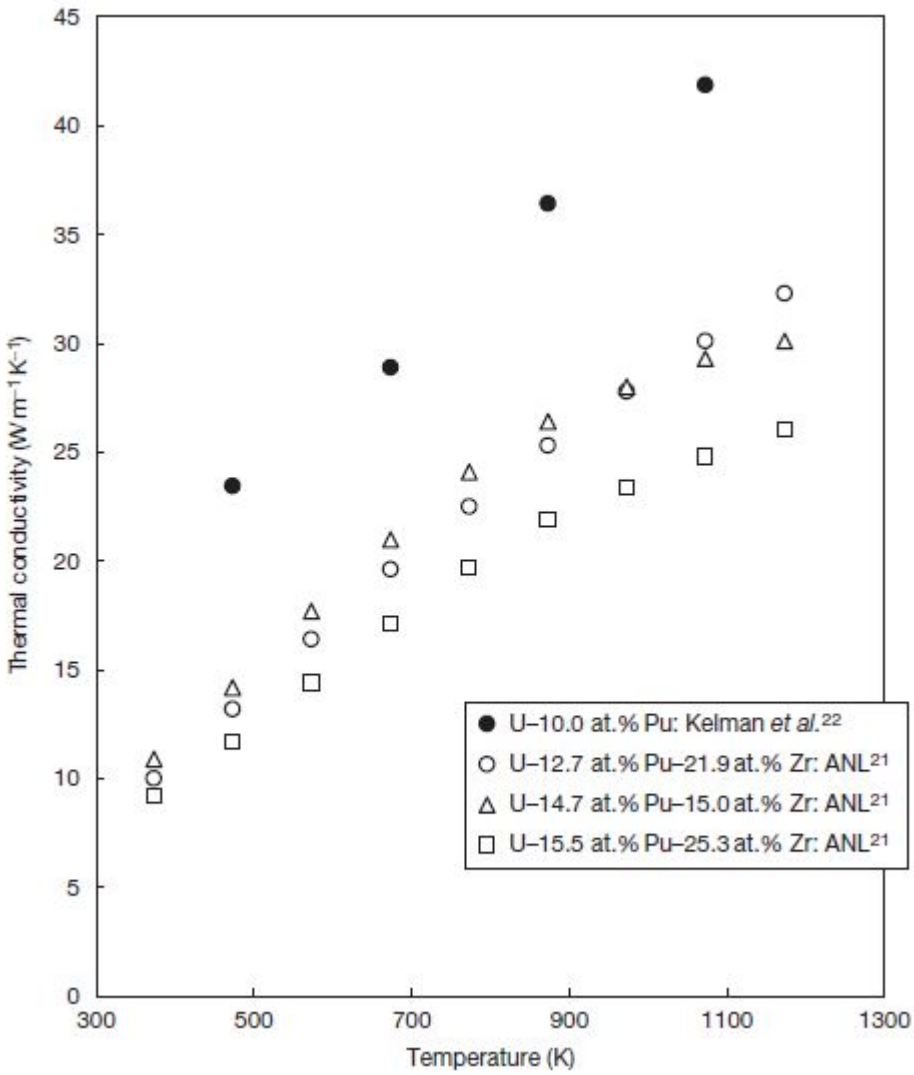

Figure 3.1. Thermal conductivity of U-Pu-Zr alloys [35].

In Section 3.01.4.6 of Reference [35], Equation 7 shows how the pores in the material may be accounted for:

$$k_f = k_0 \left(1 - P_g\right)^{3/2} \qquad \text{Equation 3.1}$$

k_f is the effective fuel thermal conductivity, k_0 is the nominal density thermal conductivity, and P_g is the pore volume fraction within the pebble. The equation in Reference [35] has an extra ε in the numerator, where ε was 0.72; however, a comparison between the values listed in the text, as well as comparing against Equation 8 (which described the thermal conductivity after sodium infiltration), indicated that this was a mistake. The pebble pore volume fraction as a function of smear density and burnup was obtained from the materials analysis and used to evaluate the effective thermal conductivity.

The clad thermal conductivity is shown in Reference [36] as a function of temperature. It varies nonlinearly with temperature, but at its lowest point in the range of interest (355 °C < T_{clad} < 590 °F), the thermal conductivity is greater than 25 W/m-K, so this value was chosen for the analysis. It was held constant, because the thermal resistance is small anyway and it does not vary greatly.

3.4.2.Pressure Drop

The largest component of the pressure drop is the frictional losses through the ordered bed. Several different correlations were considered for this portion. Ergun's equation [28] is generally considered the standard approach for systems with a random bed:

$$\frac{\Delta p_{Ergun}}{L} = 1.75 \frac{(1-\varepsilon)}{\varepsilon^3} \frac{\rho}{D_p} u_0^2 + 150 \frac{(1-\varepsilon)^2}{\varepsilon^3} \frac{\mu}{D_p^2} u_0^2 \qquad \text{Equation 3.2}$$

However, the Beaver correlation [29] better captures effects from the wall.

$$-\frac{dp_{Beaver}}{dx} = \frac{\mu u_0}{k_{perm}} + \frac{c \rho u_0^2}{k_{perm}^{1/2}} \qquad \text{Equation 3.3}$$

$$c = 0.55\left(1 - 5.5 \frac{D_p}{D_h}\right) \qquad \text{Equation 3.4}$$

where D_h is the hydraulic diameter of the assembly without any pebbles present. Susskind et al. present another correlation [30] which is valid for ordered beds with a rhomboidal lattice:

$$\frac{f \varepsilon^3}{1-\varepsilon} = 83.4 \frac{1-\varepsilon}{\mathrm{Re}} + 0.42 \qquad \text{Equation 3.5}$$

$$\Delta p_{Susskind} = 2 f \frac{L}{D} \rho_0 U^2 \qquad \text{Equation 3.6}$$

A comparison between the Susskind correlation and the Beaver and Ergun correlations (as in Figures 3.3 and 3.4) shows the large benefit in pressure drop for using an ordered bed.

Additionally, four extra analytic expressions were developed, considering the flow channels in hexagonal close packed (HCP) and hexagonal simple (HSP) lattices as either a series of gradual expansions and contractions or a series of sudden expansion and contractions. Since the analytic expressions could not account for non-ideal packing fractions or for wall effects, they are not expected to be as accurate as the Susskind correlation, but rather provide bounding values.

Additionally, the pressure drop from the hydrostatic forces was considered.

$$\Delta p_{static} = \int_0^H \rho(z)\, g dz \approx \rho_0 g H \qquad \text{Equation 3.7}$$

The hydrostatic term was less than 20 kPa for the tallest core considered, so this was nearly negligible.

Furthermore, the acceleration due to the velocity change of the coolant was considered:

$$\Delta p_{accel} = \frac{1}{2}\left(\rho_{out} U_{out}^2 - \rho_{in} U_{in}^2\right) \qquad \text{Equation 3.8}$$

This change in pressure due to acceleration was less than 1 kPa for most designs, so it was also negligible.

Lastly, the form loss due to expansion of the assembly from the inlet temperature to the outlet temperature was found. Using a value of 12.5 * 10^{-6} K^{-1} for the value of the thermal expansion coefficient of HT9 [32], the value of the form loss coefficient can be calculated from Reference [31]. For this analysis, it was approximated that the pitch of the unit cell was roughly the flat-to-flat of the assembly.

$$K_{\text{expansion}} = \left(1 - \frac{A_{in}}{A_{out}}\right)^2 2.6 \sin\left(\frac{\alpha}{2}\right) \qquad \text{Equation 3.9}$$

where α is the angle formed by the expansion.

$$\frac{A_{in}}{A_{out}} = \frac{\left(\sqrt{3}/2\right) s_{in}^2}{\left(\sqrt{3}/2\right)\left(s_{in} * \left\{1 + \left(1.25 * 10^{-5} K^{-1}\right)\Delta T\right\}\right)^2} = \frac{1}{\left(1 + \left\{1.25 * 10^{-5} K^{-1}\right\}\Delta T\right)} \qquad \text{Eq. 3.10}$$

$$\frac{A_{in}}{A_{out}} = 0.996 \qquad \text{Equation 3.11}$$

α can be calculated from the difference in the hydraulic radii and the height of the core.

$$D_h = \frac{4A_x}{P_w} = \frac{4\left(\frac{\sqrt{3}}{2}s^2\right)}{6\frac{s}{\sqrt{3}}} = s \qquad \text{Equation 3.12}$$

$$\alpha = \arctan\left(\frac{s_{in} - s_{out}}{2H}\right) \qquad \text{Equation 3.13}$$

Even in a bounding case (with an inlet pitch of 23 cm), the resulting form loss coefficient is $7.7*10^{-9}$, which is dwarfed by the friction factor from the bed (which is usually between 0.5 and 1.0). Thus, this term was neglected.

3.4.3.Heat Transfer

Several submodels were used in the heat transfer model.

3.4.3.1.Coolant Velocity

The coolant velocity can be obtained by a core energy balance along the hottest channel.

$$\rho_{Na} U A_{Na} \int_{in}^{out} C_p dT = Q_{th,ave} F_r \qquad \text{Equation 3.14}$$

Since C_p varies by less than 2.5% over the temperature range under consideration [1], the average value of 1275.66 J/kg-K will be used. A_{Na} is set by the core volume (which is set by the unit cell pitch, so both are effectively design variables) and the porosity:

$$A_{Na} = \frac{V_{core}}{H}\varepsilon \qquad \text{Equation 3.15}$$

Therefore,

$$\rho_0 U\left(\frac{V_{core}}{H}\varepsilon\right)\left(C_p \Delta T\right) = Q_{th,ave} F_r \qquad \text{Equation 3.16}$$

$$U = \frac{H Q_{th,ave} F_r}{\varepsilon \rho_0 V_{core} C_p \Delta T} \qquad \text{Equation 3.17}$$

Everything remaining in this expression is either an independent variable, a design input, or a physical parameter.

To find the superficial velocity, conservation of mass dictates that $u_0 = U*\varepsilon$, since the flow area is decreased by a factor of ε within the bed.

3.4.3.2.Heat Conduction Through the Pebble

The heat conduction equation in spherical geometry is as follows:

$$\frac{1}{r^2}\frac{d}{dr}\left(kr^2\frac{dT(r)}{dr}\right)=-\dot{q} \qquad \text{Equation 3.18}$$

Assuming constant thermal conductivity and heat generation rate, as well as no temperature difference between the cladding and the fuel, integration leads to the following result for the center temperature of a pebble.

$$T_f(0)=\frac{\dot{q}R_f^{\,2}}{3}\left(\frac{1}{2k_f}+\frac{1}{k_c}\left(1-\frac{R_f}{R_c}\right)+\frac{R_f}{hR_c^2}\right)+T_\infty \qquad \text{Equation 3.19}$$

where the *f* subscript denotes a fuel parameter, and the *c* subscript denotes cladding. Since the clad is the outer part of the pebble, R_c is the pebble radius. For the most limiting "channel" of pebbles,

$$T_f(0,z)=Z(z)\frac{\dot{q}_{ave}F_rR_f^{\,2}}{3}\left(\frac{1}{2k_f}+\frac{1}{k_c}\left(1-\frac{R_f}{R_c}\right)+\frac{R_f}{hR_c^2}\right)+T_\infty(z) \qquad \text{Equation 3.20}$$

where Z(z) is the shape function of the power. As mentioned in Section 2.2, it will be assumed for the parametric studies that the axial power shape is sinusoidal:

$$Z(z)=\frac{\pi}{2H}\sin\left(\frac{\pi}{H}z\right) \qquad \text{Equation 3.21}$$

$$T_\infty(z)=T_{inlet}+\frac{\Delta T_{core}}{2}\left(1-\cos\left(\frac{\pi}{H}z\right)\right) \qquad \text{Equation 3.22}$$

Similarly, the maximum clad temperature for a given pebble is

$$T_c(R_f)=\frac{\dot{q}R_f^2}{3k_c}\left(1-\frac{R_f}{R_c}\right)+\frac{\dot{q}R_f^3}{3hR_c^2}+T_\infty \qquad \text{Equation 3.23}$$

Since the thermal resistance of the cladding is much lower than the thermal resistance of the fuel, the cladding temperature may be more coupled to the bulk coolant temperature than the heat generation rate. Instead of creating a more detailed model to describe the power generation profile or the axial coolant temperature distribution, a very conservative upper bound for the peak clad temperature was determined by using the peak heat generation rate with the exit bulk fluid temperature. For every design, there was plenty of margin on the cladding temperature constraint.

3.4.3.3.Heat Convection to the Coolant

Reference [33] used the following correlation for liquid metal flow through a randomly packed bed:

$$Nu = \frac{hk_{Na}}{\sqrt{k_{perm}}} = \left(1 - 0.186\left(0.58 - \varepsilon\right)\right)\left(0.877\,\mathrm{Re}^{1/2} + 0.152\,\mathrm{Re}^{2/3}\right)\mathrm{Pr}^{1/2} \qquad \text{Equation 3.24}$$

Since this correlation was developed for randomly packed beds in which the flow channel is interrupted, the heat transfer is likely overestimated. Later in the project, it was discovered that Reference [34] uses two correlations for Nusselt number in ordered beds, which were developed analytically:

$$Nu_{\text{Uniform Temp}} = \sqrt{\frac{2}{\pi}\mathrm{Pe}\left(1.5639\right)} \qquad \text{Equation 3.23}$$

$$Nu_{\text{Uniform Heat Flux}} = 1.0035\sqrt{\mathrm{Pe}\left(1.5639\right)} \qquad \text{Equation 3.24}$$

Since this model was developed for a single layer of pebbles, it would not capture the differences between an HSP, HCP, or FCC lattice. This is significant, since an HSP lattice has twice the number of persistent flow channels as an HCP lattice, and FCC has no persistent flow channels.

The difference between the three correlations was small (~4.5 for uniform temp, ~5.6 for uniform heat flux, ~6.4 for random bed). Since the correlations in Reference [34] were developed for a single row of pebbles whereas the correlation in Reference [33] takes into account the layers of pebbles, the correlation from [33] is used; however, since the temperature drop between the cladding and the fuel was typically a few K, it is not expected to drastically impact the results.

3.5. Parametric Study Results

For the following studies, the effects of changing a single design variable were studied. This is not a truly physical approach: for instance, changing the pebble diameter would change the achievable packing fraction, and changing the core height would change the achievable power.

Most of the results depend strongly on the peaking factor, which is sensitive to many things, including the shuffling scheme, the material volume fractions, and the core height. For most of the parametric studies, the power peaking factors that were used were from the reference case [1], and are summarized in Table 3.3. The power was assumed to be sinusoidal axially. It should be noted that an error in the ADOPT code was discovered in this analysis; in the reference core design, the pitch was mistakenly used as diagonal distance in different instances. The pitch was reported as 23.25 cm, but in order to approximately preserve the total core volume, a hexagonal pitch of 20.135 cm was used instead. It should be noted that if a pitch of 20.135 cm were to be used in the reference core, the pressure drop and the power density would both be increased. When preserving the same number of assemblies and the overall core area, a square pitch of 18.738 cm should be used instead. In order to keep the results closer to the range of interest, the power was reduced to 1000 MW_{th}.

Table 3.3. Default values for the parameters in the T/H parametric studies.

Parameter	Value

Thermal power	1000 [MW]
Radial peaking factor	2.04
Active core height	2 [m]
Assembly pitch	18.738 [cm]
Pebble diameter	1.65 [cm]
Packing fraction	66.04% [HCP lattice]
Smeared fuel volume fraction (within assembly unit cell)	46.78%
Fuel smear density	70%

3.5.1.Changing Pebble Diameter and Packing Fraction

Using the analytic conduction equations in a spherical geometry, Figures 3.2 and 3.3 were obtained. Figure 3.4 shows the results of the empirical pressure drop correlations as well as the analytic expressions from modeling the pebble bed as a serious of expansions and contractions. The cladding thickness was changed proportionally with the pebble diameter. The specifications in Table 3.3 were used, except that the cladding diameter varied from 0.5 cm to 3.7 cm.

Figure 3.2 shows that for very small pebbles, the maximum fuel temperature is strongly dependent on the bulk sodium temperature at the exit, while for larger pebbles, the maximum fuel temperature varies linearly with pebble diameter. Figure 3.3 supports this; since the axial power shape was postulated to be sinusoidal, for infinitely small pebbles, the maximum temperature would be equal to the sodium exit temperature and it would occur at the exit. For infinitely large pebbles, the location of peak heat flux – the center – dictates the fuel temperature, and as shown in Section 3.4.3.2, the fuel temperature varies with the square of the pebble radius (since the ratio of the pebble radius to the fuel radius was held constant).

In Figure 3.4, a similar trend is observed in all correlations. It is clear that the Beaver correlation fails when the pebble diameter is large; it predicts that the pressure drop will be negative for pebble diameters larger than 3.2 cm with the chosen packing fraction in the assembly. The analytic pressure drop plotted is only for the close packed lattice; for the simple packed lattice, the pressure drop that was calculated was significantly below the limit for all pebble sizes. It should also be noted that by the analytic calculations of the pressure drop could only use the ideal close packed packing fraction (PF=0.7405). As expected, there was a significant gain in pressure drop from using an ordered bed correlation.

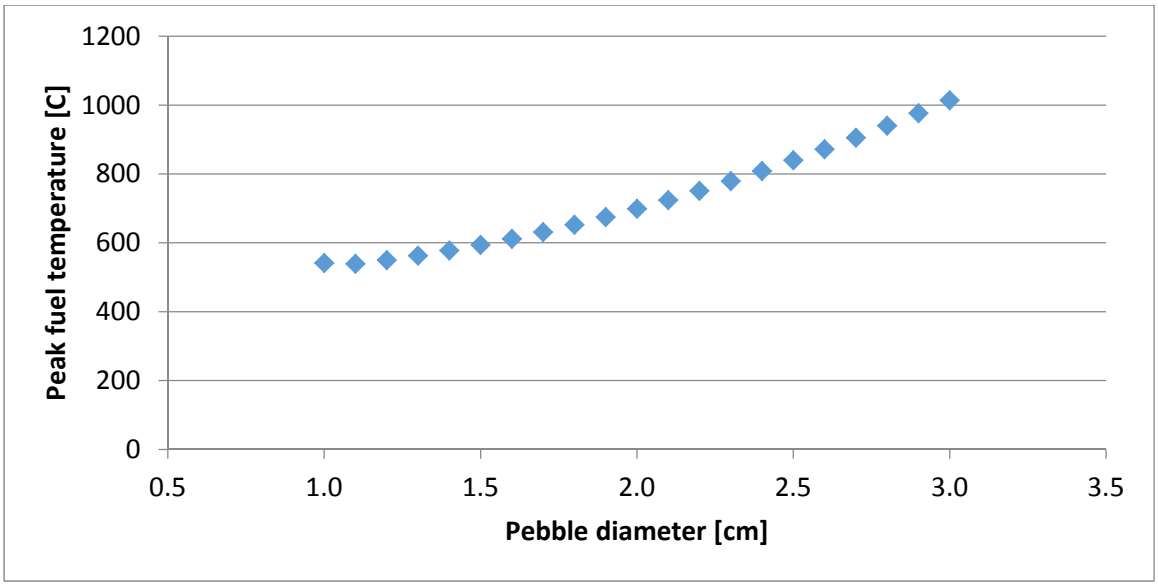

Figure 3.2. Maximum fuel temperature vs. pebble diameter.

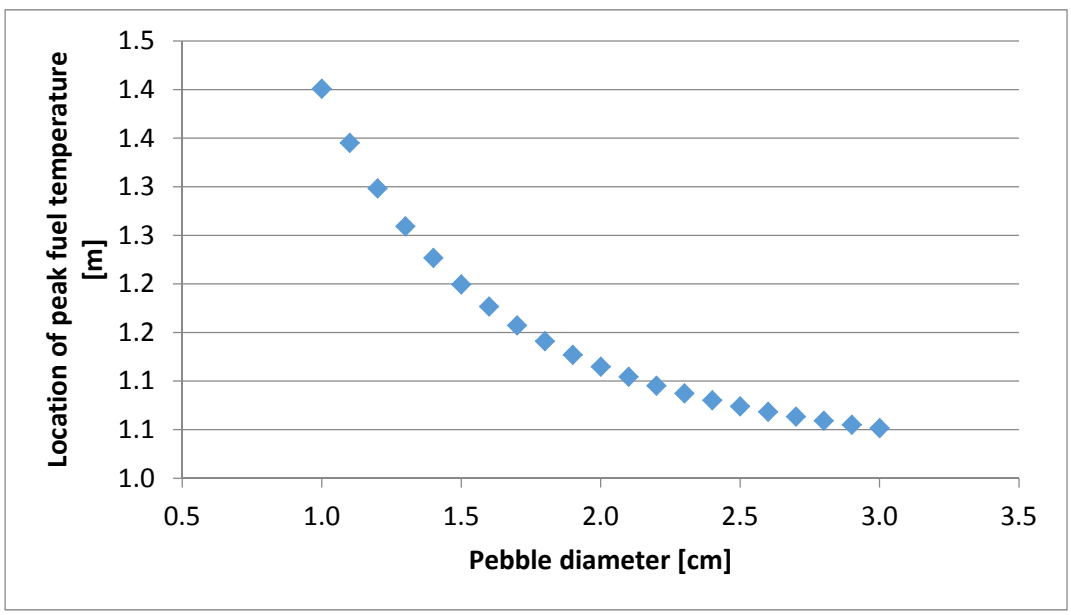

Figure 3.3. Axial position of peak fuel temperature vs. pebble diameter.

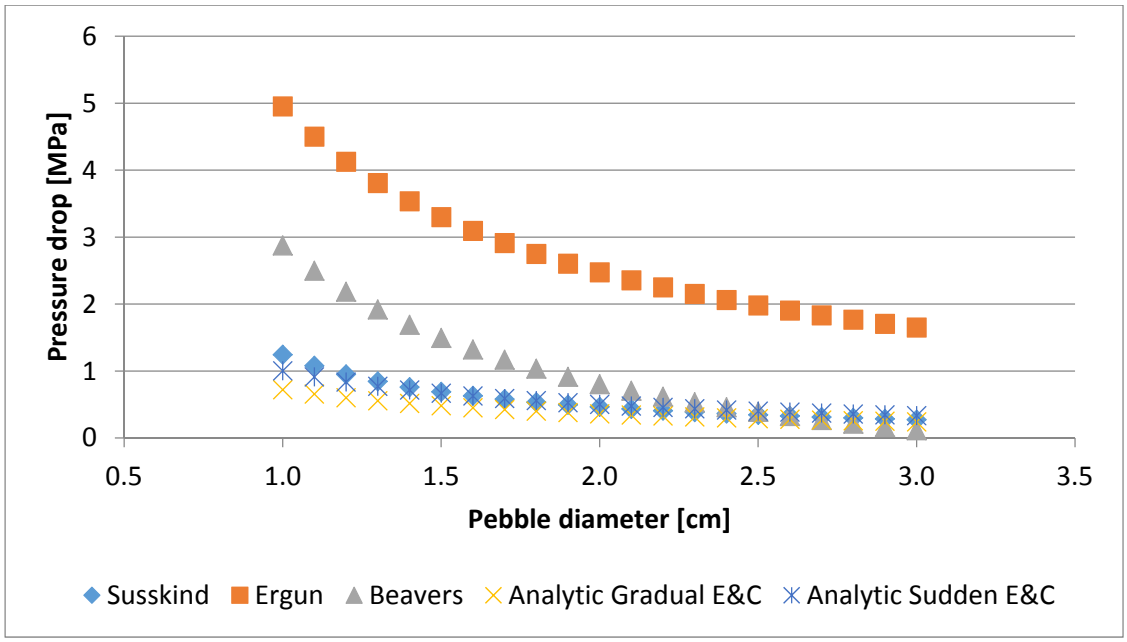

Figure 3.4. Pressure drop vs. pebble diameter for several correlations.

3.5.2.Changing Packing Factor

The pebble packing factor was changed from the ideal HCP packing factor (0.7405) to the ideal simple packing factor in hexagonal geometry (0.6046). Since the fuel volume fraction is proportional to the packing factor, the fuel volume fraction was changed accordingly as well. The other design parameters are those specified in Table 3.3.

Figure 3.5 shows the fuel temperature dependence on the packing fraction. While there is some benefit to using larger packing fractions, the dependence is small compared to the dependence on the pebble size.

Figure 3.6 shows the pressure drop variance with the packing factor. Since the analytic expressions were formulated for an HCP lattice without considering any wall effects, the pressure drop for both correlations is constant. Comparing the results for a packing factor of 0.7405 between the analytic correlations and the empirical Susskind correlation shows that the analytic expressions greatly underpredict the pressure drop. This is to be expected, as the expressions for the form losses assume that the flow fully develops before the next interruption, which is not possible in an ordered bed lattice. The differences between the experimental correlations show again the benefit of using an ordered bed.

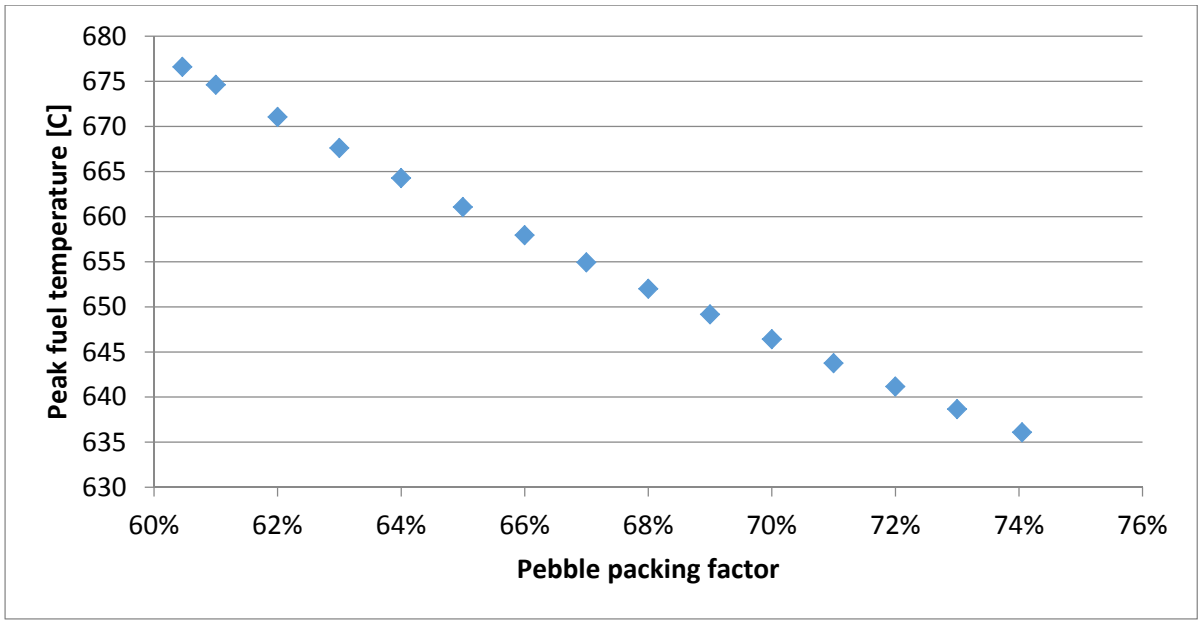

Figure 3.5. Maximum fuel temperature vs. packing factor.

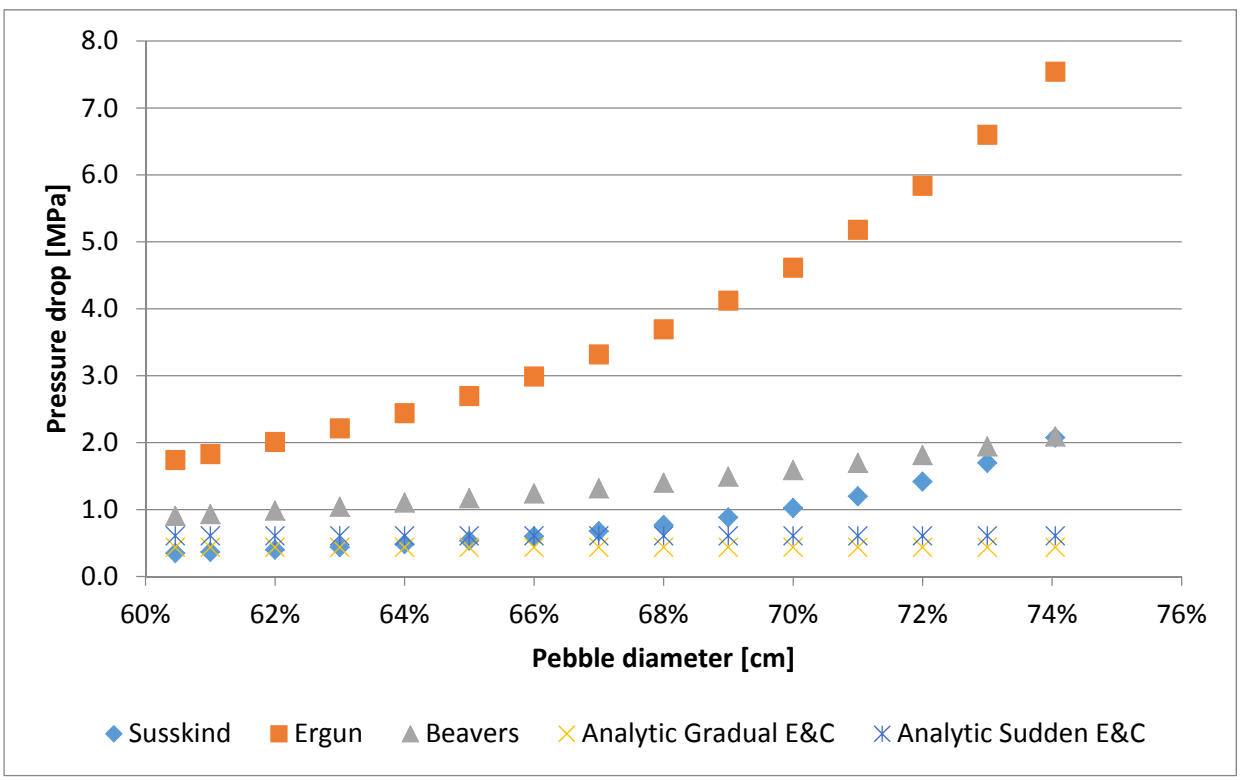

Figure 3.6. Pressure drop vs. packing factor.

3.5.3. Changing Smear Density

Changing the smear density did not affect the fluid flow at all, since the total power and the total pebble volume remained constant. Therefore, no pressure drop figures were generated.

However, increasing the smear density did increase the thermal conductivity, which reduced the peak fuel temperature, as shown in Figure 3.7. Since this affected the balance between conduction and convection in the pebbles, the temperature profile was also affected, as shown in Figure 3.8.

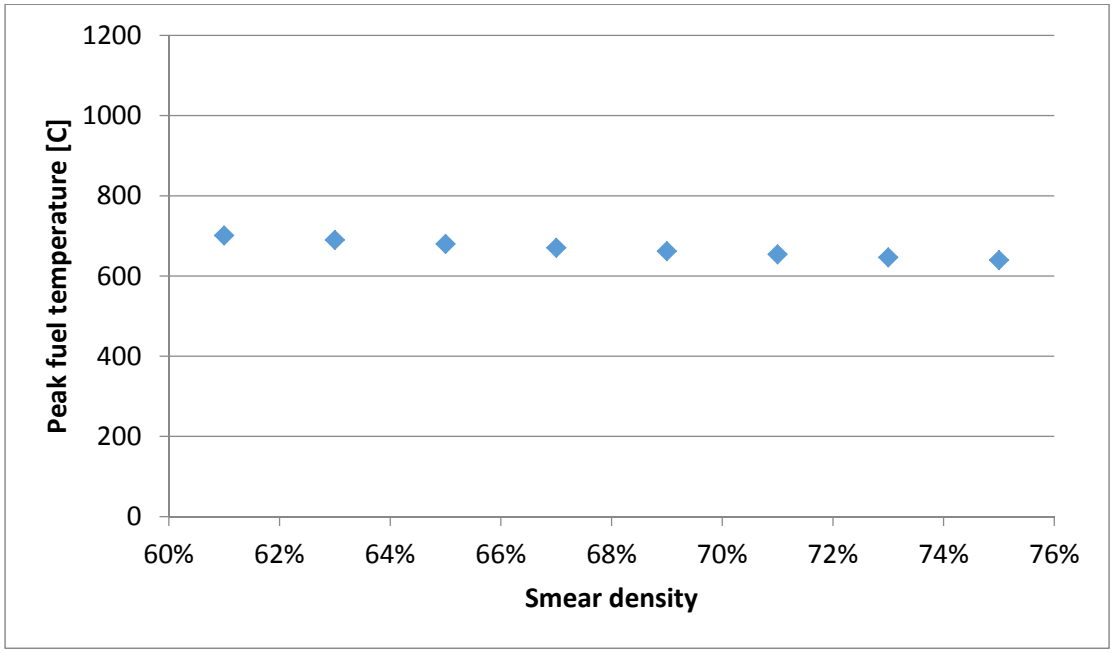

Figure 3.7. Maximum fuel temperature vs. smear density.

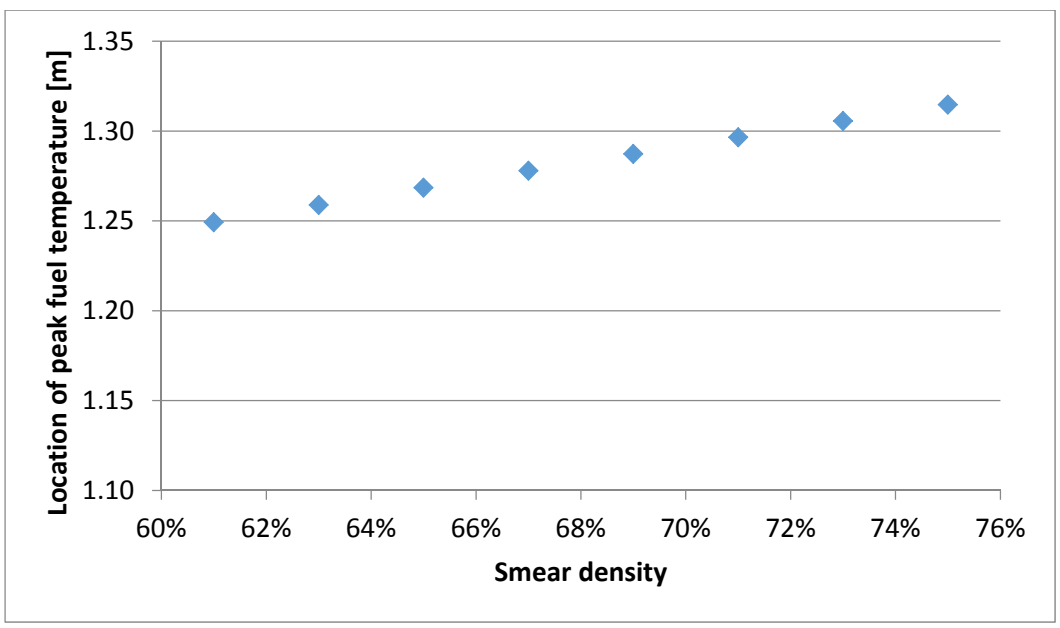

Figure 3.8. Axial location of peak fuel temperature vs. smear density.

3.5.4.Changing Core Height

Figure 3.9 shows the maximum fuel temperature dependence on the core height, and Figure 3.10 shows the pressure drop dependence. As the power density decreases, the maximum fuel temperature tapers off, whereas the pressure drop increases linearly with the core height. This is appropriate, since none of the pressure gradient terms in Section 3.4.2 depend on the core height.

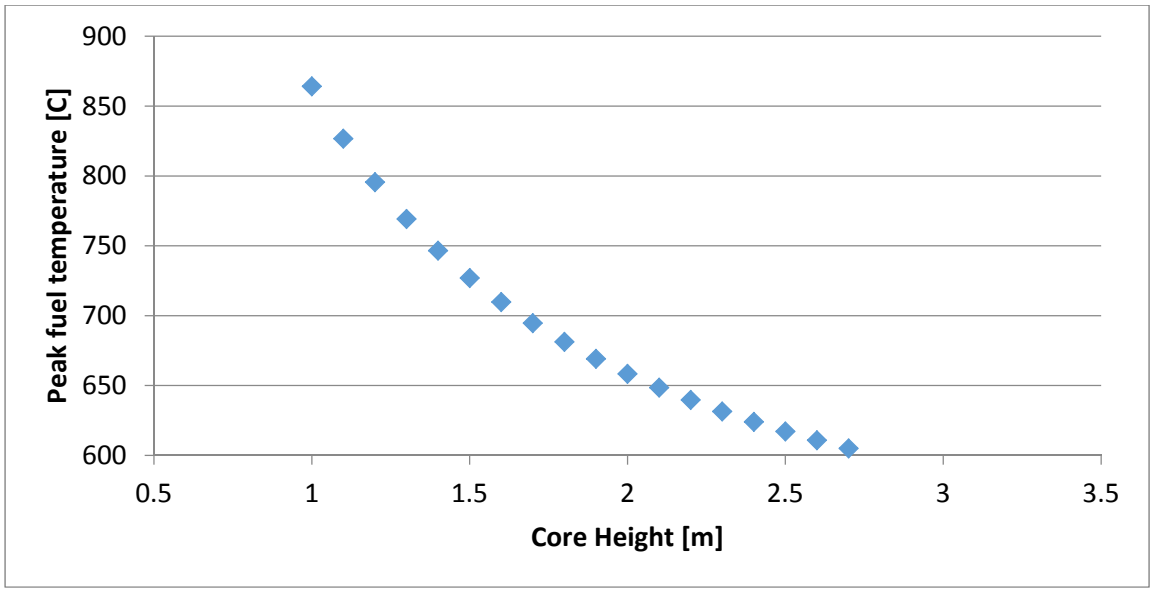

Figure 3.9. Maximum fuel temperature vs. core height.

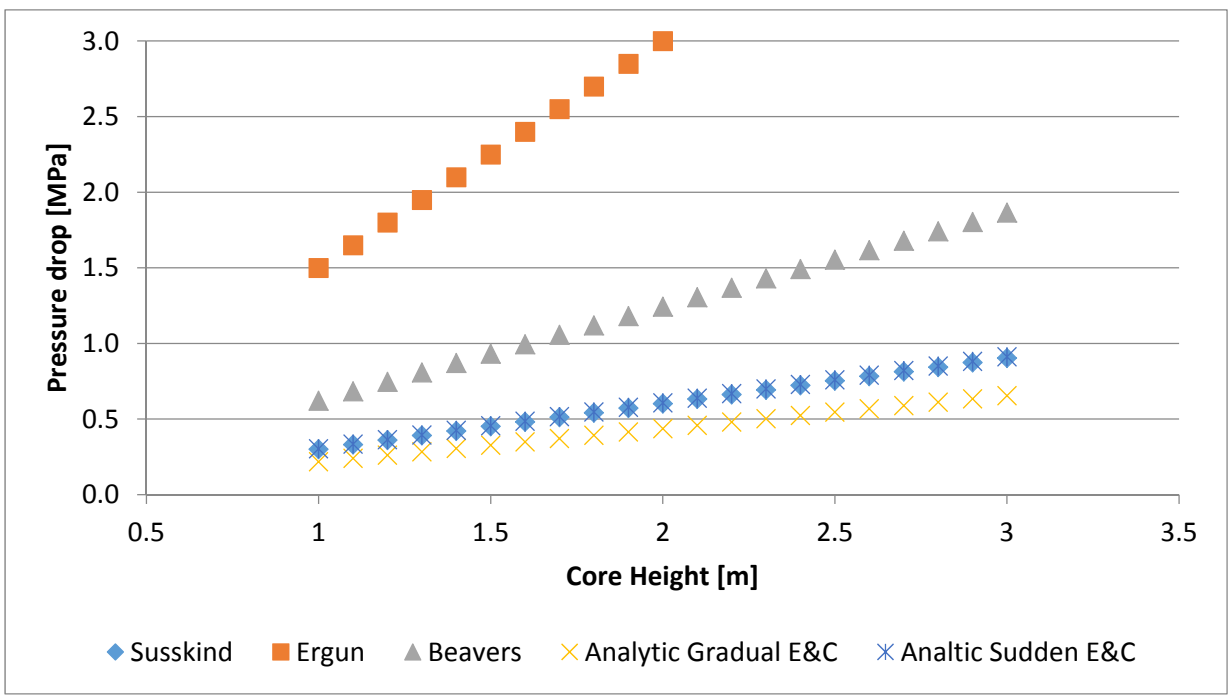

Figure 3.10. Pressure drop vs. core height.

3.5.5.Meeting all constraints

Since changing each of the independent variables would change the available design space of the others, a final study was performed in which the pebble diameter, the core height, and the power were all changed simultaneously so that a series of designs were created that just barely met the temperature and pressure drop constraints listed in Table 3.1. The independent variable for this study was the core height, since it is the one that most heavily influences the peak discharge burnup. For each core height, the pebble diameter was changed in 0.01 cm intervals and the power density was changed in 0.1 W/cc intervals until the maximum combination that met the pressure and temperature constraints was found. The assembly packing factor was maximized for each pebble diameter, and the assembly pitch was allowed to vary slightly in order to accommodate this. The actual core height was also allowed to float within a few pebble diameters from the target value. Only the Susskind pressure drop correlation was considered for this study.

As shown in Figure 3.11, the smaller cores are more economical. The high pressure drop in these cores limits the power much more than the temperature, restricting the pebble diameters to the values shown in Figure 3.12. However, as shown at the end of Figure 3.12, for very tall cores, the optimal pebble diameter decreases very slightly; in these cases, although a larger pebble will still permit a higher core power, the volume increase from using larger pebbles reduces the power density more. As shown in Figure 3.13, the pebble packing factor slightly increases with core height, as more height is available for the pebbles to squeeze into, until a sharp cutoff around 1.25 m. After this point, the packing factor remains nearly constant with step-wise increases, which correspond to the changes in the number of pebbles per plane.

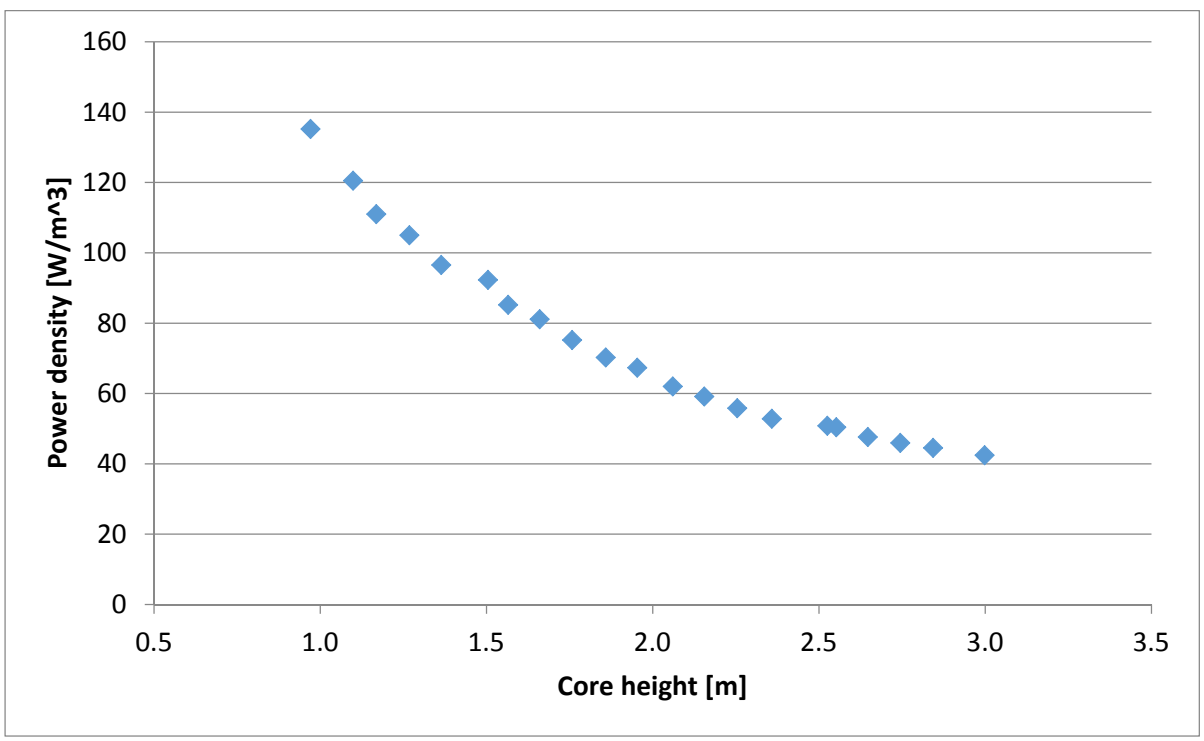

Figure 3.11. Power density vs. core height.

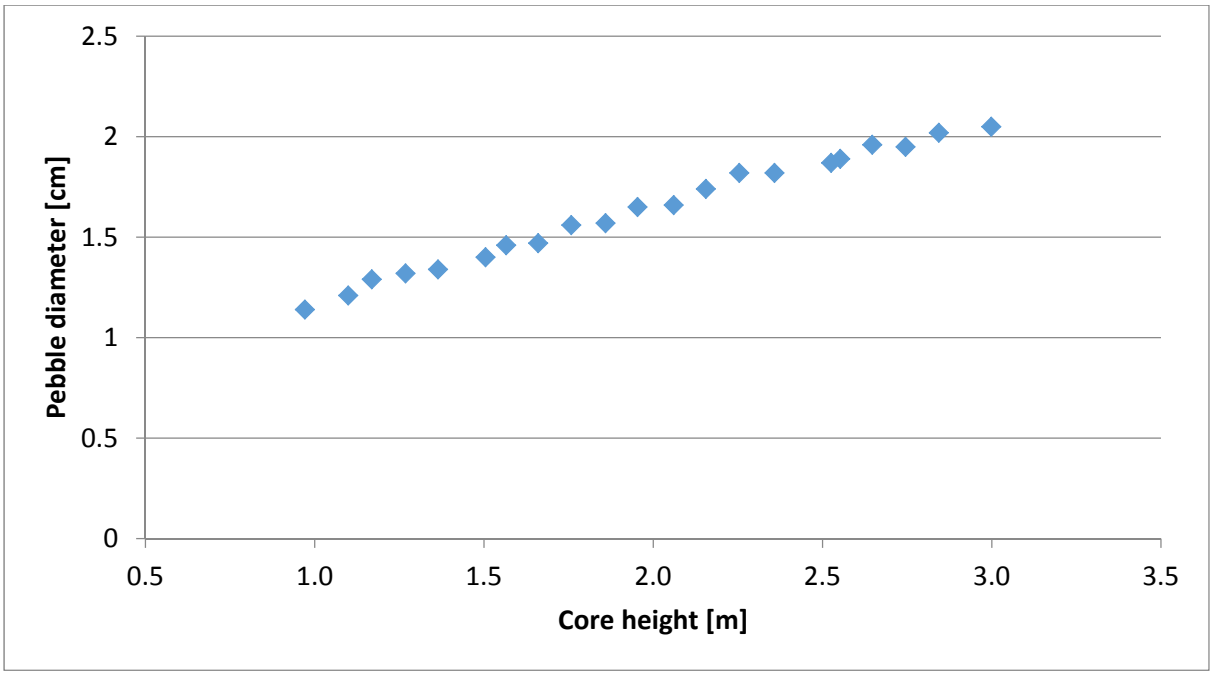

Figure 3.12. Pebble diameter vs. core height.

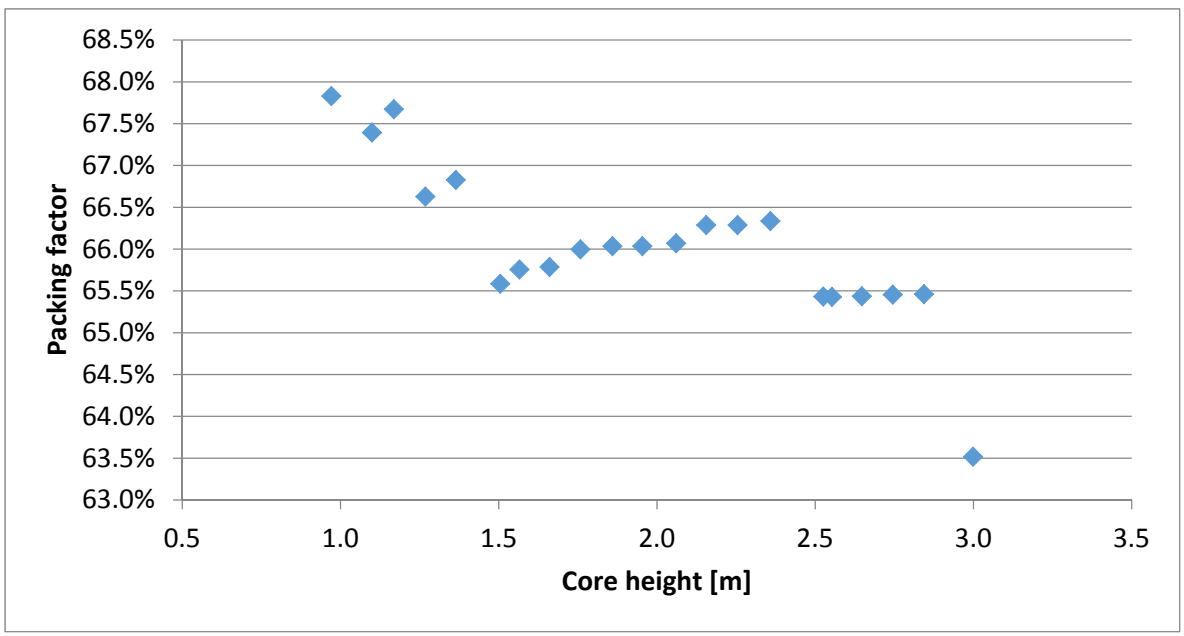

Figure 3.13. Pebble packing factor vs. core height.

3.6. Comparison against Reference Core

The reference core with 2-D fuel shuffling is shown in Table 3.4 and compared against a 2m tall core design. The power density of the reference core is 25% higher than in the pebble bed core; additionally, it has a significantly higher fuel volume fraction due to the limited achievable fuel packing fraction.

Table 3.4. Selected designs and associated metrics of thermal-hydraulic performance under the specified constraints.

Parameter	Reference	3-D PB
Power (MW)	2750	1683
Core Volume (m^3)	32.58	25.0
Power Density (W/cc)	84.4	67.3
Pebble/Rod Diameter (cm)	1.563	1.65
Bundle Pressure Drop (MPa)	0.874	1.3
Peak Fuel Temperature (°C)	798	799
Peak Clad Temperature (°C)	551	473
Exit Coolant Velocity at Hot Channel (m/s)	11.76	4.7
Fuel Volume Fraction at Smeared Density (%)	59.93	47.74

3.7. Conclusions and Future Work

The design could benefit greatly from axially dependent temperature models. It would be most desirable to implement this into a design code, such as ADOPT [1]. Ascertaining appropriate pressure drop and convective heat transfer models for an HCP lattice instead of a rhomboidal lattice could add a little more space to improve the power density (and therefore the economic attractiveness).

Unfortunately, with the specified pressure drop constraint, this reactor does not seem economically attractive, and would require a core height of about 1.5m to attain the same power density as the reference core design. At this core heights, leakage becomes an issue which threatens the feasibility of the sustaining breed and burn operation.

4. Conclusions

Although an ordered lattice of pebbles reduce the pressure drop are relatively easy to shuffle in three dimensions, the long fuel life combined with high pressures due to a lack of fission gas plenum create a large amount of thermal creep. In order to design survivable fuel, the fuel must either be vented (which does not seem feasible with pebbles), or the smear density must be reduced significantly such that the B&B mode of operation is not achievable. Additionally, the pebbles have a noticeably higher pressure drop than a rod-type design with the same fuel volume fraction, which leads to the designs being significantly less economical.

References

[1] Qvist, S. “Safety and Core Design of large liquid-metal cooled fast breeder reactors.” PhD dissertation, UC Berkeley (2013).

[2] Aydin Karahan, Jacopo Buongiorno “A new code for predicting the thermo-mechanical and irradiation behavior of metallic fuels in sodium fast reactors” J. Nuc. Mater. (2010)

[3] T. Ogata, Yeon Soo Kim, A. M. Yacout, “Metal Fuel Performance Modeling and Simulation” Comprehensive Nuclear Materials (2012)

[4] Ju Ang Jung, Seung Hyun Kim, Sang Hun Shin, In Cheol Bang, Ji Hyun Kim, “Feasibility study of fuel cladding performance for application in ultra-long fast reactor” J. Nuc. Mater. (2013).

[5] Moriyasu Tokiwai, Masaaki Horie, Kenji Kako, Masayuki Fukiwara, “Development of new ferritic steels as cladding material for metallic fuel fast breeder reactor” J. Nuc. Mater. (1993).

[6] Staffan Qvist “Optimized Standing Wave Breed & Burn Reactor Core Design”

[7] Florent Heidet, Ehud Greenspan “Performance of Large Breed-and-Burn Core” Nucl. Technol.

[8] A. A. Sorokin, B. Z. Margolin, I. P. Kursevich, A. J. Minkin, V. S. Neustroev, “Effect of neutron irradiation on tensile properties of materials for pressure vessel internals of WWER type reactors” J. Nuc. Mater. (2014).

[9] D.L. Porter, F. A. Garner J. Nuc. Mat. 159 (1988) 117-121.

[10] J.S. Straalsund, et al J. Nucl. Mater.

[11] Wang et al. J. Am. Ceram. Soc., 82 [12] 3321–29 (1999).

[12] Frank Garner, PNNL; ** Simonen, Garner, Klymyshyn and Toloczko, 2005.

[13] D. S. Gelles “Microstructural examination of commercial ferritic alloys at 200 dpa” J. Nuc. Mater. (1996).

[14] B. H. Sencer, J. R. Kennedy, J. I. Cole, S. A. Maloy, F. A. Garner “Microstructural stability of an HT-9 fuel assembly duct irradiated in FFTF” J. Nuc. Mater. (2011).

[15] B. H. Sencer, J. R. Kennedy, J. I. Cole, S. A. Maloy, F. A. Garner “Microstructural analysis of HT9 fuel assembly duct irradiated in FFTF to 155 dpa at 443 ºC” J. Nuc. Mater. (2009).

[16] J. J. Kai, G. L. Kulcinski “14 MeV nickel-ion irradiated HT-9ferritic steel with and without helium pre-implantation” J. Nuc. Mater. (1990).

[17] Bhagath Yarlagadda “ELEVATED TEMPERATURE MECHANICAL PROPERTIES AND CORROSION CHARACTERISTICS EVALUATION OF ALLOY HT-9,” Master’s thesis

[18] S. A. Maloy, T. Romero, M.R. James, Y. Dai “Tensile testing of EP-823 and HT-9 after irradiation in STIP II” J. Nuc. Mater.

[19] http://www.nrc.gov/reactors/new-reactors/design-cert/ap1000/dcd/Tier%202/Chapter%204/4-2_r14.pdf

[20] M. B. Toloczko, F. A. Garner “Irradiation creep and void swelling of two LMR heats of HT-9 at ~400ºC and 165 dpa” J. Nuc. Mater. (1996).

[21] M. B. Toloczko, F. A. Garner, C. R. Eiholzer “ Irradiation creep and swelling of the US fusion heats of HT-9 and 9Cr-1Mo to 208 dpa at ~400ºC” J. Nuc. Mater. (1994).

[22] Ning Wang, Shan-Tung Tu, Fu-Zhen Xuan, “A novel prediction method of creep rupture life of 9-12% chromium ferritic steel based on abductive work” Eng. Fail. Analy.(2013).

[23] M. D. Mathew, K. Laha, R. Sandhya, “Creep and Low Cycle Fatigue Behaviour of Fast Reactor Structural Materials” Procedia Eng. (2013).

[24] Ho Jin Ryu, Yeon Soo Kim, A. M. Yacout, “Thermal creep modeling of HT9 steel for fast reactor applications” J. Nuc. Mater. (2011).

[25] R. G. Pahl, C. E. Lahm, S. L. Hayes “Performance of HT9 clad metallic fuel at high temperature” J. Nuc. Mater. (1993).

[26] Santu Kaitya, T.R.G. Kuttya,∗, Renu Agarwalb, Arijit Laikc, Arun Kumar “Chemical compatibility of uranium based metallic fuels with T91 cladding” Nuc. Eng. Desig. (2012).

[27] http://www1.asminternational.org/AsmEnterprise/APD/

[28] Riefler, N. et al, “Pressure loss and wall shear stress in flow through confined sphere packings.” Chemical Engineering Science 69 (2012) 129-137.

[29] Beavers, G.S. et al, “Influence of bed size on the flow characteristics and porosity of randomly packed beds of spheres.” Journal of Applied Mechanics 40 (1973) 655-660.

[30] Susskind, H. & Becker, W, “Pressure drop in geometrically ordered packed beds of spheres.” Brookhaven National Lab (1966).

[31] MathWorks Documentation Center, “Gradual Area Change.” Accessed Dec 12, 2013: http://www.mathworks.com/help/physmod/hydro/ref/gradualareachange.html

[32] Yarlagadda, B. “Elevated Temperature Mechanical Properties and Corrosion Characteristics Evaluation of Alloy HT-9.” Master’s Thesis, University of Nevada, Las Vegas (2004).

[33] Gonzalez, S. “Study of the Feasibility of a Pebble Bed Breed & Burn Reactor,” MSc Project, UC Berkeley (2012).

[34] Hsu, C-J. “Analytical Study of Heat Transfer to Liquid Metals Flowing Along a Row of Spheres,” Brookhaven National Laborator (1967).

[35] Ogata, T. “Metal Fuel.” Central Research Institute of Electric Power Industry, Tokyo, Komae, Japan (2012).

[36] Leibowitz, L. and Blomquist, R. “Thermal Conductivity and Thermal Expansion of Stainless Steels D9 and HT9.” International Journal of Thermophysics, Vol. 9 (5), 1988.

[37] Epel, L.G., Levine, M.M., Nugent, G., and Parsick., R.J. “The Ordered-Bed Fast Reactor Concept [1000-MW(e) Reactor Design],” Brookhaven National Lab (1966).